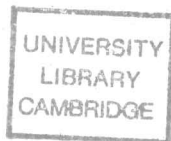


Ph.D 13099

STABLE STRATIFICATION IN THE EARTH'S CORE

by

Simon Mollett



a dissertation submitted for the degree of

Doctor of Philosophy

at the University of Cambridge

Trinity College
Cambridge

December 1983

STABLE STRATIFICATION IN THE EARTH'S CORE.

by Simon Mollett.

Summary

There has been speculation that the Earth's fluid outer core may in part be stably stratified, with evidence from studies of the magnetic field and from thermodynamic arguments. This affects possible models for the geodynamo; in particular stable stratification near the core-mantle boundary would allow more information about core surface velocities to be deduced from measurements of the secular variation of the magnetic field. The object of this dissertation is twofold: to examine the possible causes of such a stably stratified region, and to investigate the fluid dynamics of penetrative convection in a rotating system.

The possibility of thermal stratification at the core mantle boundary is investigated and rejected through the use of a numerical model of the cooling of the Earth. The model is constrained by the observed radius of the inner core, by the present heat flux to the surface of the Earth, and by palaeomagnetic evidence for an ancient geodynamo, and as a result gives reasonably well controlled estimates for the heat flux from core to mantle. Parameterised convection theory is used to model mantle convection, and the requirements of a dynamo mechanism are considered in terms of flows of entropy. Compositional gradients are reviewed as a possible mechanism for stable stratification, in terms of the rate of release of light material indicated by the cooling of the core.

Penetrative convection in a rotating system is studied in terms of the linear Boussinesq equations in simple geometries, by both analytical and numerical methods. It is shown that rotation tends to restrict the penetration of convective flows into the adjoining stable region. Experiments on penetrative convection in a rapidly rotating cylindrical tank are in broad agreement

with the linear theory, although the error estimates are large. These experiments use a tank on which the boundary temperature varies with time to create the adjoining stably and unstably stratified regions that characterise penetrative convection.

Declaration

This dissertation describes my original work except where acknowledgement is made in the text, and includes nothing which is the outcome of work done in collaboration. It does not exceed 250 pages in length and is not substantially the same in whole or in part as any that has been or is being submitted to any other University for any degree or other qualification.

Simon Mollett

December 1983

S. Mollett

Index

Page

Declaration	
Index	1
Acknowledgements	3
Nomenclature	4
1. Introduction	7
2. Review of core properties and of the fluid dynamics problem	11
2.1 Introduction	
2.2 Seismic and magnetic observations on the core	
2.3 Stable stratification in the core	
2.4 Fluid dynamics of convection	
2.5 Boussinesq approximation	
2.6 Equations of motion	
3. Heat flux from the core	53
3.1 Introduction	
3.2 The model	
3.3 Calculations	
3.4 Application of the results to the thermal history of the Earth	
3.5 Comparison of results with dynamo requirements	
3.6 Discussion of heat flux model	
4. Penetrative convection: analytical approach to the linear equations	76
4.1 Rotation parallel to gravity	
4.2 Rapid rotation limit	
4.3 General 2 layer problem	
4.4 Step function temperature profile	

4.5	Rotation perpendicular to gravity: "Busse-rolls"	
4.6	Thermal wind	
5.	Numerical solutions to the linear equations	116
5.1	Shooting program	
5.2	Testing the program	
5.3	Results: horizontal plane layer, vertical rotation	
5.4	'Overstable' convection	
5.5	Gravity normal to rotation: thin cylindrical geometry	
5.6	Summary of results from the shooting program	
6.	Experiments on penetrative convection	146
6.1	Introduction	
6.2	Tank design	
6.3	Thermal conduction model	
6.4	Observations	
6.5	Growth of convecting region	
6.6	Conclusions from the experiments	
7.	Discussion	163
7.1	Discussion of results	
7.2	Suggestions for future work	
8.	References	167
	Appendix 1	

Acknowledgements

I firstly wish to thank my supervisor, Dr David Gubbins, both for his guidance while I worked on these problems and for his patience when my work was even slower than usual. The Bullard Laboratories have been a very rewarding and enjoyable workplace: for that I wish to thank all my contemporaries in the Laboratories, but especially Professor Jack Jacobs, Dr Kathy Whaler and Dr David White for their help in many fields to do with the Earth's core and magnetic fields and with the behaviour (often unexplained!) of fluids. Many others have contributed to my work, in particular the Laboratory Technicians Roger Theobald and John Leonard who constructed the experimental tank.

A term spent with Professor F.H. Busse in the Institute of Geophysics and Planetary Physics at the University of California, Los Angeles led to much of the analytical and numerical work on penetrative convection described in chapters 4 and 5. Specific acknowledgement is made in chapter 5 for those program routines taken from UCLA, but much of the remainder of this work was heavily influenced by my discussions with Dr Busse and his students. I am also very grateful for their hospitality.

Financial support for this work was provided by a NERC studentship. The NERC also supported my visit to UCLA, with a travel grant from Trinity College. Computing time at UCLA was kindly provided from NSF grants to Professor Busse.

Finally, my thanks are due to Mrs Ann Rayner and Mrs Marion Jeffery for typing this dissertation so cheerfully and efficiently.

Nomenclature

The following is a list of the more commonly used symbols: in general they are defined when first encountered in the work. Chapter 3 is quite independent of chapters 4, 5 and 6 in this respect, and is indicated by the mark (3) where appropriate in this list.

a	horizontal wavenumber
α	proportional to, thermal expansion coefficient
a	aspect ratio
A	amplitude
b	constant (3), azimuthal wavenumber
β	variable parameter (3), density gradient
B	magnetic field
c	constant, specific heat capacity
C	heat capacity (3)
d	depth of unstable region
δ	small increment
D	geometrical constant (3), operator d/dz
e	exponential
ϵ	small parameter
η	magnetic diffusivity, radiogenic heating (3)
E	Ekman number, entropy (3)
f(z)	shape function for temperature gradient
F	normalised temperature perturbation
g	gravity
G	gravitational constant
γ	Gruneisen's constant
h	depth of a system
i	$\sqrt{-1}$

j	electric current
k	wave-number
k	thermal conductivity, compressibility
K	thermal diffusivity
K	degree Kelvin
λ	wave-length, Biot number
L	latent heat (3)
m	vertical wave-number
μ	dynamic viscosity
M	mass (3)
n	integer
ν	kinematic viscosity
N	Brunt-Vaisala frequency
Nu	Nusselt number
O	Order
p	time growth rate
π	3.14159.....
q	ratio of thermal to magnetic diffusivity
Q	energy (3), Chandrasekhar number
r	radial coordinate
ρ	density
R	Rayleigh number
s	frequency of overstable oscillation
σ	Prandtl number

t	time
τ	time scale
T	temperature (3), Taylor number
ϑ	temperature perturbation
θ	temperature
u	velocity
U	normalised vertical velocity
v	component of velocity
w	component of velocity
x	position coordinate
y	position coordinate
z	position coordinate
ζ	vorticity
Z	normalised vertical vorticity
ω	frequency
Ω	rotation rate

1. Introduction

The object of this work is to investigate some of the fluid dynamics problems that stem from observations of the magnetic field of the Earth and from thermodynamic predictions of the properties of the Earth's core. These suggest that the outermost part of the core may be stably stratified. There is no reason to suppose that core fluid dynamics has a simple structure: by analogy with the atmosphere and the oceans, one expects a great diversity of flow phenomena in the core. Not only is it a fluid body of low viscosity subject to the 'rapid' daily rotation of the Earth and to a rigid boundary, the mantle, of unknown topography, but also it is permeated by the magnetic field and is the seat of the geodynamo. It is important therefore, in studying specific topics, to realise that one's results may be applicable only to certain conditions. In particular, when modelling the behaviour of the core, one must utilise any observational constraints on the models so as to restrict the uncertainties involved.

The composition and properties of the core are not well known, owing to its inaccessibility to either direct observation or laboratory simulation. Both seismic and magnetic data give information but this is subject to the uncertainties inherent in any inverse problem. In general, what information is available is an average over a finite region of the Earth's interior and the resolution obtainable is limited, as has been discussed in works on the application of inverse theory to the deep interior (e.g. Masters, 1979). There is a general consensus that the outer core is liquid and the inner core solid, and that both regions are composed of a predominantly iron-nickel alloy with some light component (Jacobs, 1975). The magnetic field is

observed both directly in recent historic times and through the archaeo- and palaeo-magnetic records in artificial baked materials, igneous rocks and certain sediments: these studies show that the field fluctuates over both time and position and is capable of reversals on a geological time scale. Accordingly, the field is believed to arise from some self-generating dynamo mechanism. It is generally accepted that the dynamo requires convection in some region of the outer core, which is both fluid and an electrical conductor, rather than being driven by, for example, precessional torques (Loper, 1975), although gravity waves may be able to drive a dynamo (Singer & Olson, 1983). This convection occurs in a fluid subject to both Coriolis and Lorentz forces. It is not clear whether the Coriolis forces dominate or whether they are matched by the Lorentz forces in an approximately "magnetostrophic" balance. That depends on the strength of the toroidal magnetic field which is not observable at the Earth's surface, being confined to the conducting core.

Beyond that consensus, there is much discussion about the actual composition of the core, particularly of the identity of the light alloying component and of the possible presence of potassium with its attendant radiogenic heating from the decay of K^{40} , and of whether part of the outer core may be stably stratified. Higgins & Kennedy (1971) suggest that the outer part may be sub-adiabatic in its temperature gradient though this has since been disputed (Stevenson, 1980), while Fearn & Loper (1981) discuss the possibility of compositional stratification near the core-mantle boundary.

A stably stratified region adjacent to the core-mantle boundary would lead to the lack of upwelling ($\partial v_r / \partial r = 0$) reported by Whaler (1980) from secular variation data. If there is no

upwelling at the surface of the core, then much more information about the core surface velocities is available from the secular variations than is the case for unconstrained velocities (Backus, 1968); Gubbins (1982) discusses the toroidal velocity components that can be measured on this assumption of zero upwelling. Thus it is important to assess whether such a stable region can exist.

In this thesis, we investigate whether a stably stratified region can be formed, whether by compositional differences or by subadiabatic temperature gradients, and then study an idealised fluid dynamics problem, the effect of rotation on penetrative convection. The latter study is a step towards understanding whether such a stable region could persist adjacent to the convecting interior of the core.

Chapter 2 contains a review of information on core properties and of the fluid dynamics of penetrative convection and convection influenced by rotation and magnetic fields. In chapter 3, a thermal history model of the Earth yields estimates for the heat flux out of the core, constrained to fit our knowledge of the present-day inner core radius and surface heat flux and of the existence of ancient magnetic fields. This suggests that no thermal stable stratification exists and therefore that any such region would be due to the compositional stratification model put forward by Fearn & Loper (1981), which is reviewed and extended in § 2.3. Chapters 4, 5 and 6 set out an investigation of penetrative convection in rotating systems, the object being to study whether the rotation tends to enhance or to inhibit the penetration of a stable region by adjoining convection. Analytic approaches to the linear Boussinesq equations of motion are discussed in chapter 4 and extended by numerical work in chapter 5, using a "shooting" program to find

upwelling at the surface of the core, then much more information about the core surface velocities is available from the secular variations than is the case for unconstrained velocities (Backus, 1968); Gubbins (1982) discusses the toroidal velocity components that can be measured on this assumption of zero upwelling. Thus it is important to assess whether such a stable region can exist.

In this thesis, we investigate whether a stably stratified region can be formed, whether by compositional differences or by subadiabatic temperature gradients, and then study an idealised fluid dynamics problem, the effect of rotation on penetrative convection. The latter study is a step towards understanding whether such a stable region could persist adjacent to the convecting interior of the core.

Chapter 2 contains a review of information on core properties and of the fluid dynamics of penetrative convection and convection influenced by rotation and magnetic fields. In chapter 3, a thermal history model of the Earth yields estimates for the heat flux out of the core, constrained to fit our knowledge of the present-day inner core radius and surface heat flux and of the existence of ancient magnetic fields. This suggests that no thermal stable stratification exists and therefore that any such region would be due to the compositional stratification model put forward by Fearn & Loper (1981), which is reviewed and extended in § 2.3. Chapters 4, 5 and 6 set out an investigation of penetrative convection in rotating systems, the object being to study whether the rotation tends to enhance or to inhibit the penetration of a stable region by adjoining convection. Analytic approaches to the linear Boussinesq equations of motion are discussed in chapter 4 and extended by numerical work in chapter 5, using a "shooting" program to find

the eigenvalues, the critical Rayleigh numbers, of simple penetrative convection systems. Some experimental work on penetrative convection in a rapidly rotating cylindrical tank is described in chapter 6 and the results compared with the preceding numerical work. This study of the fluid dynamics is restricted to the linear equations of motion and to flows in the absence of magnetic field. It is therefore only a step towards modelling convection in the core, but a necessary one in view of the complexities of any more wide-ranging model of the convection.

2. Review of core properties and of the fluid dynamics problem

2.1 Introduction

This chapter sets out the relevant properties of the core (§2.2) and discusses the possibility of there being a stably stratified region near the core mantle boundary (§ 2.3). In addition it includes a review of the fluid dynamics literature relating to penetrative convection and convection in the presence of rotation or magnetic fields (§ 2.4), a discussion of the Boussinesq approximation (§ 2.5) and then sets out the linear equations of motion, under that approximation (§ 2.6). However, as the model of mantle convection used in the thermal history model of the Earth (§ 3) is a separate subject to this discussion of the core, the review of mantle convection work has been left to that chapter.

2.2 Seismic and magnetic observations on the core

Seismic

A recent review of seismic evidence about the composition of the Earth's core is given by Bolt (1982). Travel times and free oscillation periods yield velocity and density distributions throughout the Earth such as the "Preliminary reference Earth model" PREM (Dziewonski & Anderson, 1981). Such models are consistent with there being no stably stratified regions in the outer core, but could not resolve such regions if "thin" since the distribution are typically averaged over radial scales of about 50 km. According to Bolt (1982), "there is no definitive work precluding $7.8 < \alpha < 8.2 \text{ km s}^{-1}$, or 5% variation at the top of the outer core": here α is the P-wave velocity, but this

reflects a similar uncertainty in the density gradient. At the inner core boundary, reflection amplitudes for phase PKiKP suggest a density ratio between fluid and solid of $\rho_{oc}/\rho_{ic} = 0.87 \pm 0.04$ (Bolt, 1972), whilst the inversion of free oscillation data gives a jump $\Delta\rho = 0.87 \pm 0.32 \text{ g.cm}^{-3}$ (Masters, 1979), equivalent to a ratio $\rho_{oc}/\rho_{ic} = 0.93 \pm 0.03$. This density jump, much greater than that due solely to freezing, indicates a compositional difference between the solid inner core and the fluid outer core (Masters, 1979), as would be expected at a freezing boundary in an alloy of non-eutectic composition. From this density jump stem the possibilities both of a compositional energy source for convection and of compositional stratification near the core-mantle boundary, as will be discussed in § 2.3.

Within the outer core, there no longer appears to be a need for a transition zone at its base. The precursors observed to phase PKiKP formerly explained by such a zone can instead be accounted for by scattering from inhomogeneities near the core-mantle boundary (for a review, see Haddon, 1982). Jacobs (1975) gives a broader review of these matters, together with much information on the likely composition and thermal state of the core.

Magnetic

Models of the observed surface magnetic field and its secular variation that are continued downwards to the surface of the source region, the core (Lowes, 1974), have been used by many authors as a source of information about core motions (e.g. Bullard et al. 1950 on westward drift, Benton & Muth 1979 and Whaler 1980 on upwelling). A problem with the interpretation of these field models at the core mantle boundary is that of to what

reflects a similar uncertainty in the density gradient. At the inner core boundary, reflection amplitudes for phase PKiKP suggest a density ratio between fluid and solid of $\rho_{oc}/\rho_{ic} = 0.87 \pm 0.04$ (Bolt, 1972), whilst the inversion of free oscillation data gives a jump $\Delta\rho = 0.87 \pm 0.32 \text{ g.cm}^{-3}$ (Masters, 1979), equivalent to a ratio $\rho_{oc}/\rho_{ic} = 0.93 \pm 0.03$. This density jump, much greater than that due solely to freezing, indicates a compositional difference between the solid inner core and the fluid outer core (Masters, 1979), as would be expected at a freezing boundary in an alloy of non-eutectic composition. From this density jump stem the possibilities both of a compositional energy source for convection and of compositional stratification near the core-mantle boundary, as will be discussed in § 2.3.

Within the outer core, there no longer appears to be a need for a transition zone at its base. The precursors observed to phase PKiKP formerly explained by such a zone can instead be accounted for by scattering from inhomogeneities near the core-mantle boundary (for a review, see Haddon, 1982). Jacobs (1975) gives a broader review of these matters, together with much information on the likely composition and thermal state of the core.

Magnetic

Models of the observed surface magnetic field and its secular variation that are continued downwards to the surface of the source region, the core (Lowes, 1974), have been used by many authors as a source of information about core motions (e.g. Bullard et al. 1950 on westward drift, Benton & Muth 1979 and Whaler 1980 on upwelling). A problem with the interpretation of these field models at the core mantle boundary is that of to what

depth of the core they sample. For example, Whaler (1981) gives an estimate of the skin depth for secular variations of period one year as about 50 metres into the highly conductive core. However, as Whaler continues, this screening effect is calculated for a solid medium: in a fluid, horizontally polarised wave motions are possible that can transmit variations in the magnetic field through a conducting fluid, the MAC waves of Hide (1966) and Braginsky (1967). Benton (1979) considers the use of the unsigned flux integral U for a sphere of radius r ,

$$U(r,t) \equiv \oint |B_r(r,\vartheta,\phi,t)| \cdot dS$$

as a means of finding the source region, rather than the top of the core, following Hide (1978). The method considers the difference $\Delta U(r)$ between field models at two different times, extrapolated down to radius r : the radius at which $\Delta U(r) = 0$ is that of the surface of a good conductor in which the flux is frozen. Benton (1979) extends the argument on the grounds that if there is a core region next to the core mantle boundary that is not the site of dynamo action (because of stable stratification), then that region will react passively to the secular variation of the field and the vacuum representation of the magnetic field remains valid. Thus $\Delta U(r) = 0$ throughout this region, and the site of dynamo action should be marked by that radius at which $|\Delta U(r)|$ rises again from zero. However, the accuracy of the method (2% error, from Hide (1978)) makes it unlikely to be of use in measuring a "thin" stably stratified region.

When applied to the question of upwelling, the magnetic field data is consistent with the hypothesis of no upwelling (as measured by $\partial v_r / \partial r$) at the core-mantle boundary (Whaler

1980). This conclusion stems from the use of the radial component of the magnetic induction equation at the surface of a good conductor (so that diffusion is negligible on the time-scales of the secular variation, and $v_r = 0$ at the surface):

$$\frac{\partial B_r}{\partial t} + \underline{v} \cdot \nabla_H B_r + B_r \nabla_H \cdot \underline{v} = 0$$

where ∇_H is the horizontal divergence operator ($\nabla - \frac{\partial}{\partial r} \hat{r}$) (Backus, 1968). At points on the core mantle boundary at which $\nabla_H B_r$ vanishes, $\nabla_H \cdot \underline{v}$ can be estimated by

$$\nabla_H \cdot \underline{v} = - \frac{\partial B_r}{\partial t} / B_r$$

For an effectively incompressible fluid, this then gives $\partial v_r / \partial r$ at these points. Thus the hypothesis of no upwelling, which stemmed from thermodynamic work described in more detail in § 2.3 and § 3, is tested "at" the core mantle boundary. The question of how deep this information about core flows extends is important: if the information is very shallow, then it is merely consistent with the fluid dynamics boundary condition of a no-slip (rigid) boundary, at which $v_r = \partial v_r / \partial r = 0$. If the information extends beyond the surface boundary layer (the Ekman boundary layer in a rapidly rotating fluid body), then this lack of upwelling is significant and is consistent with suggestions of stable stratification in the core near the core mantle boundary (see § 2.3). For a typical estimate of core viscosity of $\nu = 5 \cdot 10^{-7} \text{ m}^2 \text{ s}^{-1}$ (Gans, 1972), the daily rotation of the core suggests an Ekman layer thickness, $\delta = \sqrt{\nu / \Omega}$ of approximately 10^{-1} m . Thus our information should at least extend beyond the viscous influence of a no-slip boundary, and so can be taken as supporting the proposed presence of a stable region, inhibiting the penetration of convection.

Benton & Muth (1979) give an alternative measure of the

upwelling $\partial v_r / \partial r$, using the change in area enclosed by a null-flux curve (on which $B_r = 0$) between two field models of different epoch to give the average of $\partial v_r / \partial r$ over that area and that period. They derive a value $\partial v_r / \partial r \approx 10^{-10} \text{ s}^{-1}$, indicating that the radial velocity near the surface is very much smaller than the horizontal velocities inferred from westward drift or from the measurable velocities normal to null flux curves (typically 10^{-4} ms^{-1} , again from Benton & Muth, 1979).

2.3 Stable stratification in the core

Although seismic and magnetic studies are the primary source of information on the core, it is the thermodynamics of the core that has caused most discussion of the stability or otherwise of the core. This subject is intimately linked both with speculation on the formation of the Earth and with the problem of finding an adequate source of energy to maintain a geomagnetic field. It is restrained by experimental high-pressure work on iron alloys and their phases, and by cosmological ideas on isotope abundancies. A review of this field is given by Jacobs (1975).

Higgins & Kennedy (1971) produced perhaps the greatest controversy when they suggested, on the basis of their theoretical work on both the melting temperature and the adiabatic gradient of iron at high pressures, that the outer core must be stably stratified for the surface between inner and outer cores to be a freezing interface. This ran contrary to the idea that thermal convection in the outer core, driven either by cooling (Verhoogen, 1961) or by radiogenic sources, was the cause of the geodynamo. Subsequent studies (e.g. Stevenson, 1980) have disagreed with Higgins & Kennedy's conclusions, finding

instead that the adiabatic gradient in the outer core should be less steep than the melting temperature profile, so that a well-stirred convecting core in which temperatures follow the adiabatic gradient outwards from the freezing surface is indeed consistent with the outer core being molten (fig. 2.1). However, the controversy did lead to work on the question of how much heat must flow out of the core to avoid a thermal stable stratification and also to renewed interest in the proposal of Braginsky (1963) that the release of a light fluid fraction on freezing at the inner core surface leads to compositional convection. Such compositional convection could occur even though the core might be in a state of thermal stable stratification, in which case the convection would result in a negative heat flow, in opposition to the heat flow by conduction down the adiabatic temperature gradient that is a consequence of vigorous convection and its attendant good "stirring" (Loper, 1978a and b).

Thermal models of the Earth's core such as those of Loper (1978a) (based on a constant heat flux from core to mantle) and of Gubbins et al (1979) (constant rate of cooling) have been used to test whether such cooling can lead to an adequate energy source for the dynamo. Gubbins et al (1982) considered what would be the result of a zero rate of cooling, in terms of the formation of a stably stratified layer near the core mantle boundary. This in turn led to the use of the secular variation data by Whaler (1980), to investigate fluid flows at the core surface. The work described in chapter 3 is an extension of these models, considering the effect of mantle convection in determining the thermal boundary condition to the core.

Fig. 2.1

Schematic diagram of adiabatic and melting-point profiles in the Earth's core .

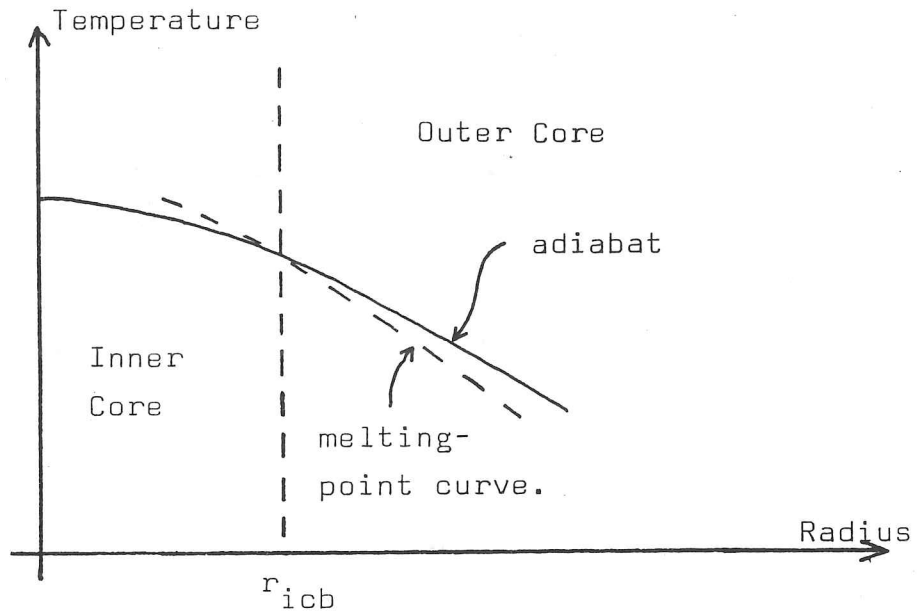


Fig. 2.2

Double diffusion regimes , reproduced from fig. 8.2 in Turner (1973) .

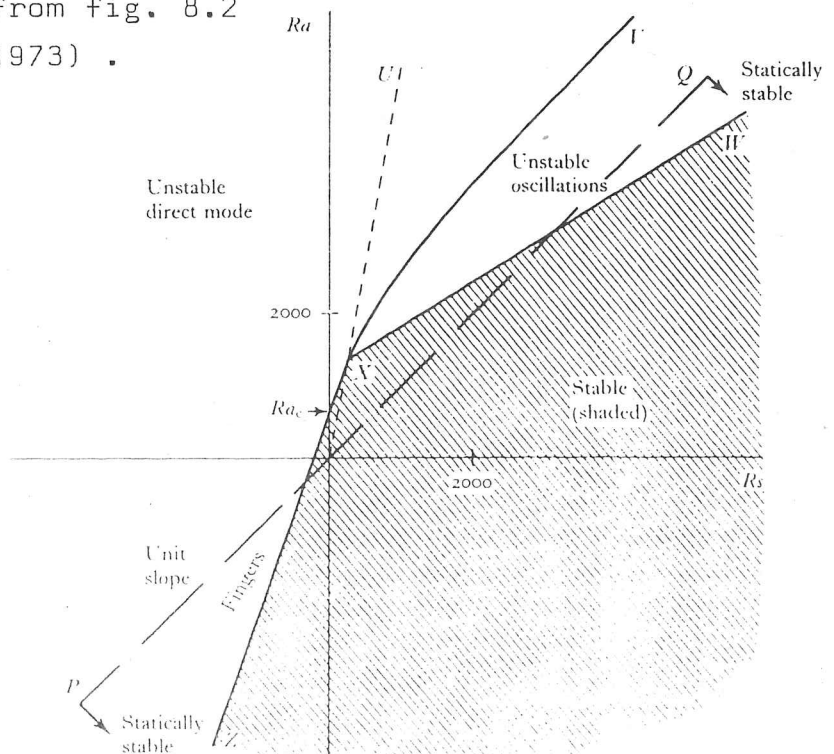


Fig. 8.2. Diagram of the various convection regimes described by (8.1.8). The sign convention is such that negative Ra and positive Rs represent stabilizing gradients of the respective components. (After Baines and Gill 1969.)

Requirement for stability

For the purpose of this work, a stable stratification in a fluid exists if, should a small parcel of fluid initially in equilibrium with its surroundings be displaced vertically in an adiabatic process, that parcel then experiences a restoring body force. An adiabatic process is one in which no irreversible changes occur (e.g. thermal conduction or diffusion of matter) and as such is an idealised occurrence, but one to which real processes approximate. The density of a fluid body is characterised by its composition, temperature and pressure and, provided there are no appreciable accelerations, the last will be determined by the equilibrium pressure of its surroundings.

Thus the requirement for stability is that, for an adiabatic move from z_1 to z_2 with composition c , temperature T and pressure p

$$\rho(c(z_1), T(z_1, p(z_2)), p(z_2)) > \rho(c(z_2), T(z_2, p(z_2)), p(z_2))$$

where position z_1 is lower than position z_2 . Note that, even though no heat flows by conduction, the temperature depends both on the original position and on the current pressure, due to the work done in any expansion. Assuming that, for small changes, the density depends linearly on these factors,

$$\rho = \rho_0(1 - \alpha_c c - \alpha_T T + \alpha_p p)$$

we require,

$$\alpha_c (c(z_2) - c(z_1)) + \alpha_T (T(z_2) - T(z_1) - \frac{\partial T}{\partial p} [p(z_2) - p(z_1)]) - \alpha_p (p(z_2) - p(z_1)) > 0$$

or, in the limit of small displacements,

$$\alpha_c \left(\frac{dc}{dz} \right) + \alpha_T \left(\frac{dT}{dz} - \frac{\partial T}{\partial p} \cdot \frac{dp}{dz} \right) - \alpha_p \left(\frac{dp}{dz} \right) < 0 \quad \text{where } z \text{ is depth.}$$



i.e.

$$\alpha_c \left(\frac{dc}{dz} \right) + \alpha_T \left(\frac{dT}{dz} - \left(\frac{\partial T}{\partial z} \right)_s \right) < 0$$

where $\left(\frac{\partial T}{\partial z} \right)_s$ is the adiabatic gradient, which is positive.

This requirement, for the fluid to be stable, is not the same as that based on an isotropic reference state (e.g. used by Fearn & Loper, 1981) if there is a compositional gradient: a distinction attributed by Gubbins et al. (1979) to Kalinin (1972).

It is very important to note that this requirement relates to adiabatic changes. If there are significant irreversible effects then it may not be a necessary criterion. Notably, this opens up the field of double-diffusive convection, in which differing rates of diffusion in a system with at least two intrinsic factors affecting density (e.g. heat and a component of composition) can lead to modes of instability even though the above criterion suggests a stable situation. Further, even in the absence of diffusive instability, the occurrence of diffusive flows of the factors causing the unstable density gradients results in the requirement being only a necessary condition on instability: there will need to be a finite excess of the unstable gradients over those required above for motion to occur. This is described by a Rayleigh number, as will be set out in more detail below.

i.e.

$$\alpha_c \left(\frac{dc}{dz} \right) + \alpha_T \left(\frac{dT}{dz} - \left(\frac{\partial T}{\partial z} \right)_s \right) < 0$$

where $\left(\frac{\partial T}{\partial z} \right)_s$ is the adiabatic gradient, which is positive.

This requirement, for the fluid to be stable, is not the same as that based on an isotropic reference state (e.g. used by Fearn & Loper, 1981) if there is a compositional gradient: a distinction attributed by Gubbins et al. (1979) to Kalinin (1972).

It is very important to note that this requirement relates to adiabatic changes. If there are significant irreversible effects then it may not be a necessary criterion. Notably, this opens up the field of double-diffusive convection, in which differing rates of diffusion in a system with at least two intrinsic factors affecting density (e.g. heat and a component of composition) can lead to modes of instability even though the above criterion suggests a stable situation. Further, even in the absence of diffusive instability, the occurrence of diffusive flows of the factors causing the unstable density gradients results in the requirement being only a necessary condition on instability: there will need to be a finite excess of the unstable gradients over those required above for motion to occur. This is described by a Rayleigh number, as will be set out in more detail below.

Adiabatic Gradient

In the absence of compositional density gradients, the above stability criterion reduces to a comparison of the temperature gradient with the adiabatic gradient. The adiabatic gradient in the core is not well-known. Anderson (1982) gives a review of recent shock-wave measurements on iron at core pressures (for reference, core-mantle boundary: 135GPa; inner core boundary: 328GPa, from Jacobs (1975)), which can be connected with the results of static measurements at pressures up to 20 GPa. His paper is primarily concerned with the melting point of iron at core pressures, but also considers the possible values for the thermodynamic Gruneisen ratio γ from which

$$\left. \frac{\partial T}{\partial p} \right)_s = \gamma T / k$$

where $k(P)$, the ⁱⁿcompressibility, can be derived from seismic data (and is tabulated in Jacobs (1975)). Anderson considers values in the range $1.1 \leq \gamma \leq 1.6$ at the core mantle boundary, $0.9 \leq \gamma \leq 1.4$ at the inner core boundary, and also notes that γ should then be increased slightly (by approximately 0.1) for electronic effects, which affect the adiabatic gradient but not the suggested melting point equations.

The adiabatic gradient can be rewritten to:

$$\left. \frac{\partial T}{\partial z} \right)_s = \gamma g T / \Phi$$

where

$$\Phi \equiv k / \rho$$

(Φ is the directly measured quantity from seismic data,

$$\Phi = v_p^2 - \frac{4}{3} v_s^2 \quad) \quad g \text{ is}$$

gravity and z depth. From inner core boundary to core mantle boundary, these change as shown in table 2.1.

The errors involved are largely "parallel": the ratio of $\left. \frac{\partial T}{\partial z} \right)_s$

Table 2.1

		<u>i.c.b.</u>	<u>c.m.b.</u>
γ	(Anderson)	1.1 ± 0.3	1.3 ± 0.3
g	(Jacobs)	4.2 ms^{-2}	10.7 ms^{-2}
$1/\phi$	(Jacobs)	$1 \times 10^{-8} \text{ s}^2 \text{ m}^{-2}$	$1.6 \times 10^{-8} \text{ s}^2 \text{ m}^{-2}$
T	(Anderson)	$4800 \pm 600 \text{ K}$	$3620 \pm 1000 \text{ K}$

(subject to errors
in the adiabatic
gradient as feedback)

Hence $\left. \frac{\partial T}{\partial z} \right|_s = \underbrace{(2.2 \pm 0.8) \times 10^{-4} \text{ K m}^{-1}}_{\text{(i.c.b.)}} ; \underbrace{(8.1 \pm 4.0) \times 10^{-4} \text{ K m}^{-1}}_{\text{(c.m.b.)}}$

at inner core boundary to that at core mantle boundary should be correct to about 20% with that error arising primarily from the feedback of uncertainty in the adiabatic gradient on the temperature at the core mantle boundary, which Anderson derives by continuation from the melting point at the inner core boundary.

The variation in $\left(\frac{\partial T}{\partial z}\right)_s$ over the range of the outer core is of interest in indicating the most likely region for stable stratification. Gubbins et al. (1982) considered this question, but state only that the top of the core is favoured by reason of the higher adiabatic gradient there, arising, as they state, primarily from the increased value of gravity there. This is in fact only obvious, on a simple model in which $\left(\frac{\partial T}{\partial p}\right)_s$ is assumed constant, if a significant heat source is localised deep in the core, rather than being distributed evenly with mass (as might be expected for specific heat from cooling or radiogenic heating), as follows:

a) Possible heat flux by conduction = $k \left(\frac{\partial T}{\partial z}\right)_s$ x area

b) Heat flux from distributed sources \propto mass enclosed (m)

c) Now $\left(\frac{\partial T}{\partial z}\right)_s = g\rho \left(\frac{\partial T}{\partial p}\right)_s$

and $g \propto [m(r)/r^2]$

\therefore possible heat flux by conduction $\propto [m(r) \cdot k\rho \left(\frac{\partial T}{\partial p}\right)_s]$

whilst distributed sources of heat $\propto [m(r)]$

d) Thus, to the extent that $k\rho \left(\frac{\partial T}{\partial p}\right)_s$ is constant with radius, so one finds that distributed sources of energy do not favour any particular region of the outer core as a candidate for being sub-adiabatic. On this simple model, it is only through the occurrence of a localised source (latent

heat or gravitational energy) at the inner core surface that the core mantle boundary becomes the favourite region for sub-adiabatic temperature gradients.

In addition, the increase in $\gamma T/\phi$ from inner core boundary to core mantle boundary indicated by the estimates in Table 2.1 does justify the conclusion of Gubbins et al. (1982) even in the absence of deep localised sources of energy. Thus, on two grounds, one can expect the outermost part of the core to be the most likely to be stably stratified by temperature. In §3 a thermal history model of the Earth is used to estimate the heat flux from the core, and thereby to investigate the possibility of a thermal stable stratification.

Compositional Stratification

As an alternative hypothesis, we may consider whether compositional gradients can lead to a stable stratification in the core. This would stem from the release of light material at the freezing surface of the inner core, as suggested by Braginsky (1963). Masters (1979) uses free oscillation data to measure the density jump across the inner core surface, and his results indicate that the jump is greater than that due to the phase change alone ($\Delta \rho = (0.7 \pm 0.3) \text{ Mg.m}^{-3}$ whereas phase change $\Delta \rho \approx 0.05 \text{ Mg.m}^{-3}$), with the inner core density being consistent with that of pure iron, the outer core being a lighter alloy. Fearn & Loper (1981) show that the concomitant release of light material at the surface during freezing would lead to a convective instability to a much greater degree than thermal flows. Further, on the assumption that the core-mantle boundary acts as an impermeable barrier to this light component, they argue that the flux of the light component must decrease to zero

as it approaches the boundary and therefore that a barodiffusive regime can account for the flux near to the boundary. Hence they suggest that a stably stratified region will result, of thickness approximately 70 km. As they point out, one must consider the time-scale for the possible emplacement of such a region and the possible disruptive effects of the convection in the remainder of the outer core as it impinges on the stratified region. This latter problem, one of penetrative convection, is analogous to that of the dispersion of a heavy gas layer in the turbulent atmospheric boundary layer, as might be formed following, say, accidental industrial release. Atmospheric studies of entrainment may be found in, for example, Deardorff (1976) or Jensen & Lenshow (1978).

The time scale for the full establishment of a compositional stable stratification, in which barodiffusion balances diffusion down the concentration gradient, would be of the order of the diffusive time-scale. If we take a length-scale $L = 70$ km (Fearn & Loper, 1981) and a diffusion constant $D \approx 10^{-8} \text{ m}^2 \text{ s}^{-1}$ (based on a viscosity $\nu = 5 \times 10^{-7} \text{ m}^2 \text{ s}^{-1}$ (Gans, 1972) and the Einstein relation, $D \nu = \frac{kT}{6\pi a \rho}$), we get a diffusive time-scale of order

$$L^2/D \approx 5 \times 10^{17} \text{ s}$$

$$\approx 15 \text{ Ga.}$$

At best diffusive equilibrium can ~~at best~~ be only partially achieved as yet, unless one argues for a markedly greater diffusion constant (and hence lower viscosity). If we now turn to the question of what would be the final equilibrium state of such a stable layer, then we can expect a Boltzmann distribution of the light component,

$$\rho = \rho_0 - \rho_1 \left\{ \exp\left(\frac{-m^*g}{kT} (Z - Z_0)\right) \right\}$$

where Z is the depth from the boundary, Z_0 , ρ_0 is the bulk density, ρ_1 is the amplitude of the density change due to the light component and m^* is the difference in molecular mass between heavy and light components (40 a.m.u. for iron and oxygen, 24 a.m.u. for iron and sulphur). This supposes an ideal solution in which there is neither volume change nor release of chemical energy on substituting one component for the other. If

$$H = \left(\frac{kT}{m^*g} \right)$$

= 60 km for $m^* = 40$ a.m.u.
and $T = 3300$ k

we have

$$\rho = \rho_0 - \rho_1 \exp\left(\frac{-(Z-Z_0)}{H}\right)$$

and, as a measure of the stability, the square of the Brunt-Vaisala frequency N :

$$N^2 = + g/\rho \partial\rho/\partial z$$

$$= \rho_1/\rho_0 \cdot \frac{g}{H} \exp\left(\frac{-(Z-Z_0)}{H}\right) \text{ for } \rho_1 \ll \rho_0$$

where we can estimate ρ_1/ρ_0 from equating the mass of light component in this distribution with the mass rejected from the inner core on freezing, using the density jump given by Masters (1979).

$H \ll R$, the radius of the outer core

$$M_L = 4\pi R^2 H \rho_1$$

$$= \left(\frac{3H}{R}\right) \cdot \rho_1/\rho_0 \times (\text{mass of core}) \quad \dots A$$

But $M_L \approx 6\%$ mass of inner core (Masters, 1979)

$$\approx 0.003 \times (\text{mass of core}) \quad \dots B$$

Equating A and B,

$$\rho_1 / \rho_0 \approx 0.003 \times \left(\frac{R}{3H} \right)$$

$$\text{Hence } N^2 \approx 0.06 \left(10^{-5} \text{s}^{-2} \right) \cdot \exp \left(\frac{-(Z-Z_0)}{H} \right)$$

This simple model thus predicts that, if diffusive equilibrium has been attained (or, more pertinently, if it is near) then the compositional gradient leads to a Brunt-Vaisala frequency N that ranges exponentially from zero deep in the outer core to approximately $(3 \times 10^{-3}) \text{ s}^{-1}$ at the core mantle boundary, with a depth scale of order 60 km (or 70 km from Fearn & Loper, 1981). The shallow depth scale makes it unlikely to be detectable by seismic means.

This model has assumed that the light component rejected on the freezing surface is convected to the core mantle boundary (or its vicinity) and then stays there, developing a locally diffusive concentration gradient. It further supposes that the intervening convecting part of the outer core, the greater part of it, remains well-mixed by the convection so that the light component already in the outer core remains in solution, not separating out under gravity to join the surface region. The separation of stable and unstable regions, even though there be no rigid barrier between the two bodies of fluid, is a concept that will be investigated below.

One further point can be made from this model of the release of light component. Using the thermal history model (chapter 3) to give a typical rate of cooling of the core of approximately $0.1 \text{ K} \cdot \text{Ma}^{-1}$ ("standard" run gives $dT_c/dt = 0.087 \text{ K} \cdot \text{Ma}^{-1}$), we can estimate the flux of light component from the inner core surface, using equation 3.7 for the inner core radius r

$$r^2/r_0^2 = (T_0 - T_1)/(T_0 - T_f)$$

where T_1 is the current core-mantle boundary temperature, and T_0 , T_f those hypothetical temperatures at which inner core formation starts and is completed respectively, so that

$$\begin{aligned} 2 \frac{dr}{dt} \cdot \frac{r}{r_0^2} &= - \frac{dT_1}{dt} / (T_0 - T_f) \\ \frac{dr}{dt} &= \frac{1}{2} \left(\frac{r_0}{0.35} \right) \cdot (10^{-4} \text{ Ma}^{-1}) \\ &\approx 500 \text{ m.Ma}^{-1} \end{aligned}$$

Hence we can estimate the mass deficit M_L being released as:

$$\frac{dM_L}{dt} = 4 \pi r^2 \cdot \frac{dr}{dt} \cdot (0.7 \text{ Mg.m}^{-3})$$

again using the density jump from Masters (1979), giving

$$\frac{dM_L}{dt} \approx 3 \times 10^5 \text{ kg.s}^{-1}$$

Double Diffusion: 2 components causing opposing density gradients.

As was mentioned above, when one relaxes the condition of changes being perfectly adiabatic, there arise possible

instabilities even though the overall density gradient is apparently stable. These are caused by the diffusive flows, and may be said to be entropy driven in that the mechanism is one of redistributing one component more rapidly than the other, thereby allowing the potential energy of the unstable component to be released by local instability. Turner (1973) (chapter 8) gives a broad review of this field, in which two new instabilities occur, the "finger" regime and the "unstable oscillations" regime. Figure 2.2 is reproduced from that book, and shows the occurrence of these two instabilities in the case of heat and salt as the two components (note: diffusivity of heat in water $\approx 100 \times$ diffusivity of salt). The finger regime in particular has been extensively studied, owing to its oceanographic applications in terms of salt transport between ocean layers.

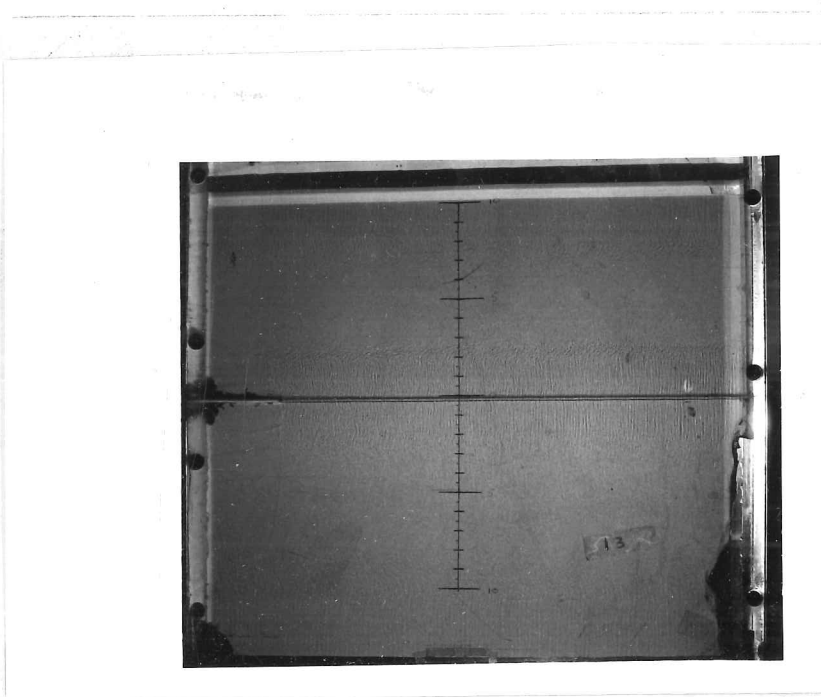
In this thesis, double diffusion is not considered in detail: the penetrative convection studies made are on single component systems, attributing the possible stable layer at the core mantle boundary to either thermal or compositional effects (probably the latter in view of the results of §3), not to a combination of the two. However, if compositional effects are significant then double diffusion is likely to be important, at least in local terms. If there is the combination of a superadiabatic temperature gradient (arising from high heat flux out of the core) and a stable compositional gradient as suggested by Fearn & Loper (1981), then since the thermal diffusivity in a liquid metal should be much greater than the material diffusivity one can expect the "unstable oscillation" regime to be a possibility near the core-mantle boundary. A "finger" regime is less likely, as it would involve a subadiabatic temperature gradient and so leads to an inefficient dynamo (see § 3).

Accordingly some experiments performed on salt fingers under rotation, following Schmitt & Lambert (1979), are not reported in this work, although Fig. 2.3 is a pair of photographs of these experiments, showing a side-effect of rotation observed, in inhibiting the formation of secondary layering at the top and bottom surfaces of the experimental tank.

The distinction between the two modes is whether the more rapidly diffusing component is the unstable (unstable oscillations) or the stable gradient (fingers): in both cases the unstable gradient component is transported preferentially across the region of instability. In the case of unstable oscillations, the oscillatory motion assists the diffusive transport of the unstable component by enhancing the local gradient of that component and then advecting the component to another region, similar in some respects to the increased heat flux in rotating annulus experiments that arises from the baroclinic instability on the thermal wind flow (e.g. Hide 1958). The finger regime on the other hand is a steady motion, most simply conceived in terms of a conducting-pipe model set out by Stommel et al. (1956), in which diffusion of the stable component through the side-walls allows a steady advection of the unstable component. Stern (1960) showed that the differing rates of diffusion of the two components can replace the rigid conducting side-walls. Double diffusion can also lead to finite amplitude subcritical convection in cases in which the unstable component is the more rapidly diffusing (Proctor, 1981a).

Fig. 2.3

Experiments on the formation of salt fingers ,
firstly non-rotating , secondly rotating about
a vertical axis at approximately 0.5 rev. s^{-1} .

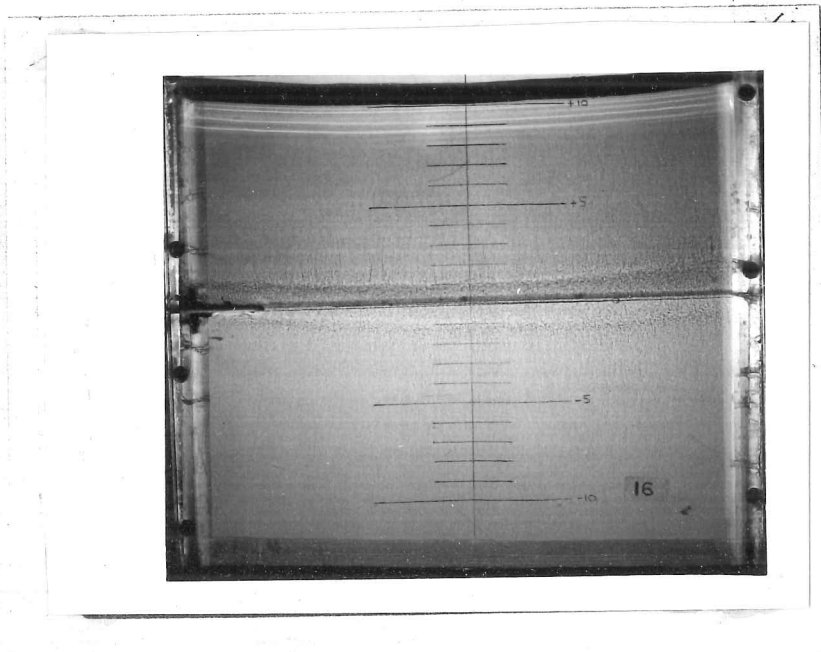


Non-rotating

← Boundary
(secondary)
finger layer .

← Main finger
layer .

Apparatus scale is shown by the vertical grid
which is marked in 1cm steps .



Rotating

← No secondary
finger layer.

← Main finger
layer .

Note that the bright
horizontal lines seen
at the top boundary
are merely reflections
from the meniscus .

Penetrative Convection

Penetrative convection theory applies to cases in which stable and unstable density gradients exist in adjacent regions of fluid, and is primarily concerned with the extent to which convection can penetrate the stable region. In this sense it is a study of convection in a region in which the density gradient is not constant, as in the Rayleigh-Benard problem, but rather changes sign. An alternative approach is to consider the fluid as two distinct regions, interacting at their mutual boundary through pressure and viscous forces.

The former approach was studied for a non-rotating system by Sparrow et al. (1964) as part of an investigation into broadening the range of the convection problems studied using linear theory. Part of the work concerns the effect of changing the thermal boundary condition, revealing the long horizontal wavelengths associated with fixed flux or low Biot number boundaries (where the thermal boundary condition is $\frac{d\vartheta}{dz} = \pm\lambda\vartheta$, $\lambda = \text{Biot number}$, $\vartheta = \text{temperature perturbation}$), and part investigates the non-linear temperature profiles that can result from internal heating, rather than heating from the base. This latter part mainly considers the effect on the Rayleigh number at onset (defined in terms of the maximum temperature difference within the system), but Sparrow et al. also note that for strongly peaked temperature profiles the lower boundary becomes shielded from the convective motions by the immediately adjacent stably stratified region.

Veronis (1963) investigates a specific penetrative problem, that of convection in an ice-water system, in which the coefficient of expansion α changes sign so that the density

gradient is one of penetrative convection even though the temperature gradient is the constant one of simple one-dimensional thermal conduction. His approach is based on Fourier series expansions of the perturbation variables, using the idealised boundary conditions of stress-free and perfectly conducting surfaces to simplify the analysis, and he achieves a high degree of accuracy in the evaluation of the critical Rayleigh number despite severe truncation of the series. Equivalent results for rigid boundaries are also given, from the analogous problem of Couette flow (Chandrasekhar, 1954). This problem is used as a test case in § 5, in which the numerical integration used, a "shooting" method, yields similar values for the Rayleigh number but suggests that the countercell found by Veronis is partly due to the extent of truncation of the series. Veronis continues in the same paper to a weakly non-linear calculation in which he demonstrates a finite amplitude sub-critical instability: as he explains, this is to be expected in view of the results of mixing in a system with such a variation of the coefficient of expansion. Moore & Weiss (1973) extend this work in a nonlinear numerical study.

Stix (1970) also employs a Galerkin approach, a series expansion of the solution, but considers two special cases of a two layer problem, one of a perfectly conducting and therefore isothermal upper ("stable") layer and the other of a very strongly stratified upper layer. These allow analytic expressions for the solutions at the onset of convection, and as a result Stix shows that the strongly stratified region can act as a more severe boundary condition to the unstable region than would a rigid wall (the critical Rayleigh numbers being 2435 and 1708 respectively). A similar conclusion is reached by Whitehead

(1971), who shows that as the stable region becomes of infinitely strong stratification it becomes equivalent to a boundary on which $W = DW = D^2W = 0$

(where W is the normal velocity, parallel to z), a combination of the conditions of no slip and no tangential stress.

Sun (1976) investigates the atmospheric problem of the morning disruption of the night-time temperature inversion by considering a two layer problem. The layer adjacent to the ground (a rigid boundary, taken to be perfectly conducting) is allowed a cubic temperature profile, which is matched to an upper semi-infinite stable layer of uniform stability, and a power series method used. Subsequent finite amplitude convection is described in terms of a mixed convecting region bounded by a thermal boundary layer of superadiabatic temperature gradient by the ground and by an inversion layer under an undisturbed stable region. This is similar qualitatively to the situation in the cylindrical tank experiments described in chapter 6, though without rotation.

A finite degree of stable stratification is investigated numerically in a 3 layer model by Latour and Zahn (1978), the unstable layer of unit depth being sandwiched between semi-infinite stable layers, the modulus of the density gradient being the same in each layer. The computational domain is of restricted extent, with matching conditions at its boundaries to analytic solutions in the stably stratified regions that extend the solution to infinity. In their paper, the layering is assumed due to variations in the underlying adiabatic gradient, with the motive for the work coming from convection in the interior of stars.

A non-linear approach to a particular problem in penetrative

convection is to use the long-wavelength solutions arising from fixed flux boundary conditions to separate horizontal and vertical scales of the solutions (Roberts, 1982, following the use of the method by Chapman & Proctor, 1980, and Proctor, 1981b). Roberts notes that an extensive stable region inhibits the long-wavelength solutions and so limits the applicability of the method. In chapter 5, we shall see a similar limitation arising from rotation of the system.

The alternative non-linear approach to penetrative convection is that developed by Townsend (1966), who considers the effect of thermals impinging on a stably stratified region, causing wave motions in the latter which can be of considerable amplitude and are therefore of interest in explaining and predicting the phenomenon of clear air turbulence. The only penetration considered is that of the buoyant rise of the thermals into the stable region until the density contrast becomes zero. Thermals penetrating in this way then act as discrete sources of waves, which are subject to diffusive losses as they propagate away from the disturbance. Entrainment of stable fluid by such thermals is a model for the growth of unstable regions in certain cases (e.g. Denton & Wood, 1981).

The effect of rotation and magnetic fields on convection

Chankrasekhar (1961) gives a detailed review of the linear stability of convection in a plane layer when rotation and magnetic fields are present. His numerical results for critical

Note: in the remainder of this chapter and in chapters 4, 5, 6, T is the Taylor number, and so Θ represents the temperature.

$$(T \equiv 4\Omega^2 d^4 / \nu^2)$$

Rayleigh numbers and horizontal wavenumbers are used in § 5 for comparison purposes with the shooting program used for this work. In his chapter on rotation there is a discussion of the $R_c = 0$ ($T^{2/3}$), $a_c = 0$ ($T^{1/6}$) relationships in the limit of $T \rightarrow \infty$ and also work on the occurrence of overstability when the Prandtl number ($\sigma \equiv \nu/\kappa$) is sufficiently small and the rotation rate sufficiently large. Linear temperature profiles only are considered. The discussion of cell planforms follows Veronis (1959), and experimental evidence is from Nakagawa & Frenzen (1955). A similar chapter on the effect of magnetic fields is then followed by one on the joint effects of magnetic fields and rotation, in which it is shown that the critical Rayleigh number may be appreciably lower when both influences are present than if only one is.

Veronis (1959 and 1966) considers the possible occurrence of finite amplitude instabilities and of overstability in much more detail, using the method of a small amplitude expansion about the linear solution previously set out in Malkus & Veronis (1958). Both overstable solutions and finite amplitude instabilities occur in certain parameter ranges in order to relax the constraint of rotation: both require fluids of low Prandtl number. The prediction of a finite amplitude instability at modest values of the Taylor number has been verified experimentally by Rossby (1969). This instability depends on the dual role played by viscosity, in releasing energy as well as in dissipating it. Stress-free, perfectly conducting boundaries are considered in this work of Veronis as they permit an analytical solution to the linear problem. The finite amplitude instability at low Prandtl number is also studied numerically by Veronis (1968).

Spherical geometry greatly increases the difficulty of analysis (e.g. Chandrasekhar, 1961, chapter 6), but a great simplification in the case of rapid rotation leads to the non axisymmetric "Busse-roll" solutions, in which the inclination of the boundaries restricts the convection to a tightly packed cylindrical form (Busse, 1970, following earlier work by Roberts, 1968). In such cases, in which the Coriolis forces must be dominant, a spherical shell such as the Earth's outer core can be divided into two very distinct regions of convection: polar, in which essentially plane-layer solutions occur, and equatorial, in which Busse-rolls occur (figure 2.4).

The existence of Busse-rolls has been demonstrated experimentally (Busse & Carrigan, 1974). Whether they are a suitable form of solution in the Earth's core depends on the strength of the magnetic field, for which Hide and Roberts (1979) review the arguments. In models incorporating a toroidal magnetic field of the same approximate strength as the observed poloidal field (weak field dynamo models), Busse-rolls should be important. However, in strong field models, in which the toroidal field is much stronger than the poloidal and an approximate balance of magnetic and rotational forces is assumed (a "magneto-strophic" balance), the rotational constraints are so weakened that the motion can again be fully three-dimensional. The analysis leading to Busse-rolls is described in § 4.5, as background to numerical (§ 5) and experimental (§ 6) studies in a cylindrical geometry, in which inclination of the boundaries is not significant. A point of interest from the experiments of Busse & Carrigan (1974) is that no finite amplitude subcritical instability was observed, unlike the plane layer case discussed above.

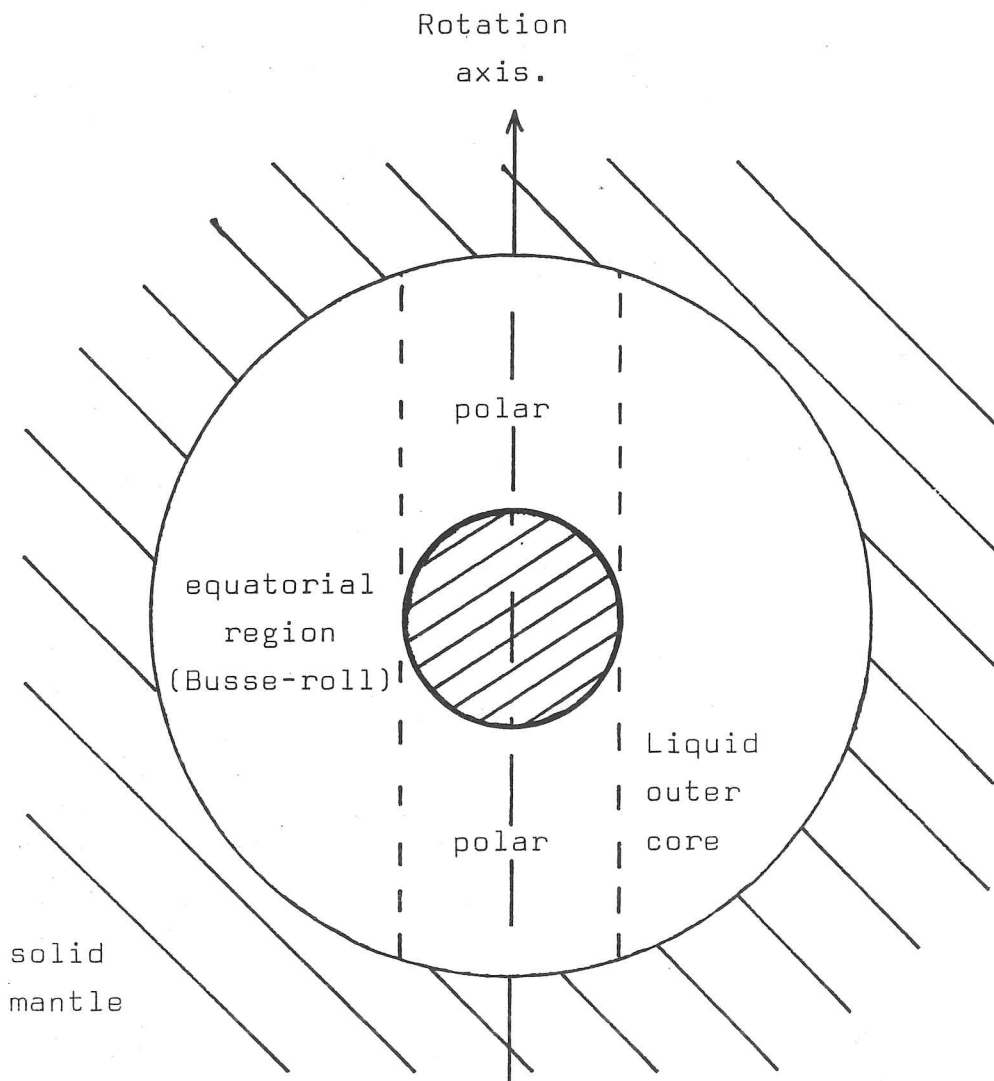


Fig. 2.4

Schematic diagram of the division of the Earth's core into two distinct regions of convection, polar, in which the boundary inclination is small and equatorial, in which it dominates.

The interaction of rotation and magnetic fields to give relatively low critical Rayleigh number solutions when Coriolis and Lorentz forces are of similar magnitude has been studied in such works as Eltayeb (1972, 1975) and Fearn (1979). Eltayeb (1972) describes the boundary layer structure in his plane-layer study, noting that a magnetic field reduces the strength of the Ekman suction that is a major part of the rotational constraint on convection. The various boundary layers (Ekman, Hartmann and mixed) are discussed in more detail by Tough & Roberts (1968). Soward (1979 and 1980) extends the plane layer investigation, for vertical (1979) and horizontal (1980) magnetic fields, in particular noting that overstable solutions occur only for $q > 1$ ($q = \kappa/\eta$). Fearn (1979) considers a spherical shell geometry with a fluid that is a weak conductor of electricity, so that $q = \kappa/\eta$ is small, where κ is the thermal and η the magnetic diffusivity, and with a strong toroidal field ($Q = \frac{B_0^2}{2\Omega\mu\rho\eta} = O(1)$). He finds that the critical Rayleigh number is a minimum for $Q = O(1)$ and is associated with a slowly drifting wave of azimuthal wavenumber $m = 1$, an oscillatory solution.

Wave solutions to the Boussinesq equations of motion in a stratified, rotating perfectly conducting fluid are discussed by Hide (1969) in the simplest geometry, namely small amplitude plane waves in a fluid of infinite extent in which both the Brunt-Vaisala frequency ($N \equiv (\frac{g}{\rho} \cdot \frac{\partial \rho}{\partial z})^{\frac{1}{2}}$) and the Alfvén velocity ($V \equiv B_0 / (\mu\rho)^{\frac{1}{2}}$) are uniform, and there is no dissipation. This indicates that the effect of stratification is negligible on the oscillations if $N \ll 2\Omega$. In the absence of stratification, hydromagnetic waves can be described in a spherical shell using the plane geometry (Hide, 1966), resulting in two classes of wave modes: "inertial", which are of high frequency, and

"magnetic", of lower frequency. The latter are put forward by Hide (1966) as a possible cause of the secular variation, whose time scale is hundreds of years. A review of this work and of more recent developments is given by Eltayeb (1981a), who then concentrates on the role of diffusion in modifying the waves in a spherical geometry. The combination of diffusion and of spherical boundaries leads to very different solutions in certain parameter regimes, just as Busse-rolls reflect their influence in the non-magnetic case. In the weak field case ($Q \leq 0(\sigma^{2/3}.E^{1/3})$, where $Q \equiv B_0^2/2\Omega\mu\rho\eta$, the modified Chandrasekhar number in Eltayeb's notation), solutions are of Busse-roll form, an inertial wave in a thin cylindrical cell, propagating eastwards because of the constraint of the inclination of the boundary. Three-dimensional motions are the critical mode of convection in the strong field case. These 'waves' are oscillatory solutions of a convection problem, in which there is a driving buoyancy force. They therefore refer to an unstable stratification and so are very different to the waves considered by Hide (1969). The latter may be of interest as a response to forcing by convection originating elsewhere, in which case the problem would resemble that considered by Townsend (1966) in the context of gravity waves excited in the atmosphere by the impact of thermals. Townsend considered dissipation of the waves only as a means of estimating the extent of their propagation from the source, his object being to put forward an explanation for 'clear air turbulence'.

In a separate paper to that described above, Eltayeb (1981b) considers the effect of a stably stratified outer region on convection in a spherical shell, prompted by the stable region suggested by Higgins & Kennedy (1971). His results show that in

the weak field case ($Q \ll 0$ ($\sigma^{2/3} E^{1/3}$)), the Busse-roll form of solutions persists. The analysis is performed in the limit of small σ , using an expansion scheme in powers of σ , which results in the solutions being wave motions that are diffusionless and independent of the stratification. He anticipates that for $\sigma \gg 0(1)$ the solutions would be of decaying amplitude in the stably stratified part of the spherical shell, but no such calculations are described. In the strong field case, preliminary results are that instability occurs in the whole volume of the spherical shell: detailed calculations are not given by Eltayeb (1981b). These studies are very different from the qualitative model put forward by Yukutake (1981), in which a two layer outer core is invoked to explain the westward drift (in similar analysis to that of Bullard et al., 1950) and a stable stratification in the outer region is supposed to lead to 'spherical' motions rather than 'cylindrical'.

The role of rotation and of magnetic fields in convection also includes double diffusive effects analogous to those discussed previously. Busse (1975) describes the effect of the magnetic field on the nonlinear stability of a plane layer convection problem. In the case of large q ($q = \kappa/\eta$), oscillations can occur, with amplification of magnetic energy and distortion of the originally uniform and vertical magnetic field so as to allow finite amplitude convection at subcritical Rayleigh numbers. However, in the Earth's core q is expected to be small ($q \approx 10^{-6}$ per Eltayeb, 1981b) and so such a subcritical instability should not occur. A triply diffusive regime has also been investigated (Acheson, 1980), but is outside the scope of this work.

The full equations describing a fluid, expressing conservation of mass, momentum and energy, are unwieldy in that they include effects such as compressibility that are often observed to be of little influence on the large scale flows found in geophysics. In order to simplify mathematical analysis, a set of approximations known collectively as the "Boussinesq approximation" is frequently applied to the equations in convection problems, to reduce them to the following form:

$$\nabla \cdot \underline{v} = 0$$

$$\rho_0 \cdot \frac{D\underline{v}}{Dt} = - \nabla p + \mu \nabla^2 \underline{v} + \rho(\theta) \cdot \underline{g}$$

$$\rho_0 c_v \frac{D\theta}{Dt} = - \kappa \nabla^2 \theta$$

where the parameters μ, c_v, k are constants, \underline{v} is the velocity, ρ_0 a reference density, $\rho(\theta)$ the density at temperature θ and p the pressure.

In this section, the nature of the Boussinesq approximation is reviewed, relying heavily on the unpublished notes of Malkus (1964) and on the earlier work of Spiegel and Veronis (1960) and Mihaljan (1962). Malkus notes that the traditional rationale for the approximation is based on the following four assertions, plausible for a fluid in which density contrasts are small and velocities slow compared to that of sound:

- (a) the fluid behaves as though the density is constant (ρ_0) except for the buoyancy force,
- (b) the fluid behaves as though incompressible,
- (c) the fluid parameters μ, c_v, k are constant, and

(d) mechanical dissipation is negligible in the energy equation.

The approach followed by Malkus in quantifying the requirements needed to justify the Boussinesq approximation is to consider the effect on the equations of small departures from an ideal "Boussinesq" fluid, in terms of two parameters that are to be small:

$$\eta = d / \left(\frac{c_p \theta_o}{g} \right)$$

$$\epsilon = \left| \frac{\Delta \theta^1}{\theta_o} \right|$$

where θ_o is a reference temperature of the system, d the depth and $\Delta \theta^1$ the maximum potential temperature contrast. Thus $(\eta + \epsilon)$ represents the overall scaled temperature contrast in the system, η being due to depth and ϵ to contrasts of potential temperature. A reference state based on the adiabatic temperature profile through θ_o and $z = 0$ and on a hydrostatic pressure field is adopted and perturbations about this state considered in terms of new variables scaled as follows:

$$z^1 = z/d$$

$$\rho^1 = \rho / \epsilon \rho_o$$

$$v^1 = v / v_o$$

$$\mu^1 = \mu(\theta) / \mu(\theta_o)$$

$$\theta^1 = \theta / \epsilon \theta_o$$

$$p^1 = p / \rho_o v_o^2$$

$$t^1 = t / (d/v_o)$$

$$k^1 = k(\theta) / k(\theta_o)$$

where θ and p are perturbations from the reference state and v_o is a characteristic velocity for the system, based on the speed of sound, c , and the expansion parameters:

$$v_o = (\epsilon \eta)^{1/2} c$$

The characteristic time scale, $\tau = d/v_0$ is thus

$$\tau = \left(\frac{d}{\epsilon g} \right)^{\frac{1}{2}}$$

which Malkus compares with "free-fall" under buoyancy forces in the system. It is thus the shortest time-scale for either convective motions if the temperature differences are destabilising or gravity waves if stabilising. Thus acoustic phenomena are excluded by the scaling and cannot be represented accurately in the Boussinesq approximation.

This time scale is dependent on the Rayleigh number, through

$$\tau = O(R^{-\frac{1}{2}})$$

In a rapidly rotating system, following Chandrasekhar (1961), one typically finds

$$\begin{aligned} R_c &= O(T^{2/3}) \\ &= O(\Omega^{4/3}) \\ \therefore \tau &= O(\Omega^{-2/3}) \end{aligned}$$

Thus there are likely to be problems in using the Boussinesq approximation in a rapidly rotating system, in which the rotation time scale Ω^{-1} is much shorter than the natural convective time scale. In particular, inertial waves are in general on too short a time-scale to be resolved by the Boussinesq approximation under this scaling. However, one may anticipate that τ is still sufficiently short to be an appropriate time-scale for convective motions.

If one considers the non-rotating case, Malkus uses the ideal gas equation of state to write the full equations in terms

of the expansion parameters ϵ, η and the non-dimensional state parameters R, σ, s , where

$$\begin{aligned} \text{Rayleigh number} & R \equiv \frac{gd^3 \Delta\theta}{\kappa v \theta^0} \\ \text{Prandtl number} & \sigma \equiv v/\kappa \\ \text{and} & s \equiv R/c_p \end{aligned}$$

(his equations 2.22-24)

and shows that the Boussinesq equations are the zero order terms of the expansion of the equations in the parameters ϵ, η . Thus the magnitudes of ϵ and η are measures of the departure of a real system from that represented by the Boussinesq approximation.

Rotation of the system introduces two sources of pressure fields beyond the hydrostatic field due to gravity. The resulting pressure differences represent additional terms to be included in η , the measure of the pressure depth of the system. In the atmosphere, the Coriolis acceleration leads to pressure drops in cyclonic depressions of order 0.05 bar, which is small but not negligible. In the core, the greater ~~rigidity~~ ^{bulk modulus} k_s of the fluid ensures that Coriolis accelerations are negligible in terms of density changes, as is now shown:-

$$\text{Pressure differences} \approx \Omega U L \rho$$

$$\text{where rotation rate } \Omega \approx 10^{-4} \text{ rad. s}^{-1}$$

$$\text{fluid speed scale } U \ll V_p \quad (\text{compressional wave speed})$$

$$\text{and } V_p \approx 10^4 \text{ ms}^{-1} \quad (\text{Jacobs, 1975})$$

$$L \lesssim 10^6 \text{ m}$$

$$\rho \approx 10^4 \text{ kg.m}^{-3}$$

$$\therefore \text{Coriolis pressure differences} \ll 10^{10} \text{ Pa}$$

But $\kappa_s \approx 6 \times 10^{11}$ Pa (Jacobs, 1975)

∴ density changes due to Coriolis accelerations,

$$\Delta\rho_{\text{COR}} \ll 10^{-2}\rho_0$$

and so are negligible for any plausible (i.e. subsonic) convection velocity in the core.

The centrifugal acceleration can be regarded as part of the effective local gravity field and, since the core-mantle boundary will be, to first approximation, an equipotential surface for this effective gravity field, any effect of centrifugal acceleration can be considered as included in the radial density profile of the outer core. Taking density values from Jacobs (1975), it is apparent that depth scales of order 100 km or less involve only small density changes (and so small values of η).

<u>depth from c.m.b.</u>	<u>density (10^3 kg.m⁻³)</u>
<u>(km)</u>	
0	9.90
85	10.04
485	10.62
2270 (i.c.b.)	12.11

Thus for the purpose of considering motions effectively confined to the outermost 100 km or less of the core, the Boussinesq approximation should involve error terms due to η of order

$$\eta = \cdot 0 (10^{-2})$$

which can reasonably be taken as negligible. The suggested stratified region due to compositional effects is within this depth scale.

The other scale parameter ϵ depends on the differences in density relative to the adiabatic equilibrium density profile. In an unstable region, they are limited by the rapid transport by convection occurring when the Rayleigh number markedly exceeds its critical value. This is readily shown to require only negligible superadiabatic temperature (or density) differences (Gubbins et al. 1979 derived a superadiabatic gradient $\frac{\partial\theta}{\partial z} \approx (10^{-11} \text{ K km}^{-1})$ from the work on convection of Busse (1970), revealing a maximum superadiabatic temperature difference $\Delta\theta = 0 (10^{-8} \text{ K})$ across the outer core). Thus ϵ is negligible in a convecting region of outer core size. However, in a stably stratified region there is no equivalent mechanism to limit ϵ and so we need an estimate of the potential sub-adiabatic temperature gradient (or of the stabilising compositional density gradient). Thermal gradients, even immediately adjacent to the core mantle boundary, cannot plausibly be more sub-adiabatic than to be isothermal, and so thermal density differences in ϵ must be negligible in the same way that the adiabatic density depth η is negligible in the outermost 100 km or less. Compositional gradients are not so constrained, and so we require the estimate of them made in § 2.3 above. This suggested a maximum density perturbation of $\rho/\rho_0 \approx 0.06$ which is still small even if not fully negligible. Accordingly, the Boussinesq approximation should be accurate to within terms of order η, ϵ where

$$\eta \approx 0.01$$

$$\epsilon \lesssim 0.06$$

for the outermost 100 km or so of the core, which is acceptable. For motions extending throughout the outer core however, one has

$$\eta \approx 0.22 \text{ (from the measured densities, above)}$$

and so the error involved in the Boussinesq approximation is correspondingly increased.

For the purposes of the analyses of penetrative convection given in chapters 4 and 5, the Boussinesq approximation is assumed, as being appropriate to the outermost part of the core.

2.6 Equations of Motion

The equations of motion for a fluid in a rotating frame of reference are given in many textbooks (e.g. Chandrasekhar 1961). We have:

Continuity

$$\frac{\partial \rho}{\partial t} + \nabla \cdot (\rho \underline{u}) = 0 \quad (2.1a)$$

Momentum

$$\frac{\partial}{\partial t} (\rho \underline{u}) + (\underline{u} \cdot \nabla) \rho \underline{u} = \underline{X} - \nabla p + \frac{\rho}{2} \nabla (\underline{\Omega} \wedge \underline{r})^2 + \mu \nabla^2 \underline{u} + 2\rho (\underline{u} \wedge \underline{\Omega}) \quad (2.1b)$$

where \underline{X} are external forces, such as gravity, which are assumed to be conservative.

Heat transport

$$\frac{\partial}{\partial t} (\rho C_v \theta) + (\underline{u} \cdot \nabla) \rho C_v \theta = \nabla \cdot (\kappa \nabla \theta) - p \nabla \cdot \underline{u} + \Phi \quad (2.1c)$$

where Φ is internal heating, such as viscous dissipation,

and θ the temperature.

The analysis will be based on linear theory, in which quadratic terms in \underline{u} can be neglected. Clearly this is suitable only for either the onset of motion or else motions of small amplitude.

If we assume the Boussinesq approximation as discussed above in § 2.5 we can take all of the material properties of the fluid to be constant throughout its body, except in so far as density changes introduce buoyancy forces. Thus the above equations, in the linear Boussinesq approximation become:

$$\nabla \cdot \underline{u} = 0 \quad (2.2a)$$

$$\begin{aligned} \frac{\partial \underline{u}}{\partial t} = & \frac{\underline{X}}{\rho} - \frac{\nabla p}{\rho} + \frac{\nabla}{2} (\underline{\Omega} \wedge \underline{r})^2 + \nu \nabla^2 \underline{u} \\ & + 2(\underline{u} \wedge \underline{\Omega}) \end{aligned} \quad (2.2b)$$

$$\frac{\partial \theta}{\partial t} + \underline{u} \cdot \nabla \theta = \kappa \nabla^2 \theta + \frac{\Phi}{\rho c_v} \quad (2.2c)$$

Let us operate on (2.2b) with curl, and then again with curl

$$(\text{curl } \underline{a} \equiv \nabla \wedge \underline{a} \equiv \epsilon_{ijk} \frac{\partial}{\partial x_j} a_k) \quad \text{to give}$$

$$\frac{\partial \underline{\zeta}}{\partial t} = \frac{\nabla \rho^1 \wedge \underline{g}}{\rho_0} + \nu \nabla^2 \underline{\zeta} + 2(\underline{\Omega} \cdot \nabla) \underline{u} \quad (2.3)$$

$$\text{and } \frac{\partial}{\partial t} (\nabla^2 \underline{u}) = \frac{1}{\rho_0} (\underline{g} \nabla^2 \rho^1 - (\underline{g} \cdot \nabla) \nabla \rho^1) + \nu \nabla^4 \underline{u} - 2(\underline{\Omega} \cdot \nabla) \underline{\zeta} \quad (2.4)$$

where $\underline{\zeta} \equiv \nabla \wedge \underline{u}$ is the vorticity and ρ^1 is the density perturbation from the reference density ρ_0 . In the Boussinesq approximation and assuming we are dealing with thermal buoyancy,

and θ the temperature.

The analysis will be based on linear theory, in which quadratic terms in \underline{u} can be neglected. Clearly this is suitable only for either the onset of motion or else motions of small amplitude.

If we assume the Boussinesq approximation as discussed above in § 2.5 we can take all of the material properties of the fluid to be constant throughout its body, except in so far as density changes introduce buoyancy forces. Thus the above equations, in the linear Boussinesq approximation become:

$$\nabla \cdot \underline{u} = 0 \quad (2.2a)$$

$$\begin{aligned} \frac{\partial \underline{u}}{\partial t} = & \frac{\underline{X}}{\rho} - \frac{\nabla p}{\rho} + \frac{\nabla}{2} (\underline{\Omega} \wedge \underline{r})^2 + \nu \nabla^2 \underline{u} \\ & + 2(\underline{u} \wedge \underline{\Omega}) \end{aligned} \quad (2.2b)$$

$$\frac{\partial \theta}{\partial t} + \underline{u} \cdot \nabla \theta = \kappa \nabla^2 \theta + \frac{\Phi}{\rho c_v} \quad (2.2c)$$

Let us operate on (2.2b) with curl, and then again with curl

$$(\text{curl } \underline{a} \equiv \nabla \wedge \underline{a} \equiv \epsilon_{ijk} \frac{\partial}{\partial x_j} a_k) \quad \text{to give}$$

$$\frac{\partial \underline{\zeta}}{\partial t} = \frac{\nabla \rho^1 \wedge \underline{g}}{\rho_0} + \nu \nabla^2 \underline{\zeta} + 2(\underline{\Omega} \cdot \nabla) \underline{u} \quad (2.3)$$

$$\text{and } \frac{\partial}{\partial t} (\nabla^2 \underline{u}) = \frac{1}{\rho_0} (\underline{g} \nabla^2 \rho^1 - (\underline{g} \cdot \nabla) \nabla \rho^1) + \nu \nabla^4 \underline{u} - 2(\underline{\Omega} \cdot \nabla) \underline{\zeta} \quad (2.4)$$

where $\underline{\zeta} \equiv \nabla \wedge \underline{u}$ is the vorticity and ρ^1 is the density perturbation from the reference density ρ_0 . In the Boussinesq approximation and assuming we are dealing with thermal buoyancy,

we can write

$$\rho' = -\alpha\rho_0\theta$$

where θ is the potential temperature perturbation.

Thus we have three dimensional equations

$$\text{vorticity: } \frac{\partial \zeta}{\partial t} = -\alpha(\nabla\theta \wedge \underline{g}) + \nu\nabla^2\zeta + 2(\underline{\Omega} \cdot \nabla)\underline{u} \quad (2.5a)$$

$$\text{velocity: } \frac{\partial}{\partial t} (\nabla^2 \underline{u}) = -\alpha(g\nabla^2\theta - (\underline{g} \cdot \nabla)\nabla\theta) + \nu\nabla^4 \underline{u} \quad (2.5b)$$

$$\text{temperature: } \frac{\partial \theta}{\partial t} = -\underline{u} \cdot \nabla\theta + \kappa\nabla^2\theta \quad (2.5c)$$

where ζ , \underline{u} and θ are our small perturbations in vorticity, velocity and temperature, and $\nabla\theta$ may be a function of position. In the case of penetrative convection, $\nabla\theta$ reverses sign within the region being studied.

Time dependence

Since the equations (2.5) are valid only in the linear case, when the perturbations are sufficiently small for non-linear terms to be neglected, they can only be used for 2 cases. Firstly one can consider the case of marginal stability when the growth-rate of any convection mode is zero (although it may have a frequency and therefore a time-dependence if the onset is "overstable" rather than "stationary" convection, in the nomenclature of Chandrasekhar (1961)). Secondly one may use the equations to derive the initial growth-rate of a mode: this may be a guide to which mode is likely to dominate the subsequent finite amplitude motion, at least in the short term. The use of the linear equations gives only a sufficient condition for instability. In order to find a necessary condition and thereby to

allow for finite amplitude instabilities, one can use energy arguments such as those of Joseph & Shir (1966a, 1966b). This is not pursued in this work.

Boundary Conditions

The traditional boundary condition to be placed on the equations for the onset of convection are based on the bounding surface being either rigid or stress-free, perfectly conducting or constant heat flux. For a rigid boundary, one has:

$$u_n = 0$$

$$\frac{\partial u_n}{\partial n} = 0$$

$$\zeta_n = 0$$

where n indicates the component normal to the boundary

For a stress-free boundary,

$$u_n = 0$$

$$\frac{\partial^2 u_n}{\partial n^2} = 0$$

$$\frac{\partial \zeta_n}{\partial n} = 0$$

The thermal boundary condition is either

$$\vartheta = 0 \quad (\text{perfectly conducting})$$

$$\text{or } \frac{\partial \vartheta}{\partial n} = 0 \quad (\text{constant heat flux})$$

$$\text{or } \lambda \vartheta + \frac{\partial \vartheta}{\partial n} = 0 \quad (\text{imperfectly conducting, } \lambda = \text{Biot number})$$

For the derivation of these, see Chandrasekhar (1961) pp. 21-22, and Hurle et al. (1967) for the imperfectly conducting case.

Separation of Variables

The linear equations (2.5) and the boundary conditions may be separated simply between the independent variables for certain geometries. In particular, a layer of fluid confined between infinite horizontal boundaries, rotating about a vertical axis and in which the set temperature gradient $\nabla\theta$ is vertical and solely a function of vertical position z can be separated: the traditional Rayleigh-Benard problem is the particular case of $\nabla\theta = \text{constant}$. In this geometry we may try a solution of the form

$$\underline{u} = \underline{u}_0(z) \cdot \exp(pt + i(k_1 x_1 + k_2 x_2)) \quad (2.6)$$

where x_1, x_2 are the horizontal co-ordinates; and so get the following equations for $(\zeta)_z$, (\underline{u}) , and ϑ

$$p\zeta_z = \nu(D^2 - a^2)\zeta_z + 2\Omega(Du_z) \quad (2.7a)$$

$$p(D^2 - a^2)u_z = -\alpha g a^2 \vartheta + \nu(D^2 - a^2)^2 u_z - 2\Omega(D\zeta_z) \quad (2.7b)$$

$$p\vartheta = -u_z D\theta + \kappa(D^2 - a^2)\vartheta \quad (2.7c)$$

where $D \equiv \frac{d}{dz}$, $a^2 = k_1^2 + k_2^2$ and $\underline{g} = -g \hat{z}$

$$\text{i.e. } \left[D^2 - a^2 - p/\nu \right] \zeta_z = -\frac{(2\Omega)}{\nu} Du_z \quad (2.8a)$$

$$\left[(D^2 - a^2)(D^2 - a^2 - p/\nu) \right] u_z = + \frac{(2\Omega)D\zeta_z}{\nu} + \frac{\alpha g a^2}{\nu} \vartheta \quad (2.8b)$$

$$\left[D^2 - a^2 - p/\kappa \right] \vartheta = \left(\frac{D\theta}{\kappa} \right) u_z \quad (2.8c)$$

This is only a valid solution if it satisfies the horizontal boundary condition: an arbitrary horizontal wave number (a) is allowable only in the limit of infinite horizontal extent. In a bounded fluid, there will be a discrete spectrum for a even if those horizontal boundaries are idealised as stress-free and perfectly conducting. Less ideal horizontal boundaries destroy the periodicity and so the separation of variables (e.g. Buell & Catton, 1983).

Definition of a Rayleigh number

In the Rayleigh-Benard problem, there is a natural length-scale given by the depth of the layer and a natural temperature scale given by the overall temperature difference. However, once we allow $\nabla\theta$ to be a function of position z , that is no longer necessarily the most appropriate scaling. For example it becomes quite possible to have a problem in which the overall temperature difference is zero and yet there is a region sufficiently unstable to allow convection to occur. This is a very similar problem of definition to that found by workers on convection in fluids of variable viscosity: no one definition of the Rayleigh number is adequate as a universal description of a system's stability to convection.

I propose to use the depth d of the region in which the temperature gradient $\nabla\theta$ is destabilising as the characteristic length scale of the problem, as suggested by Whitehead & Chen (1970). The maximum unstable temperature gradient will be used to define the temperature scale, following Roberts (1982). We

can write equations (2.8) in non-dimensional form on the following scaling:

length	d
temperature	$\beta_0 d$
time	d^2/ν
where	$\nabla \theta = -\beta_0 f(\underline{z})$
	and $f(\underline{z}) \leq 1$

Thus, indicating non-dimensional terms by primes,

$$\left[D'^2 - a'^2 - p' \right] \zeta'_z = - \left(\frac{2\Omega d^2}{\nu} \right) D' u'_z \quad (2.9a)$$

$$\left[(D'^2 - a'^2)(D'^2 - a'^2 - p') \right] u'_z = + \left(\frac{2\Omega d^2}{\nu} \right) D' \zeta'_z + \left(\frac{\alpha g d^4 \beta_0}{\nu} \right) a'^2 \vartheta' \quad (2.9b)$$

$$\left[D'^2 - a'^2 - p' \sigma \right] \vartheta' = -\sigma f(z') u'_z \quad (2.9c)$$

where $\sigma \equiv \nu/k$ is the Prandtl number.

Now let us rescale the variables, following Chandrasekhar (1961), by introducing

$$F \equiv \left(\frac{\alpha g d^4 \beta_0 a'^2}{\nu} \right) \vartheta' \quad (2.10a)$$

$$Z \equiv \left(\frac{2\Omega d^2}{\nu} \right) \zeta'_z \quad (2.10b)$$

$$U \equiv u'_z$$

and writing $T \equiv \frac{4\Omega^2 d^4}{\nu^2}$ Taylor number

$R \equiv \frac{\alpha g d^4 \beta_0}{\kappa \nu}$ Rayleigh number

Dropping primes from now on on the non dimensional equations, we have:

$$\left[D^2 - a^2 - p \right] Z = - T, DU \quad (2.11a)$$

$$\left[(D^2 - a^2)(D^2 - a^2 - p) \right] U = + DZ + F \quad (2.11b)$$

$$\left[D^2 - a^2 - \sigma p \right] F = -Ra^2 f(z) U \quad (2.11c)$$

The only difference from the equations for Rayleigh-Benard convection is the presence of the function $f(z)$ which can be regarded as the shape of the set temperature profile. In the case $f(z) = 1$ both the equations and the definitions for R and T reduce to those standard for the Rayleigh-Benard problem.

Effect of rotation on penetrative convection

A qualitative view of the effect of rapid rotation on any fluid motion is traditionally sought by applying the concepts of the Taylor-Proudman column, of Ekman boundary layers and of geostrophic balance. In addition high frequency motions will involve inertial wave modes. Such concepts are explored thoroughly by Greenspan (1968).

The Taylor-Proudman theorem relates to an inviscid fluid in slow steady motion. This is also the state that yields the geostrophic balance. Starting with equation (2.1a),

$$\left(\underline{u} \cdot \nabla \right) \underline{u} + \frac{\partial \underline{u}}{\partial t} = \frac{\underline{X}}{\rho} - \frac{\nabla p}{\rho} + \frac{\nabla}{2} \left(\underline{\Omega} \cdot \underline{r} \right)^2 + \nu \nabla^2 \underline{u} + 2 \left(\underline{u} \wedge \underline{\Omega} \right)$$

and supposing we are dealing with motions of characteristic velocity V , length-scale L and time-scale τ , then if

- a) viscous effects are small, i.e. if the Ekman number
 $E \equiv \nu/\Omega L^2$ is small,
- b) inertial effects are small, i.e. if the Rossby number
 $\epsilon \equiv V/\Omega L$ is small
- c) the time-scale is long, $\tau \Omega$ large,
- then

$$0 = \frac{\underline{x}}{\rho} - \nabla p / \rho + \nabla / 2 \left(\underline{\Omega} \wedge \underline{r} \right)^2 + 2 \left(\underline{u} \wedge \underline{\Omega} \right) \quad (2.12)$$

Taking curl of this, assuming incompressibility

$$0 = \frac{1}{\rho} \left(\nabla \rho \wedge \nabla p \right) + 2 \left(\underline{\Omega} \cdot \nabla \right) \underline{u} \quad (2.13)$$

In the absence of any baroclinic term $\left(\nabla \rho \wedge \nabla p \right)$ this reduces to

$$0 = \left(\underline{\Omega} \cdot \nabla \right) \underline{u} \quad (2.14)$$

which is the Taylor-Proudman theorem, that \underline{u} does not vary along the axis of rotation under these conditions. Clearly this can lead to problems in fitting boundary conditions, and so one has to consider the effect of thin Ekman boundary layers in which the local length scale is sufficiently short for viscosity to destroy the applicability of the Taylor-Proudman theorem. Not only will such short length-scales avoid the constraint of the Taylor-Proudman theorem, they also introduce a region of very high viscous dissipation which may turn out to be the dominant form of dissipation when one considers the onset of convection in a rotating body. This will be seen more clearly in a later section (§ 4.5), dealing with the onset of convection in a cylindrical annulus and the formation of "Busse-rolls" (Busse 1970).

If one applies the qualitative view of the usual effects of rotation to the onset of convection, then as the Taylor number increases one might expect:

- a) the vertical form of u_z to become more uniform, except for thin boundary layers,
- b) the horizontal planform to be of smaller scale, to match more closely the scale thickness of the boundary layers,
- c) as a result of (b), the critical Rayleigh number should increase.

This appears to work well for convection in a rotating Rayleigh-Benard problem, with a uniform temperature gradient and so a uniform baroclinic term (equation 2.18). The horizontal scale diminishes sufficiently for the baroclinic term and viscosity to match the rotational constraint. Figure 2.5 shows U as a function of position z for various rotation rates (results derived from the shooting program described in § 5): as T becomes large, U tends to a sine-wave with the influence of the rigid boundaries at $z = 0, z = 1$ being removed by thin boundary layers.

Extending this reasoning to penetrative convection, one might expect rapid rotation to result in more uniform vertical velocity and therefore in greater penetration of the stable region. This prediction is tested and disproved in chapters 4 and 5.

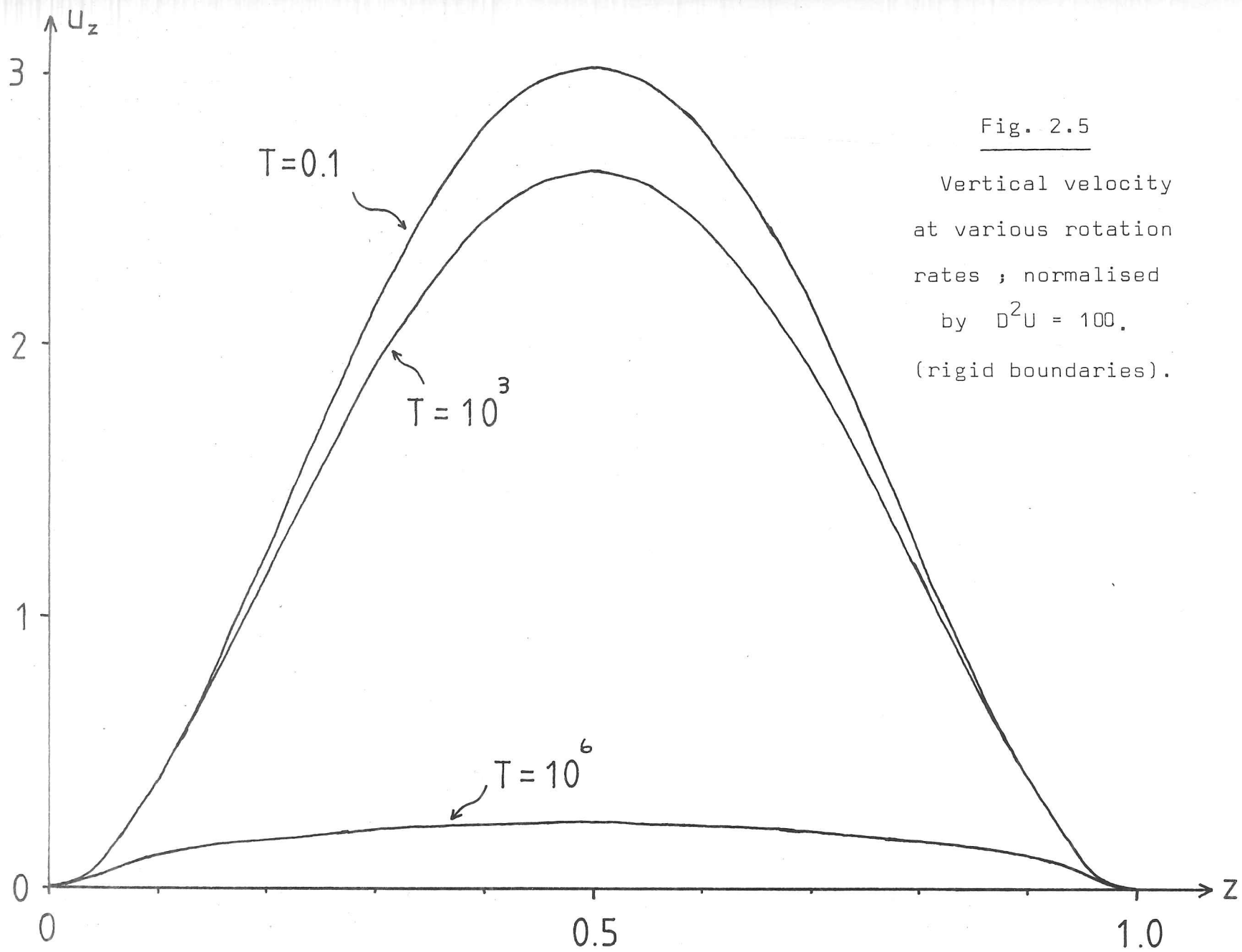


Fig. 2.5

Vertical velocity
at various rotation
rates ; normalised
by $D^2U = 100$.
(rigid boundaries).

3. Heat flux from the core

3.1. Introduction

The maintenance of the Earth's magnetic field by some dynamo mechanism in the core requires the dissipation of energy and an associated heat flux out of the core. That heat flux may serve as a constraint on dynamo models. For each given type of energy source, a lower bound can be placed on the heat flux by considering the entropy requirements of a dynamo (Backus 1975, Hewitt et al 1975). Such calculations show that a source of gravitational energy arising from the release of a light component during the freezing of the inner core would be markedly more efficient than a thermal source such as radiogenic heating or an overall cooling of the core (Gubbins 1977, Loper 1978a). In the case of a thermal source, the lower bound on the heat flux from the core is a substantial fraction of the observed heat flux from the Earth's surface. A model of the cooling Earth will now be used to investigate what values are possible for the heat flux from core to mantle, given the constraints imposed by our knowledge of the present size of the inner core, of the heat flux from mantle to the surface and of the existence of a magnetic field. The resulting heat flux can then be compared with the estimate of the conductive heat flux arising from the adiabatic gradient in the outer core, so as to decide whether a thermally stratified layer is possible at the top of the outer core.

Previous studies of the cooling of the core have incorporated simplifying assumptions as to the appropriate thermal boundary condition at the core-mantle interface. Loper (1978a) adopted a constant heat flux condition whereas Gubbins et al (1979) adopted one of constant rate of cooling. Subsequently the

effect on the core of a constant temperature boundary has been considered (Gubbins et al 1982). The last condition was intended to correspond to an extreme case of temperature dependent viscosity controlling mantle convection. In this work, a model of the heat flow through the mantle is used to give a more realistic thermal boundary condition for the core.

Parameterised convection theory has been applied in several thermal history studies to calculate the heat flux through the mantle (e.g. McKenzie & Weiss 1975, Sharpe & Peltier 1979, Schubert et al 1980, Davies 1980, Spohn & Schubert 1982, Stevenson et al. 1983). These studies include a variation of mantle viscosity with temperature following the argument that this temperature dependence makes mantle convection self regulating (Tozer 1972). However doubt has been cast on the applicability of the parameterised convection theory to the case of variable viscosity: it seems that such a parameterised model will overstate the effect of the variation on the heat flux (McKenzie & Weiss 1980). The present work therefore follows the suggestion of McKenzie & Weiss that a model based on a constant viscosity parameterisation is more suitable for studies of heat flux than is one purporting to incorporate variable viscosity. They warn that such a constant viscosity model will show average temperatures that respond too slowly to changes in boundary conditions: in this respect one must apply caution in interpreting the results from the model. The application of the parameterised convection theory in this problem assumes that the convection in each spherical shell can be regarded as effectively homogeneous in a statistical sense, with the instabilities in the boundary layers occurring sufficiently frequently and evenly both spatially and over time that they have no marked individual

effect on the heat flux. In particular, it supposes that surface plate tectonics can be regarded as a manifestation of the boundary layer activity at the top of the upper mantle, as opposed to being a largely independent phenomenon which, through the large thermal and mechanical anomalies associated with subduction regions, can control the upper mantle circulation in certain areas. If such control of the convection is in fact significant, then the effective surface boundary condition to the Earth's mantle may well have changed during geologic history as the configuration of the surface plates has changed. No attempt has been made in this study to allow for such variations in surface conditions.

The core of the Earth is known from seismic observations to have a solid inner region and this is assumed to be growing by the freezing of the liquid outer core (e.g. Jacobs 1975). Accordingly the model includes the latent heat arising from the cooling and freezing of the core. This term may be made to include all the sources of energy arising at the freezing surface; not only the latent heat of solidification, which includes a term for the decrease in volume on solidification (Hage & Muller 1979), but also the gravitational energy and chemical energy arising from a difference in composition between the solid and liquid phases. Such a difference is indicated by the observed densities (Masters 1979).

3.2. The Model

The model used is based on four concentric spherical layers, corresponding to the core, lower mantle, upper mantle and surface. These are numbered 1 to 4 respectively. It is assumed that the three inner layers convect independently, with the heat

fluxes through the boundary layers at their interfaces being the sole thermal connection. The outermost layer is assumed to be at constant temperature.

Two separate layers are used for the mantle on the grounds of the seismological (Richter 1979) and geochemical (O'Nions et al 1979) evidence. This tends to delay the loss of heat from the core (McKenzie & Richter 1981). The results of this present work cannot be taken as an argument in favour of two layers, as part of the numerical scheme involves a fitting of parameters to the imposed thermal constraints. A similar procedure can be followed for a single layer mantle model, and the results of doing this are reported in section 3.3.4. Arguments in favour of single layer "whole mantle" convection have been based primarily on the problem of matching the viscosity distribution in the mantle, known from glacial rebound (e.g. Peltier, 1983), to a temperature distribution that includes a thermal boundary layer at about 650 km depth (for a recent review of this problem, see Kenyon & Turcotte (1983)).

Parameterised convection theory is applied to the two mantle layers. The theory is based on the premise that the heat flux is controlled by the thermal boundary layers and is independent of the overall depth of the convecting layer (McKenzie & Weiss 1975). It is assumed however that the boundary layer at the surface of the core can be neglected, owing to the high thermal conductivity and low viscosity of the liquid metal core compared to the mantle. For a viscosity ν less than $1\text{m}^2\text{s}^{-1}$, one can expect the temperature drop across the core thermal boundary layer to be less than 10^{-2}K for heat fluxes of up to 10^{14}W , on the basis of equation (3.1). As a result, temperatures throughout the core are taken to be uniquely determined by the tem-

perature at the core-mantle boundary, with no dependence on the heat flux. The curvature of the boundary layers in the mantle is neglected on the grounds that they are thin relative to their radius (the parameterised convection theory and the values of parameters in Table 3.1 give a thickness of approximately 20 km), and so the spherical geometry is reflected only in the different surface area of each boundary layer. Thus the Earth has been reduced to a 1-dimensional model (Fig. 3.1).

Equation 3.1 is used to calculate the heat flux through each boundary layer. One has to consider the individual boundary layers as the flux per unit area will differ between top and bottom surfaces of each layer of the model, owing to internal radiogenic heating, to internal cooling and to the dependence of surface area on radius.

$$\text{Flux per unit area} = k \left(\frac{g\alpha}{\kappa\nu} \right)^{1/3} \cdot (D \cdot \Delta T)^{4/3} \quad (3.1)$$

where k = thermal conductivity

κ = thermal diffusivity

g = gravity

α = coefficient of thermal expansion

ν = kinematic viscosity

D = geometrical constant of order 1

ΔT = temperature drop across boundary layer

(based on McKenzie & Weiss 1975). A further factor β will be applied by an iterative procedure in order to fit the imposed thermal constraints (see equations 3.9a to 3.9c and section 3.3.1). Accordingly the geometrical constant D has been taken to be 1.0 at the start of the calculations. The value of the exponent of $(D \cdot \Delta T)$, $4/3$, is given by the parameterised convection theory, but has only approximately been confirmed by experiment (Kulacki & Emara, 1977). However, trial runs with the

Fig. 3.1

Model of heat flow in the Earth.

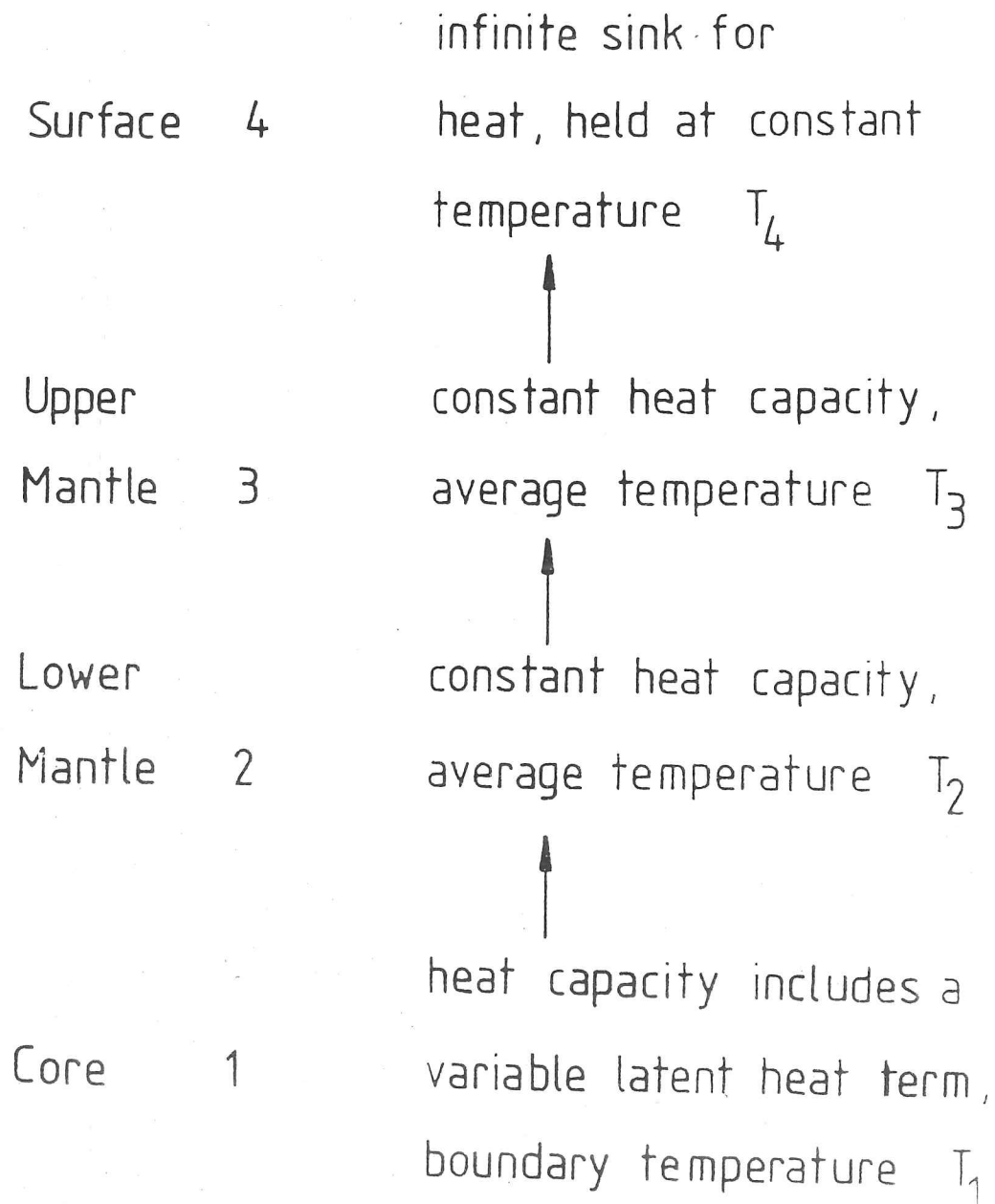


Table 3.1

Standard Parameters

Parameter	Value	Source
Masses:		
core	1.9×10^{24} kg	1
lower mantle	2.8×10^{24} kg	1
upper mantle	1.2×10^{24} kg	1
Specific heats:		
core	700 J kg ⁻¹ K ⁻¹	3
mantle	1200 J kg ⁻¹ K ⁻¹	2
Latent heat (core)	1.0×10^6 J kg ⁻¹	3
Radii:		
inner core	1215 km	1
outer core	3485 km	1
lower mantle	5700 km	1
upper mantle	6370 km	1
Radioactive decay constant (exponential basis)	4×10^9 years	3 (note 1)
Adiabatic lapses across layers		
lower mantle	700 K	2)
upper mantle	400 K	2) (note 2)
Core freezing range ($T_O - T_F$)	1000 K	Estimate (note 3)
Mantle:		
thermal conductivity	6-12 Wm ⁻¹ K ⁻¹	2
thermal diffusivity	$1-2 \times 10^{-6}$ m ² s ⁻¹	2
thermal expansion	$1-2 \times 10^{-5}$ K ⁻¹	2 (note 4)
kinematic viscosity	$1-10 \times 10^{17}$ m ² s ⁻¹	
gravity	10 ms ⁻²	
Geometric factor D	1	4

Sources

1. Jacobs 1975
2. Jeanloz & Richter 1979
3. Gubbins et al 1979
4. McKenzie & Richter 1981

Notes

1. with further calculations to derive an average
2. subject to scaling, therefore approximate
3. uncertain owing to the effects of alloying constituents
4. hence the standard value for the transmission factor $A_{-4/3} \bar{k} (g\alpha/kv)^{1/3} D^{4/3}$ has been taken as 4.10^{-5} Wm⁻² K^{-4/3}, but is subject to scaling by β .

exponent set to 5/4 or 3/2 showed that the model is not sensitive to its exact value, again owing to the applied constraints (section 3.3.5).

It is assumed that layers 1, 2 and 3 have specific heat capacities constant with temperature. Layer 1, the core, is also given a term for a latent heat capacity, λ , which will be a function of the radius of the inner core, and so of temperature.

$$\lambda = 4\pi\rho Lr^2 \cdot dr/dT_1 \quad (3.2)$$

where ρ is the density, L the specific latent heat, r the radius of the inner core and T_1 the temperature of the core-mantle boundary used to characterise the temperature throughout the core.

In order to derive d^2r/dT_1^2 , I make the following

assumptions:

$$\left. \frac{\partial T}{\partial p} \right)_m - \left. \frac{\partial T}{\partial p} \right)_s = b_1 \quad (3.3)$$

$$\frac{\partial p}{\partial r} = -b_2 r \quad (3.4)$$

$$\frac{\partial T}{\partial T_1} = T/T_1 = b_3 \quad (3.5)$$

where T is the temperature at the inner core boundary, m and s represent the melting and adiabatic profiles and b_1 , $b_2 (= \frac{4}{3} \pi G \rho^2)$ and b_3 are assumed to be constants. (3.4) and (3.5) amount to ignoring any radial variation in the density and temperature of the inner core, and are reasonable approximations because the gravitational field and the pressure gradient are relatively

small in the inner core.

$$\text{Hence } dr/dT_1 = - \frac{b_3}{b_1 b_2} \cdot \frac{1}{r} \quad (3.6)$$

$$\text{Integrating, } r^2/r_0^2 = (T_0 - T_1) / (T_0 - T_f) \quad (3.7)$$

where r_0 is the radius of the whole core and $(T_0 - T_f)$ is the hypothetical range of temperatures for the core to freeze from centre to surface.

$$\begin{aligned} \therefore \lambda &= - 4\pi\rho Lr \cdot \frac{b_3}{b_1 b_2} \\ &= - \frac{3 M L}{2(T_0 - T_f)} \cdot \left(\frac{T_0 - T}{T_0 - T_f} \right)^{\frac{1}{2}} \end{aligned} \quad (3.8)$$

where M is the mass of the entire core. In this expression $(T_0 - T_f)$ is a poorly known parameter of the model.

This expression for λ is equivalent to the latent heat term considered by Gubbins et al (1979) in their section 4.1 and equations (40) and (41) subject to the simplifying assumptions in (3.3), (3.4) and (3.5) above which allow the expression of λ in terms of gross properties of the layer. Furthermore, λ can obviously be interpreted as including terms for any other energy source similarly dependent on the freezing process. Thus, if one assumes further that the compositional density jump and the chemical energy per unit mass can be regarded as constants, then one can include the gravitational energy, chemical energy and adiabatic heating terms given by Gubbins et al in their sections 4.3, 4.4 and 4.6 by calculating:

$$L = L_0 + L_g + L_c + L_a$$

where L_0 is the latent heat,

$$L_g = \frac{\Delta\rho}{\rho} \cdot \left(\psi(r) - \bar{\psi} \right) \quad \text{is the gravitational energy,}$$

$$L_c = cQ_H \cdot \overline{\ln \left(\frac{T}{T(r)} \right)} \quad \text{is the chemical energy of rearrangement}$$

$$\text{and } L_a = \frac{G\alpha\Delta\rho}{M_{oc}\rho} \int_0^r 4\pi T(r') r'^2 \int_{r'}^{r_0} \frac{\rho(r'')}{r''^2} \left[\int_{r''}^{r_0} 8\pi\rho(r''') r'''^2 dr''' - M \right] dr'' \cdot dr'$$

is the adiabatic heating due to the rearrangement

(note that the last term differs from the expression evaluated by Gubbins et al. (1979) on their p. 81, due to an error in their term for \dot{p}), and ψ is the gravitational potential,

$\frac{\Delta\rho}{\rho}$ the fractional density jump on freezing due to composition,

Q_H the chemical heat of reaction, c the concentration of light material in the fluid, M_{oc} and M the masses of the outer core and entire core respectively,

G, α, ρ, T are conventional and \bar{X} indicates the average of X over the mass

of the outer core,

$$\bar{X} = \int_{oc} \rho X dV / M_{oc}$$

Radiogenic heating is an energy input to each of layers 1, 2 and 3, with the values given in Table 3.2. This heating decays exponentially with time, with a single decay constant designed to approximate the average of the principal radiogenic species in a chondritic composition over a time span of 4.5 Ga.

The equations derived by applying conservation of energy to each layer are:-

$$\frac{dT_i}{dt} = \left(\eta_i + \beta \left[-a_{12} \cdot \Delta T_{12}^{4/3} \right] \right) / (c_i + \lambda) \quad (3.9a)$$

Table 3.2 Sets of input values for initial temperatures
and for radiogenic heating

Initial temperature conditions

	<u>'Hot'</u>	<u>'Cold'</u>
	K	K
Core-mantle boundary	6000	4000
Lower mantle average	4500	3000
Upper mantle average	2500	1800
Surface (constant)	1000	1000

Radiogenic heating distributions
(values as at present time)
Units : 10^{12} W

	<u>1</u>	<u>2</u>	<u>3</u>
1 Core	0	2	5
2 Lower Mantle	20	18	15
3 Upper Mantle	<u>2</u>	<u>2</u>	<u>2</u>
Total	<u>22</u>	<u>22</u>	<u>22</u>
	<u>4</u>	<u>5</u>	<u>6</u>
1 Core	0	2	5
2 Lower Mantle	10	8	5
3 Upper Mantle	<u>2</u>	<u>2</u>	<u>2</u>
Total	<u>12</u>	<u>12</u>	<u>12</u>

$$dT_2/dt = \left(\eta_2 + \beta \left[a_{12} \cdot \Delta T_{12}^{4/3} - a_{23} \cdot \Delta T_{23}^{4/3} \right] \right) / c_2 \quad (3.9b)$$

$$dT_3/dt = \left(\eta_3 + \beta \left[a_{23} \cdot \Delta T_{23}^{4/3} - a_{34} \cdot \Delta T_{34}^{4/3} \right] \right) / c_3 \quad (3.9c)$$

$$T_4 = \text{constant} \quad (3.9d)$$

$$\Delta T_{ij} = (T_i - T_j) - \tau_{ij} \quad (3.9e)$$

Here T_i is the temperature of layer i ,

ΔT_{ij} is the potential temperature difference between layers i and j , which is the temperature drop across the boundary layer,

τ_{ij} is the adiabatic lapse between the 'centres' of layers i and j : these τ_{ij} are varied as one parameter only by the iteration described in section 3.3.1,

η_i is the radiogenic heating in layer i ,

βa_{ij} is the transmission factor between layers i and j , calculated from equation 3.1. The common factor β is varied by the iteration described in section 3.3.1,

c_i is the heat capacity of layer i ,

λ is the latent heat term given by equation (3.8).

In all runs of the model, the age of the Earth is taken to be 4.5 Ga.

Two thermal constraints are placed on the model by the variation of the two parameters β and τ_{ij} . Firstly the radius of the inner core at present time must be that observed seismically. Secondly the present time heat flux from upper mantle to surface, the term $\beta a_{34} \cdot \Delta T_{34}^{4/3}$ in equation (3.9c), should be equal to a preset value, to

correspond to that for the Earth. Values of 2, 3, 4 and 5×10^{13} W were used for this constraint: these may be compared with the recent estimate of 3.6×10^{13} W for this flux (Sclater et al 1980).

The first constraint sets a fixed value for the heat to be lost from the core over the full 4.5 Ga life of the model Earth for any given values for the latent and specific heat and for the radiogenic heating. It also leads to an approximate value for the total heat supply from the model. If that latter supply is inadequate for the required surface heat flux, the model will fail to converge to a solution. On the other hand, the model can more readily adapt to a plentiful supply of heat compared to the required surface heat flux by increasing both β and τ_{ij} in order to exaggerate the variation of the heat fluxes through the boundary layers as the temperature differences between layers diminish.

The time interval over which the inner core freezes out from the core depends heavily on the assumed range of freezing temperature, $(T_o - T_f)$ in equations (3.7) and (3.8). It is a very poorly known parameter, depending as it does on the difference b_1 between the melting and adiabatic gradients, neither of which is well known at core pressures and temperatures. However, a useful upper bound to physically plausible estimates of $(T_o - T_f)$ is given by using equation (3.7) to note that the present size of the inner core $r/r_o = 0.35$, corresponds to a temperature that is only about 0.12 down the freezing range. The remaining 0.88 $(T_o - T_f)$ must be accommodated by further cooling from the present temperature of the core-mantle boundary. Thus a range of $(T_o - T_f) = 1000^\circ\text{K}$ is feasible, but one of 3000°K becomes implausible (and has been taken as the upper limit for this parameter in running the model). This argument does of course depend on extending the

approximations (3.3) - (3.5) to a large inner core when they are likely to be much less accurate. However, one major source of inaccuracy is the omission of any depression of freezing temperatures by compositional changes during the growth of the solid inner core and this if taken into account would tend to make the real freezing temperature range greater than the hypothetical range $(T_o - T_f)$, thereby strengthening the argument.

3.3 Calculations

3.3.1 Numerical scheme

A first order forward difference procedure was used to solve equations (3.9a) to (3.9c). The two imposed thermal constraints are met by an iterative routine that chooses the appropriate values for β and τ_{ij} given the other input parameters. Lower and upper limits of 0.05 and 20.0 are placed on β to avoid both instability in the model and physically unreasonable solutions. Similarly negative values for τ_{ij} are discarded as solutions. These criteria exclude runs in which the total supply of energy is inadequate.

3.3.2 Results of a "standard" run

Figs, 3.2 and 3.3 show the temperature and heat flux profiles (marked 'A') resulting from the following input parameters:

- i) specific and latent heats and a range of freezing temperatures as in Table 3.1,
- ii) distribution '2' for radiogenic heating and "cold" initial boundary conditions, from Table 3.2, and
- iii) a surface heat flux constraint of $4 \times 10^{13} \text{ W}$.

(Profiles marked 'B' are for "hot" initial boundary conditions).

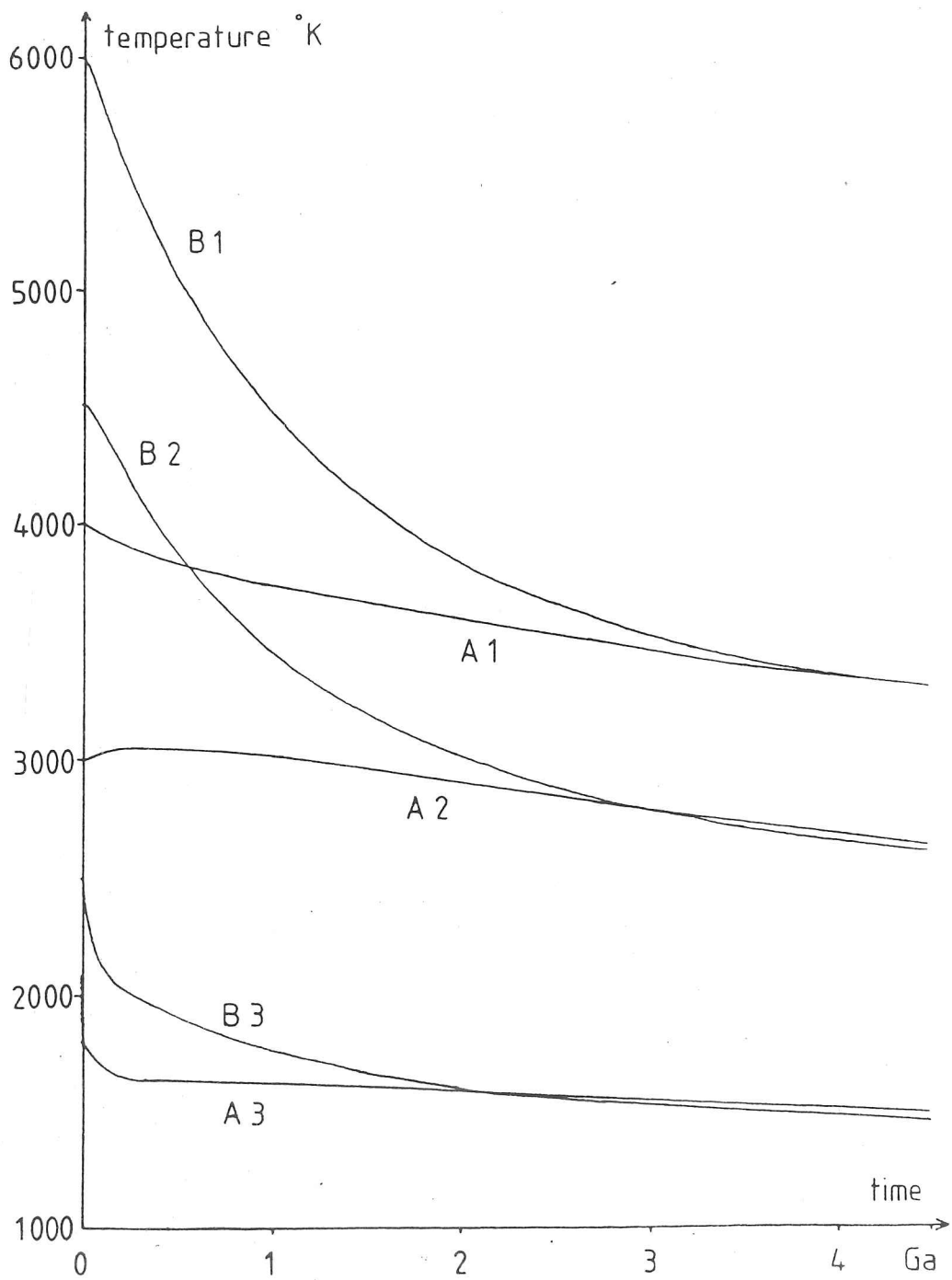


Fig. 3.2

Temperature profiles resulting from two runs :

'A' : 'standard' , 'B' : 'hot' ;

'1' : core , '2' : lower mantle , '3' : upper mantle.

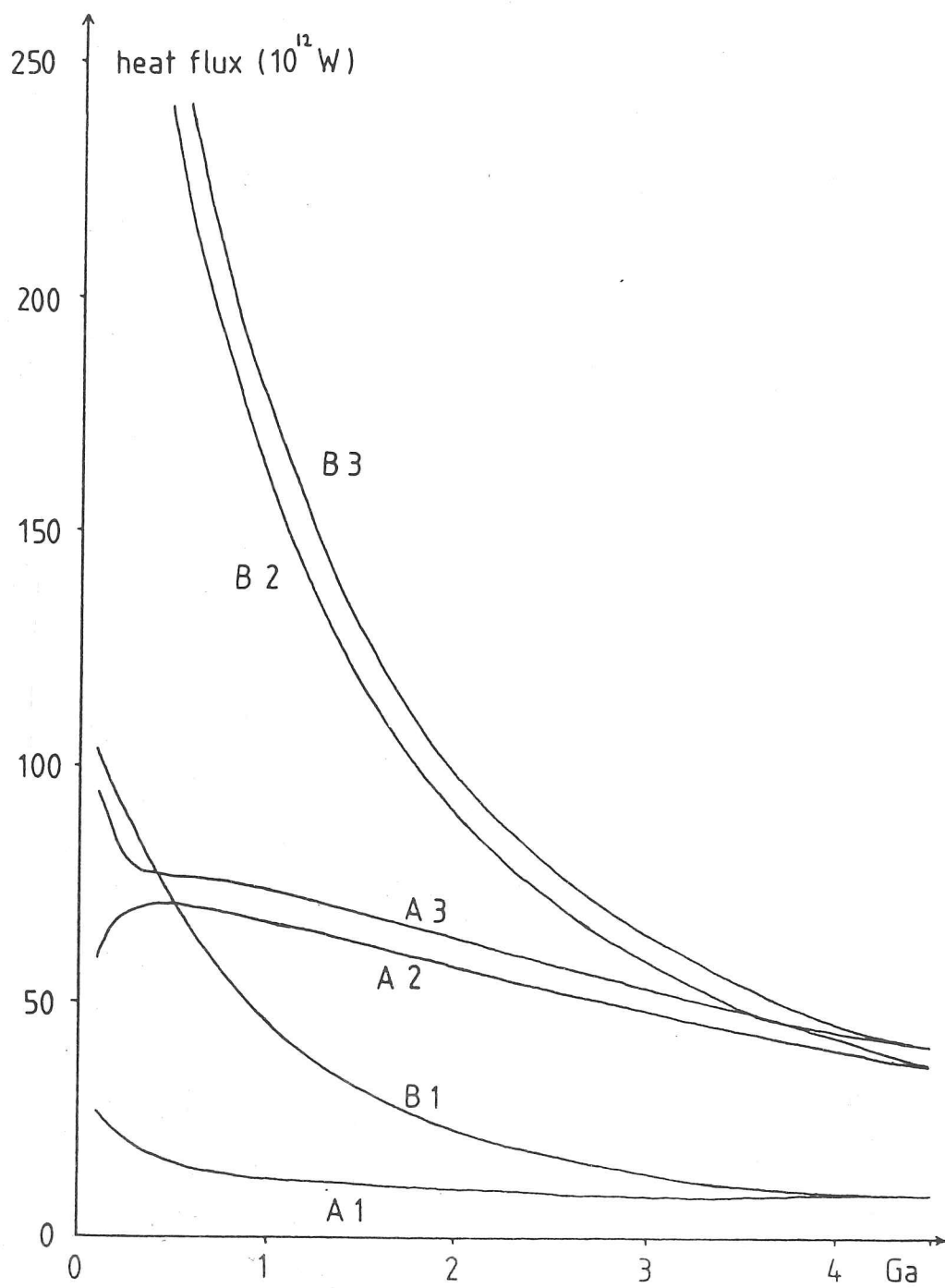


Fig. 3.3

Heat flux profiles resulting from two runs :

'A' : 'standard' , 'B' : 'hot' ,

'1' : flux from core , '2' : flux from lower mantle ,

'3' : flux from upper mantle to surface .

Table 3.3 Heat fluxes arising from the 'standard' run

Units: 10^{12}W

Time (Ga):	1	2	3	4	4.5 (present)
<u>Layers</u>					
1 to 2	12.1	10.0	8.9	8.8	8.8
2 to 3	67.1	57.5	48.0	39.9	36.6
3 to 4	73.5	63.2	52.8	43.8	40.0 (constrained)

The inner core begins to form in layer 1 at 3.2 Ga: after then latent heat is evolved.

Table 3.4. Temperatures and rates of temperature drop arising from the 'standard' run

Units: K , K Ga^{-1} respectively

Time (Ga):	1	2	3	4	4.5 (present)
T_1	3732	3586	3450	3344	3300 (constrained)
$-dT_1/dt$	161	139	132	91	87
T_2	3012	2901	2785	2681	2637
$-dT_2/dt$	96	117	112	94	85
T_3	1622	1584	1543	1506	1491
$-dT_3/dt$	32	41	39	34	30

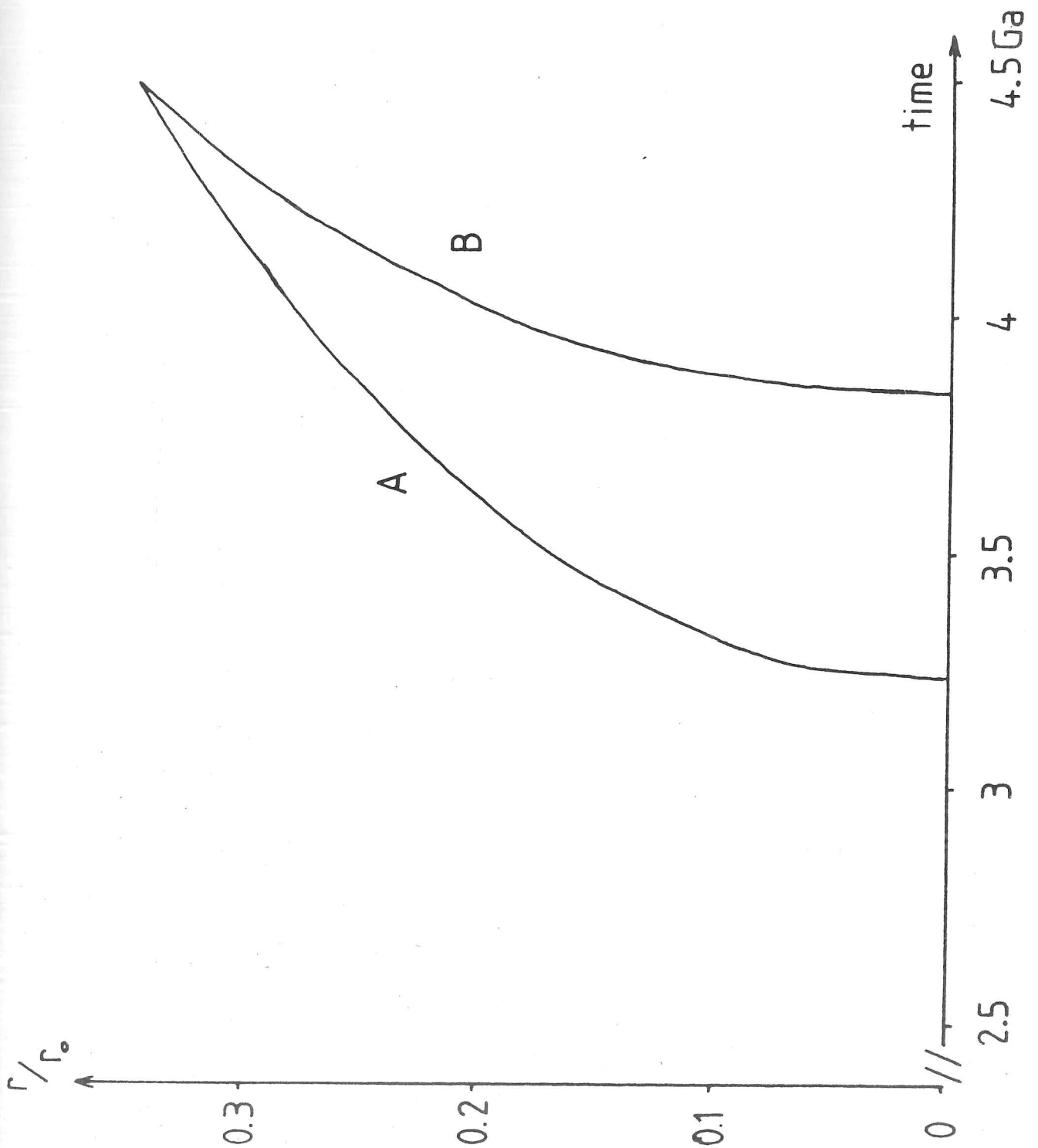


Fig. 3.4

Radius of inner core as a function of time . 'A' : 'standard' run ,
 'B' : 300 K freezing range.

Tables 3.3 and 3.4 give values for heat fluxes, temperatures and rates of change of temperature at selected times for this standard run.

The inner core begins to form at 3.2 Ga in this run. At later times, the heat flux from layer 1 varies by only about 2% whilst the rate of temperature drop decreases from $130^{\circ}\text{K Ga}^{-1}$ to $87^{\circ}\text{K Ga}^{-1}$. Thus in this period the simplifying assumption of constant heat flux from the core, as used by Loper (1978), is appropriate. For earlier times, neither simplifying assumption as to the boundary conditions is well justified. Figure 3.4 shows the radius of the inner core as a function of time, as given by equation (3.7).

3.3.3 Effects of varying parameters

The variations of input parameters tried in the model were:-

- 1) all specific and latent heats : doubled, halved,
- 2) latent heat only: tripled, divided by three,
in both cases based on values from Table 3.1 as the standards,
- 3) initial temperature conditions : 2 sets (Table 3.2),
- 4) radiogenic heating distribution : 6 sets (Table 3.2),
- 5) core freezing temperature range : 3000 K, 1000 K, 300 K or 100 K

Table 3.5 gives the average effect of each variation on the heat flux out of layer 1 at present time (4.5 Ga). Clearly this heat flux is relatively insensitive to the initial temperatures, the heat capacities and the range of freezing temperatures. This is mainly a result of the imposed thermal constraints and the consequent adjustment of the parameters β and τ_{ij} .

The effects of changing the constraint on the surface heat

Table 3.5

Effect of varying parameters

<u>Parameter</u>	<u>Change therein</u>	<u>Effect on core heat flux</u> $10^{12}W$
Constraint on surface heat flux	+ $10 \times 10^{12}W$	+ 3.9 ± 0.9
Total radiogenic heating (layer 2)	+ $10 \times 10^{12}W$ (present day value)	- 4.4 ± 0.8
Distribution of radiogenic heating between core and lower mantle	+ $3 \times 10^{12}W$ into core (present day value)	+ 3.5 ± 0.3
Initial temperatures	Increase as in table 3.2	+ 0.4 ± 0.6
Specific and latent heat capacities	Doubled	+ 0.5 ± 0.5
Latent heat	Tripled	+ 1.8 ± 1.0
Freezing temperature range	Tripled, for standard latent heat	- 0.6 ± 0.3
Change to single-layer mantle model	-	+ 0.3 ± 0.3
Change of exponent in equation (1)	From $3/2$ to $5/4$	+ 0.05 ± 0.05

flux and of changing the total radiogenic heating are complementary to each other, as might be expected. The difference between the two is due to the time lag involved in radiogenic heat of deep origin (layer 2) affecting the flux to the surface.

A change in the distribution of radiogenic heating between layers 1 and 2 by some amount has an effect of almost equal value on the flux out of layer 1. The effect is slightly larger in value than the cause, again due to the time lags involved. These result in the flux being associated with the radiogenic heating of an earlier period when the decay of the radiogenic heating is less advanced.

3.3.4 Effect of a single layer mantle model

A limited set of variations of the parameters was also run on a single layer mantle model in which the thermal capacities and radiogenic heating of upper and lower mantle were combined. The effect on the present day heat flux from core to mantle was slight (Table 3.5). This reflects the effect of the fitting of the two parameters β and τ_{ij} to the imposed constraints, and emphasises how restrictive are those constraints. Only a core freezing temperature range of 1000 K and a constrained mantle to crust heat flux of either 30 or 40 x 10¹²W were applied, with the full range of variation of the other parameters, as the effect of this change of the model on the heat flux results was so slight. Similarly the change has little effect on the time of onset of formation of the inner core: the single layer models giving times of onset typically later by 100 \pm 50 Ma only.

3.3.5 Effect of varying the exponent in equation (1)

As there is little experimental evidence for the parameterised convection expression for the heat flux used in equation (3.1), test runs were made with the exponent set to 5/4 and to 3/2 instead of the value of 4/3 given by the theory. The effect on the present time heat flux from the core was negligible, being $(0.05 \pm 0.05) \times 10^{12} \text{W}$ for the change in exponent from 3/2 to 5/4. This again emphasises the strength of the applied thermal constraints.

3.3.6. An example of a high flux run (N32)

Let us take the run in which, compared to the "standard" run, radiogenic heating is changed to distribution "6" and hot initial conditions are applied. From table 3.5, we may expect a present core heat flux of:-

	10^{12}W
Standard run	8.8
Decrease in total radiogenic heating	+ 4.4 \pm 0.8
Move $3 \times 10^{12} \text{W}$ from mantle to core	+ 3.5 \pm 0.3
Hot initial conditions	+ 0.4 \pm 0.6
	<hr/>
Prediction	17.1 \pm 1.0
	<hr/>

The model in fact gives a present core flux of $16.9 \times 10^{12} \text{W}$ for this run. Tables 3.6 and 3.7 give values for heat fluxes, temperatures and rates of change of temperature at selected times.

In this run, the inner core begins to form at 3.8 Ga. In order to comply with the constraints, $\beta = 1.65$ and $\tau_{ij} = 1.20 \times$ standard, whereas for the standard run the model requires $\beta = 1.65$ and $\tau_{ij} = 1.31 \times$ standard.

Table 3.6

Heat fluxes from run N32

Units 10^{12}W

Time (Ga):	1	2	3	4	4.5 (present)
Layers					
1 to 2	52.9	34.4	23.6	17.5	16.9
2 to 3	134.9	85.6	58.1	41.4	35.9
3 to 4	149.9	95.5	65.0	46.4	40.0 (constrained)

The inner core begins to form in layer 1 at 3.8 Ga at which time the heat flux from layers 1 to 2 is $17.9 \times 10^{12} \text{W}$.

Table 3.7 Temperatures and rates of temperature drop arising from run N32

Units: $^{\circ}\text{K}$, $^{\circ}\text{K Ga}^{-1}$ respectively

Time (Ga):	1	2	3	4	4.5 (present)
T_1	4844	4127	3676	3383	3300 (constrained)
$-dT_1/dt$	914	557	363	187	152
T_2	3641	3139	2828	2620	2547
$-dT_2/dt$	647	386	250	168	129
T_3	1853	1677	1568	1495	1468
$-dT_3/dt$	227	135	88	60	47

3.3.7. An example of a low flux run (N26)

In this case, the "standard" run is altered by a change in radiogenic heating to distribution '1' and a change in the surface heat flux to $30 \times 10^{12} \text{W}$. Again applying Table 3.5, we have:-

	<u>10^{12}W</u>
Standard run	8.8
Move 2×10^{12} from core to mantle	- 2.3 ± 0.2
Decrease surface heat flux constraint	- 3.9 ± 0.9
Prediction	<hr/> 2.6 ± 0.9 <hr/>

The model gives instead a present core flux of 3.0×10^{12} for this run. Heat fluxes, temperature and rates of change of temperature are given in table 3.8 and 3.9.

The inner core begins to form much earlier in this run, at 2.2 Ga, while in order to comply with the constraints $\beta = 5.74$ and $\tau_{ij} = 1.87 \times$ standard. Those lead to a rapid diminution with time of the heat transport through the boundary layers, in order to meet the reduced constraint on the surface heat flux. That causes the early formation of the inner core. In so far as the model requires these less "realistic" values for β and τ_{ij} , one can conjecture that such a run is less likely to correspond to the Earth.

3.4. Application of the results to the thermal history of the Earth

As described above, the model can be expected to give a reasonable range of values both for the present heat flux out of the Earth's core and for its variation with time, provided that

Table 3.8

Heat fluxes from run N26
Units 10^{12} W

Time (Ga):	1	2	3	4	4.5 (present)
<u>Layers</u>					
1 to 2	8.8	4.3	3.5	3.1	3.0
2 to 3	73.8	51.2	38.9	30.7	27.4
3 to 4	81.0	56.2	42.7	33.7	30.0 (constrained)

The inner core begins to form in layer 1 at 2.2 Ga at which time the heat flux from layers 1 to 2 is 3.9×10^{12} W.

Table 3.9

Temperatures and rates of temperature
drop arising from run N26Units: K, $K Ga^{-1}$ respectively

Time (Ga):	1	2	3	4	4.5 (present)
T_1	3572	3434	3367	3320	3300 (constrained)
$-dT_1/dt$	210	95	54	42	38
T_2	2837	2733	2672	2628	2610
$-dT_2/dt$	149	78	50	39	35
T_3	1526	1490	1468	1453	1446
$-dT_3/dt$	52	27	18	14	12

the input parameters are sufficiently accurate. Table 3.1 sets out the "standard" parameters used, which are based on literature sources relating to the Earth. Table 3.5 shows how sensitive the heat flux calculated by the model is to changes in these parameters. Clearly the crucial parameters are the quantity and location of radiogenic heating and the values taken for the heat flux from mantle to surface. In particular the value adopted for radiogenic heating in the core itself is both important and, unfortunately, very ill-known.

Despite that caution, the model does show that the heat flux out of the core, both at present and in the past, is a significant contribution to the heat flow in the mantle, supporting the case put by Sharpe & Peltier (1979). Using the "standard" input parameters, the model gives a present time heat flux from the core of 22% of that from mantle to surface. The applied range of parameters makes that vary from 7% to 60%.

If one considers the energetics of the core at recent times, i.e. with the presence of an inner core, then the results from the model are closer to those from an assumption of constant heat flux at the core-mantle boundary (Loper 1978a) than to those from one of constant rate of change of temperature. The model does not yield a well determined time for the onset of the inner core : it ranges from 0.5 Ga to 4.3 Ga after the start of the model for the parameter range tried, with 3.2 Ga for the "standard" run. The time of onset does tend to be rather later in the Earth's history than has usually been suggested (e.g. Gubbins et al (1979) consider an inner core starting to form early). However Stevenson et al (1983), using a model based on an exponential variation of viscosity with temperature, have recently suggested an inner core starting to form quite late, at

2.3 - 3.0 Ga for the six models used.

As stated in the introduction, the model used is likely to give mantle layer temperatures that are substantially in error, being too slow to respond to changing conditions. However, the upper mantle temperatures, T_3 , given by the model are in fact remarkably steady over recent periods. This reinforces one's confidence in the use of the constant viscosity parameterisation. For example the run with "standard" parameters yields a drop in T_3 over the last 2.5 Ga of only 93 K (see Table 3.4). That value may be compared with the suggestion (Green 1972) that the compositions of certain Archaean lavas indicate a decline in upper mantle temperature over that period of some 200 K. As can be seen in Fig. 3.2, a change in the initial temperatures of the model has little effect on this (for the "hot" set of initial conditions, the corresponding decline was 140 K).

In this work, our main interest in the results from the model lies in the comparison of the heat flux with the conductive heat flux due to the adiabatic gradient, in order to investigate the suggestion that the outermost part of the core may be stably stratified. Gubbins et al (1979, 1982) consider the possibility of thermal stratification if the core-mantle boundary were cooling slowly or were at constant temperature, and give a maximum value for the heat flux for this to occur of $4.5 \times 10^{12} \text{ W}$. That is based on an assumed thermal conductivity $k = 50 \text{ W m}^{-1} \text{ K}^{-1}$ and an adiabatic gradient $\left. \frac{\partial T}{\partial p} \right|_s = 2.6 \times 10^{-9} \text{ K.Pa}^{-1}$ at the top of the outer core. The model gives a heat flux from the core lower than that for runs in which there is zero core radiogenic heating combined with the minimum contribution ($8 \times 10^{12} \text{ W}$) from cooling, but otherwise the heat flux is greater than the limit. Thus the model suggests that the top of the core will not be

stably stratified by thermal effects. As will be seen in section 3.5, those runs in which the heat flux from the core is so low as to suggest a stably stratified top of the core are also runs in which the requirements of a dynamo would not have been met prior to the formation of the inner core (when there could be no "gravitational" drive for the dynamo). The only exceptions to this, runs for which there can now be a stably stratified top of the core and yet there is sufficiently high flux to drive a dynamo before the formation of the inner core, are runs performed with a very large range (3000 K) of freezing temperatures of the core.

3.5. Comparison of results with dynamo requirements

Gubbins et al (1979) give expressions for the generation of entropy E by the sources of energy Q , as follows:

$$\text{Radiogenic} \quad E_R/Q_R = 3.05 \times 10^{-5} \text{ K}^{-1} \quad (3.10a)$$

$$\text{Cooling} \quad E_C/Q_C = 3.3 \times 10^{-5} \text{ K}^{-1} \quad (3.10b)$$

$$\text{Latent (including chemical)} \quad E_L/Q_L = 5.3 \times 10^{-5} \text{ K}^{-1} \quad (3.10c)$$

$$\text{Gravitational and adiabatic} \quad E_G/Q_G = 2.9 \times 10^{-4} \text{ K}^{-1} \quad (3.10d)$$

These sources of entropy can then be compared with the various dissipative sinks, again from Gubbins et al:

$$\text{Thermal conduction} \quad E_k = 1.14 \times 10^8 \text{ W/K} \quad (3.11a)$$

$$\text{(based on adiabatic gradient } \left. \frac{\partial T}{\partial p} \right)_s = 2.6 \times 10^{-9} \text{ K/Pa)}$$

$$\text{Molecular diffusion} \quad E_\alpha = 1.43 \times 10^{10} \times \left(\frac{\Delta \rho}{\rho} \right)^2 \text{ W/K} \quad (3.11b)$$

where $\left(\frac{\Delta \rho}{\rho} \right)$ is the fractional density jump at the inner core

surface due to compositional differences.

$$\text{Ohmic dissipation } E_0 = 1.4 \times 10^8 \text{ W/K} \quad (3.11c)$$

for the dynamo of Kumar & Roberts (1975).

A representation of the dynamo requirements in terms of entropy is necessary in order to account properly for the feedback of Ohmic dissipation into thermal buoyancy in the fluid (compare Olson, 1981).

3.5.1 The thermally powered dynamo, at present time

Excluding any contribution from gravitational energy, equations 3.10 and 3.11 give the values for the minimum heat flux from the core to power a dynamo set out in Table 3.10.

In the case of the standard range of core freezing temperatures (1000°K), the model gives sufficiently high values for the heat flux except for the runs in which both the core radiogenic heating and the difference between surface heat flux and total radiogenic heat flux are at low values (less than $2 \times 10^{12}\text{W}$ and $8 \times 10^{12}\text{W}$ respectively). Changing the range of core freezing temperatures to 300 K does not affect this result.

Hence at present time the heat flux alone can be sufficient to drive the terrestrial dynamo, unless there is the combination of properties set out above. This conclusion is sensitive to the assumed value of the adiabatic gradient: a higher value would make it less likely that the heat flux alone can drive the dynamo.

3.5.2 The thermally powered dynamo, prior to onset of freezing

Prior to the onset of freezing, there could necessarily be neither latent heat nor gravitational energy from differential freezing as source of energy. Thus we can approximate by noting that:

Table 3.10

Dynamo requirements for heat flux from core
with no gravitational energy
Units = 10^{12} W

<u>Radiogenic Heating:</u>	<u>High</u>		<u>Low</u>		<u>Zero</u>	
	$(5 \times 10^{12}W)$		$(2 \times 10^{12}W)$			
Freezing Temperature Range:	<u>1000^oK</u>	<u>300^oK</u>	<u>1000^oK</u>	<u>300^oK</u>	<u>1000^oK</u>	<u>300^oK</u>
Standard heat capacities or all doubled or halved	7.6	7.3	6.8	6.3	6.2	5.5
Latent heat tripled	7.3	7.2	6.3	6.0	5.5	5.1
Latent heat divided by 3	8.0	7.6	7.4	6.8	7.0	6.2

$$E_R/Q_R \approx E_c/Q_c \quad (\text{since both are 'distributed' sources})$$

$$\text{and } Q_R \approx Q_c$$

$$E_R + E_c \approx (3 \times 10^{-5} \text{K}^{-1}) \times (\text{core to mantle heat flux})$$

This places a lower limit to the heat flux for a dynamo to be possible, of approximately $8 \times 10^{12} \text{W}$.

At the onset of freezing, the only runs that failed to provide sufficient flux were under the same combination of low core radiogenic heating and low contribution from cooling required for failure in section 3.5.1, but also required a value for the heat capacities not greater than the "standard" parameters.

Thus the model again indicates that the heat flux alone can be sufficient to drive the dynamo prior to the onset of freezing. This result can, in reverse, be used as a constraint on possible values for the adiabatic gradient in the core, because of the lack of complications from the inner core freezing surface in this case. In the case of the standard set of parameters, the lowest value of heat flux from the core prior to freezing was $8.6 \times 10^{12} \text{W}$. This could only satisfy the dissipation given by (11) for values of the adiabatic gradient not more than 10% greater than that used hitherto. This requirement depends on the evidence for an ancient magnetic field. Palaeomagnetic studies indicate that the field is at least 3.5 Ga old (McElhinny & Senanayake, 1980) and this is older than the inner core for most parameter ranges used, the only exceptions occurring with the freezing range $(T_o - T_f)$ set to its highest value, of 3000 K.

3.5.3 The gravitationally powered dynamo

For a dynamo to be feasible, we now need

$$E_o \leq (E_R + E_c + E_L + E_g) - (E_k + E_\alpha) \quad (15)$$

which can again be expressed in terms of a minimum heat flux from the core, though now this flux may be less than the conductive heat loss down the adiabatic gradient, since convection can be driven against a thermally stable gradient by the compositional difference. Some solutions are given in Table 3.11.

Except for runs with a combination of zero core radiogenic heating and lowest contribution from cooling, failure of the dynamo requirement is now rare for the range of parameters used: if the density contrast is 0.75 g cm^{-3} and the freezing range is 1000 K , then only 4 runs now fail. These are among those failing in section 3.5.1, but now failure only occurs for doubled values of the specific and latent heats, as this reduces the effect of the gravitational contribution.

3.6. Discussion of heat flux model

The most interesting results of this work are that the heat flux out of the core can be sufficiently large to:-

- i) drive a dynamo both at present time and at times previous to the formation of the inner core,
- ii) avoid thermal stable stratification of the core near the core mantle boundary, and
- iii) influence mantle convection significantly.

Exceptions to these results occur for values of the radiogenic heating in the core lower than approximately $2 \times 10^{12} \text{ W}$ combined with high values for mantle radiogenic heating. The uncertainty

Table 3.11

Dynamo requirements for heat flux from core
including gravitational energy
Units $10^{12}W$

<u>Radiogenic Heating</u> <u>in core:-</u>	<u>"High"</u> <u>$5 \times 10^{12}W$</u>		<u>"Low"</u> <u>$2 \times 10^{12}W$</u>		<u>"Zero"</u>	
<u>Freezing Temperature</u> <u>Range:-</u>	<u>$1000^{\circ}K$</u>	<u>$300^{\circ}K$</u>	<u>$1000^{\circ}K$</u>	<u>$300^{\circ}K$</u>	<u>$1000^{\circ}K$</u>	<u>$300^{\circ}K$</u>
<u>Density Jump at Inner</u> <u>Core Boundary¹:-</u>						
0.25 g cm ⁻³	7.0	6.6	5.7	4.9	4.9	3.8
0.75g cm ⁻³	6.7	6.3	4.7	4.1	3.5	2.7
1.25 g cm ⁻³	7.0	6.6	4.9	4.2	3.4	2.6

Note 1 of these 0.1 g cm^{-3} is assumed due to solidification, the balance to composition.

2 "standard" values for specific and latent heat are used in calculating the above.

in estimates of the adiabatic gradient near the core mantle boundary is such that (i) and (ii) above are themselves not certain.

The model used is successful in producing thermal histories that fit the observational constraints for most sets of input parameters. The resulting temperature profiles are remarkably steady after the first 1 - 2 Ga, despite the exclusion from the model of any temperature dependence of viscosity. Varying the input parameters leads to the estimates of the resulting effects on heat flux out of the core, given in Table 3.5. These show that the present time heat flux is relatively independent both of the initial temperature conditions (provided they are "hot") and of the values used for the specific heats.

The combination of the thermal model and the dynamo requirements suggests that, if one requires a dynamo at early times (prior to about 2.0-2.5 Ga before present), then the present heat flux from core to mantle is sufficient to avoid a stable thermal stratification. It is the dynamo problem in the absence of an inner core (and hence the absence of any complications from compositional differences yielding a "gravitational" source of energy) that leads to this stronger conclusion from the thermal model. In this context, it is important that the present inner core radius (35% of the whole core) corresponds, under plausible assumptions, to cooling through a small fraction of the range of freezing temperatures (12% of that range). This is of course a consequence of the low value of g near the centre of the core, which leads to small pressure gradients in the inner core. As a result, it becomes physically implausible that the freezing range for the core can be very much larger than 1000 K, if about 88% of that range has

yet to be covered by future cooling of the core-mantle boundary. In turn, this results in it being likely that the geodynamo precedes the formation of an inner core.

4. Penetrative convection: analytical approach to the linear equations.

The remaining chapters of this thesis are devoted to a study of penetrative convection. The object is to assess the effect of rotation on the extent to which an unstable convecting layer can disrupt an adjoining stably stratified region. In this chapter, the linear equations are studied and the results given will serve as a framework for the numerical solutions, again of the linear equations, set out in chapter 5 and the experimental work described in chapter 6. The analysis does not include the influence of magnetic fields, and so is only a step towards understanding the dynamics of the core.

4.1 Rotation parallel to gravity

The normalised linear equations of motion and heat transport (2.11) are:

$$\left[D^2 - a^2 - p \right] Z = - TDU \quad (4.1a)$$

$$\left[(D^2 - a^2)(D^2 - a^2 - p) \right] U = +DZ + F \quad (4.1b)$$

$$\left[D^2 - a^2 - \sigma p \right] F = Ra^2 f(z) U \quad (4.1c)$$

If we operate on (4.1b) with

$$\left[(D^2 - a^2 - p)(D^2 - a^2 - \sigma p) \right]$$

and substitute from (4.1a) and (4.1c), this becomes an 8th order differential equation in U:

$$\left[(D^2 - a^2)(D^2 - a^2 - p)^2(D^2 - a^2 - \sigma p) + TD^2(D^2 - a^2 - \sigma p) \dots \right]$$

$$\dots + Ra^2(D^2 - a^2 - p)f(z) \Big] U = 0 \quad (4.2)$$

Note that the term in the Rayleigh number,

$$\left[Ra^2(D^2 - a^2 - p)f(z) \right] U$$

includes an operator that acts on $f(z)U$, not just on U . This makes the penetrative convection problem rather more interesting than a mere juxtaposition of solutions for different constant values of $f(z)$. Only in the special case of marginal steady stability, $p = 0$, can the equations be simplified to the 6th order form:

$$\left[(D^2 - a^2)^3 + TD^2 + Ra^2f(z) \right] U = 0 \quad (4.3)$$

Even in this case we must exercise care in the boundary conditions (see Chandrasekhar, 1961, p.90): only for stress-free perfectly conducting boundaries does one find complete solutions in terms of the sixth order equation.

We shall first investigate the limit of rapid rotation, $T \rightarrow \infty$, as this leads to a useful simplifying approximation (§ 4.2) and then in § 4.3 and § 4.4 investigate certain especially simple forms for $f(z)$.

4.2 Rapid rotation limit

The equations (4.1a) to (4.1c) can be simplified in the limit $T \rightarrow \infty$ for regions that do not include boundaries to the fluid. In such "interior" regions, we may anticipate from boundary layer theory that viscous forces become negligible so that the order of the differential equations may be reduced from 8 to 2. Boundary conditions must then be met through matching

the interior solutions to the boundaries by way of thin boundary layers. Greenspan (1968) gives a review of the relevant boundary layer theory. In the interior region the vertical length-scale for variations in the flow will continue to be the layer depth but the horizontal length-scale may become short to counteract the rotational constraint.

Let us adopt a new non-dimensionalisation of the linear equations (4.1) on scales that reflect the rapid rotation. We shall later see that the length-scale is that appropriate only to the boundary layer thickness: the horizontal length-scale of convective motions reflects a compromise between the layer depth and the rotational scale.

$$\begin{aligned} \text{Length} \quad L &= \sqrt{\nu}/\Omega \\ \text{Time} \quad \tau &= \Omega^{-1} \\ \text{Temperature} \quad \theta &= \beta_0 d \end{aligned}$$

Let us define new non-dimensional variables:

$$\begin{aligned} F_1 &\equiv \frac{d}{\sigma} \sqrt{\frac{\Omega}{\nu}} \vartheta^1 \\ Z_1 &\equiv \zeta_z^1 \\ U_1 &\equiv u_z^1 \end{aligned}$$

where ϑ^1 , ζ_z^1 , u_z^1 are the non-dimensionalised temperature, vertical vorticity and vertical velocity perturbations respectively.

Thus we get the non-dimensional equations

$$\left[D^2 - a^2 - p \right] Z_1 = 2 D U_1 \quad (4.4a)$$

$$\left[(D^2 - a^2)(D^2 - a^2 - p) \right] U_1 = 2 D Z_1 + R_1 a^2 F_1 \quad (4.4b)$$

$$\left[D^2 - a^2 - p\sigma \right] F_1 = -f(z) U_1 \quad (4.4c)$$

where a new Rayleigh number has been defined as

$$R_1 \equiv \frac{g\alpha\beta_0\sigma}{\Omega^2} \quad (4.5)$$

and D , a , p are non-dimensional.

We now consider the terms in equations (4.4) in terms of a small parameter ϵ :

$$\epsilon \equiv L/d = \sqrt{2} T^{-\frac{1}{4}}$$

where T is the Taylor number. Further let us consider the marginal case, $p = 0$. We may note that a diffusive time-scale would imply $p = 0 (\epsilon^2)$. We note that the horizontal wave-number a and the Rayleigh number R_1 are as yet of undetermined magnitude, and that our vertical scale-length implies that $D U_1 = 0 (\epsilon) U_1$, etc.

Combining the three equations (4.4), just as (4.1) were combined into (4.3) in the marginal case, we have

$$\left[(D^2 - a^2)^3 + 4D^2 + R_1 a^2 f(z) \right] U_1 = 0 \quad (4.6)$$

which may be expanded as

$$\left[(-a^6 + R_1 a^2 f(z)) + (4 + 3a^4) D^2 + (-3a^2) D^4 + D^6 \right] U_1 = 0 \quad (4.7)$$

and then approximated by

$$\left[(-a^6 + R_1 a^2 f(z)) + (4 + 3a^4)(0(\epsilon^2)) + (-3a^2)(0(\epsilon^4)) + \dots \right] U_1 = 0 \quad (4.8)$$

Let us consider 2 cases:-

$$(i) \quad a \geq 0(1)$$

Then (4.8) can be approximated by

$$\left[(-a^6 + R_1 a^2 f(z)) + O(\epsilon^2) \right] U_1 = 0 \quad (4.9)$$

which implies $R_1 = O(a^4)$

$$\geq 0(1) \quad (4.10)$$

$$(ii) \quad a \ll 0(1)$$

Then (4.8) can be approximated by

$$\left[(-a^6 + R_1 a^2 f(z)) + 4D^2 \right] U_1 = 0$$

which implies

$$R_1 a^2 = O(\epsilon^2) + O(a^6) \quad (4.11)$$

which minimises R_1 for

$$a = O(\epsilon^{1/3}) \quad (4.12a)$$

$$R_1 = O(\epsilon^{4/3}) \quad (4.12b)$$

Comparing the 2 cases, the latter leads to the lower critical Rayleigh number and is therefore the appropriate physical scaling. Thus (4.8) should be approximated by:-

$$\left[4D^2 + a^2 (R, f(z) - a^4) \right] U_{,1} = 0 \quad (4.13)$$

with the 1st correction terms being $O(\epsilon^{4/3})$

relative to the terms retained in (4.13).

Boundary conditions

Now that we have reduced the interior equations to 2nd order in U , (4.13), we are left with the problem of what are appropriate boundary conditions. In the case of stress-free boundaries, Chandrasekhar (1961) adopts $U_{,1} = 0$ on each (pp. 104-106) and this would appear valid since the absence of stress at the boundary would seem to rule out the possibility of Ekman-layer "pumping" as described by Greenspan (1968) (p.46). On the other hand, a rigid boundary will result in Ekman layer pumping associated with any transverse interior motion: this is equivalent to a boundary condition of $U \neq 0$, thereby allowing a longer vertical-scale and so a lower Rayleigh number. This prediction is in general agreement with the results of the variational principle used by Chandrasekhar (1961) for the cases with rigid boundaries (see Table 4.1).

At high rotation rates, although boundary layer pumping still occurs, it can be shown that it becomes small relative to interior velocities. Using the boundary layer flux given as equation 2.17.3 by Greenspan (1968) and converting it to our non-dimensionalisation based on a length-scale $L \equiv \sqrt{\nu/\Omega}$, we have

$$U_{1n} = \left(\frac{1}{2} \frac{\partial}{\partial x_1} - \frac{\partial}{\partial y_1} \right) U_{,1x} \quad (4.14)$$

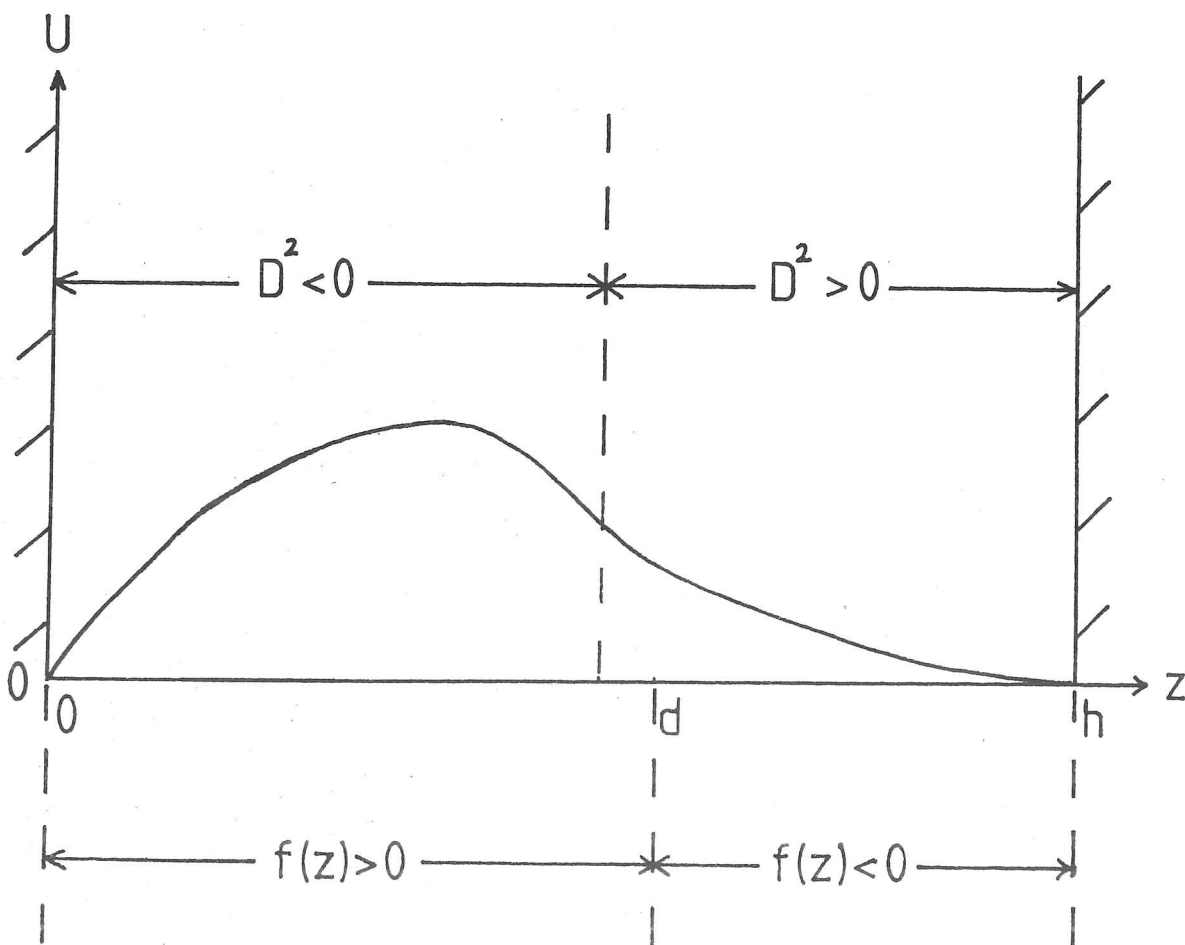
Table 4.1

Comparison of critical Rayleigh numbers for free-free and rigid-rigid boundaries. Values taken from Chandrasekhar (1961)

T	R_{C-free}	$R_{C-rigid}$	Ratio
0 ₂	6.575×10^2	1.708×10^3	0.385
10 ₂	8.263×10^2	1.757×10^3	0.470
10 ₄	5.377×10^3	4.713×10^3	1.141
10 ₆	9.222×10^4	7.113×10^4	1.296
10 ₈	1.897×10^6	1.531×10^6	1.239
10 ₁₀	4.047×10^7	3.464×10^7	1.168

Fig. 4.1

Schematic diagram of the interior solution for the vertical velocity U under rapid rotation.



where x_1, y_1 are the normalised transverse co-ordinates and U_{1x} a typical interior velocity. Thus the normal flow, U_{1n} is of order:

$$U_{1n} = O(a) \cdot U_{1x} \quad (4.15)$$

where, from (4.12a),

$$a = O(\epsilon^{1/3}) = O(T^{-1/12})$$

This $O(T^{-1/12})$ relationship has previously been noted by Eltayeb (1972). Clearly we must consider T very large for $T^{-1/12}$ to be small (and so for the above to be valid). Table 4.1 shows critical Rayleigh numbers for stress-free and for rigid boundaries in the rotating plane layer convection problem, taken from Chandrasekhar (1961). As T increases, and $T^{-1/12}$ starts to become small, the ratio of Rayleigh numbers is seen to diminish. Thus, rather than the two types of boundary leading to critical Rayleigh numbers of asymptotic form

$$R_c = c T^{2/3}$$

where the constant c differs depending on the boundary conditions (Chandrasekhar, 1961, p. 106), one should have an asymptotic limit

$$R_c = c T^{2/3}$$

with c independent of boundary conditions, being of the form

$$\frac{c \text{ (stress-free)}}{c \text{ (rigid)}} = 1 + O(T^{-1/2}) \quad (4.16)$$

In reducing the equations to 2nd order as $T \rightarrow \infty$, not only do we lose the 2 viscous boundary conditions, by substituting an Ekman boundary layer, but also we lose the thermal boundary condition. In the full equations this condition represents the relative conductivity of the boundaries and the fluid and might typically be given as:

$$DF = \pm \lambda F \quad (4.17)$$

on the boundaries, where F is the normalised temperature perturbation and λ is the Biot number. The loss of this boundary condition through the introduction of a viscous boundary layer is at first sight surprising, but physically is a result of the small horizontal length-scales imposed by the rapid rotation.

The Biot number λ is the inverse of the thermal thickness of the boundary. If we scale on our rotational length-scale, we find the Biot number λ_1 is given by

$$\lambda_1 = \epsilon \lambda \quad (4.18)$$

Thus for any real boundary, for which $0 < \lambda < \infty$ the rescaled Biot number λ_1 in our rotational scaling will tend to zero in the limit $T \rightarrow \infty$. This tendency towards a fixed flux character is reflected in the limit of the horizontal wavenumber given above (4.12a): $a_1 = O(\epsilon^{1/3}) \rightarrow 0$ as $T \rightarrow \infty$.

Now that we are satisfied that $U = 0$ is the appropriate boundary condition for the interior region for $T \rightarrow \infty$, we can

consider the interior eigenvalue problem given by (4.13). Clearly, in order to have a non-trivial solution satisfying the boundary condition at both top and bottom boundaries, D^2 must be a negative operator on U in at least some part of the region. Therefore $a^4 < R$, $f(z)$ in some part of the fluid.

If $f(z)$ changes sign, then clearly D^2 becomes a positive operator on U , in that stable region. Thus in this limit $T \rightarrow \infty$ we may expect that the interior solution for U , has separated into two regions distinguished by the sign of $D^2 U$ (Figure 4.1).

The boundary, where $D^2 U = 0$ (to within $O(\epsilon^{4/3})$), will be at the point where

$$R, \quad f(z) = a^4 \quad (4.19)$$

i.e. within the unstable region of $f(z) > 0$. Note that this boundary is one on which $D^2 U = 0$ but $U \neq 0$: it is not correct to describe it as a stress-free (albeit permeable) surface since if one considers the horizontal elements of the viscous stress tensor, P_{xz} , P_{yz} ,

$$P_{xz} = \mu \left(\frac{\partial u_x}{\partial z} + \frac{\partial u_z}{\partial x} \right)$$

$$P_{yz} = \mu \left(\frac{\partial u_y}{\partial z} + \frac{\partial u_z}{\partial y} \right)$$

then to achieve $p_{xz} = p_{yz} = 0$ in an incompressible fluid we require

$$\frac{\partial u_x}{\partial z} = - \frac{\partial u_z}{\partial x}$$

and
$$\frac{\partial u_y}{\partial z} = - \frac{\partial u_z}{\partial y}$$

and so
$$\frac{\partial}{\partial z} \left(- \frac{\partial u_z}{\partial z} \right) = - \frac{\partial^2 u_z}{\partial x^2} - \frac{\partial^2 u_z}{\partial y^2}$$

i.e. $(D^2 + a^2) U_z = 0$ in our normalised units (4.20). Thus $D^2 U_z = 0$ is a stress-free boundary in the special case of $U_z = 0$ but not in the case being considered.

Approximate solutions, as $T \rightarrow \infty$

Let us consider the approximate equation of motion (4.13), valid as $T \rightarrow \infty$:

$$TD^2U = a^2 (a^4 - R_1 f(z)) U$$

in $0 \leq z \leq h$

with $U = 0$ on $z = 0, h$.

If $f(z)$ is an analytic function in the region $0 \leq z \leq h$, then the equation can in principle be solved by a series expansion method. The choice of a suitable basis for the expansion depends on the form of $f(z)$. For example, if $f(z)$ can readily be expressed as a trigonometric series

$$f(z) = \sum_{n=0}^{\infty} f_n \cdot \cos \left(\frac{n\pi z}{h} \right) \tag{4.21}$$

then an expansion for U of the form

$$U(z) = \sum_{n=1}^{\infty} u_n \cdot \sin \frac{n\pi z}{h} \tag{4.22}$$

is appropriate, in that the boundary conditions are satisfied and one can use the relation

$$\sin z_1 \cdot \cos z_2 = \frac{1}{2} \left[\sin(z_1 - z_2) + \sin(z_1 + z_2) \right]$$

on substituting the series expansions into equation (4.13). However, if u_n , f_n are not small for large n , there are problems arising from the "difference" sine term ($\sin(z_1 - z_2)$ above). Alternatively one could use expansions in (z/h) ,

$$f(z) = \sum_{n=0}^{\infty} f_{1n} \cdot (z/h)^n \quad (4.23)$$

$$U(z) = \sum_{n=1}^{\infty} U_{1n} \cdot (z/h)^n \quad (4.24)$$

in which case the series expansion of the cross-product ($f(z) \cdot U(z)$) term is simpler and one is left with the boundary condition on $U(z)$ at $z = h$ as the criterion for the eigenvalue R :

$$U(h) = 0 \quad (4.25)$$

$$\therefore \sum_{n=1}^{\infty} U_{1n} = 0 \quad (4.26)$$

Except for very simple forms of $f(z)$ the simplest approach to equation (4.13) is numerical integration. Unlike the 8th order equations for slow rotation, this 2nd order equation lends itself to a straightforward initial value integration from the normalised initial conditions:

$$U(0) = 0$$

$$DU(0) = 1.0$$

Results from such an integration are reported briefly in § 5.3.3

As a brief example of the series expansion method, let us consider a parabolic temperature profile, with temperature

gradient given by $f(z) = 1-z$ in $0 \leq z \leq h$. Such a profile approximately describes the density gradient in an ice-water system with a linear temperature profile (e.g. Veronis (1963)).

1) Expansion in $\left(\frac{z}{h}\right)^m$

$$f_0 = 1 \quad (4.27a)$$

$$f_1 = -h \quad (4.27b)$$

$$f_2, f_3, \dots = 0 \quad (4.27c)$$

For $m > 1$, we have the recurrence relationship

$$\frac{T}{h^2} (m+2)(m+1) \cdot U_{m+2} = a^6 U_m - a^2 R_1 U_m + a^2 R_1 h \cdot U_{m-1} \quad (4.28)$$

and similarly we find for $m \leq 1$

$$U_2 = 0 \quad (4.29)$$

$$U_3 = \frac{h^2}{6T} \cdot (a^6 - a^2 R_1) U_1 \quad (4.30)$$

Inspection of the recurrence relation confirms that it will give a convergent series for $u(z)$ in $0 \leq z \leq h$, since for large m we can approximate it by:

$$U_{m+2} \approx \left(\frac{a^2 R_1 h^3}{T}\right) \frac{U_{m-1}}{m^2} \quad (4.31)$$

Indeed, provided $f(z)$ is itself analytic in that range of z , we can see that for any $f(z)$ the recurrence relation will be of the

form

$$u_j = 0 \left(\frac{1}{j^2}\right) u_{j-k} \quad (4.32)$$

for some finite integer k and sufficiently large j . In our example, we have

$$u_1 \quad (4.33a)$$

$$u_2 = 0 \quad (4.33b)$$

$$u_3 = \left(\frac{h^2}{6T}\right)(a^6 - a^2R_1) u_1 \quad (4.33c)$$

$$u_4 = \left(\frac{h^2}{12T}\right)(a^2R_1h) u_1 \quad (4.33d)$$

$$u_5 = \left(\frac{h^2}{20T}\right)\left(\frac{h^2}{6T}\right)(a^6 - a^2R_1)^2 u_1 \quad (4.33e)$$

and so on.

The boundary condition at $z = h$ is equivalent to $\sum_{n=1}^{\infty} u_n = 0$. and so we might take as a first approximation the series up to $m = 3$ only, giving

$$R_1 = a^4 + \frac{6T}{a^2h^2} \quad (4.34)$$

which can be minimised by choosing $a^6 = 3T/h^2$ to give an estimate

$$R_{1c} = 3(3T/h^2)^{2/3} \quad (4.35a)$$

$$a_c = (3T/h^2)^{1/6} \quad (4.35b)$$

The corresponding eigenfunction is:

$$u_1$$

$$u_2 = 0$$

$$u_3 = -u_1$$

i.e.
$$u(z) = u_1 \left(\left(\frac{z}{h} \right) - \left(\frac{z}{h} \right)^3 \right) \quad (4.36)$$

This is the lowest order of truncation at which the boundary condition at $z = h$ can be met in this problem. The inclusion of further terms leads to multiple roots for the Rayleigh number (for $m \geq 5$), of which the lowest is the one of interest.

2) Expansion in $\sin(m\pi z/h)$

$$f(z) = \sum_{n=0}^{\infty} f_n \cdot \cos(n\pi z/h) \quad (4.37a)$$

$$\text{where } f_0 = 1 - h/2 \quad (4.37b)$$

$$f_{2m} = 0 \quad (4.37c)$$

$$f_{2m-1} = \frac{4h}{\pi^2(2m-1)^2} \quad (4.37d)$$

} for $m \geq 1$

The recurrence relation is

$$U_m \left(a^6 + \frac{17m^2\pi^2}{h^2} \right) = \frac{Ra^2}{2} \left(\sum_{n=0}^{m-1} u_{m-n} \cdot f_n + \sum_{n=0}^{\infty} u_{m+n} \cdot f_n \right) \quad (4.38)$$

and in order to avoid the problem of the infinite series in the

last term on the R.H.S. we must make the approximation of truncating the solution for $u(z)$.

For truncation at $m = 1$, we have

$$u(z) = u_1 \sin(\pi z/h) \quad (4.39)$$

and so $(1-h/2)Ra^2 = a^6 + \frac{T\pi^2}{h}$ (4.40)

which gives $R_{1c} = 3\left(\frac{T\pi^2}{2h^2}\right)^{2/3} / (1-h/2)$ (4.41)

$$a_c = \left(\frac{T\pi^2}{2h^2}\right)^{1/6} \quad (4.42)$$

provided $h < 2$

This level of truncation only "sees" the average value of $f(z)$,

$$\overline{f(z)} = (1-h/2) \quad (4.43)$$

For truncation at $m = 2$, we get

$$u_1\left(a^6 + \frac{T\pi^2}{h^2}\right) = \frac{Ra^2}{2}(2f_0 \cdot u_1 + f_1 \cdot u_2) \quad (4.44a)$$

and $u_2\left(a^6 + \frac{4T\pi^2}{h^2}\right) = \frac{Ra^2}{2}(2f_0 \cdot u_2 + f_1 \cdot u_1)$ (4.44b)

which gives a quadratic in (Ra^2) :

$$\begin{aligned} & (Ra^2)^2 \left(1-h+h^2\left(\frac{1}{4} - \frac{4}{\pi^4}\right)\right) - (Ra^2) \left(\left(1-\frac{h}{2}\right)\left(2a^6 + \frac{5T\pi^2}{h^2}\right)\right) \\ & + \left(a^6 + \frac{T\pi^2}{h^2}\right)\left(a^6 + \frac{4T\pi^2}{h^2}\right) = 0 \end{aligned} \quad (4.45)$$

For given a , T , h this is readily solved, but it is clear that even at this modest level of truncation the series expansion is of little general use. Thus numerical integration is to be preferred.

It is worth noting that, having made the approximation of reducing the equations to 2nd order, based on $T \rightarrow \infty$, the solutions for critical Rayleigh number and wavenumber will now be of the form $R_c = O(T^{2/3})$, $a_c = O(T^{1/6})$ for all values of T . This occurs as a result of neglecting all the terms leading to deviation from those relationships. Thus the critical Rayleigh numbers plotted in figure 5.16 based on the 2nd order equations fit the straight line

$$\log (R_c) = 2/3 \log (T) + \text{constant}.$$

The solutions have a common form, depending only on the chosen $f(z)$ and h to determine the constants of proportionality. In particular, under this approximation there can be no change in the shape of the eigenfunctions (and thus of the extent of penetration) as one varies T for given $f(z)$, h . It is for this reason that the numerical work in § 5 is devoted to the full 8th order equations, as a study of the influence of rotation on the extent of penetration.

Two layer case

The concept of the internal boundary separating the stable and unstable regions in the limit $T \rightarrow \infty$ according to the sign of D^2U/U suggests that a study of a simple two layer problem will be of interest. Let us consider the case

$$f(z) = +1 \quad \text{in } 0 \leq z < 1 \quad (4.46a)$$

$$= -A \quad \text{in } 1 < z \leq h \quad (4.46b)$$

The solutions in the two regions that satisfy our 'interior' boundary condition $U = 0$ on $z = 0$ and $z = h$ are:

$$U = u_1 \sin(\lambda_1 z) \text{ in } 0 \leq z < 1 \quad (4.47a)$$

$$U = u_2 \sin h(\lambda_2(z-h)) \text{ in } 1 < z \leq h \quad (4.47b)$$

where in order to satisfy equation 4.13 we must have'

$$T\lambda_1^2 = R_1 a^2 - a^6 \quad (4.48a)$$

$$T\lambda_2^2 = A R_1 a^2 + a^6 \quad (4.48b)$$

and $R_1 > a^4$ so that λ_1 is real.

At the interior boundary, continuity of velocity is required, though not necessarily any higher derivation of U since we may have an internal Ekman layer. Therefore U , DU are continuous (the latter reflecting the continuity of the transverse velocities V and W).

$$u_1 \sin \lambda_1 = u_2 \sin h(\lambda_2(1-h)) \quad (4.49a)$$

$$u_1 \lambda_1 \cos \lambda_1 = u_2 \lambda_2 \cos h(\lambda_2(1-h)) \quad (4.49b)$$

Combining these, we have

$$\frac{\tan \lambda_1}{\lambda_1} = \frac{\tan h \lambda_2(1-h)}{\lambda_2} \quad (4.50)$$

which for given values of a , T , h may be solved graphically,

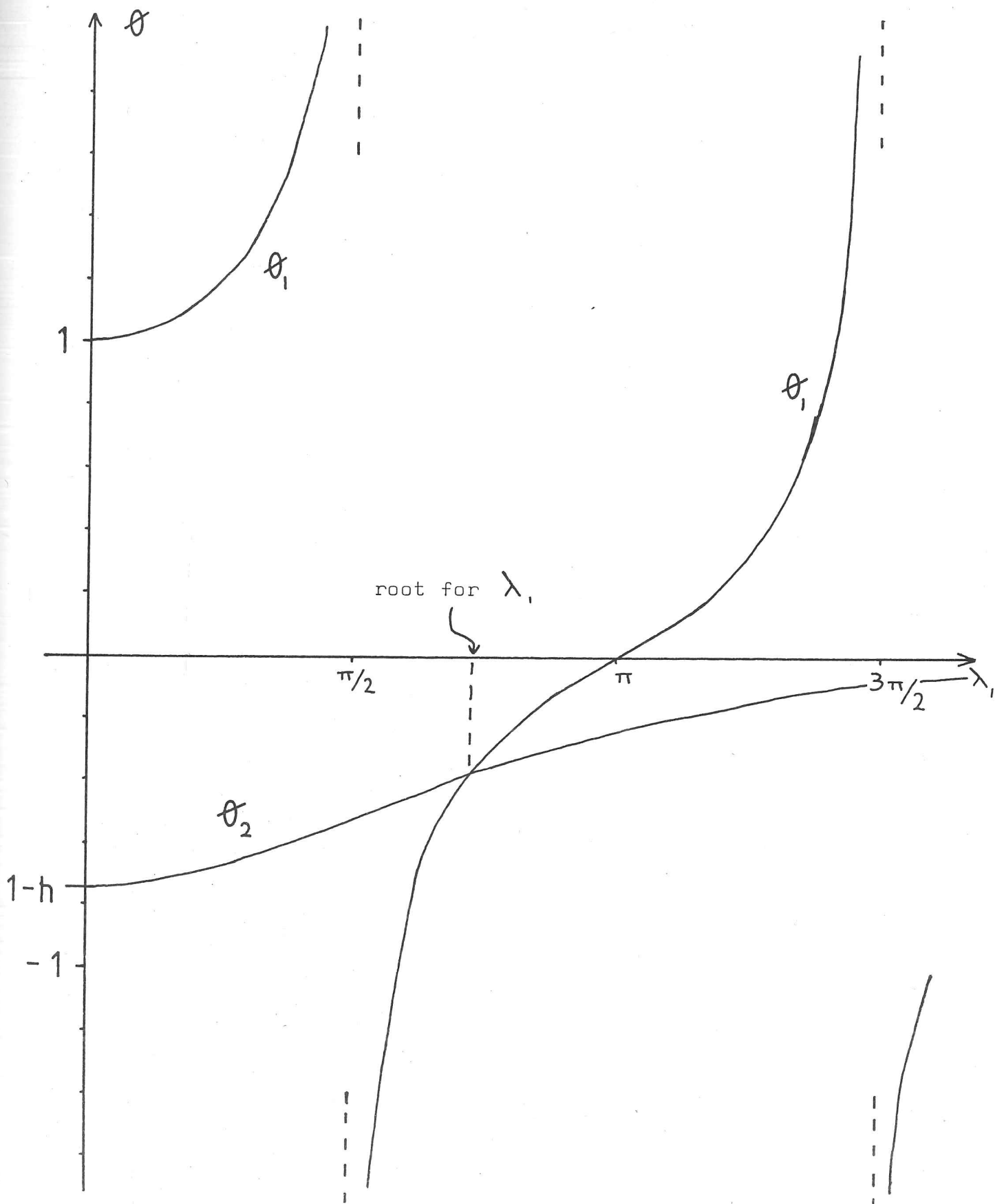


Fig. 4.2

Schematic graphical solution for $\theta_1 = \theta_2$, where
 $\theta_1 = \tan \lambda_1 / \lambda_1$, $\theta_2 = \tanh \lambda_2(1-h) / \lambda_2$

noting that λ_1 and λ_2 both increase monotonically with the Rayleigh number R , (fig. 4.2).

Regardless of the actual values of a , T and h , the first eigenvalue R , clearly must correspond to $\pi/2 < \lambda_1 < \pi$. Thus, if T is sufficiently large that the 2nd order equation 4.13 is a reasonable approximation, then regardless of the value of A we can perform a minimisation of the Rayleigh number with respect to a , T to show that

$$R_c = O(T^{2/3}) \quad (4.51a)$$

$$a_c = O(T^{1/6}) \quad (4.51b)$$

just as for the case $f(z) = 1$.

4.3 General two layer problem: $f(z) = +1$ in $0 \leq z < 1$ $= -A$ in $1 < z \leq h$

In the case of general values of rotation rate, the problem of the onset of convection in even the simple geometry of two layers of constant density gradient becomes much more difficult. The obvious analytical approach is to consider solutions of the form.

$$U \propto e^{mz} \quad (4.52)$$

in each layer.

Stress-free and perfectly conducting boundaries at $z = 0$, $z = h$ lead to a simplification, in that the relevant differential equation for onset is sixth order:

$$\left[(D^2 - a^2)^3 + TD^2 + Ra^2 \cdot f(z) \right] U = 0 \quad (4.53)$$

with boundary conditions $U = D^2U = D^4U = 0$ at $z = 0$, $z = h$ and an internal boundary $z = 1$ at which U and D^jU ($j = 1$ to 5) are continuous. Rigid boundaries introduce such difficulties that no analytical treatment is useful.

In this simple geometry, solutions will be of the form:

$$U = u_1 \sin(m_1 z) + u_2 \sin(m_2 z) + u_3 \sin(m_3 z) \quad (4.54a)$$

in $0 \leq z < 1$

and

$$U = u_4 \sin h(m_4(z-h)) + u_5 \sin h(m_5(z-h)) + u_6 \sin h(m_6(z-h)) \quad (4.54b)$$

in $1 < z \leq h$

where m_1, m_2, m_3 are the roots from the cubic in m^2 :

$$(m^2 + a^2)^3 + Tm^2 = Ra^2 \quad (4.55a)$$

and m_4, m_5, m_6 from

$$(m^2 - a^2)^3 + Tm^2 = ARa^2 \quad (4.55b)$$

In principle, these can be solved for given a, T, R and then the matching condition at $z = 1$ leads to discrete eigenvalues for R , for the given a, T . In practice it will be difficult. We next describe the problem for large A , i.e. a strongly stably stratified region, whilst the following section (4.4) discusses

the problem of a thin unstable region imbedded in a stable stratification. Chapter 5 introduces numerical solutions of selected cases of interest.

Strong stable region, $A \gg 1$

Consider equation (4.55b) for the strongly stably stratified region :

$$(m^2 - a^2)^3 + Tm^2 = A Ra^2$$

If A is very large, we may assume that the rotational term Tm^2 is negligible, influencing the solution only through equation (4.55a), from which we expect

$$O(1) \leq a \leq O(T^{1/6}) \quad (4.56a)$$

$$o(1) \leq R \leq O(T^{2/3}) \quad (4.56b)$$

From (4.55b), we expect

$$|m| = O(ARa^2)^{1/6} \quad (4.57)$$

Let us consider two cases:

- 1) T small: $a = O(1)$, $R = O(1)$
and so $|m| = O(A^{1/6})$.

For large A , matching conditions at the boundary will tend to:

$$D^5 U(1_-) = D^5 U(1_+) \quad (4.58a)$$

and $D^4 U(1_-) = O(A^{-1/6}) \quad (4.58b)$

$$D^3 U(1_-) = O(A^{-2/6}) \quad (4.58c)$$

etc.

Thus the strong stable region acts as a very restrictive boundary to the unstable region $0 \leq z < 1$, as noted by Stix (1970) and Whitehead (1971).

$$2) \quad O(1) \ll T$$

Rotation dominates the unstable layer, so that

$$a = O(T^{1/6}) \quad (4.59a)$$

$$R = O(T^{2/3}) \quad (4.59b)$$

$$\text{Suppose } m = O(A^\mu) \quad (4.60a)$$

$$T = O(A^\tau) \quad (4.60b)$$

then we have terms in equation (4.55b) as follows:

$$m^6 = O(A^{6\mu}) \quad (4.61a)$$

$$m^4 a^2 = O(A^{4\mu + \tau/3}) \quad (4.61b)$$

$$m^2 a^4 = O(A^{2\mu + 2\tau/3}) \quad (4.61c)$$

$$a^6 = O(A^\tau) \quad (4.61d)$$

$$T m^2 = O(A^{2\mu + \tau}) \quad (4.61e)$$

$$ARa^2 = O(A^{1 + \tau}) \quad (4.61f)$$

If $\tau < 2$, the leading terms are

$$m^6 \quad \text{and} \quad ARa^2$$

giving $\mu = 1/6 (1 + \tau)$, so that the rotation increases μ and the decay rate, already rapid, of solutions in the stable region.

If $\tau = 2$, we have a balance of three terms,

$$m^6, \quad Tm^2, \quad ARa^2$$

with $\mu = 1/2, \quad \tau = 2$

If $\tau > 2$, we have a two term balance of Tm^2 against ARa^2 , so that $\mu = 1/2$

In each of these cases, the decay rate of the solutions in the stable region is rapid, and so the boundary $z = 1$ remains a very restrictive one. At finite but large values of A , the effect of increasing rotation is to increase m and so increase this restriction at $z = 1$. Thus rotation tends to reinforce the effect of the stable stratification.

4.4 Step-function temperature profile

An idealised case of the layered problem is that in which the unstable layer is reduced in depth whilst the temperature drop across it remains constant, so that the temperature profile tends towards a step-function. This may be imbedded in symmetric deep layers of neutrally or stably stratified fluid. For the non-rotating case with deep neutral surroundings, such a step-function profile will result in convective instability for an arbitrarily small temperature step, provided the problem will accommodate a sufficiently long horizontal wavelength. The aim of this section is to investigate the effect of rotation and of the stability of the surrounding layers on the critical Rayleigh number of such a step temperature profile.

We have a problem in defining a suitable length-scale, d ,

for this case: clearly the depth of the stable region is not useful. Two intrinsic measures exist, namely the stable gradient length-scale, over which the stable gradients result in an equal temperature change to that in the step, and the rotational Ekman depth, $d \equiv (\nu/\Omega)^{\frac{1}{2}}$. Since the case of neutrally stable layers is to be considered, the latter is adopted here. Clearly the form of analysis does not extend to the irrotational case.

Scaling on this length-scale, on the rotational time scale, $\tau \equiv \Omega^{-1}$, and a temperature scale of the unstable jump (ΔT), we get at marginal steady stability the equivalent of equation (4.6), namely:

$$\left[(D^2 - a^2)^3 + 4D^2 + R_1(z) \cdot a^2 \right] U = 0 \quad (4.62)$$

where $R_1(z) = - \left(\frac{g \alpha \sigma}{\Omega^2} \right) |\nabla T|$ in $z < 0$
and $z > 0$

$$= - R_s$$

and $R_1(z) = + \left(\frac{g \alpha \sigma}{\Omega^2} \right) \Delta T \cdot \delta(z)$ across $z = 0$

where $\delta(z)$ is the Dirac delta function, normalised by

$$\int_{-\infty}^{+\infty} \delta(z) \cdot dz = 1$$

In the stable regions, let us consider solutions of the form

$$U = u \cdot e^{mz} \cdot e^{iax}$$

which can be substituted into (4.62) to give:

$$(m^2 - a^2)^3 + 4m^2 - R_s a^2 = 0 \quad (4.63)$$

Across the unstable step, integration of (4.62)

shows that $D^5 U$ suffers a discontinuity,

$$D^5 U \Big|_{0^-}^{0^+} = a^2 U(0) \cdot \left(\frac{g\alpha\sigma}{\Omega^2} \cdot \Delta T \right) \quad (4.64)$$

and then $D^4 U$, $D^3 U$, $D^2 U$, DU and U are continuous.

Let us suppose that the stable gradients are 'weak' in so far as they allow convection on scales long compared with the Ekman depth, i.e. let us assume both

$$\left. \begin{array}{l} |a| \ll 1 \\ R_s \leq O(1) \end{array} \right\} \quad (4.65)$$

Further, let us assume that the roots of (4.63) are of the form:

$$m = m_0 + am_1 + a^2 m_2 + \dots \quad (4.66)$$

Substitution into equation (4.63) leads to

$$\begin{aligned} & (m_0^6 + 4m_0^2) + a(6m_0^5 m_1 + 8m_0 m_1^2) \\ & + a^2 (15m_0^4 m_1^2 + 6m_0^5 m_2 - 3m_0^4 + 8m_0 m_2 + 4m_1^2 - R_s) \\ & + O(a^3) = 0 \end{aligned} \quad (4.67)$$

The roots for m are in 2 groups, m small or $m = O(1)$

$$\begin{aligned} 1. \quad m_0 &= 0 \\ m_1 &= \frac{R_s^{1/2}}{2} \\ m_2 &= 0 \\ m_3 &= 0 \\ m_4 &= 0 \\ m_5 &= 1/4 R_s^{1/2} \quad \text{if } R_s^{1/2} \ll 1 \end{aligned} \quad (4.68)$$

$$2. \quad m_0^4 = -4$$

$$\therefore m_0 = \sqrt{2} \cdot \exp\left(\frac{i\pi}{4}(2n-1)\right) \quad (4.69)$$

(for integer n)

$$m_1 = 0$$

$$m_2 = \frac{\sqrt{2}}{32} \cdot (12-R_s) \cdot \exp\left(\frac{-i\pi}{4}(2n-1)\right)$$

Thus a general solution in the region $z > 0$, applying a boundary condition that the motions decay to infinity, is:

$$U = A_1 e^{-\mu z} + B_1 e^{-\nu z} \cos \rho z + C_1 e^{-\nu z} \sin \rho z \quad (4.70)$$

where $\mu = \frac{aR_s^{\frac{1}{2}}}{2} + \frac{a^5}{4R_s^{\frac{1}{2}}}$

$$\nu = 1 + \frac{a^2(12-R_s)}{32} + O(a^4)$$

$$\rho = 1 - \frac{a^2(12-R_s)}{32} + O(a^4)$$

the corresponding general solution in $z < 0$ is:

$$U = A_2 e^{+\mu z} + B_2 e^{+\nu z} \cos \rho z + C_2 e^{+\nu z} \sin \rho z \quad (4.71)$$

The constants $A_1, B_1, C_1; A_2, B_2, C_2$ are linked by the 5 continuity conditions at the boundary region $z = 0$. The algebra

is given in Appendix 1, leading to

$$A_1 = A_2 = A \quad (4.72a)$$

$$B_1 = B_2 = \frac{\mu(\rho^2 - 3v^2)}{2v(v^2 + \rho^2)} \cdot A \quad (4.72b)$$

$$C_1 = -C_2 = \frac{\mu(3\rho^2 - v^2)}{2\rho(v^2 + \rho^2)} \cdot A \quad (4.72c)$$

and the difference in D^5U across the step in temperature is given by:

$$D^5U \Big|_{0^-}^{0^+} = \left(\frac{g\alpha\sigma a^2 \cdot \Delta T}{\Omega^2} \right) (A + B)$$

$$= -2\mu^5 A + 2B_1 v(-v^4 + 10v^2\rho^2 - 5\rho^4) + 2C_1 \rho(5v^4 - 10v^2\rho^2 + \rho^4) \quad (4.73)$$

from Appendix 1.

Noting that μ, B, C are $O(a)$ or less

$$\text{and } \mu, \rho \text{ are } [1 + O(a^2)]$$

we get the approximate relationship, to $O(a^3)$

$$\left(\frac{g\alpha\sigma a^2 \cdot \Delta T}{\Omega^2} \right) (1 - \mu/2) = 8(-\mu/2) - 8(\mu/2) + O(a^2\mu) \quad (4.74a)$$

$$\therefore \left(\frac{g\alpha\sigma a^2 \cdot \Delta T}{\Omega^2} \right) = -8\mu + O(a^2\mu) + O(\mu^2) \quad (4.74b)$$

$$\therefore \left(\frac{g\alpha\sigma \cdot \Delta T}{\Omega^2} \right) = - \left[\frac{4 R_S^{\frac{1}{2}}}{a} + \frac{2 a^3}{R_S^{\frac{1}{2}}} \right] + O(\mu) \quad (4.74c)$$

The critical Rayleigh number thus calculated is minimised by choosing

$$a = \left(\frac{2 R_S}{3} \right)^{\frac{1}{4}} \quad (4.75)$$

Accordingly, the expansion of m in terms of a as a small parameter is only valid for very small values of R_s ($R_s = O(a^4)$). Further, the critical Rayleigh number is then

$$\left(\frac{g \alpha \sigma_s \Delta T}{\Omega^2} \right)_c \equiv R_c = \frac{16}{3} \left(\frac{3}{2} R_s \right)^{\frac{1}{4}} + O(\mu) \quad (4.76)$$

which is itself $O(a)$.

The "waveform" for U in the stable regions $z < 0$ and $z > 0$ is a combination of a slow exponential decay function of the form $e^{-\mu z}$, which may be identified with the conventional decay solution in an homogeneous stable layer, and an oscillatory convective wave of the form $e^{-\nu} \cos \rho z$ or $e^{-\nu} \sin \rho z$, where ρ and ν are of order unity. These latter therefore have a "wavelength" of order the Ekman depth $d_2 \equiv (\nu/\Omega)^{\frac{1}{2}}$, decaying on the same scale. Thus increased rotation rates lead to shorter length scales for the convective wave-like part of the solution. In turn, this may be regarded as a lesser extent of penetration into the stable regions, if one regards the other, $e^{-\mu z}$, part of the wave form as being just a response to the forcing by the $e^{-\nu z} \cos \rho z$ and $e^{-\nu z} \sin \rho z$ convection. That $e^{-\mu z}$ response is on a decay wavelength, in dimensional terms of

$$\begin{aligned} \text{wavelength} &= \mu^{-1} \cdot \left(\frac{\nu}{\Omega} \right)^{\frac{1}{2}} \\ &= O \left(\Omega^{3/2} \times \Omega^{-\frac{1}{2}} \right) \\ &= O(\Omega) \end{aligned} \quad (4.77)$$

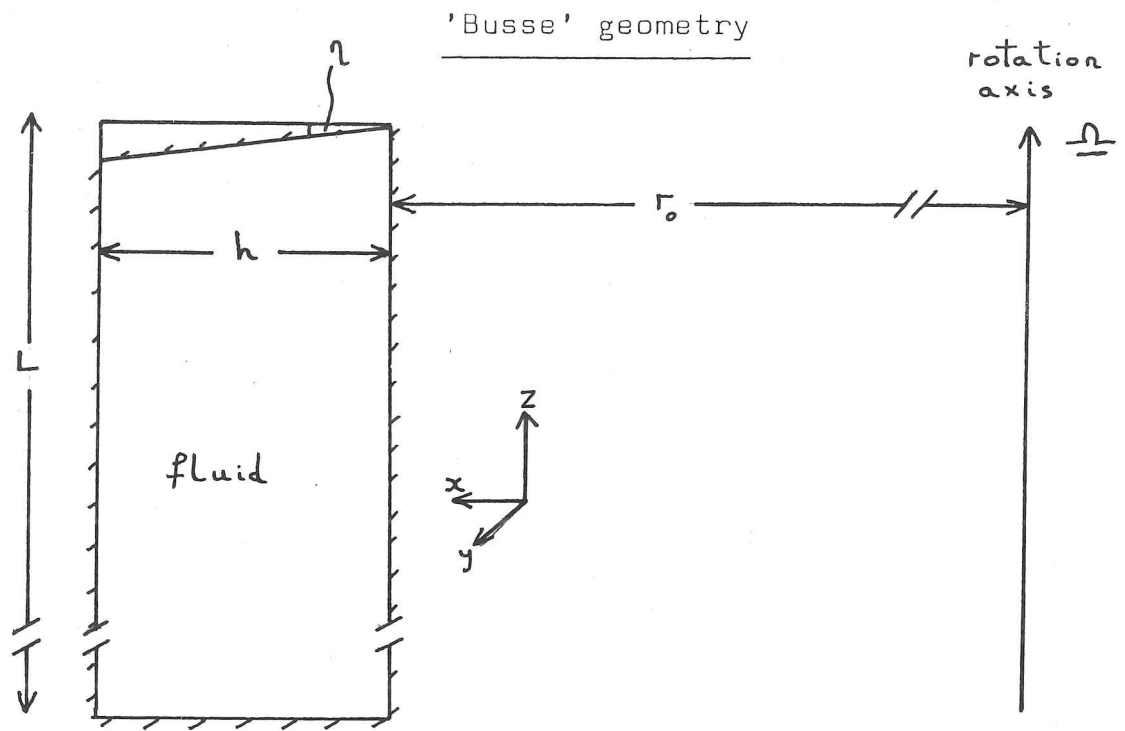
Thus this decay function is on a longer length-scale as rotation increases.

This analysis fails for $R_S \geq O(1)$ since the horizontal wavenumber a , used as the expansion parameter, is then no longer small. In such a case, the roots for m (equation 4.63) no longer divide into one pair of "small" roots and two pairs of $O(1)$ roots and so the analysis of the complete solutions in each stable layer becomes unwieldy. As one moves to the other extreme, $R_S \gg 1$, the problem becomes rather ill-posed physically in that one expects very short wave lengths to be involved, with rotation becoming of negligible importance. These cases will not be pursued further.

4.5 Rotation perpendicular to gravity: "Busse-Rolls"

Busse (1970) considered the case of the onset of convection in a thin cylindrical annulus rotating about its axis with a radial body-force, following earlier work by Roberts (1968). His analysis drew attention to the role of the end-walls at top and bottom of the annulus in inhibiting convection through the dissipation in the end-wall boundary layers and, if inclined, in restricting the radial extent of the motion. The latter effect allowed the application of the model, which uses locally rectangular coordinates to simplify the analysis, to the deep spherical shell that models the Earth's outer core. In this section, this analysis is extended to the case of penetrative convection and is then, in chapter 6, applied to observations made using a rapidly rotating cylindrical tank. Figure 4.3 shows the geometry involved.

Fig. 4.3



This geometry, in which axial variations of the flow are negligible except for the flows induced by the boundary layers, results in the equations being reduced to 6th order. The axial (\hat{z}) variation of the radial (\hat{x}) component of vorticity is converted into an operator on the radial velocity through the boundary layer theory (Greenspan, 1968).

Taking the linear Navier-Stokes equations for the perturbations \underline{u} , ϑ , $\underline{\zeta}$ of velocity, temperature and vorticity, radial component of velocity:

$$\frac{\partial}{\partial t} (\nabla^2 u_x) = \nu \nabla^4 u_x - \alpha g \frac{\partial^2 \vartheta}{\partial y^2} - 2 \Omega \frac{\partial}{\partial z} (\zeta_x) \quad (4.78a)$$

(where $g = \Omega^2 r_0$ is taken to be constant), heat flow:

$$\frac{\partial}{\partial t} (\vartheta) = -\underline{u}_x \cdot \frac{\partial \theta}{\partial x} + \kappa \nabla^2 \vartheta \quad (4.78b)$$

radial component of vorticity:

$$\frac{\partial}{\partial t}(\zeta_x) = \nu \nabla^2 \zeta_x + 2 \Omega \frac{\partial}{\partial z} (u_x) \quad (4.78c)$$

In the limit of rapid rotation, we use boundary layer theory to give the induced boundary flows at the top and bottom surfaces ($z = \pm L/2$) and thereby decouple the third equation

$$\underline{u}_n = - \frac{E^{1/2} L \cdot \underline{n} \cdot \nabla \wedge \left[(\underline{n} \wedge \underline{v}) + \frac{\underline{n} \cdot \underline{z}}{|\underline{n} \cdot \underline{z}|} \underline{v} \right] / |\underline{n} \cdot \underline{k}|^{1/2}}{2} \quad (4.79)$$

where $E \equiv (\nu/L^2 \Omega)$, \underline{n} is the normal to the boundary layer and \underline{z} the axis of rotation (Greenspan, 1968, eq'n 2.17.3). This gives:

$$\frac{\partial u_z}{\partial z} = -E^{1/2} \left[\frac{\partial u_y}{\partial x} - \frac{\partial u_x}{\partial y} \right] - \frac{1}{L} \left[\eta_1 u_x + \eta_2 u_y \right] + O(E) u_x \quad (4.80)$$

$$\text{and } \frac{\partial \zeta_x}{\partial z} = +E^{1/2} \left[\frac{\partial^2 u_x}{\partial x^2} + \frac{\partial^2 u_x}{\partial y^2} \right] - \frac{1}{L} \left[\eta_1 \frac{\partial u_x}{\partial y} - \eta_2 \frac{\partial u_x}{\partial x} \right] \quad (4.81)$$

where η_1, η_2 are small inclinations of one boundary in the \hat{x}, \hat{y} directions from being a plane perpendicular to the axis of rotation.

Substituting for $\frac{\partial \zeta_x}{\partial z}$, one gets

$$\left[(\nu \nabla^4 - p \nabla^2) + 2 \Omega \left(-E^{1/2} \nabla_H^2 + \frac{\eta_1}{L} \frac{\partial}{\partial y} - \frac{\eta_2}{L} \frac{\partial}{\partial x} \right) \right] u_x = \alpha g \frac{\partial^2 \theta}{\partial y^2} \quad (4.82a)$$

$$\text{and } \beta_0 f(x) u_x = [K \nabla^2 - p] \theta \quad (4.82b)$$

where p is the growth-rate of the perturbation. Let us now use normalised variables, indicated by primes, based on scales:

length L

time L^2/ν

temperature $\beta_0 d$, where d is the unstable layer

depth, and write $\alpha = L/d$, the aspect ratio. L is used as

the primary length-scale because of the boundary layer behaviour depending on $E \equiv \nu/L^2\Omega$

$$\left[(\nabla'^4 - p' \nabla'^2) + 2E^{-1} \left(-E^{1/2} \nabla_H'^2 + \eta_1 \frac{\partial}{\partial y'} + \eta_2 \frac{\partial}{\partial x'} \right) \right] u'_x = \frac{\alpha g \beta_0 d L^3}{\nu^2} \frac{\delta \theta'}{\delta y'^2} \quad (4.83a)$$

$$\text{and } \sigma \mathbf{a} \cdot \mathbf{f}(x') u'_x = [\nabla'^2 - \sigma p'] \vartheta' \quad (4.83b)$$

$$\text{Now write } F \equiv \frac{\alpha g \beta_0 d L^3 b^2}{\nu^2} \vartheta' \quad (4.84a)$$

$$U \equiv u'_x \quad (4.84b)$$

$$R \equiv \frac{\alpha g \beta_0 d^4}{\nu \kappa} \quad (4.84c)$$

$$\text{and } -b^2 = \frac{\partial^2}{\partial y'^2} \quad (\text{azimuthal dependence}) \quad (4.84d)$$

$$\left[\nabla'^2 (\nabla'^2 - p') - 2E^{-1/2} \nabla_H'^2 + 2E^{-1} \left(\eta_1 \frac{\partial}{\partial y'} - \eta_2 \frac{\partial}{\partial x'} \right) \right] U = -F \quad (4.85a)$$

$$\left[R \mathbf{a} \cdot \mathbf{b}^2 \cdot \mathbf{f}(x') \right] U = [\nabla'^2 - \sigma p'] F \quad (4.85b)$$

Note that R is defined here in a "conventional" manner, in terms of the depth of the unstable layer.

Some numerical solutions for the two equations (4.85a) and (4.85b) with various boundary conditions will be investigated in §5.5. These will explore the effect of rotation on an idealised penetrative convection profile, $f(x') = \cos\left(\frac{\pi \mathbf{a} \cdot \mathbf{x}'}{2}\right)$, for various boundary positions. The same numerical scheme will also be applied in §5.5 to a simulation of the experimental observations of chapter 6.

If one considers the equations (4.85a) and (4.85b) in comparison with the case of \mathbf{g} parallel to $\underline{\Omega}$ given by equations 4.1a

to 4.1c, it is clear that much higher rotation rates are going to be necessary for the rotation to be dominant, in that rotation only appears as a term in $E^{-1/2} \nabla'^2 U$ and as one in $E^{-1} \eta \frac{\partial U}{\partial x'}$, instead of as $T \frac{\partial U}{\partial z}$ in equation 4.1 (note: $T \equiv 4E^{-2}$). This is because in the present case the convective transport of heat is transverse to the rotation axis and is therefore not affected by the rotation except through the effects of the top and bottom boundaries. These latter are a secondary effect on the flow. Busse (1970) considered the special case of constant temperature gradient and cylindrical symmetry

$$f(x') = 1$$

$$\eta_2 = 0$$

with constant temperature, stress-free boundaries so that solutions were of the form

$$U = \sin(a x') \sin(b y')$$

where $a = \pi a$ to fit the boundary conditions.

By considering the real and imaginary parts of equations (4.85a) and (4.85b), remembering that at the onset of convection there can be an imaginary part to the growth-rate p' ,

$$p' = i \omega,$$

one gets

$$\omega = \frac{-2\eta b}{2\sigma E^{1/2} + (\sigma+1)(a^2+b^2)E} \quad (4.86)$$

and then

$$R a^4 b^2 = (a^2 + b^2)^3 + 2 E^{-1/2} (a^2 + b^2)^2 + \frac{(2\eta_1 b \sigma)^2 (a^2 + b^2 + 2 E^{-1/2})}{((\sigma + 1)(a^2 + b^2) E + 2 \sigma E^{1/2})^2} \quad (4.87)$$

This notation differs from that used by Busse (1970) in order to give a "conventional" definition for R and to show the relative contributions to the Rayleigh number from Bénard-type convection, from boundary-layer suction and from end-wall inclination respectively. One can use this special case with its relatively simple solution to determine the conditions under which each of these mechanisms should be dominant, still following Busse (1970)

Case (i) $a \gg E^{-1/4}$ (cp Busse (1970) misprint, $a \gg E^{-1/2}$)
 $\eta_1 \ll E^{1/4} \sigma^{-1}$

Bénard-type convection

$$b_c = \frac{a}{\sqrt{2}} \quad (4.88a)$$

$$(R a^4)_c = \frac{27}{4} a^4$$

$$R_c = \frac{27}{4} \pi^4 \quad (4.88b)$$

Case (ii) $a \ll E^{-1/4}$
 $\eta_1 \ll E^{1/4} \sigma^{-1}$

Boundary-layer dominates

$$b_c = a \quad (4.89a)$$

$$\begin{aligned} (Ra^4)_c &= 8E^{-1/2} a^{+2} \\ R_c &= 8\pi^2 E^{-1/2} a^{-2} \end{aligned} \quad (4.89b)$$

Case (iii) $1 \gg \eta_1 \gg E^{1/4} \sigma^{-1}$

and $\eta_1 \gg a^3 E \sigma^{-1}$

End-wall inclination dominates

$$b_c = \left(\frac{\sqrt{2} \eta_1 \cdot \sigma}{E(\sigma+1)} \right)^{1/3} \quad (4.90a)$$

$$(Ra^4)_c = 3 \left(\frac{\sqrt{2} \eta_1 \cdot \sigma}{E(\sigma+1)} \right)^{4/3} \quad (4.90b)$$

$$\omega_c = - \left(\frac{4\sqrt{2} \eta_1^2}{E^2 \sigma (\sigma+1)^2} \right)^{1/3} \quad (4.90c)$$

Now we can see that the effect of rotation is to shift the emphasis away from interior dissipation (case 1) towards Ekman layer dissipation (case 2). Further, as rotation increases, it becomes more likely that any inclination will become significant. In the limit $T \rightarrow \infty$, for finite aspect ratio a , one gets either

$$R_c \propto T^{1/4} a^{-2} \quad \text{for zero inclination} \quad (4.91a)$$

$$\text{or } R_c \propto T^{2/3} a^{-4} \quad \text{for finite inclination} \quad (4.91b)$$

Thus in any practical situation, one can expect

$$R_c \propto T^{2/3} \quad \text{as } T \rightarrow \infty \quad (4.92)$$

as end-wall inclination will come to dominate the onset of convection. However, the numerical solutions in the next chapter

are for the case $\eta = 0$ in order to model the experimental cylindrical tank. This also avoids the oscillatory nature of the marginal solution that necessarily accompanies any significant inclination.

4.6 Thermal wind

The 'thermal wind' is the azimuthal velocity field that balances Coriolis forces against baroclinic buoyancy forces in a rotating system. It is not a primary feature of any part of this work, but does occur in the experimental work reported in chapter 6 and so a brief summary of the theory describing it is given here. A more complete review is given by Pedlosky (1979): the following deals only with the nature of the thermal wind, not with the instabilities that arouse interest in atmosphere studies.

The convection theory that has been dealt with considers cases of unstable equilibrium: $\underline{g} \cdot \nabla \rho < 0$, $\underline{g} \wedge \nabla \rho = 0$. If $\underline{g} \wedge \nabla \rho \neq 0$, i.e. if the gravity and density gradients are inclined to each other rather than being antiparallel, then there is an overturning force acting on the fluid, generating vorticity. In a non-rotating system such a baroclinic density distribution leads to convection and the system cannot be in static equilibrium. Rotation of the system introduces the possibility of the existence of azimuthal flows that, through the Coriolis force, set up a dynamic pressure field to balance the buoyancy forces and so prevent convection. The creation of such a flow pattern involves the deflection of the initial convection flows (which obey Ekman boundary layer theory in a rapidly rotating system) by the Coriolis forces until a dynamic equilibrium is reached: this time dependent behaviour is not

dealt with here. A similar problem in stellar fluid dynamics is that of Eddington-Sweet currents, which should be modified by rotational effects (Busse, 1981).

Consider the non-linear vorticity equation:

$$\frac{\partial \omega}{\partial t} + (\underline{u} \cdot \nabla) \omega = \frac{\nabla \rho \wedge \underline{g}}{\rho} + \nabla \wedge \underline{g} + \nu \nabla^2 \omega + 2(\underline{\Omega} \cdot \nabla) \underline{u} \quad (4.93)$$

The body force acceleration \underline{g} , which may be a combination of gravity and of centrifugal accelerations, is conservative, so that $\nabla \wedge \underline{g} = 0$. Let us consider the azimuthal ($\hat{\phi}$) component of vorticity in the steady state ($\frac{\partial \omega}{\partial t} = 0$):

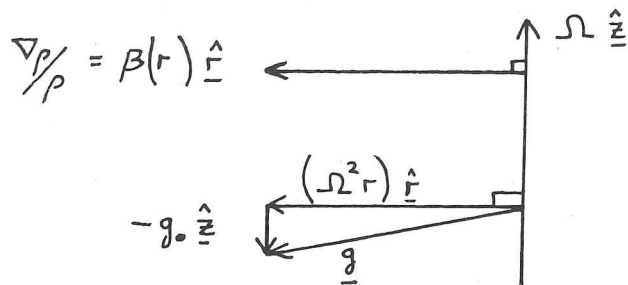
$$(\underline{u} \cdot \nabla) \omega_{\phi} = \left(\frac{\nabla \rho \wedge \underline{g}}{\rho} \right)_{\phi} + \nu \nabla^2 \omega_{\phi} + 2 \Omega \frac{\partial}{\partial z} (u_{\phi}) \quad (4.94)$$

In the case of slow rotation or in the neighbourhood of boundaries the viscous term is significant. However, in many geophysical applications the typical length-scale L of the system is sufficiently large that we can consider the rapid-rotation limit in the interior of the fluid:

$$(\underline{u} \cdot \nabla) \omega_{\phi} = \left(\frac{\nabla \rho \wedge \underline{g}}{\rho} \right)_{\phi} + 2 \Omega \frac{\partial}{\partial z} (u_{\phi}) + O(E) \quad (4.95)$$

where $E \equiv \nu / \Omega L^2$, the Ekman number, is small. This holds in the atmosphere or core for $L \gtrsim 1$ m if we consider non-turbulent processes and take $\nu \approx 10^{-7} \text{ m}^2 \text{ s}^{-1}$ for the core or $\nu \approx 10^{-5} \text{ m}^2 \text{ s}^{-1}$ for air.

Now let us consider the specific cylindrical geometry of the experiments described in chapter 6.



There is cylindrical symmetry and the dominant body force in the region of interest ($r \approx r_0$) is the radial centrifugal force. However there is also an axial body force, the laboratory gravity, $-g_0 \hat{z}$. It is this that gives rise to baroclinic effects.

$$u_r \cdot \frac{\partial \omega_\phi}{\partial r} + u_z \cdot \frac{\partial \omega_\phi}{\partial z} = \beta(r) g_0 + 2 \Omega \cdot \frac{\partial u_\phi}{\partial z} \quad (4.96)$$

Neglecting boundary layer effects, we can put $u_r = u_z = 0$ and hence get a solution:

$$u_\phi = - \frac{\beta(r) \cdot g_0 \cdot (z + c)}{2\Omega} \quad (4.97)$$

for some constant c , zero if there is symmetry about $z = 0$.

This solution requires modification for the effect of Ekman boundary layers on the rigid surfaces of the experimental tank, similarly there are internal viscous forces arising from the non-uniformity of the flow and it assumes cylindrical symmetry. That symmetry is broken in certain of the experiments by the introduction of a radial thermistor array.

Rigid surfaces

Following Greenspan (1968), the modification to the interior flow arising from the surface $z = \pm L/2$ is an axial flow (i.e. normal to the surfaces)

$$\begin{aligned}
u_z &= - \frac{E^{1/2} L}{2} \left[\frac{\partial u_\phi}{\partial r} + \frac{u_\phi}{r} \right]_{z = L/2} \\
&= + \frac{\nu^{1/2} g_0 L}{8 \Omega^{3/2}} \left[\frac{\partial \beta(r)}{\partial r} + \frac{\beta(r)}{r} \right]
\end{aligned}
\tag{4.98}$$

Note that this velocity is constant with respect to z and represents a flow from one Ekman boundary layer to the other, its sign depending on $\beta(r)$. The counterflow to maintain the boundary layers occurs in the inner side-wall boundary layer (thickness $O(E^{1/3})$). Side-wall boundary conditions are satisfied over a thicker ($O(E^{1/4})$) boundary layer. In the limit of rapid rotation ($E \rightarrow 0$), these sidewall effects are negligible compared with the end surface $z = \pm L/2$. Greenspan (1968) gives a description of the various boundary layers (§ 2.18).

Internal shear

The boundary layer suction velocity is correct only to $O(E^{1/2})$ and cannot accurately describe a basic state for any finer corrections. Internal shears, leading to viscous stresses, are of $O(E)$, provided that the radial variation of $\beta(r)$ is on a length-scale comparable to L . Only if variations of $\beta(r)$ are on radial length scales $O(E^{1/2})L$ or less do internal shears become significant compared to the boundary layer suction in modifying the velocity profile. Accordingly such effects are ignored in this work.

Lack of symmetry

The experimental tank is cylindrically symmetric except in the cases in which a radial thermistor array is deployed. The array acts as a radial barrier to azimuthal flows by virtue of changing the available depth of the tank: a geostrophic path of constant depth is no longer available for the thermal wind. The change of depth is approximately 6 mm in a tank of depth 200 mm, much greater than the Ekman layer thickness. Such a change of depth can support a pressure difference sufficient to prevent the

thermal wind if its Rossby number $\epsilon \equiv U/d\Omega$ is small, where d is the length-scale of the obstacle and U the thermal wind speed in the absence of the obstacle. In a typical experiment,

$$\begin{aligned}\beta &\approx 10^{-2} \text{ m}^{-1} \\ g_0 &\approx 10 \text{ m s}^{-2} \\ 2\Omega &\approx 10^2 \text{ rad.s}^{-1} \\ z &\approx 10^{-1} \text{ m}\end{aligned}$$

so the expected thermal wind velocity is

$$U \approx 10^{-4} \text{ ms}^{-1}$$

and the critical depth d for "blocking" on the criterion $\epsilon \ll 1$ is

$$\begin{aligned}d &\gg U/\Omega \\ &\gg 10^{-6} \text{ m}\end{aligned}$$

The Ekman layer thickness is of order 10^{-4} m and so is of more significance in this case than the Rossby number criterion: obstacles can only have a "blocking" effect if they are large enough to affect the internal region of inviscid flow.

Clearly any feasible radial thermistor array is likely to act as an effective barrier to the thermal wind. On the other hand, isolated bumps in the top and bottom boundaries have no comparable blocking effect, provided there exist geostrophic paths around such bumps. The radial array effectively changes the degree of connectedness of the cylindrical annulus, owing to the combination of its "large" size and its continuity across the annulus.

The effect of the blocking of the thermal wind by the

thermistor array is to eliminate the dynamic pressure field that opposes the buoyancy forces associated with the laboratory gravity. It is for this reason that the measured temperature profiles in § 6.3 are distorted by the convective heat transport, compared with the experiments performed without the thermistor array. Note that similar experiments performed in a spherical tank would not suffer such an effect, as geostrophic paths exist around a radial array (by deflection inwards in radius, to enjoy a matching increase in depth between the spherical boundary walls). (fig. 6.8).

5. Numerical solutions to the linear equations

5.1 Shooting program

In the last chapter it is apparent that analytical solutions even of the linear equations in convenient geometries are rarely simple, or indeed obtainable. On the other hand, numerical integration of simultaneous linear differential equations such as (2.11) is generally quite easy, using a standard integration routine, and such integrations may therefore be used to test the result of 'guesses' for the desired eigenvalue R , the Rayleigh number, and thence to find the eigenvalues by an iterative routine. The problem becomes one of finding a starting condition, in terms of both initial values for the variables at one boundary and of the parameter R , such that integration of the differential equations through the region of the problem yields values for the variables at the boundaries that fit the boundary conditions. Only one dimensional regions of integration are investigated in this work, owing to the simple geometries of the problems investigated. This method is known as a "shooting" method of finding eigenvalues and functions of such problems. It involves both a linear inversion of results from trial integrations in order to fit all but one of the boundary conditions by varying the starting values for the variables, and a non-linear iteration in the parameter R to fit the final boundary-condition. In general we are dealing with simultaneous differential equations in $(2n)$ variables, with (n) boundary conditions on each of the two boundaries, and this requires a linear inversion of a $((n-1) \times (n-1))$ results matrix followed by the non-linear iteration. The case $n = 1$ occurs, in the plane layer problem in the limit $T \rightarrow \infty$ (see § 4.2 for analysis), and

in this there need be no linear inversion stage: the one unknown variable at the opening boundary can be normalised to unity. $n = 4$ or 8 is required for the general plane layer problem, the latter if overstability is to be considered. $n = 3$ is required for the cylindrical annulus problem, with end-walls of zero inclination.

The program will now be described in the version for $n = 4$, appropriate for solving the steady convection problem in a plane layer (see flowchart in Fig. 5.1). The equations to be solved are (2.11) which are:

$$\begin{aligned} [D^2 - a^2] Z &= -T \cdot DU \\ [D^2 - a^2]^2 U &= DZ + F \\ [D^2 - a^2] F &= -Ra^2 \cdot f(z) \cdot U \end{aligned}$$

The shooting program treats these as the following eight simultaneous equations (subroutine 'RHT')

$$\begin{aligned} D Y(8) &= -T Y(2) + a^2 Y(7) \\ D Y(7) &= Y(8) \\ D Y(6) &= -(R F(Z) a^2) Y(1) + a^2 Y(5) \\ D Y(5) &= Y(6) \\ D Y(4) &= Y(5) + Y(8) + 2a^2 Y(3) - a^4 Y(1) \\ D Y(3) &= Y(4) \\ D Y(2) &= Y(3) \\ D Y(1) &= Y(2) \end{aligned}$$

where U, DU, D^2U, D^3U are to be identified with $Y(1)$ to $Y(4)$, F, DF with $Y(5), Y(6)$ and Z, DZ with $Y(7), Y(8)$ respectively. Integration of these equations over the interval $Z = 0$ to $Z = h$ is performed by a standard 4th order Runge-Kutta integration subroutine ('RKM'), from Dr. Busse's group at UCLA, modified to

Subroutine

Fig. 5.1

Flowchart for the
'SHOOTING' program.

MAIN

Set geometry and
Taylor number.

MAIN

Set horizontal
wavenumber 'a'.

SOLVE

Set Rayleigh number.

SOLVE

Set four initial
boundary conditions.

RHT / RKM

Runge-Kutta integration.

INVERT

Linear inversion to fit three
closing boundary conditions.

SOLVE

Calculate error in the
fourth boundary condition.

CONVRG

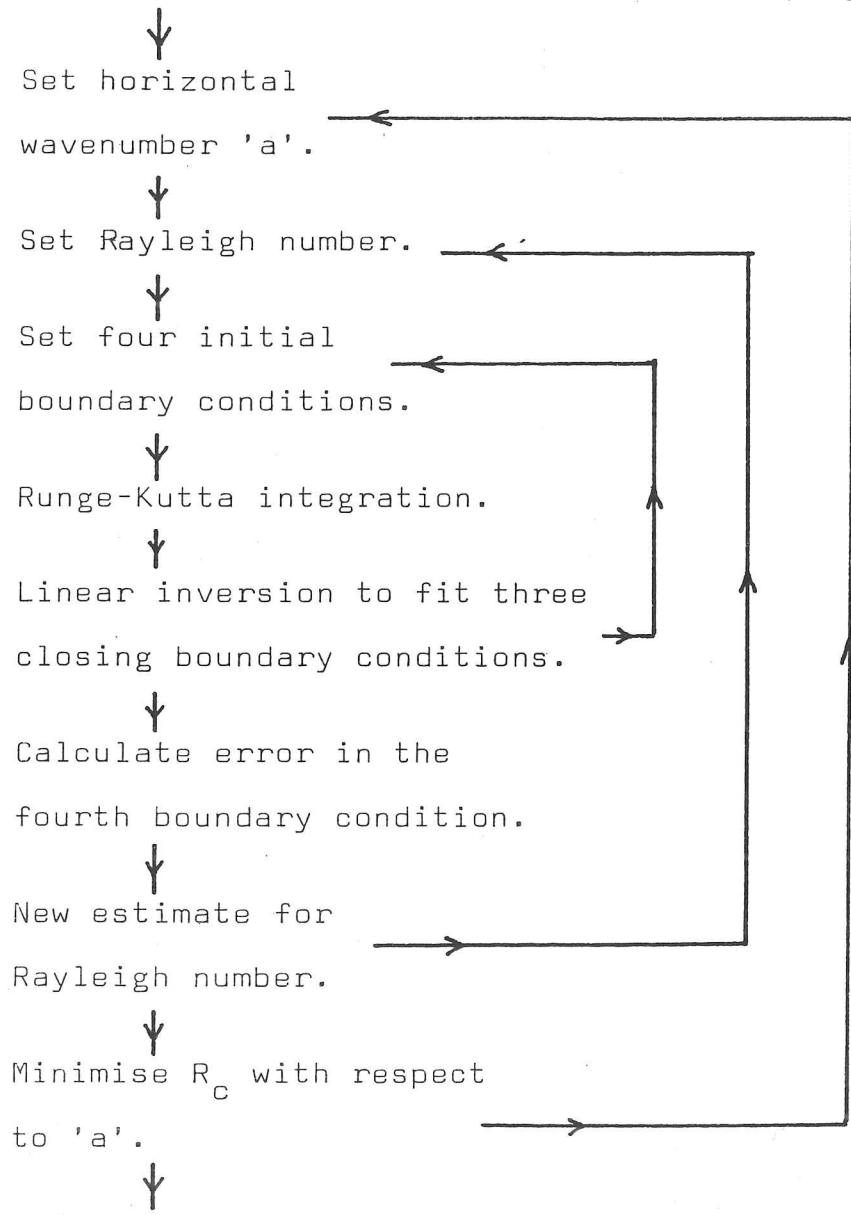
New estimate for
Rayleigh number.

MAIN /
PARAB

Minimise R_c with respect
to 'a'.

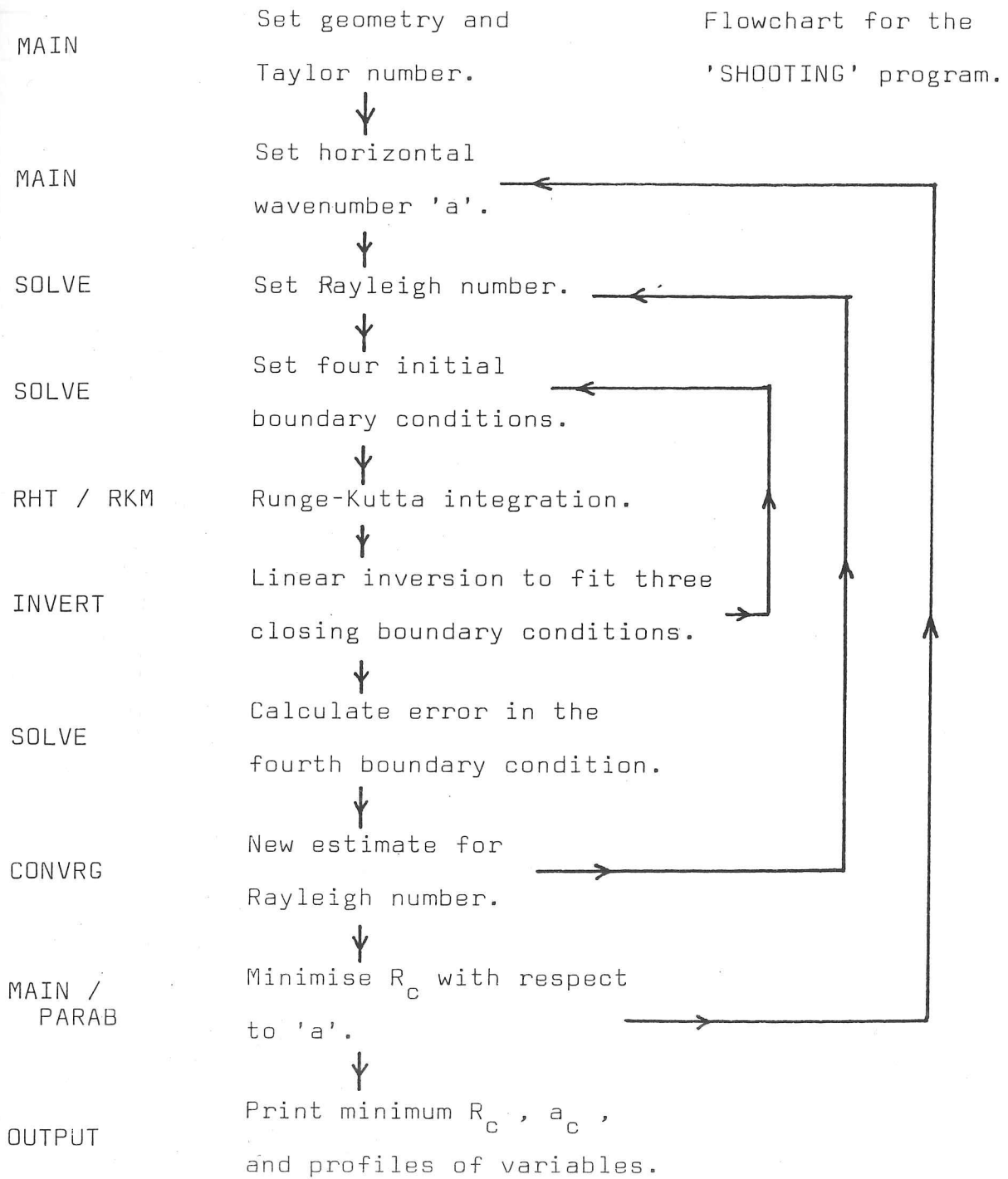
OUTPUT

Print minimum R_c , a_c ,
and profiles of variables.



Subroutine

Fig. 5.1



incorporate a shortened step length ($\times 1/10$) in the step nearest the boundaries in order to improve the resolution of boundary layers.

Typical opening boundary conditions at $Z = 0$ are (rigid, constant temperature boundary):

$$U \equiv Y(1) = 0$$

$$DU \equiv Y(2) = 0$$

$$F \equiv Y(5) = 0$$

$$Z \equiv Y(7) = 0$$

which leaves four opening values to be set, which can be expressed as a vector \underline{X} :

$$\underline{X} \equiv (x_1, x_2, x_3, x_4)$$

for the opening boundary values ($z = 0$)

$$Y(3) = x_1$$

$$Y(4) = x_2$$

$$Y(6) = x_3$$

$$Y(8) = x_4$$

After integration, one has an 'error' value on each of the closing boundary conditions, which can be expressed as a vector \underline{E} :

$$\underline{E} \equiv (e_1, e_2, e_3, e_4)$$

where at the closing boundary, again taking a rigid constant temperature boundary as our example,

$$Y(1) = e_1$$

$$Y(2) = e_2$$

$$Y(5) = e_3$$

$$Y(7) = e_4$$

The aim is now $\underline{E} \equiv 0$, and we can achieve this by varying \underline{X} and the parameter R . From inspection of the equations (2.11), \underline{E} is a linear function of \underline{X} . Trial integrations are made with

$$\underline{X}_1 = (1, 0, 0, 0)$$

$$\underline{X}_2 = (0, 1, 0, 0)$$

$$\underline{X}_3 = (0, 0, 1, 0)$$

and $\underline{X}_4 = (0, 0, 0, 1)$

and a results matrix F (3 x 3) constructed

$$F_{ij} = e_j(\underline{X}_1) - e_j(\underline{X}_i)$$

for $i, j = 2, 3, 4$ (subroutine 'SOLVE')

This matrix is then inverted to give the input initial conditions \underline{X} , normalised as

$$\underline{X} = (1, x_2, x_3, x_4)$$

that will yield

$$\underline{E}(\underline{X}) = (e_1, 0, 0, 0)$$

so that three boundary conditions are satisfied (subroutine 'INVERT').

If $n = 3$ or $n = 4$, the inversion routine is explicit and algebraic but for the program version $n = 8$ the inversion routine is a standard Gauss-Jordan inversion, from Dr. Busse's group at UCLA.

We now have an error estimate, e_1 , for our chosen value R and the set parameters $a, T, h, f(z)$. The object now is to reduce e_1 to zero by manipulation of R and then to test the effect on this eigenvalue R of varying the horizontal wavenumber a . The minimum of R with respect to a yields the critical Rayleigh number R_c and wavenumber a_c for the given conditions.

Manipulation of R is performed by a Newton-Raphson iteration subroutine (CONVRG), which includes tests on successive values of R to deal with both diverging predictions and the physically unacceptable prediction of negative R . Iteration continues until the error estimate e_1 has been reduced by some preset factor, typically 10^3 , which is taken as being adequate convergence.

Minimisation of R with respect to a is achieved by the adoption of linearly stepped values of a until the result $R(a)$ is found to increase. The last 3 results

$$R(a_0 - 2\delta)$$

$$R(a_0 - \delta)$$

$$R(a_0)$$

where δ is the steplength and $R(a_0) > R(a_0 - \delta)$, are fitted by a parabola in 'a' (subroutine PARAB, from E. Bolton, UCLA) to give a prediction for the minimum in $R(a)$ at some value a_1 of a . The computation of R is then repeated for

$$a = a_1 - \delta / 10$$

$$a = a_1$$

$$a = a_1 + \delta / 10$$

and 'PARAB' employed again to give a final prediction of R_c, a_c , which is then tested by computing $R(a_c)$.

Thus we have a value for the critical Rayleigh number R_c and wavenumber a_c for the set boundary conditions, rotation rate (T), fluid depth (L) and temperature profile ($f(z)$). Inspection of the form of the eigenfunctions for $Y(1)$ to $Y(8)$ acts as a check both on the adequacy of the convergence and on whether the lowest eigenvalue has been found. Judicious selection of the initial guesses for the Rayleigh number 'R' and the range of wavenumbers 'a' tested is of practical importance in running the program: if prior knowledge of similar set conditions is not available, it is best to perform an initial study of the results for a sequence of values of 'R' and of 'a', by switching the routines 'CONVRG' and 'PARAB' out of the program.

Boundary conditions (n = 4 version, as example)

- 1) Impermeable boundary: $Y(1) = 0$
- 2) Either a) rigid boundary: $Y(2), Y(7) = 0$
or b) stress-free boundary: $Y(3), Y(8) = 0$
- 3) Either a) perfectly conducting: $Y(5) = 0$
or b) fixed flux: $Y(6) = 0$
or c) finite conductivity, Biot number $\lambda = k_s/l.k_f$

where k_s is wall conductivity,

k_f is fluid conductivity

and l is non-dimensional wall thickness,

$$\Phi \equiv \lambda Y(5) \pm Y(6) = 0$$

where the sign depends on which boundary is being considered.

Various combinations of these are reported in the following results. Condition (3c) is only used in the case of the cylindrical annulus, in order to model the experimental tank.

5.2 Testing the program

To an extent the shooting program is self-checking in that it yields values of the eight variables at all the integration steps: one can therefore check that the solution provided does indeed meet the set boundary conditions at both ends of the fluid region. In addition it was run for well-known problems as a check on the numerical value of the critical Rayleigh number R_c and the optimum horizontal wavenumber a_c .

1. Rayleigh-Benard problem, with vertical rotation.

Rigid - rigid, constant temperature boundaries

$$f(z) = 1$$

Integration step = 0.05

Taylor No.	Variational Method		Program	
	(Chandrasekhar, 1961)			
I	$\underline{R_c}$	$\underline{a_c}$	$\underline{R_c}$	$\underline{a_c}$
0.0	1707.8	3.117		
0.1			1,707.2	3.11
10^3	2151.7	3.50	2151.1	3.49
10^4	4713.1	4.80	4712.4	4.78
10^5	16721	7.20	16719	7.17
10^6	71132	10.80	70800 ^a	10.8 ^a

a: not properly converged, so uncertain.

Agreement is satisfactory. The variational method used by Chandrasekhar (1961) is of limited accuracy in locating the critical wavenumber a_c , owing to the spacing used between values of a . At $T = 10^6$, the shooting program only gives poorly converged results and so is inaccurate, particularly in locating a_c . This problem is discussed further in § 5.3.

2. $f(z) = 1 - z$ in $0 \leq z \leq 2$

Stress-free, constant temperature boundaries.

Integration step = 0.10

This case was investigated by Veronis (1963) as being an approximation to the ice-water system, in which the coefficient of thermal expansion α changes sign at 4°C . Veronis used a truncated Fourier expansion of the velocity field to compute the critical Rayleigh number.

Veronis ($T = 0$): $\frac{g \cdot \Delta \rho d^3}{\rho K \nu} \equiv \frac{R}{2\lambda^4}$ in Veronis' notation

The comparable case is Veronis $\lambda = 2$, in which case $R = \left(\frac{R}{2\lambda^4}\right)_{\text{Ver.}} \times 2$ is the appropriate conversion. For the horizontal wave-number, $a = \left(\frac{a}{\lambda}\right)_{\text{Veronis}} \times \pi$. Hence:-

$$\begin{aligned} \left(\frac{R}{2\lambda^4} \right)_{\text{Veronis}} &= 2.72 \pi^4 \quad \text{for } \lambda = 2 \\ &= 264.9 \\ \therefore R &= 529.9 \quad \text{from Veronis} \\ \text{Compare } R_c &= 531.1 \quad \text{from shooting program} \\ &\quad (\tau = 10^{-3}) \end{aligned}$$

$$\begin{aligned} \left(\frac{a}{\lambda} \right)_{\text{Veronis}} &= (0.233)^{1/2} \\ &= 0.483 \\ \therefore a &= 1.516 \quad \text{from Veronis} \\ \text{Compare } a_c &= \underline{1.513} \quad \text{from shooting program} \end{aligned}$$

Agreement here is again satisfactory. However, comparison of the wave-form for the vertical velocity component (w_0 in Veronis' notation) at the onset of convection shows differences (fig. 5.2). Veronis noted a countercell in the uppermost part of his fluid region, in which $w_0 < 0$, and attributed this to a secondary circulation cell driven by viscous forces. No such countercell exists in the solution from the shooting program for $h = 2$. It appears that Veronis' countercell may be an artifact of using a Fourier expansion truncated at the fourth term. Using the shooting program, no countercell is observed until $h = 2.5$. As h increases beyond $h = 2.5$, the beginning of the countercell is found to occur between $Z = 2.0$ and $Z = 2.1$, so that the first cell only extends as far as the position of zero overall temperature difference. In the cases $2.0 < h < 2.5$, there is no countercell because of the constraint of the upper boundary. This inhibition of the optimum form of convection results in an increased value for R_c in this range of h , as can be seen in Table 5.1.

Table 5.1

Critical Rayleigh number and wavenumber for a parabolic density profile at low rotation rate ($T = 10^{-3}$). Stress-free, constant temperature boundaries. $f(z) = 1 - z$

h	R_c	a_c	Start of counter-cell
1.0	1308.8	2.23	-
1.1	990.8	2.03	-
1.2	784.0	1.86	-
1.3	646.8	1.73	-
1.4	555.7	1.61	-
1.5	497.8	1.51	-
1.6	466.3	1.44	-
1.7	458.2	1.39	-
1.8	472.1	1.38	-
1.9	501.5	1.43	-
2.0	531.1	1.51	-
2.1	549.7	1.58	-
2.2	557.6	1.61	-
2.3	558.8	1.62	-
2.4	556.8	1.62	-
2.5	554.1	1.61	2.2
2.6	551.8	1.60	2.1
2.7	550.4	1.59	2.1
2.8	549.9	1.59	2.1
2.9	549.8	1.59	2.1
3.0	550.2	1.59	2.1

Fig. 5.2

Copy of fig. 2 from Veronis (1963), showing the counter-cell found by a truncated series expansion analysis. This case is equivalent to $h=2.0$, for which the shooting program finds no counter-cell (see above, Table 5.1).

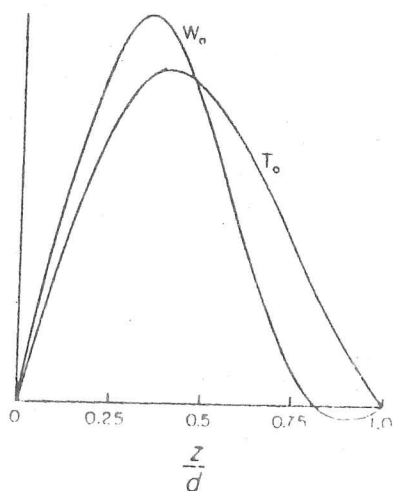


Fig. 2.—A plot of w_0 versus z for $\lambda = 2$ with T_0 normalized, i.e., $(T_0)_m = 1$, and w_0 deduced from eq. (28). A small secondary cell near the upper boundary is driven by viscous forces and is shown as the region in which w_0 is negative.

$$3. f(z) = \cos(\pi z/2) \text{ in } 0 \leq z \leq 2$$

Stress-free, constant temperature boundaries.

Vertical rotation.

An alternative method of finding the critical Rayleigh number in this particular case is to use the Fourier series expansion method set out before in § 4.2, utilising the properties of the cross-product term:

$$f(z) \cdot \sin\left(\frac{n\pi z}{2}\right) = \frac{1}{2} \left[\sin\left(\frac{(n-1)\pi z}{2}\right) + \sin\left(\frac{(n+1)\pi z}{2}\right) \right]$$

The problem is therefore to find values for R such that the following determinant is zero:

$$\begin{vmatrix} A_1 & B & 0 & \dots \\ B & A_2 & B & 0 \\ 0 & B & A_3 & B \\ 0 & 0 & B & A_4 \\ \vdots & \vdots & \vdots & \vdots \end{vmatrix}$$

where the diagonal terms are

$$A_i \equiv -(i^2 \pi^2 + a^2)^3 - T \pi^2$$

and the off diagonal terms are either zero or

$$B \equiv R a^2/2$$

with T and a specified.

If the determinant is truncated at some order, it defines approximate roots for the Rayleigh number R, which may be found numerically by the use of an iterative procedure similar to the subroutine 'CONVRG' in the shooting program, combined with an evaluation of the truncated determinant. It is found that truncation at the 3rd order determinant

$$\begin{vmatrix} A_1 & B & 0 \\ B & A_2 & B \\ 0 & B & A_3 \end{vmatrix} = 0$$

gives reasonable estimates for the Rayleigh number, in that the

change to truncating at the 4th order determinant results in no significant change in the root R. The critical values R_c , a_c can then be found by the use of successively finer test grids of values of a.

A comparison of the results at two different rotation rates from the two methods, the above determinant method and the shooting program, is given below:

I	<u>Determinant method</u>		<u>Shooting program</u>	
	$\underline{R_c}$	$\underline{a_c}$	$\underline{R_c}$	$\underline{a_c}$
0.0625	383.2	1.514	383.3	1.511
	(3rd order truncation)			
	383.2	1.514		
	(4th order truncation)			
62.5	582.8	2.072	582.9	2.072
	(3rd order truncation)			
	582.8	2.072		
	(4th order truncation)			

Agreement is satisfactory. The determinant method is of limited use: only this particular case of $f(z) = \cos(\pi z/2)$ gives such a simple determinant and it is only for the stress-free, constant temperature boundaries that a Fourier series expansion for U satisfies the boundary conditions.

Numerical Accuracy

In general a grid spacing of 0.1 is used for the Runge-Kutta integration routine, so that the Rayleigh number is evaluated at intervals of 0.05 (using a normalisation of unstable region being $0 \leq z < 1.0$). No appreciable gain in resolution of the critical Rayleigh number or of the critical horizontal wavenumber results from decreasing the spacing to 0.05 or 0.025: the following results relate to the case of:-

$$f(z) = \cos(\pi z/2)$$

rigid, constant temperature boundaries

$$T = 1$$

$$h = 1.6 \text{ or } 2.0$$

Grid spacing	<u>h</u> = <u>1.6</u>		<u>h</u> = <u>2.0</u>	
	<u>R_c</u>	<u>a_c</u>	<u>R_c</u>	<u>a_c</u>
0.1	828.84	2.035	826.66	2.006
0.05	828.65	2.029	826.43	1.999
0.025	828.64	2.029	826.41	1.999

Only in the case of $f(z)$ being discontinuous (plane layer case, reported below in § 5.3.2, Tables 5.5 to 5.7) does the finite spacing used affect the results to a marked degree. In other cases, $f(z)$ is a continuous function and $D f(z)$ is never so large as to cause substantial changes between grid points.

As noted above in the description of the shooting program, the ^{step} length is reduced by a factor of 10 in the intervals next to the boundaries, in order to assist in resolving the Ekman layers that form at high T . Since the highest rotation rate generally used in running the program is $T = 10^5$, for which the Ekman layer thickness $O(T^{-1/4})$ is approximately 0.05, this is adequate: again a test of reducing the grid spacing to 0.025 for a run with $T = 10^5$ resulted in a change of less than 0.01% in R_c , 0.1% in a_c .

5.3 Results: horizontal plane layer, vertical rotation

5.3.1 Case 1: $f(z) \equiv \cos \pi z/2$

A temperature gradient of the form $f(z) = \cos \pi z/2$ in the region $0 \leq z \leq h$ for $1 \leq h \leq 2$ is used as being a convenient function of smooth form. Note that the overall temperature difference across the layer $Z = 0$ to $Z = 2$ is zero. The layer is unstably stratified in $0 \leq z < 1$, stably in $1 < z \leq 2$. The object of using a smooth function $f(z)$ is to avoid the risk of spurious effects stemming from a discontinuity in one or more terms. A layered stratification, with a step-function for $f(z)$, will be considered separately, in § 5.3.2.

The shooting program is run for different positions of the top boundary, $h = 1.0, 1.1, \dots, 2.0$. These correspond first to having no stable layer, then to adding a stable region above the unstable layer. As a result of the manner in which the scale-depth d is defined for the purpose of the Rayleigh number R and Taylor number T , R is proportional to $\nabla\theta$ for all of the cases and similarly a given value for T implies the same rotation rate for all of the cases.

$$R \equiv g\alpha\beta_0 d^4 / \kappa\nu$$
$$T \equiv 4\Omega^2 d^4 / \nu^2$$

1) Rigid, constant temperature boundaries

(Figs. 5.3 to 5.5 and Table 5.2)

At low rotation rates, $T = O(1)$, and a top boundary at $z = h = 1.0$, the profile of vertical velocity U at the onset of steady convection is very similar in shape for both $f(z) = \cos(\pi z/2)$ and $f(z) = 1.0$. The asymmetry of the density profile $f(z) = \cos(\pi z/2)$ scarcely deflects the velocity U from being symmetric about the mid-point, $z = 0.5$. As one considers the top boundary moved to $h = 1.5$ and then to $h = 2.0$, the profile of U penetrates

into the stable region, allowing a longer effective length-scale and so a lower value for the critical Rayleigh number (fig. 5.3 and Table 5.2).

The effect of increasing the rotation rate, as measured by T , is to bias the profile of U towards the region of greatest instability. For $T \geq 10^3$, this effect is sufficiently great that the profiles for $h = 1.5$ and $h = 2.0$ become very similar in the unstable region (see fig. 5.3): the combination of rapid rotation and a stable layer shields the solution from the actual position of the upper boundary, $z = h$. Thus the rotation emphasizes the effect of the stable layer. This may be seen more clearly in the profiles of D^2U plotted in fig. 5.4. Increasing the rotation rate from $T = 1$ to $T = 10^3$ causes a shift in the profiles of D^2U towards the unstable region, particularly marked for a deep stable region, $h = 2.0$. A further increase, to $T = 10^5$ results in D^2U being small except in the neighbourhood of the rigid boundaries, indicating that Ekman boundary layer theory and a reduction in the effective order of the equations to 2 in the interior region become applicable for $T \geq 10^5$.

Figure 5.5 shows the variation of critical Rayleigh number with the position of the upper boundary, h , for various rotation rates (see also Table 5.2). Medium rotation rates, $T = 10^3$ or 10^4 , show minima for the critical Rayleigh number at about $h = 1.6$, rather than at $h = 1.8$ as for $T = 1$. This reflects the decreased advantage to the system of any penetration of the stable region. At $T = 10^5$ however, R_c appears to continue decreasing with h , although this conclusion is limited by the difficulty in achieving convergence for $T = 10^5$, $h \geq 1.7$ (see §5.3.3 for this problem). From Table 5.2, it is clear that changing the top boundary position from $h = 1.0$ to, say, $h = 1.6$

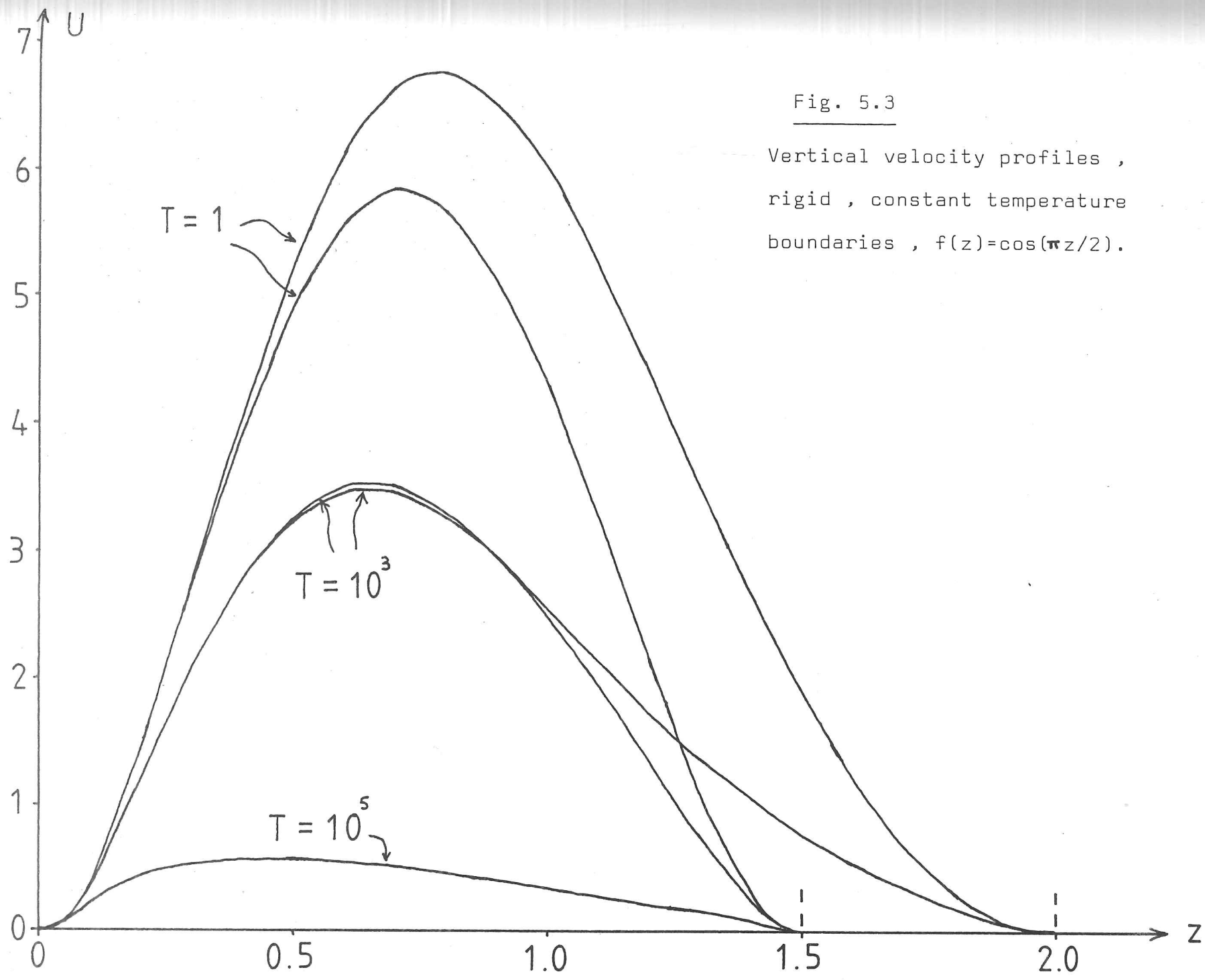


Fig. 5.3

Vertical velocity profiles ,
rigid , constant temperature
boundaries , $f(z)=\cos(\pi z/2)$.

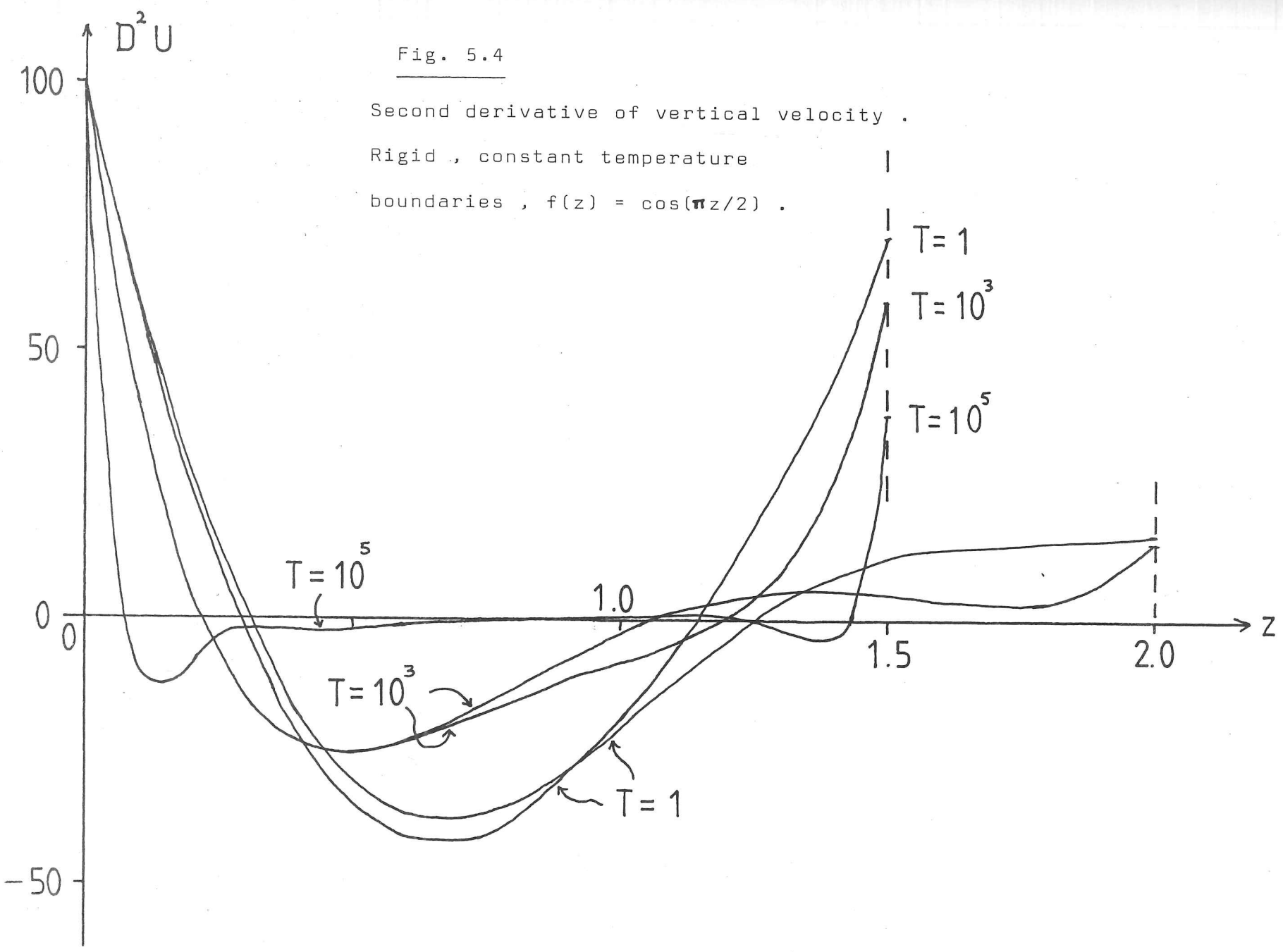


Fig. 5.4

Second derivative of vertical velocity .
 Rigid , constant temperature
 boundaries , $f(z) = \cos(\pi z/2)$.

$T = 1$
 $T = 10^3$
 $T = 10^5$

$T = 10^5$

$T = 10^3$

$T = 1$

Fig. 5.5

Variation of critical Rayleigh number with depth h . Rigid, constant temperature boundaries.

$$f(z) = \cos(\pi z/2).$$

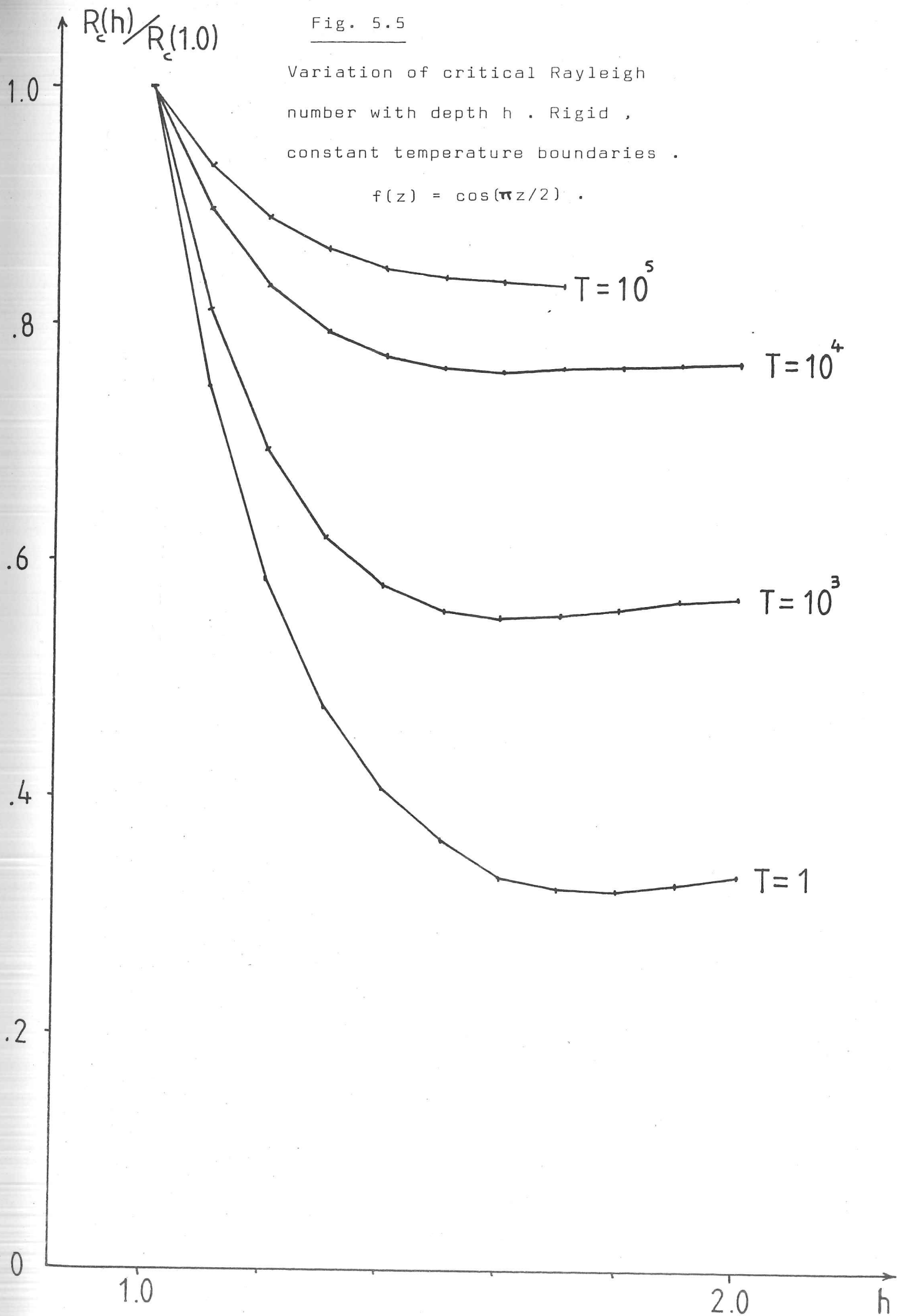


Table 5.2

Critical Rayleigh numbers and wavenumbers
 Rigid, constant temperature boundaries
 $f(\xi) = \cos(\pi \xi / 2)$

I	$h =$	1.0	1.1	1.2	1.3	1.4
1	R_c	2483	1855	1450	1185	1009
	a_c	3.13	2.85	2.62	2.42	2.27
10^3	R_c	3125	2527	2158	1933	1804
	a_c	3.50	3.31	3.16	3.06	2.99
10^4	R_c	6829	6118	5675	5410	5265
	a_c	4.81	4.69	4.60	4.53	4.49
10^5	R_c	24158	22508	21445	20790	20416
	a_c	7.25	7.09	6.98	6.89	6.84
10^6	R_c	102420				
	a_c	10.98 ^a				

a: step length = 0.025

I	1.5	1.6	1.7	1.8	1.9	2.0
1	896	829	799	797	810	827
	2.14	2.04	1.97	1.95	1.97	2.01
10^3	1740	1720	1727	1743	1760	1772
	2.95	2.94	2.96	2.99	3.01	3.04
10^4	5202	5184	5191	5204	5215	5227
	4.48	4.48	4.49	4.51	4.53	4.54
10^5	20221	20138	20087		failed	
	6.82	6.81	6.83			
10^6						

has a much greater effect in decreasing the critical Rayleigh number R_c at low rotation rates ($T = 1$, $R_c(h=1.0) = 2483$, $R_c(h=1.6) = 829$, a reduction of 67%) than at medium ($T = 10^3$, $R_c(h=1.0) = 3125$, $R_c(h=1.6) = 1720$, a reduction of 45%) or at high rotation rates ($T = 10^5$, $R_c(h=1.0) = 24158$, $R_c(h=1.6) = 20138$, a reduction of 17%).

2) Stress-free, constant temperature boundaries.

figs. 5.6 and 5.7, table 5.3

The same effect of increasing the rotation rate on the extent of penetration into the stable region occurs with stress-free boundaries. Fig. 5.6 shows U , fig. 5.7 shows D^2U : the compression of the flow pattern into the unstable region is clearer than for rigid boundaries as there is no Ekman boundary layer effect to obscure fig. 5.7. The profile of D^2U for $h = 1.5$ shows how at fast rotation ($T = 10^5$) D^2U changes sign near $z = 1.0$: the cross-over occurring for z less than 1.0 by a small amount, in accordance with our expectations from the 2nd order approximate equations (see § 5.3.4 for discussion of the rapid rotation limit).

3) Rigid-Rigid, constant heat flux boundaries

figs. 5.8 to 5.10, table 5.4

The case of constant heat flux boundaries has been investigated in recent years primarily as a result of the long horizontal wavelengths associated with it, which have been of interest to studies of mantle convection (Sparrow et al. 1964, Chapman & Proctor, 1980). Penetrative convection, in the form of an idealised ice-water system, $f(z) = 1-z$, with fixed-flux boundaries was investigated by Roberts (1982) who found that the critical wavenumber for the onset of convection remains zero for layer depths $h < 1.6492$. For $h > 1.6492$, he found a bifurcation

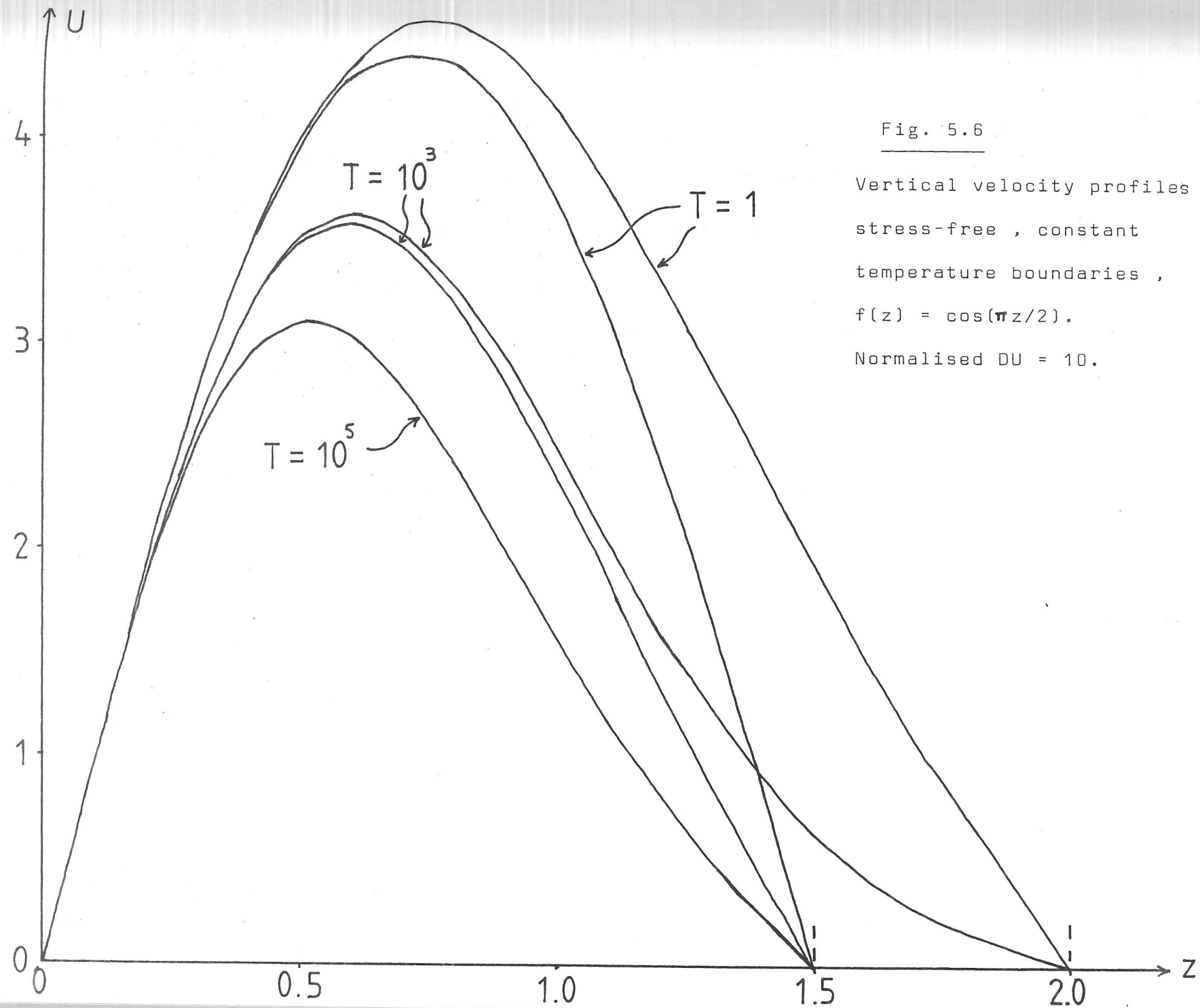


Fig. 5.6

Vertical velocity profiles
 stress-free , constant
 temperature boundaries ,
 $f(z) = \cos(\pi z/2)$.
 Normalised $DU = 10$.

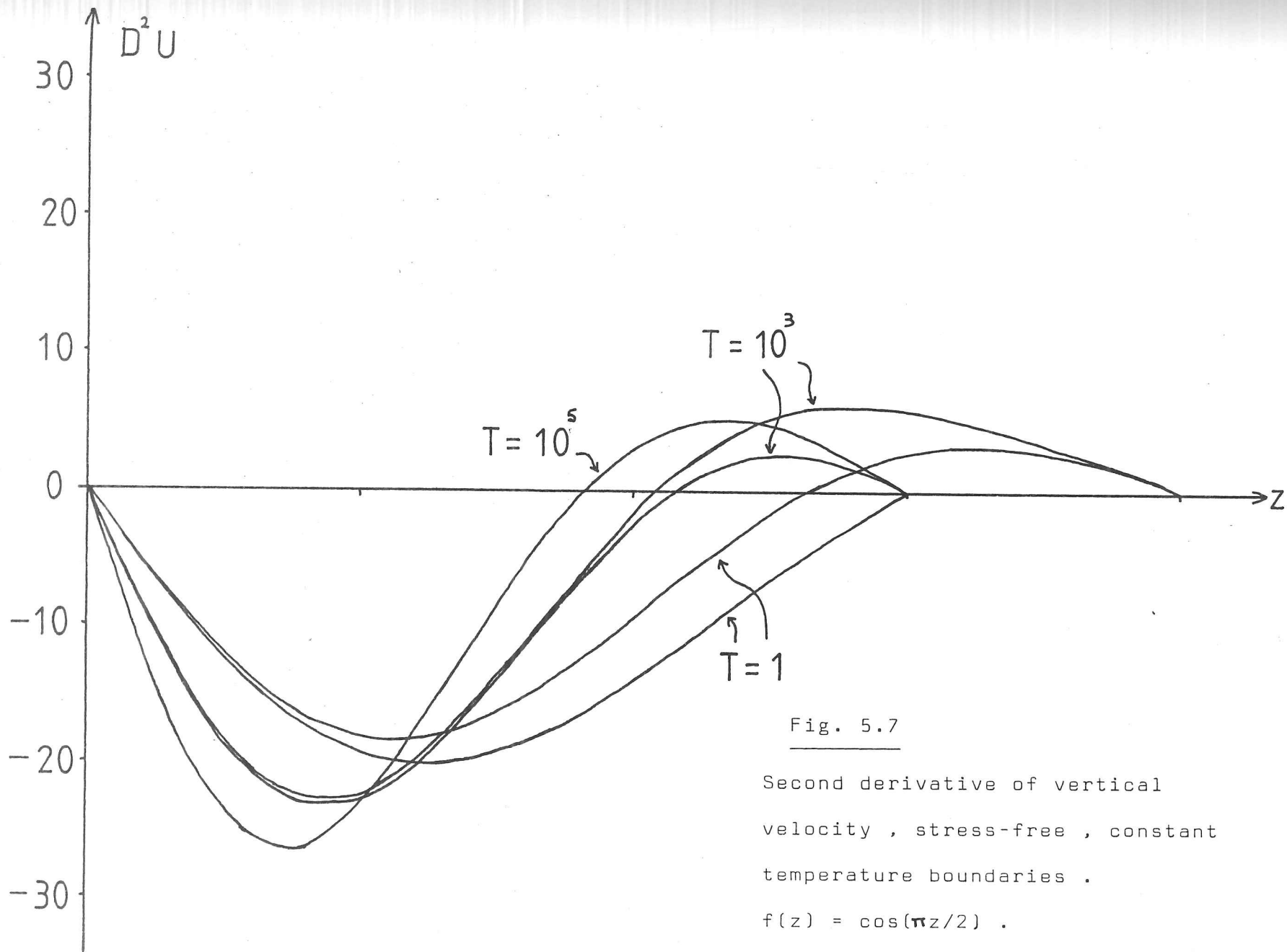


Fig. 5.7

Second derivative of vertical velocity , stress-free , constant temperature boundaries .

$$f(z) = \cos(\pi z/2) .$$

Table 5.3

Critical Rayleigh numbers and wavenumbers
 Stress-free, constant temperature boundaries
 $f(\xi) = \cos(\pi \xi / 2)$

Γ	$h =$	1.0	1.5	2.0
1	R_c	968.5	362.4	389.2
	a_c	2.24	1.54	1.54
10^3	R_c	2441.7	1724.4	1684.1
	a_c	3.72	3.42	3.37
10^4	R_c	7739.8	6095.2	5970.7
	a_c	5.72	5.26	5.18
10^5	R_c	30416	25121	
	a_c	8.67	7.96	
10^6	R_c	131190		
	a_c	12.95		

to a non-zero critical wavenumber, more akin to the case of perfectly-conducting boundaries. This limits the use of the simplification $a_c = 0$ in a non-linear analysis to cases in which the stable region is not too large. In the cases of $a_c = 0$, the vertical velocity perturbation profile becomes independent of $f(z)$, so that penetration may be said to be complete, with the stable layer having no effect on the form of the convection.

The effect of rotation on these results tends to be to restrict the range of applicability of the solution $a_c = 0$. Using our standard penetrative profile, $f(z) = \cos(\pi z/2)$, at $T = 1$ we find that $a_c = 0$ is the solution for layer depths $h \leq 1.6$, whereas $a_c \neq 0$ for $h \geq 1.7$, in broad agreement with Roberts' results (given the slight difference in $f(z)$). However, at $T = 10^3$, $a_c = 0$ is the critical solution only for the cases $h \leq 1.1$, whilst at $T = 10^4$, $a_c \neq 0$ even for $h = 1.0$.

Figures 5.8 to 5.10 plot the vertical velocity profile, U , $D U$ and the temperature perturbation F for the critical states. In the cases where $a_c = 0$, the profiles are symmetric about the mid-point in z , $z = h/2$, demonstrating the independence of the solution from $f(z)$ in these cases. This is especially marked in the profiles of F , the temperature perturbation, in which the cases $a_c = 0$ correspond to $F = \text{constant}$ throughout the layer, as is obvious from the equations.

Table 5.4 gives the critical wavenumber a_c and Rayleigh number R_c for various cases, to show the variation with rotation and with the depth of layer h . Except in the region of both ($h = 1.0$) and T small, in which $a_c = 0$, there is no qualitative difference from the behaviour of convecting layers with constant temperature boundaries.

In terms of geophysical applications, the daily rotation of

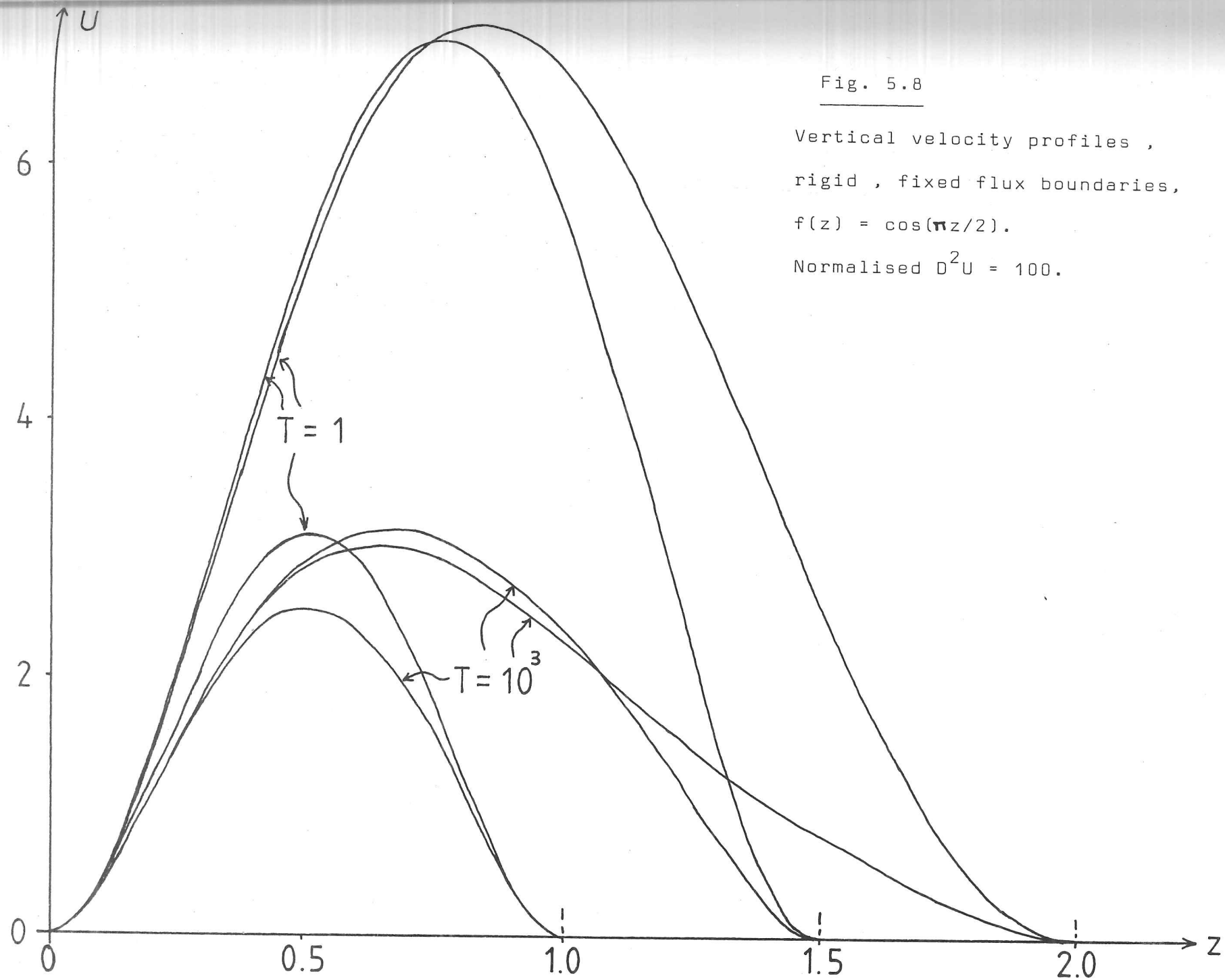


Fig. 5.8

Vertical velocity profiles ,
rigid , fixed flux boundaries,
 $f(z) = \cos(\pi z/2)$.
Normalised $D^2U = 100$.

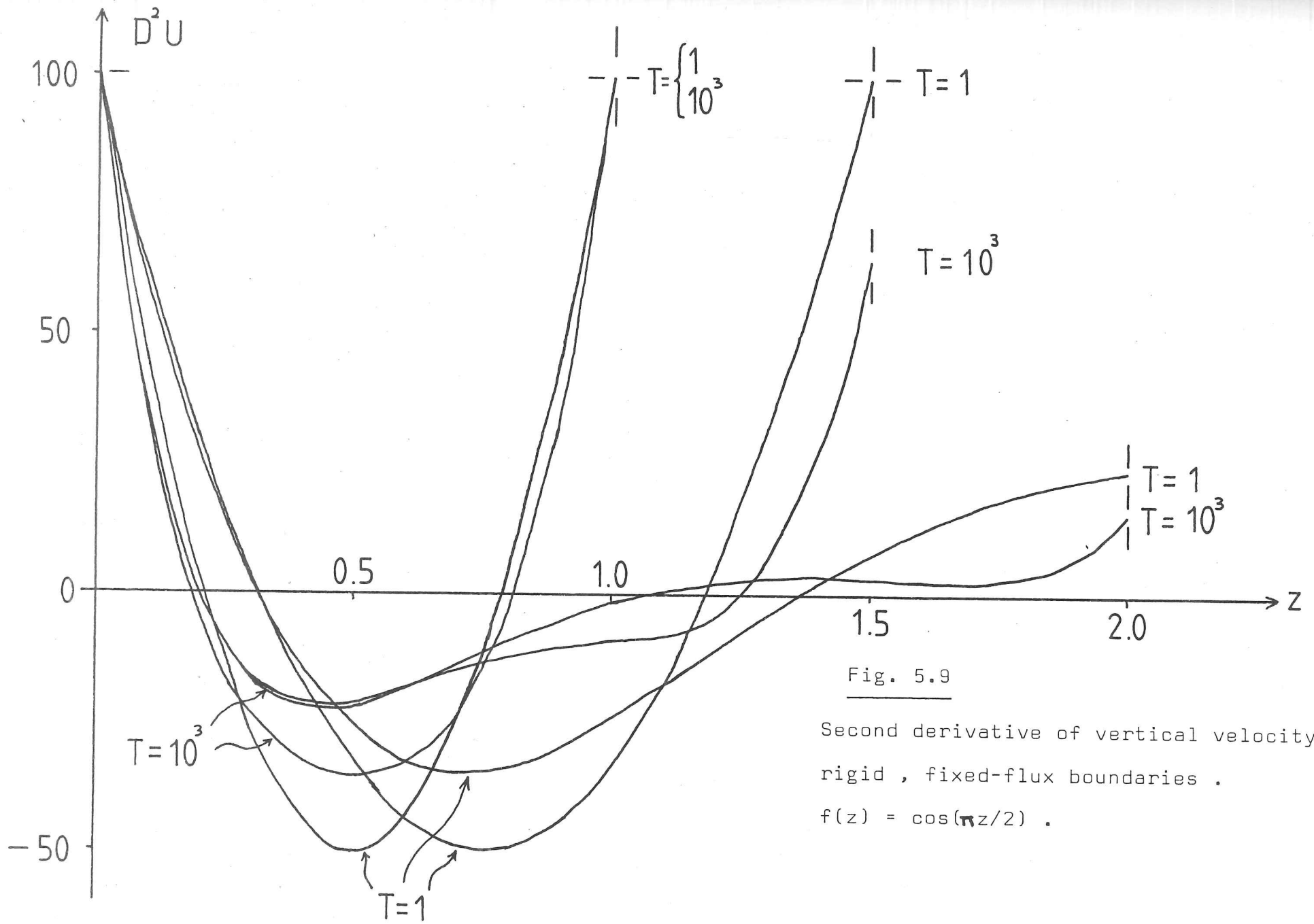


Fig. 5.9

Second derivative of vertical velocity,
 rigid, fixed-flux boundaries.

$$f(z) = \cos(\pi z/2).$$

Fig. 5.10

Temperature perturbation F ,
rigid, fixed-flux boundaries,
 $f(z) = \cos(z/2)$.

Normalised by $D^2U = 1.0$.

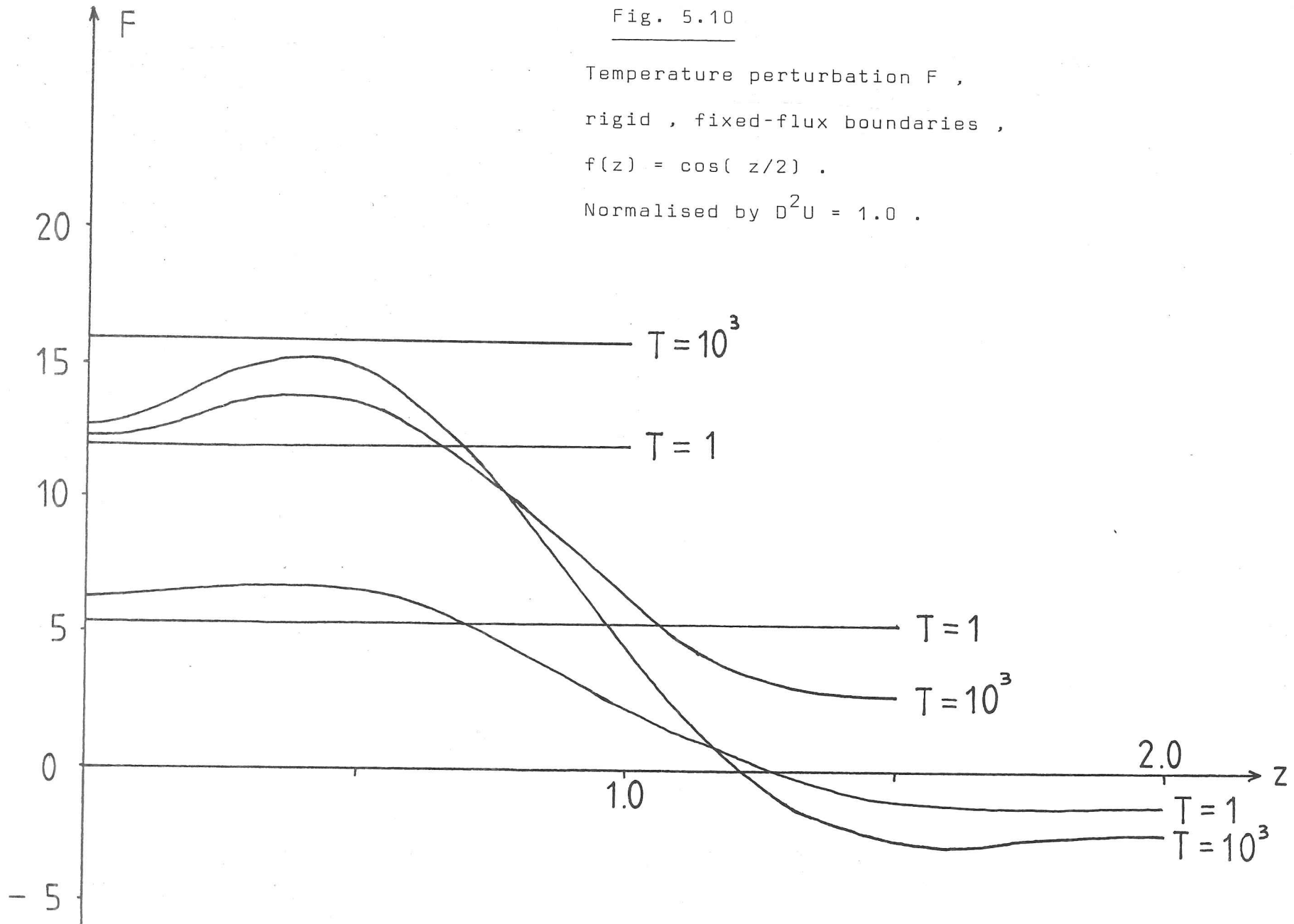


Table 5.4

Critical Rayleigh numbers and wavenumbers.

Rigid, fixed-flux boundaries $f(z) = \cos(\pi z/2)$

I	h =	1.0	1.1	1.2	1.3	1.4
1	R_{ac}^c	1065 0	800 0	631 0	521 0	452 0
10^3	R_{ac}^c	1675 0	1460 0	1344 1.19	1285 1.62	1264 1.91
10^4	R_{ac}^c	5320 3.51				
10^5	R_{ac}^c	21815 6.52				
I	1.5	1.6	1.7	1.8	1.9	2.0
1	412 0	400 0	417 0.68	447 1.08	476 1.31	497 1.44
10^3	1268 2.11	1287 2.27	1311 2.39	1332 2.48	1348 2.54	1358 2.57
10^4	4491 3.97					4508 4.11
10^5	18728 6.44					

the Earth often gives rise to cases in which $T \geq 10^4$. For example, if one considers the convection problem in solar energy ponds, one only needs a depth of pond of approximately 1 metre to give $T \approx 10^4$ (based on $\nu \approx 10^{-6} \text{ m}^2 \text{ s}^{-1}$ for water). Thus only very small-scale convective phenomena, or those in which the viscosity is great (such as mantle convection) are likely to be affected by the large aspect ratios associated with constant heat flux boundaries. In other cases, one can expect "normal" horizontal wavenumbers even if constant heat flux is the appropriate thermal boundary condition. In particular, for the core the rotation rate is very high ($T \approx 10^{30}$) and so the poorly conducting mantle will not lead to long wavelength convection cells.

5.3.2. Case 2: Layered profile

$$f(z) = 1.0 \quad \text{in } 0 \leq z \leq 1.0^*$$

$$= -A \quad \text{in } 1.0 < z \leq h$$

The advantage of using a layered profile of this form rather than $f(z) = \cos(\pi z/2)$ or $f(z) = 1-z$ is that it becomes easy to introduce an asymmetry about $z = 1$ in order to investigate the effect of a relatively thin but strongly stratified stable region on the onset of convection. Rigid, constant temperature boundaries are used in the calculations for this case: boundary condition effects should be qualitatively similar to those for the previous section ($f(z) = \cos \pi z/2$) after allowing for the greater shielding of the upper boundary by the strong stable layer.

The critical Rayleigh numbers, horizontal wavenumbers and the point at which a countercell starts (if any) are listed in Tables 5.5 to 5.7, for values of A in the range 10 to 1000. In

each case, as h increases to sufficiently large values (e.g. $h \geq 1.8$ for $A = 10$, $h \geq 1.4$ for $A = 100$), the results tend to constant values, those for low A being of lower Rayleigh number and wavenumber as is expected for a less "constricted" system. At low Taylor number, these results for large h feature lower values for both Rayleigh number and wavenumber than for $h = 1.0$ (the linear temperature profile end-member of this case) but at high Taylor number coupled with high value for A this is not so. In these latter cases, the stable layer acts as a more restrictive boundary to the convection than would a rigid boundary. Similarly, in these cases, lower values of h (e.g. $h = 1.1$) do not display the initial relaxation of R_c , a_c that is clear for the cases of lower values for A or for T .

A countercell is associated with the solutions for sufficiently large h (as in the parabolic profile with zero rotation investigated by Veronis (1963)): once well established, this is responsible for the lack of effect of any further increase in h , noted above. Increased values of A result in the countercell appearing at smaller values of h , as might be expected. Increased rotation rate increases the value of h for onset however. From the analysis in § 4.2, one predicts that as T is increased still further countercells will no longer feature in the solution, regardless of h . This is a result of the tendency of fast rotation rate to change the effective order of the differential equations from 8 to 2.

footnote * The finite spacing using in the Runge-Kutta integration leads to $f(z) = -A$ being applied first for $z = 1.05$, except in the runs for $A = 1000$ (see Table 5.7)

Table 5.5 Critical Rayleigh numbers and wavenumbers
 Rigid, constant temperature boundaries
 $f(\infty) = 1$ for $z \leq 1$, $= -10$ for $1 < z \leq h$

I	h	1.0	1.1	1.2	1.3	1.4
1	R_c	1709	1186	923	913	1023
	a_c	3.12	2.83	2.60	2.50	2.65
10^3	R_c	2152	1622	1396	1488	1611
	a_c	3.49	3.29	3.16	3.21	3.39
10^4	R_c	4711	3988	3867	4186	4307
	a_c	4.79	4.66	4.67	4.90	5.03
10^5	R_c	16719	15145	15528	16133	16250
	a_c	7.17	7.06	7.29	7.51	7.5

I	1.5	1.6	1.7	1.8	2.0
1	1061	1050	1035	1028	1029
	2.76	2.76	2.74	2.71	2.71
10^3	1640	1636	1632	1631	1630
	3.47	3.48	3.48	3.48	3.47
10^4	4326	4328	4326	4326	4326
	5.06	5.06	5.06	5.06	5.06
10^5	16269	16272	16272	16273	16260 \pm 10
	7.59	7.59	7.60 \pm .02	7.59	7.7 \pm 0.1

Table 5.6

Critical Rayleigh numbers and wavenumbers
Rigid, Constant temperature boundaries

$$f(z) = 1 \quad \text{for } z \leq 1$$

$$= -100 \quad \text{for } 1 < z \leq h$$

T	h	1.0	1.1	1.2	1.3	1.4	1.5	1.6
1	R_c	1709	1343	1623	1670	1610	1607	1610
	a_c	3.12	2.84	3.09	3.26	3.19	3.16	3.17
10^3	R_c	2152	1855	2199	2222	2188	2190	2189
	a_c	3.49	3.32	3.66	3.78	3.75	3.74	3.74
10^4	R_c	4711	4709	5117	5109	5102	5099	5099
	a_c	4.79	4.85	5.25	5.29	5.28	5.28	5.28
10^5	R_c	16719	18172	18141	18123	18117	18120 \pm 10	failed
	a_c	7.17	7.64	7.87	7.88	7.87	7.9 \pm 1	

Table 5.7

Critical Rayleigh numbers and wavenumbers

Rigid, constant temperature boundaries

$$f(z) = 1 \quad \text{for } z \leq 1$$

$$= -1000 \quad \text{for } 1 < z \leq h$$

T	h	1.0	1.1	1.2	1.3	1.4	1.5	1.6
1	R_c	1708	2129	2182	2152	2153	2151	2151
	a_c	3.12	3.34	3.55	3.48	3.49	3.49	3.48
10^3	R_c	2151	2708	2727	2716	2713	2713	2713
	a_c	3.49	3.83	3.97	3.95	3.95	3.95	3.95
10^4	R_c	4712	5808	5767	5763	5763	5763	failed
	a_c	4.79	5.36	5.41	5.41	5.41	5.41	
10^5	R_c	16720	19718	19625	failed	failed	failed	failed
	a_c	7.17	8.02	8.02				

A second reversal of the velocity field is observed in some cases, generally those at high h and T , but this is not properly resolved within the convergence error of the iteration scheme and so may be just numerical error. Its occurrence has no effect on the convective part of the solutions.

Counter-cell Position: slow rotation ($T = 1$)

see Fig 5.11 for a schematic diagram of the flow

Fig. 5.11

Schematic diagram of vertical velocity

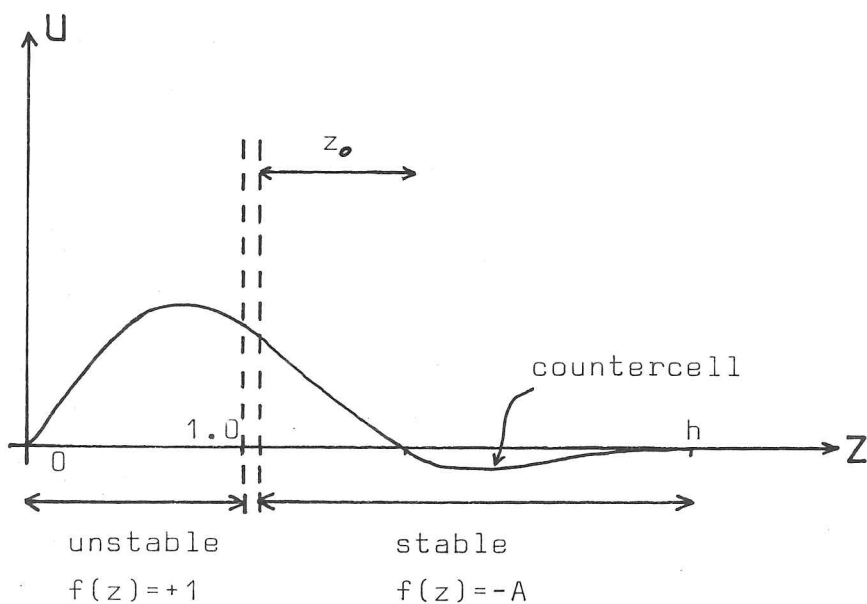


Table 5.8 lists the positions z_0 at which flow reverses for various values of A and $T = 1$. For $1 \leq A \leq 20$ the grid spacing is reduced to 0.05 and so $f(z) = -A$ is first applied at $z = 1.0 + \frac{1}{2}(0.05)$ in the Runge-Kutta routine, whilst for $20 < A$, the grid spacing is again reduced to 0.02.

No simple power-law relates the depth of penetration to the counter-cell, z_0 , to the strength A of the stable layer (figure 5.12 for logarithmic plot). In particular, a $z_0 = \text{constant}$ is not valid, so there is no relationship based directly on the

Table 5.8

Counter-cell Position ($T = 1$)

A	h	Intrapolated position of reversal z (a)	Adjusted position z_0 = (z - 1.025)
1	3.0	1.910	0.885
2	3.0	1.640	0.615
5	3.0	1.415	0.390
10	2.5	1.305	0.280
20	2.5	1.235	0.210
100	1.6	1.129b	0.119b
1000	1.6	1.068b	0.058b
10^4	1.3	1.060b	0.050b

Notes: a: error ± 0.010 , based on integration spacing = 0.05

b: Integration spacing = 0.02

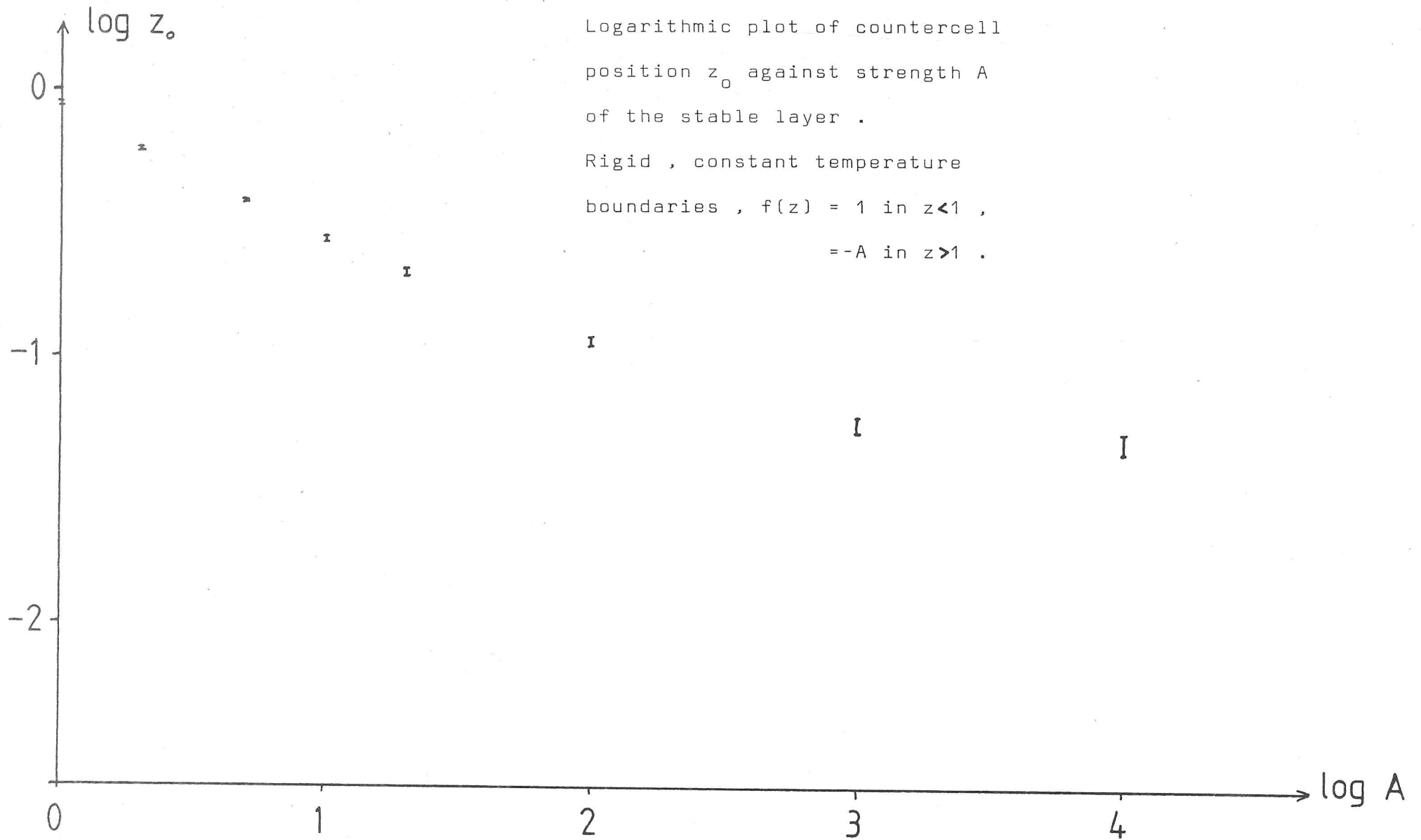
$$z_0 = (z - 1.01)$$

error ± 0.004

Fig. 5.12

Logarithmic plot of countercell position z_0 against strength A of the stable layer .

Rigid , constant temperature boundaries , $f(z) = 1$ in $z < 1$,
 $= -A$ in $z > 1$.



overall temperature difference across the first convective cell. For large A , $A z_0 \gg 1$, indicating that the countercell starts at a point whose density is stable relative to the base $z = 0$ of the system (fig. 5.13).

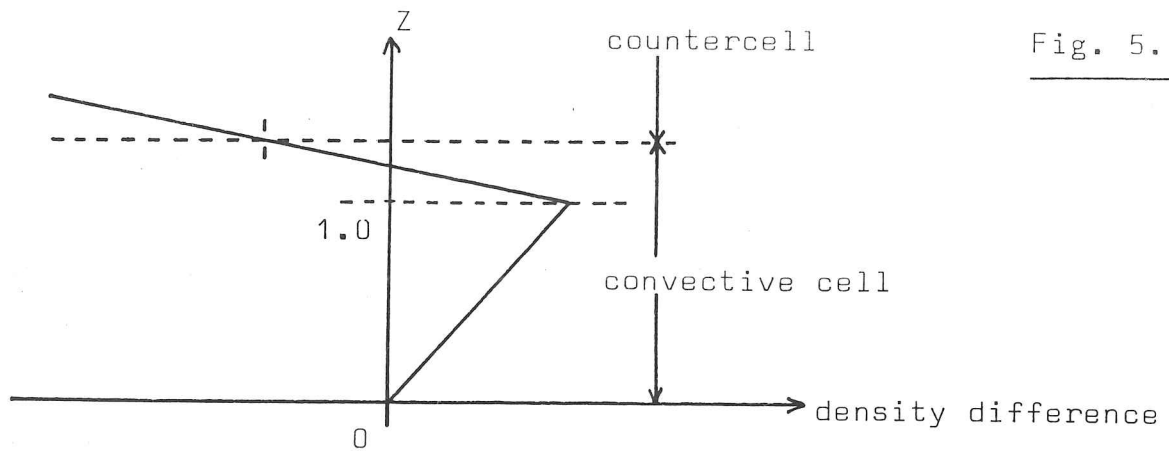


Fig. 5.13

Effect of rotation on countercell position

At high rotation rates ($T \rightarrow \infty$) there should be no countercell since, following § 4.2, the equations are effectively reduced to 2nd order and the flow in the stable region becomes one of exponential decay. In order to illustrate the transition to this, figure 5.14 shows the vertical velocity profile for the case $A = 100$ and $T = 1, 10^3$ and 10^4 . A grid spacing of 0.02 is used in the calculations and the upper boundary is at $h = 1.4$. Figure 5.14 shows that the increased rotation rates result both in the convection being more closely confined to the unstable region $0 \leq z \leq 1.0$ (as in the case of $f(z) = \cos(\pi z/2)$ considered previously) and in a weakening of the countercell in the stable region

5.3.3 shooting program failures at large T, R and use of 2nd order approximate equations

For large values of T and R , the 8th order shooting program fails to converge, owing to the combination of two problems.

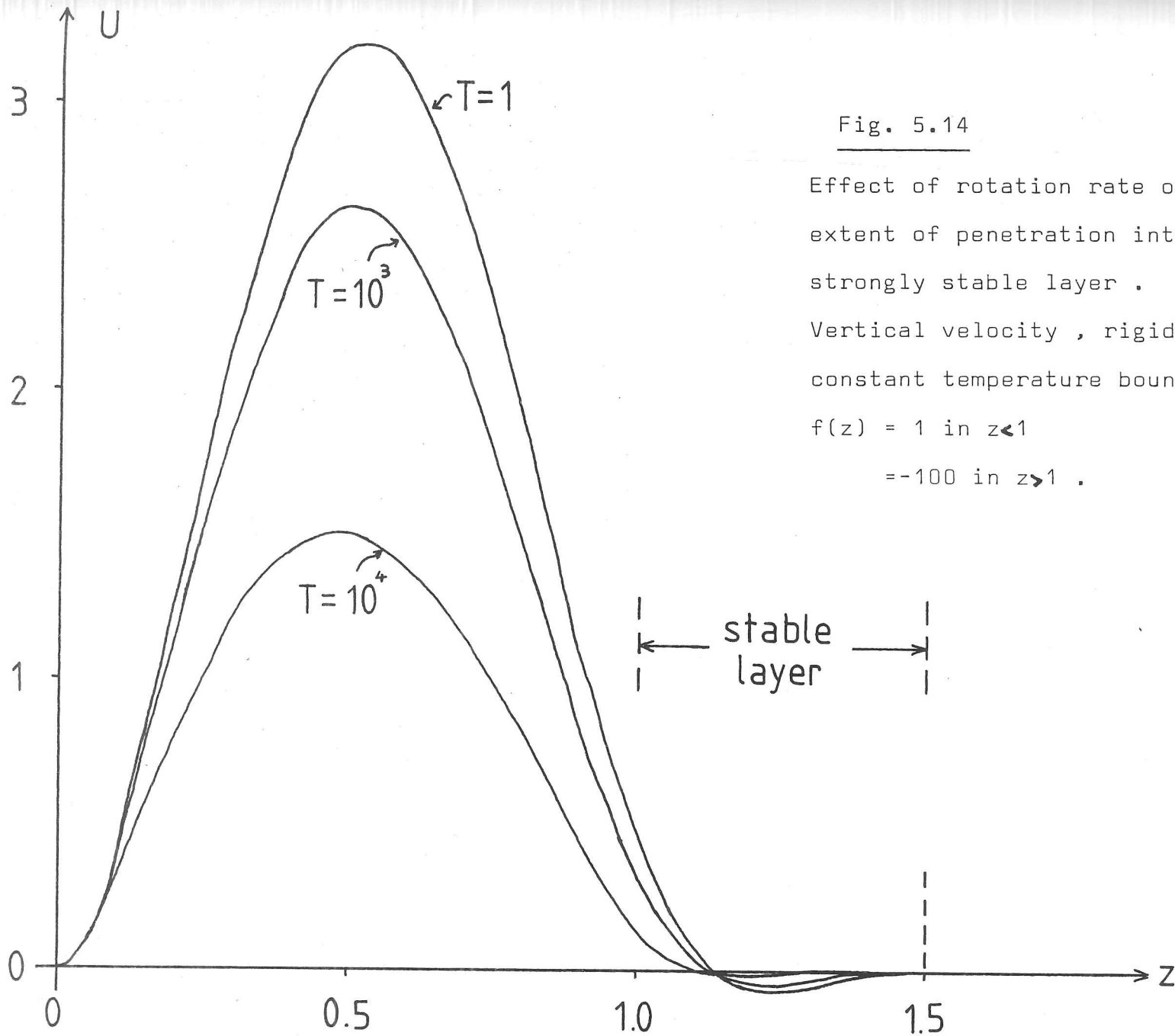


Fig. 5.14

Effect of rotation rate on the extent of penetration into a strongly stable layer .

Vertical velocity , rigid , constant temperature boundaries .

$f(z) = 1$ in $z < 1$

$= -100$ in $z > 1$.

Firstly, in cases where a stable region exists ($h > 1.0$) there is the exponential growth in each shot trial solution in the region of $f(z) < 0$, which becomes more extreme as the Rayleigh number is increased. Secondly, as T becomes large the equations become similar to the 2nd order $T \rightarrow \infty$ approximation discussed in § 4.2: as this occurs, there is increasing difficulty in inverting the results matrix (which tends towards singularity). The limits of use of the shooting program are mapped out in figure 5.15.

In order to extend solutions into the high T region, it is best to take the approximate 2nd order equations from the $T \rightarrow \infty$ analysis. Numerical integration of these is a simple initial value problem in which the one unknown starting boundary condition (DU) can be set arbitrarily to $DU = 1.0$. Results from such an integration are given in Table 5.9, with those from the 8th order equations for rigid boundaries and $T = 10^4$ and 10^5 for comparison. Figure 5.16 shows a logarithmic plot of critical Rayleigh numbers against Taylor number for $h = 1.0$ by both methods. For $T \geq 10^5$, it appears that the approximation of $T \rightarrow \infty$ is reasonable, with the viscous boundary conditions becoming negligible.

5.3.4. Physical explanation for reduced penetration

One physical view of penetrative convection is that it occurs in order to increase the effective depth of the system, even at the expense of a decrease in the overall temperature difference, so as to increase the Rayleigh number of the convecting region (Veronis, 1963). With a smooth temperature profile, the overall temperature difference will of course be a maximum if the boundary for convection is at the point where

Fig. 5.15

Stability of 8th order
shooting program, in
terms of the Taylor No.
and the depth of layer.

program unstable

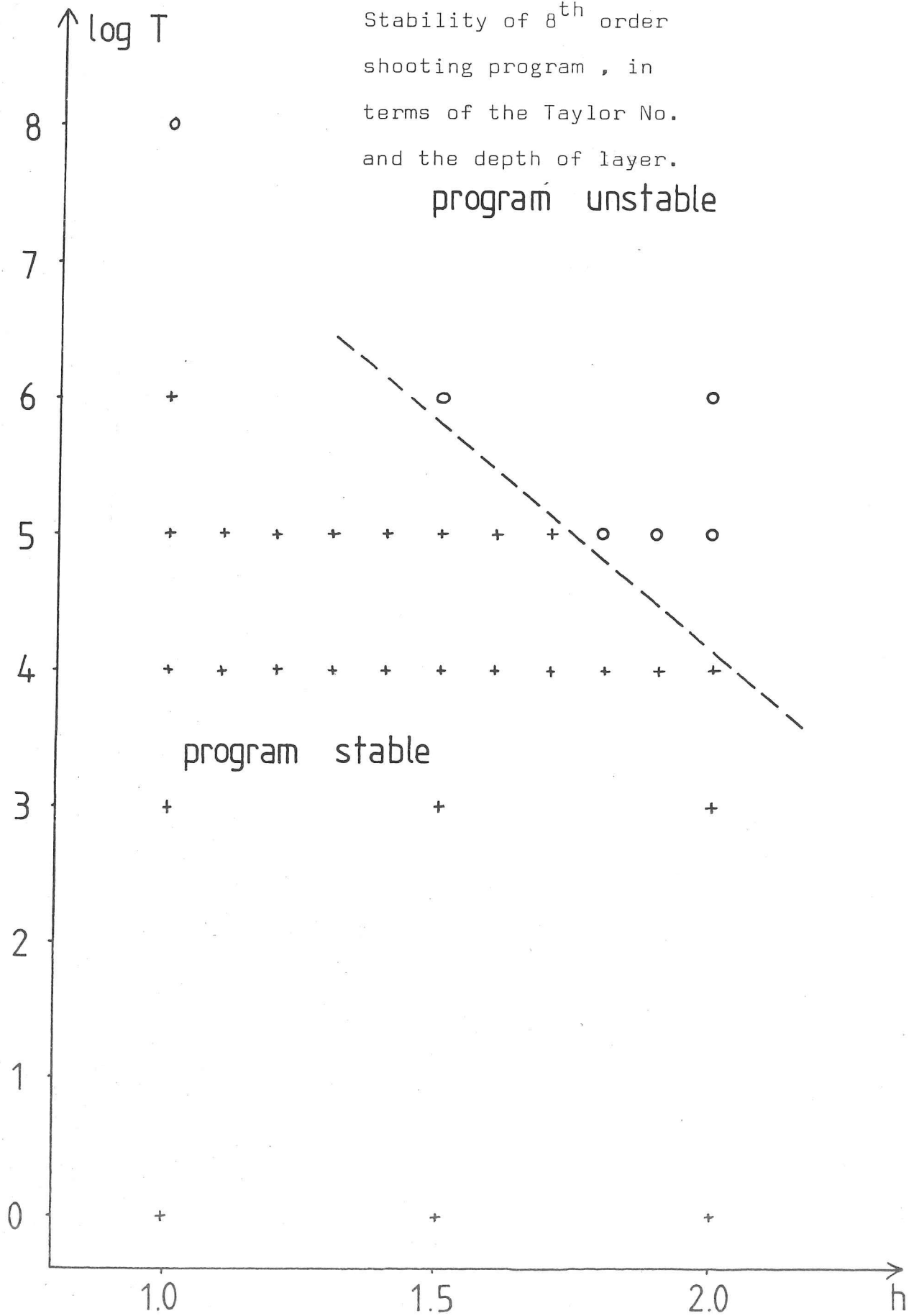


Table 5.9

Critical Rayleigh numbers and wavenumbers

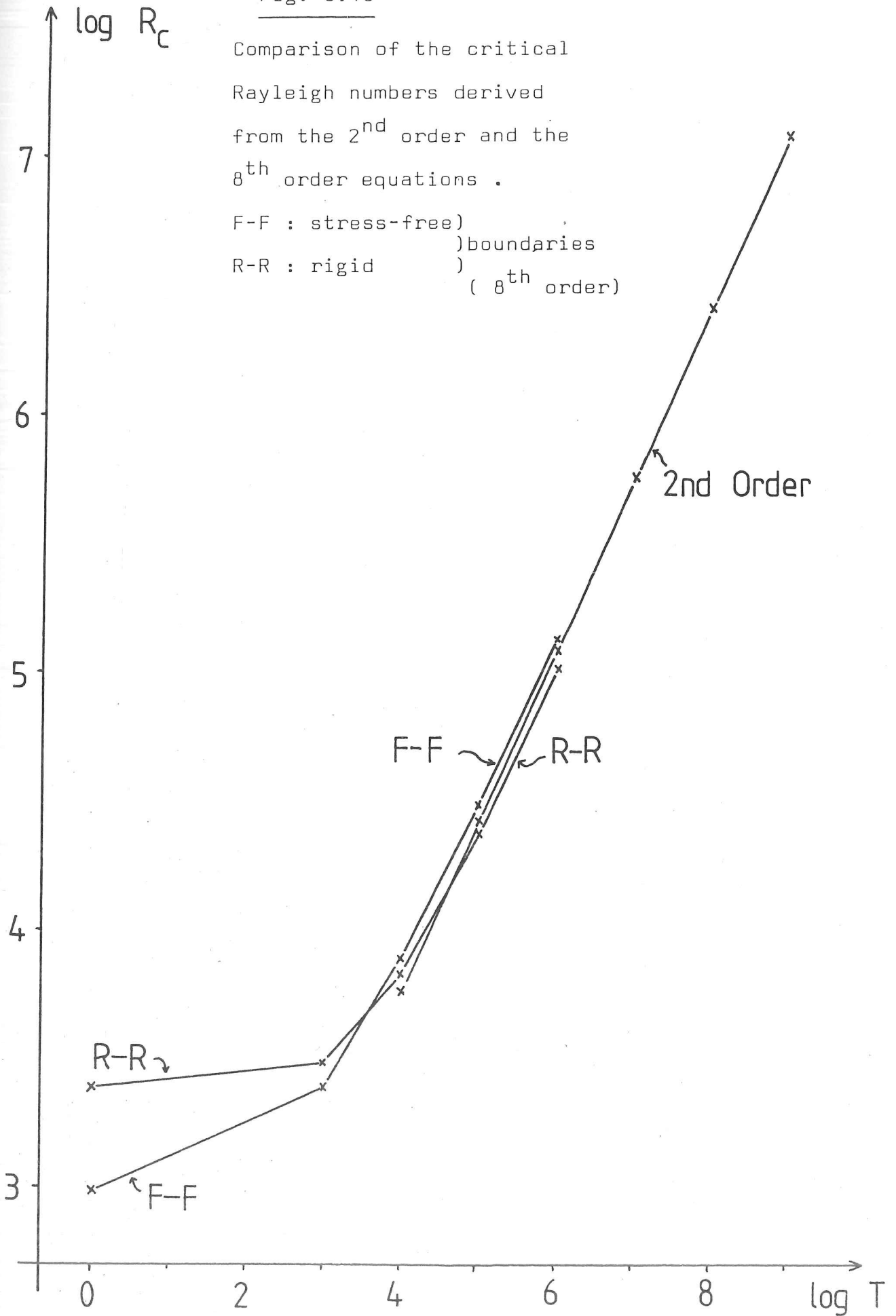
2nd order equations, with comparison to 8th order for $T = 10^4, 10^5$
 $f(z) = \cos(\pi z/2)$

T		h =		
		1.0	1.2	1.4
10^4	8th order	6829	{ 7740 }	5675
	R.R. {F-F}	4.81	{ 5.72 }	4.60
	2nd order	5726		5204
		6.11		5.81
10^5	8th order	24,158	{ 30,416 }	21,445
	R.R. {F-F}	7.25	{ 8.67 }	6.98
	2nd order	26,575		24,152
		8.97		8.53
10^6	2nd order	1.23×10^5	1.12×10^5	1.07×10^5
		13.17	12.53	12.14
10^7		5.72×10^5	5.20×10^5	4.97×10^5
		19.33	18.39	17.83
10^8		2.66×10^6	2.42×10^6	2.31×10^6
		28.4	27.0	26.1
10^9		1.23×10^7	1.12×10^7	1.07×10^7
		41.6	39.6	38.4
T		h =		
		1.6	1.8	2.0
10^4	8th order	5184	5204	5227
	R.R.	4.48	4.51	4.54
	2nd order	4894	4872	4867
		5.54	5.51	5.50
10^5	8th order	20,138	failed	failed
	R.R.	6.81		
	2nd order	22,700	22,615	22,582
		8.14	8.09	8.07
10^6	2nd order	1.05×10^5	1.05×10^5	1.05×10^5
		11.95	11.88	11.85
10^7		4.89×10^5	4.87×10^5	4.87×10^5
		17.51	17.42	17.39
10^8		2.27×10^6	2.26×10^6	2.26×10^6
		25.7	25.6	25.5
10^9		1.05×10^7	1.05×10^7	1.05×10^7
		37.8	37.5	37.4

Fig. 5.16

Comparison of the critical Rayleigh numbers derived from the 2nd order and the 8th order equations .

F-F : stress-free) boundaries
R-R : rigid) (8th order)



$f(z) = 0$, but will diminish but slightly as one considers other nearby positions for the effective boundary. As a result, the d^3 term in the expression for the non-rotating Rayleigh number is dominant:

$$R = \frac{g\alpha(\nabla T \cdot d)d^3}{\kappa\nu}$$

$(\nabla T \cdot d)$ is nearly constant in this region

$$\therefore R/R_c \propto d^3, \text{ favouring penetration.}$$

However, in the limit of rapid rotation, we may expect $R_c \propto T^{2/3}$

(Chandrasekhar, 1961)

$$\text{where } T = 4\Omega^2 d^4/\nu^2$$

$$\therefore R/R_c \propto d^{1/3}$$

Clearly in this limit there is little "incentive" for the system to convect on a deeper length-scale, so that penetration of the stable region is not favoured.

Alternatively, we can consider the reduced equation (4.13) in the limit $T \rightarrow \infty$.

$$T D^2 U = a^2 \left[a^4 - R \cdot f(z) \right] U$$

When $R \cdot f(z)$ is large and positive, we get a 'sine' solution, as in Benard convection. When $R \cdot f(z)$ is negative, we get exponentially decaying solutions. The changeover occurs when

$$\left[a^4 - R \cdot f(z) \right]$$

changes sign, i.e. at a point where $f(z)$ is positive. Thus the

effective region for convection is restricted to only part of the unstable region: the rapid rotation therefore reduces the extent of penetration through the reduction in the order of the equation from 8 to 2.

5.4 "Overstable" Convection

The foregoing results refer to the onset of steady convection, in which the marginal case is that of zero growth, $p = 0$. From equations 4.1a to 4.1c it is possible to envisage solutions which are marginal in the sense that $\text{Re}(p) = 0$ (no growth or decay) but which are oscillatory, with $\text{Im}(p) \neq 0$. In order to investigate such solutions, one must consider both the real and the imaginary parts of the variables U, F, Z . Thus the shooting program has to be extended to 16 simultaneous linear differential equations, with 8 boundary conditions at each boundary, those for the imaginary parts being the equivalent conditions to those for the real parts. The linear inversion of the trial solutions is now that of a (7 x 7) matrix, derived from 8 trial initial condition.

Using this method, one has to set both the horizontal wavenumber 'a' and the overstable frequency 's' ($\equiv \text{Im}(p)$) and then search for the Rayleigh number that will satisfy the boundary conditions. Although the Rayleigh number must in fact be real, being a physical value, the root for the problem for arbitrary pairs of 'a', 's' will not necessarily be real and so one is faced with the additional problem of finding the value of 'a' for given 's' (or vice versa) that will yield a purely real root. Chandrasekhar (1961, pp 114-124) discusses this at greater length. Mismatched pairs of 'a', 's' will yield no real value for R at which the error in fitting the boundary-conditions is

zero (or, in practice, is less than a small limit). If 'a', 's' are close to being a matched pair, one finds that the error converges towards zero as R approaches to its "root" except in a small region, in which it diverges. This region is found to become smaller as one refines the matching of 'a', 's', but can never be eliminated. As a result the convergence routine cannot be used on the Rayleigh number, and finding a root becomes a step by step manual inspection of the results from a grid of trial values of R. This procedure is cumbersome and time consuming: accordingly few results are given in this section. One guide to finding the appropriate value of 'a_c' to match to 's' is to follow the variation of 'a_c' and R_c with 's' away from s = 0, which must correspond to the steady convection solution. Table 5.10 sets out a comparison of results between Chandrasekhar (1961) and the shooting program, for the one specific case of a plane layer, linear temperature profile, rigid constant temperature boundaries and $T=10^4$. Agreement is good, except that the shooting program reveals that the critical wavenumber and frequency are displaced from those given by Chandrasekhar (1961).

5.5 Gravity normal to rotation: thin cylindrical geometry

A further variant of the shooting program is used to investigate the convection equations 4.85a and 4.85b, for cylindrical convection with the body force perpendicular to the axis of rotation. The object is both to investigate the effect of rotation on an idealised penetrative convection profile $f(x)$, and to be able to apply the program to the observations on laboratory experiments set out in chapter 6, for which we need to establish an effective inner boundary to the convection solution in order to avoid problems of large variations of the body force

Table 5.10

Overstability

$f(z) = 1.0$: rigid, constant-temperature boundaries, $h = 1.0$

From shooting program, $T = 10^4$

S	a_c	R_c
0	4.785	4712.4
10		no root found
20		no root found
30	$3.60 \pm .05$	4570 ± 10
40	$3.28 \pm .03$	4410 ± 20
45	$3.065 \pm .005$	4370 ± 5
46	$3.023 \pm .002$	4368 ± 3
47	$2.978 \pm .002$	4366 ± 3
48	$2.935 \pm .005$	4367 ± 3
50	$2.840 \pm .005$	4379 ± 3

Hence critical value is

$$R_c = 4366 \pm 3, S = 47 \pm 1$$

$$a_c = 2.978 \pm .002 \text{ (for } S = 47)$$

Note that near the critical value, a_c varies approximately linearly with S .

Compare Chandrasekhar (1961) for $T = 10^4$:

critical value is

$$R_c = 4390, S = 44.5$$

$$a_c = 3.08 \text{ (which agrees for } S = 44.5)$$

and of curved geometry.

The program used needs to deal with only 6 variables and so can use an explicit algebraic inversion of just a (2 x 2) matrix. In order to test it, the results of Busse's (1970) theory in the case of stress-free perfectly conducting boundaries can be applied (see § 4.5 for this theory and table 5.11 for the results). In the case of $\eta_1 = \eta_2 = 0$, we need not map out the results in both T and a space, since the equations depend on $(E^{\frac{1}{2}} a^2)$. Thus $(a=1, T=1)$ is equivalent to $(a=10, T=10^8)$. If $\eta \neq 0$, no such simplification is available unless the term in η_1, η_2 becomes dominant. The case $\eta \neq 0$ has not been studied in this work, as it leads to the distinct "Busse-roll" solutions that have been studied elsewhere (Busse 1970).

Penetrative convection profiles

1) $f(x) = \cos(\pi a x/2)$, where a is the aspect ratio (see § 4.5)

The cylindrical version of the shooting program produces the results set out in Tables 5.12 to 5.15 when applied with the above profile of temperature gradient and the four combinations of boundary conditions: rigid/stress-free and constant temperature/fixed flux. The results refer to an aspect ratio $a=10$, but for ease of comparison with the plane layer case the

Table 5.11

Shooting-program applied to "Busse-rolls" case, as a test.
 $\eta = 0, \alpha = 10, f(x) = 1.0$, stress-free perfectly conducting boundaries

T	Rayleigh number R	Horizontal wavenumber b	Notes
1	658	22.23	(1)
10^2	660	22.24	
10^4	664	22.27	
10^6	677	22.38	
10^8	720	22.72	
10^{10}	852	23.59	
10^{12}	1257	25.40	
10^{14}	2497	27.76	
10^{16}	6339	29.78	(2)

Notes: 1 In limit $T \rightarrow 0$, Busse predicts $R_c \rightarrow 657.5$
 $b_c \rightarrow \frac{\pi \alpha}{\sqrt{2}} = 22.214$

2 From § 4.5, equation 4.87, predict $R_c = 6341$ for
 $b_c = 29.78$ and
 $a = \pi \alpha$

Rayleigh number R_n and horizontal wavenumber are normalised:

$$R_n \equiv R/a^4$$

$$b_n \equiv b/a$$

As predicted in § 4.5, the effect of increasing the rotation rate is much less than in the plane layer case. The effect is again to decrease the depth of penetration, as indicated by the position h of lowest critical Rayleigh number.

In the two cases of fixed flux boundaries (tables 5.14, 5.15), there is again the effect of the stable region on whether $b_n = 0$ is the critical solution, just as in the plane layer case. However, the effect of rotation on this is much weaker and is only observed in the results for stress-free boundaries (table 5.15).

Figure 5.17 shows the vertical velocity profile in the case of rigid, constant temperature boundaries, $h = 2.0$ and $T = 1, 10^8$ or 10^{16} . The profiles are normalised by $D^2U(x=0) = 1.0$ in each case. Higher rates of rotation are associated with a slight movement of the peak velocity further into the unstably stratified region.

2) Parabolic profile $f(x) = 1-ax$

The cylindrical version of the program has been applied to a parabolic temperature profile in order to serve for comparison with the experiments described in chapter 6, both in terms of *the* observed shape of the temperature profile and as an extension of the model to cases in which the stable region is deep. In all cases, a rigid boundary at $x = 0$ is applied (to correspond to the apparatus side-wall) and in general another rigid boundary is applied at $x = h$. A few runs (marked by square brackets in Table 5.16) include a stress-free boundary at $x = h$ and these indicate that for $ah \geq 2.0$ this change of boundary condition has

Table 5.12

Critical Rayleigh numbers and wavenumbers

Rigid, constant temperature boundaries

$f(x) = \cos(\pi a x / 2)$, $a = \text{aspect ratio} = 10$

Rayleigh No. and wavenumber normalised: $R_n = R_c / a^4$, $b_n = b_c / a$

T	ah =	1.0	1.2	1.4	1.6	1.8	2.0
1	R_n	2845	1449	1009	828	796	826
	b_n	3.12	2.61	2.26	2.03	1.94	2.00
10^4	R_n	2493	1456	1015	835	803	833
	b_n	3.12	2.61	2.26	2.03	1.94	2.00
10^8	R_n	2575	1525	1079	900	873	904
	b_n	3.13	2.62	2.27	2.04	1.96	2.02
10^{12}	R_n	3391	2205	1708	1535	1533	1566
	b_n	3.17	2.66	2.33	2.13	2.09	2.15
10^{16}	R_n	11301	8734	7660	7372	7419	7479
	b_n	3.26	2.75	2.43	2.27	2.27	2.33

Table 5.13

Critical Rayleigh numbers and wavenumbers

Stress-free, constant temperature boundaries

$f(x) = \cos(\pi a x / 2)$, $a = 10$

I	ah =	1.0	1.2	1.4	1.6	1.8	2.0
1	R_n	966	568	400	336	342	382
	b_n	2.23	1.86	1.61	1.44	1.39	1.51
10^4	R_n	975	575	406	343	350	391
	b_n	2.23	1.87	1.61	1.45	1.40	1.52
10^8	R_n	1057	644	471	410	421	459
	b_n	2.28	1.92	1.67	1.52	1.49	1.60
10^{12}	R_n	1841	1293	1069	1009	1030	1058
	b_n	2.55	2.20	1.96	1.83	1.84	1.90
10^{16}	R_n	9228	7407	6645	6459	6510	6559
	b_n	3.00	2.56	2.29	2.17	2.18	2.23

Table 5.14

Critical Rayleigh numbers and wavenumbers
 Rigid, fixed flux boundaries
 $f(x) = \cos(\pi ax/2)$, $a = 10$

T	ah =	1.0	1.2	1.4	1.6	1.8	2.0
1	R_n	1065	630	451	399	446	495
	b_n	0	0	0	0	1.07	1.43
10^4	R_n	1068	633	454	402	450	500
	b_n	0	0	0	0	1.07	1.43
10^8	R_n	1101	660	480	433	491	544
	b_n	0	0	0	0	1.08	1.44
10^{12}	R_n	1419	930	742	734	876	951
	b_n	0	0	0	0	1.14	1.46
10^{16}	R_n	4347	3380	3094	3424	4146	-
	b_n	0	0	0	0	1.34	

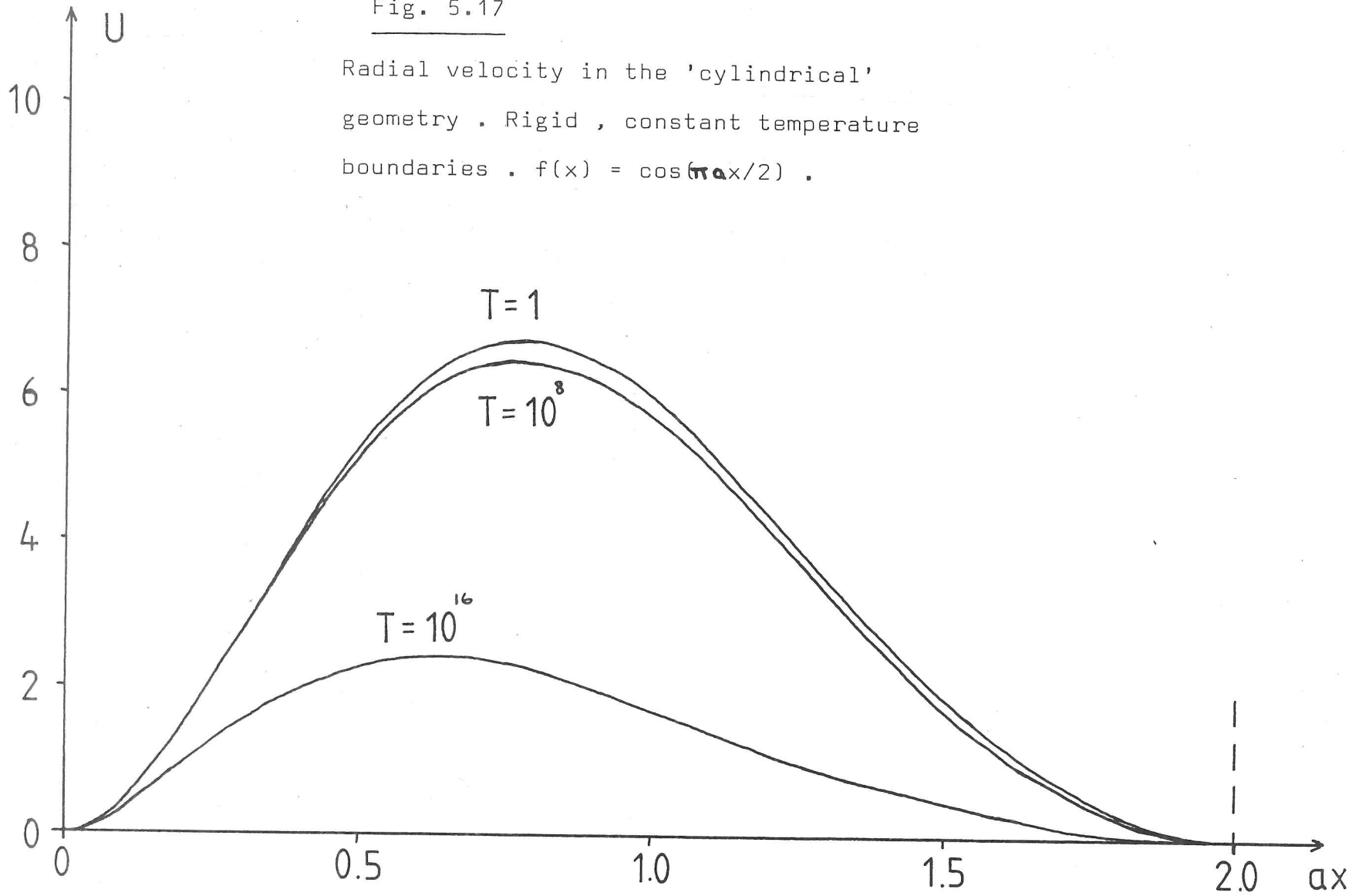
Table 5.15

Critical Rayleigh numbers and wavenumbers
 Stress-free, fixed flux boundaries
 $f(x) = \cos(\pi ax/2)$, $a = 10$

I	ah =	1.0	1.2	1.4	1.6	1.8	2.0
1	R_n	180	107	78	69	89	155
	b_n	0	0	0	0	0	0.97
10^4	R_n	183	109	80	72	93	158
	b_n	0	0	0	0	0	0.98
10^8	R_n	206	129	99	94	130	194
	b_n	0	0	0	0	0	1.04
10^{12}	R_n	438	328	294	322	448	506
	b_n	0	0	0	0	0.85	1.22
10^{16}	R_n	2744	2307	2238	2594	3215	-
	b_n	0	0	0	0	1.13	

Fig. 5.17

Radial velocity in the 'cylindrical'
geometry . Rigid , constant temperature
boundaries . $f(x) = \cos(\pi ax/2)$.



no appreciable effect: the stable layer acts as a shield for that boundary. Tables 5.16 and 5.17 show the results for constant temperature and fixed flux boundary conditions respectively. In both cases there is only a small variation in the results as h increases beyond $ah = 2.0$, less than 10% in b_c and less than 5% in R_c . The only qualitative change as h increases is that a countercell does appear for $ah \geq 2.4$ ($ah \geq 2.2$ as rotation rates increase to $T = 10^{12}$). This is very similar to the behaviour shown in § 5.2 in which the horizontal plane layer version of the program was tested on a parabolic profile. For $ah \approx 3.0$, the countercell appears in $2.0 < \alpha x < 2.1$ and so corresponds to the region that is stable relative to all parts of the fluid (figure 5.18).

From this, we may compare observations made on a system with a deep stable layer with numerical models based solely on the region $0 \leq \alpha x \leq 2.0$, neglecting the remainder of the stable region. Thus we can avoid both excessive computation and the difficulty of specifying a suitable internal boundary.

Biot number

The experimental tank is one in which the sidewall is an imperfect conductor of finite thickness and so the shooting program has been applied to the mixed thermal boundary conditions, $DF = \pm (\alpha \lambda) F$, where λ is the Biot number.

$$\lambda \equiv \frac{k_s \cdot d}{k_f \cdot l}$$

where k_s , k_f are the thermal conductivities of the solid wall and of the fluid, l is the wall thickness and d the unstable layer depth. The aspect ratio α enters into the boundary-

Table 5.16

Critical Rayleigh numbers and wavenumbers
 Rigid, constant temperature boundaries, unless marked
 for which $x = h$ boundary is stress-free
 $f(x) = 1 - ax$, $a = 10$

I	$ah =$	1.0	1.2	1.4	1.6	1.8	2.0
1	R_n	3393	2025	1426	1173	1125	1168
	b_n	3.13	2.62	2.26	2.03	1.94	2.00
		2383					1187
		2.70					2.04
10^4	R_n	3405	2034	1434	1182	1135	1178
	b_n	3.13	2.62	2.27	2.03	1.94	2.00
		2395					1197
		2.71					2.05
10^8	R_n	3516	2131	1524	1275	1234	1278
	b_n	3.13	2.62	2.27	2.05	1.97	2.02
		2513					1296
		2.73					2.06
10^{12}	R_n	4625	3075	2407	2165	2159	2206
	b_n	3.17	2.67	2.33	2.14	2.10	2.15
10^{16}	R_n	15343	12087	10683	10286	10342	10417
	b_n	3.27	2.77	2.44	2.29	2.29	2.30

I	$ah =$	2.2	2.4	2.6	2.8	3.0	5.0
1		1188	1184	1180	1180	1180	1180
		2.05	2.05	2.04	2.03	2.03	2.03
						1180	
10^4		1198	1197	1190	1190	1190	1190
		2.05	2.05	2.04	2.04	2.04	2.04
						1190	
10^8		1296	1295	1289	1289	1289	1289
		2.07	2.07	2.06	2.06	2.06	2.06
						1289	
10^{12}		2219	failed				
		2.18					
10^{16}		failed					

Table 5.17 Critical Rayleigh numbers and wavenumbers
 Rigid fixed flux boundaries
 $f(x) = 1 - ax, \quad a = 10$

I		ah =	1.0	1.2	1.4	1.6	1.8
1	R_n		1441	869	625	550	612
	b_n		0	0	0	0	1.05
10^4	R_n		1445	872	629	554	618
	b_n		0	0	0	0	1.05
10^8	R_n		1489	910	666	596	674
	b_n		0	0	0	0	1.06

T		2.0	2.2	2.4	2.6	2.8	3.0
1	R_n	685	707	703	695	692	692
	b_n	1.43	1.53	1.53	1.51	1.50	1.49
10^4	R_n	691	713	709	701	698	698
	b_n	1.43	1.53	1.53	1.51	1.50	1.50
10^8	R_n	752	774	770	763	760	760
	b_n	1.43	1.53	1.54	1.52	1.50	1.50

condition because of the non-dimensionalisation of the equations, but the results depend only on λ for all values of α . Table 5.18 gives selected critical Rayleigh numbers and wavenumbers for a range of values for λ , T and ah : in each case the boundaries are rigid. In these results, the stable region is large enough to prevent $b_c = 0$ being the critical solution for a fixed flux boundary condition: the effect of changing λ on R_c and b_c is therefore quite regular. Experimental conditions ($\lambda \approx 0.15$, $\alpha \approx 100$, $T \approx 10^{12}$) are approximately equivalent to ($\lambda = 0.15$, $\alpha = 10$, $T = 10^4$) through the dependence on $(T\alpha^{-8})$, and so we expect a critical Rayleigh number for the tank of approximately $R_c = 730$. Figure 5.18 is plotted for $\lambda = 0.10$, $\alpha = 10$, $T = 10^4$ and so is similar to the expected velocity profile at the onset of convection in the tank. Note in particular the countercell for $2.05 \leq \alpha x \leq 3.0$: the main convection cell is effectively confined to $0 \leq \alpha x \leq 2$.

At low λ (i.e. nearly fixed-flux), the stable layer acts to inhibit long wavelength convection just as it does for strictly fixed flux boundaries. As for that latter case, there is some value of depth of the stable region at which a high wavenumber solution has an equally low Rayleigh number to the low wavenumber critical solution, and so the critical wavenumber shows a jump with increasing depth ah . Table 5.19 shows this effect for $\lambda = 10^{-5}$. Near the low wavenumber critical solutions the Rayleigh number is only very weakly dependent on the wavenumber, and so the critical wavenumber is not well located (fig. 5.24, for $\lambda = 10^{-5}$, $ah = 1.0$). In the 'deep' cases ($ah \geq 1.7$) with high wavenumber solutions, the effect of rotation is the usual one of increasing both R_c and b_c . However, in the "shallow" cases ($ah \leq 1.6$) with a low wavenumber solution, an increased rotation rate

Table 5.18

Effect of Biot number λ on critical Rayleigh numbers and wavenumbers
 Rigid boundaries, $f(x) = 1 - ax$, $a = 10$

T		$\lambda =$	0 (fixed flux)	0.1	1	10	∞ (constant temperature)	
$ah = 2.0$	1	R_n	685	708	833	1071	1168	
		b_n	1.43	1.48	1.70	1.94	2.00	
	10^4	R_n	691	714	840	1080	1178	
		b_n	1.43	1.48	1.70	1.94	2.00	
	10^8	R_n	752	777	913	1172	1278	
		b_n	1.43	1.49	1.71	1.96	2.02	
	$ah = 3.0$	1	R_n	692	713	838	1081	1180
			b_n	1.49	1.53	1.73	1.97	2.03
		10^4	R_n	698	719	845	1090	1190
b_n			1.50	1.53	1.73	1.97	2.04	
10^8		R_n	760	783	918	1181	1289	
		b_n	1.50	1.54	1.74	1.99	2.06	

Table 5.19

Dependence of critical solution on depth of layer at low Biot number λ .
 Rigid boundaries, $\lambda = 10^{-5}$, $a = 10$, $f(x) = 1 - ax$

I	$ah =$	1.0	1.6	1.7	2.0
1	R_n	1443	550	570	685
	b_n	0.160	0.13	0.62	1.43
10^4	R_n	1448	554	575	692
	b_n	0.160	0.13	0.62	1.43
10^8	R_n	1491	597	625	752
	b_n	0.160	0.14	0.62	1.43
10^{12}	R_n	1921	1008	1100	1308
	b_n	0.159	0.131	0.66	1.46
10^{16}	R_n	5858	4625	5323	failed
	b_n	0.14	0.095	0.09 5198 0.76	

Note: Rayleigh number is only weakly dependent on wavenumber and so in some cases b_n is given to only a limited accuracy.

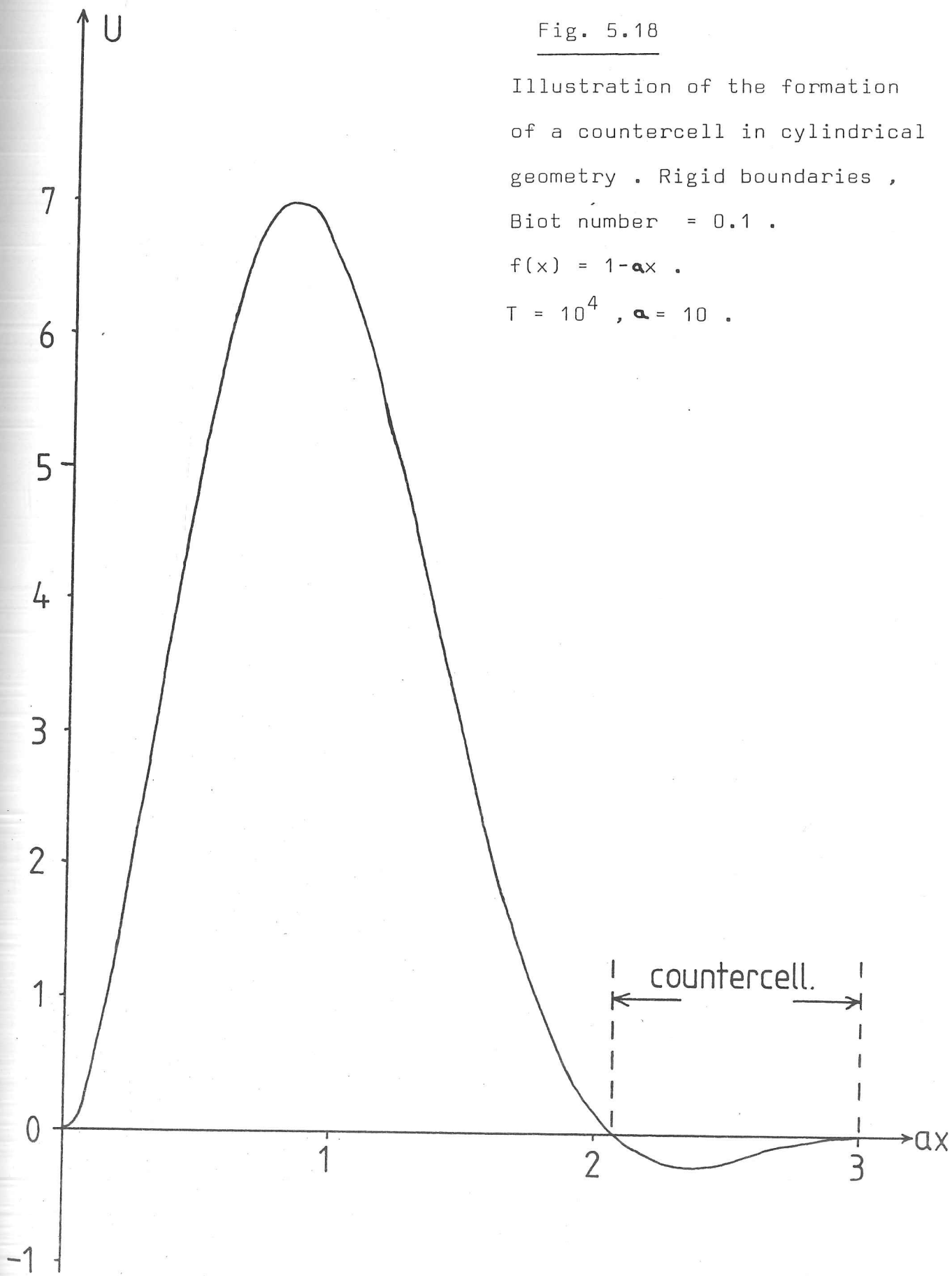


Fig. 5.18

Illustration of the formation
of a countercell in cylindrical
geometry . Rigid boundaries ,
Biot number = 0.1 .

$$f(x) = 1 - ax .$$

$$T = 10^4 , a = 10 .$$

leads to longer critical wavelengths (lower wavenumbers), opposite to the usual behaviour. However one must note that the differences in Rayleigh number involved in selecting the critical wavenumber are very small, and so this effect is of no practical significance.

5.6 Summary of results from the shooting program

1) Plane-layer: steady convection, g parallel to $\underline{\Omega}$

The effect of increasing rotation is to restrict the convection more to the unstable region of a penetrative convection profile, whilst leading to higher critical Rayleigh numbers and horizontal wavenumbers as in the standard non-penetrative case. This restriction of the extent of the convection is clearly seen in graphs of D^2U , in which, as rotation rate increases, $z = 1$ (the changeover point from unstable to stable density gradients) comes to be near a zero of D^2U .

In the case of fixed-flux boundaries, increased rotation rates enhance the effect of a deep stable region in inhibiting zero wavenumber from being the critical solution. $T = 10^4$ is sufficiently fast rotation for the critical solution to occur for non-zero wavenumber even with no stable region ($h = 1$). This limits the geophysical applicability of non-linear theories based on scale separation for fixed flux boundary convection problems (e.g. Proctor (1981)).

The shooting program shows that countercells are only excited for rather deeper stable layers than was previously predicted by methods based on truncated series expansions: in the case of a smooth density profile such as $f(z) = 1-z$. an upper boundary $Z = h$ of $h \geq 2.5$ is required. On the other hand, with an asymmetric density profile such that the stable region is much

stronger than the unstable, a countercell occurs at lower values of h . No simple power-law relation is found between the position of the countercell and the relative strength of the stable layer (figure 5.16). Increasing the rotation rate in such cases results in the inhibition of the countercell (for $T \geq 10^4$), as is expected as one approaches the limiting case $T \rightarrow \infty$.

2) Plane-layer: overstability

Few results have been obtained for the overstable case, which is a double eigenvalue problem (in frequency and Rayleigh number) as noted by Chandrasekhar (1961). Although the shooting program can locate the eigenvalues to any required accuracy, it cannot then produce a set of eigenfunctions: a good fit to the boundary conditions is never achieved in the close neighbourhood of the eigenvalues. Thus the method is of limited use in this case.

3) Cylindrical convection, \underline{g} perpendicular to $\underline{\Omega}$

The effect of rotation is much less marked than in the plane layer case, as is expected from the equations. In particular, increasing T has much less effect on inhibiting $b_c = 0$ from being the critical solution for fixed flux thermal boundary conditions. A parabolic temperature profile extending to $ah = 3.0$ has been investigated in order to compare results with the experimental tank (chapter 6), and it is shown that increasing the stable region beyond $ah = 2.0$ has little effect on the eigenvalues R_c and b_c , although a countercell in the region $ax > 2.0$ occurs for $ah > 2.5$. The effect of Biot number is also investigated, and is quite regular for $ah = 2.0$ or 3.0 , which would apply to the experimental results. However, for $ah \leq 1.6$, in which case one has the long wavelength $b_c = 0$ solution for fixed flux thermal

boundaries, there is an anomalous behaviour with increasing rotation rate in that increased rotation leads to lower critical wavenumbers, appropriate to lower Biot numbers. This effect is slight (up to $T = 10^{18}$, the limit of the numerical technique) but anomalous and as yet unexplained.

6.1 Introduction

The object of the experimental work has been to test the predictions of the theory set out in §4.5, which was based on the work of Busse (1970), for the onset of convection and further to investigate the growth of the resulting convecting region into the stably stratified region. In distinction to the experimental work on "Busse-rolls" of Busse & Carrigan (1974) and of Chamberlain (1980), a cylindrical tank has replaced the spherical tanks, so that effects due to the inclination (η) of the end-walls have been eliminated. A penetrative convection type of density profile is set up by the use of a time-dependent boundary temperature: such a procedure was suggested by Veronis (1963) for the non-rotating case of penetrative convection in a plane layer.

The temperature differences involved are small, of the order of 0.05°C across the unstable region, and the depth of the unstable region is of the order of 3 mm only. Thus direct temperature measurements, for example by the use of bead thermistors, are not feasible. Instead a thermal conduction model is used to calculate the temperature profile at various times, the model being checked by separate experiments using widely-spaced thermistors (§ 6.3). This approach is only valid before the onset of convection, although if the Rayleigh number of the system becomes only marginally supercritical then one can expect the temperature profile to be but little affected by the resulting convective flows and heat transport.

The apparatus consists of a rotating experimental tank enclosed within a water jacket whose temperature can be varied and measured. The water jacket and associated temperature control are those built by Carrigan and Chamberlain and a full description, in particular of the temperature control, is given in Chamberlain (1980).

The experimental tank (shown in figs. 6.1 and 6.2) for this work is cylindrical, with top and bottom walls positioned, by machining, to be normal to the rotation axis to ± 0.1 mm. Thus any inclination of the top and bottom boundaries, (equation 4.87), is negligible. The side walls are of thin (3 mm) perspex, the top and bottom walls are double 3 mm sheets of perspex, with a 3 mm air-gap. As a result, the side-walls are relatively good conductors whilst the top and bottom walls may be taken to be insulating when calculating the temperature profile of the tank. Distilled water is used as the working fluid in the experiments.

The main constraint on the design of the tank side walls and joints is the need for sufficient mechanical strength to withstand the centrifugal pressure generated by the tank's rotation. Rotation rates in the range 30 - 100 radians s^{-1} are needed for the centrifugal forces to dominate laboratory gravity, given the size limitation of the water jacket, and for the upper end of that range a 3 mm walled perspex cylinder gives an adequate safety factor in tension. Glued joints on perspex are liable to cracking and so the only such joint is designed to be under compression when the tank rotates (figure 6.2). In practice some leaking of water occurs through the greased and bolted end-joint when the tank is in use, but several experimental runs of 2 hours duration are possible before the resulting

Fig. 6.1

Schematic diagram of the
experimental tank .

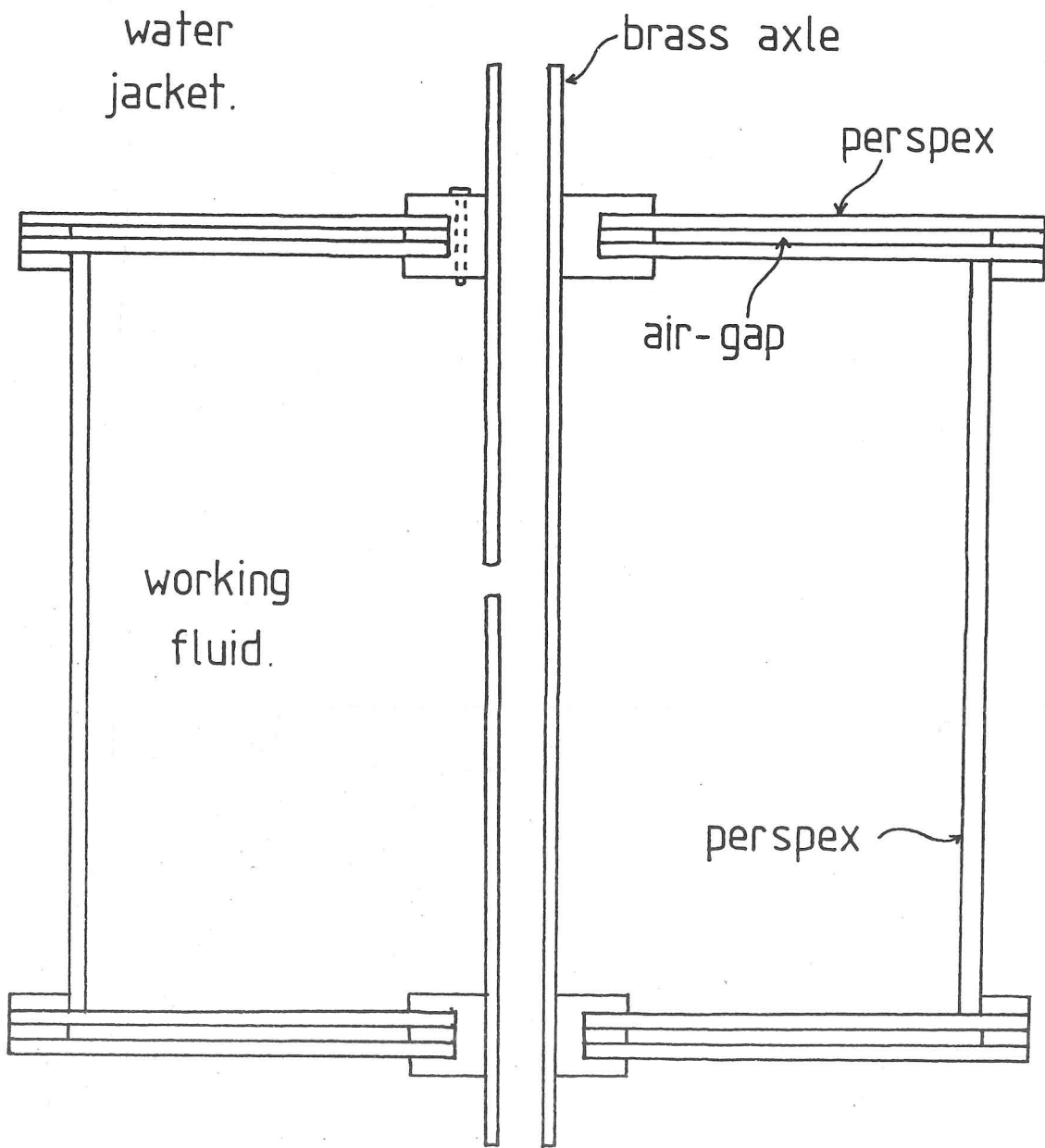


Fig. 6.2

Detail of joint construction
of the experimental tank .

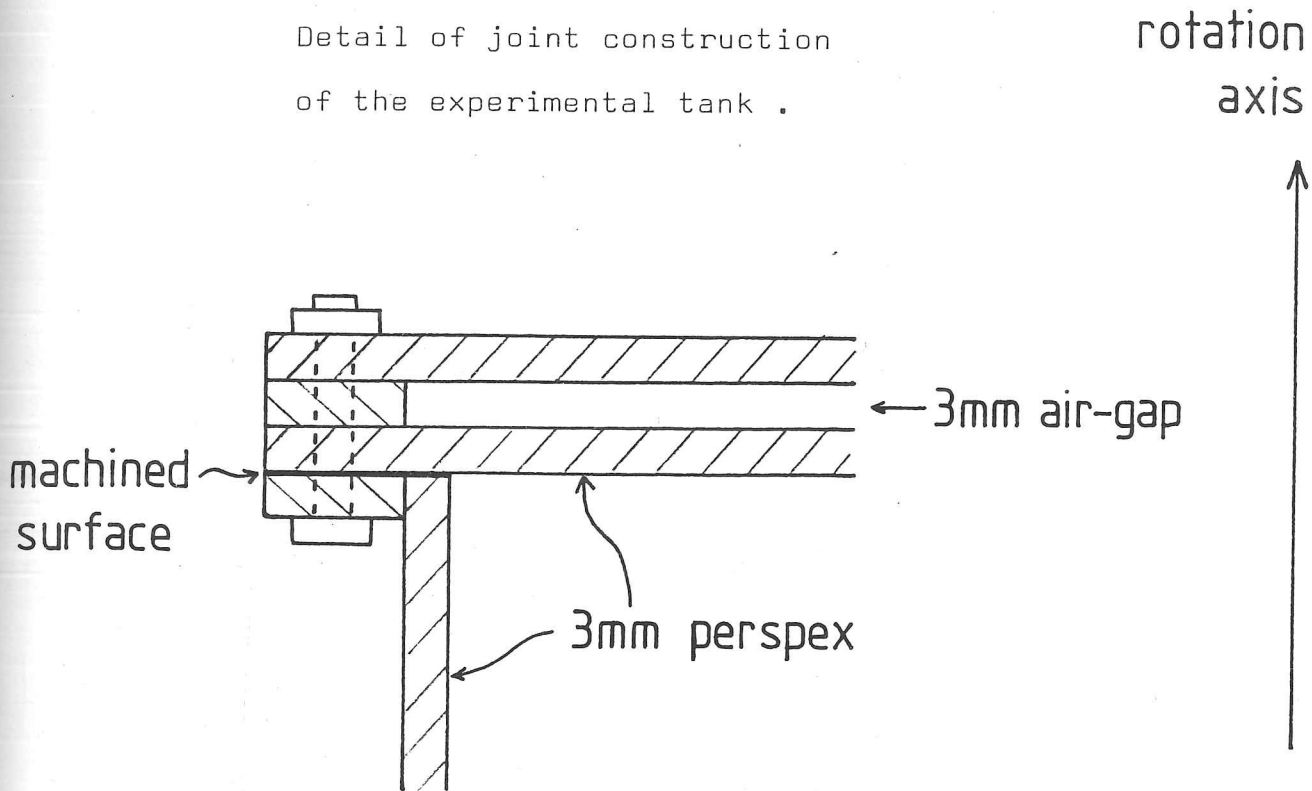
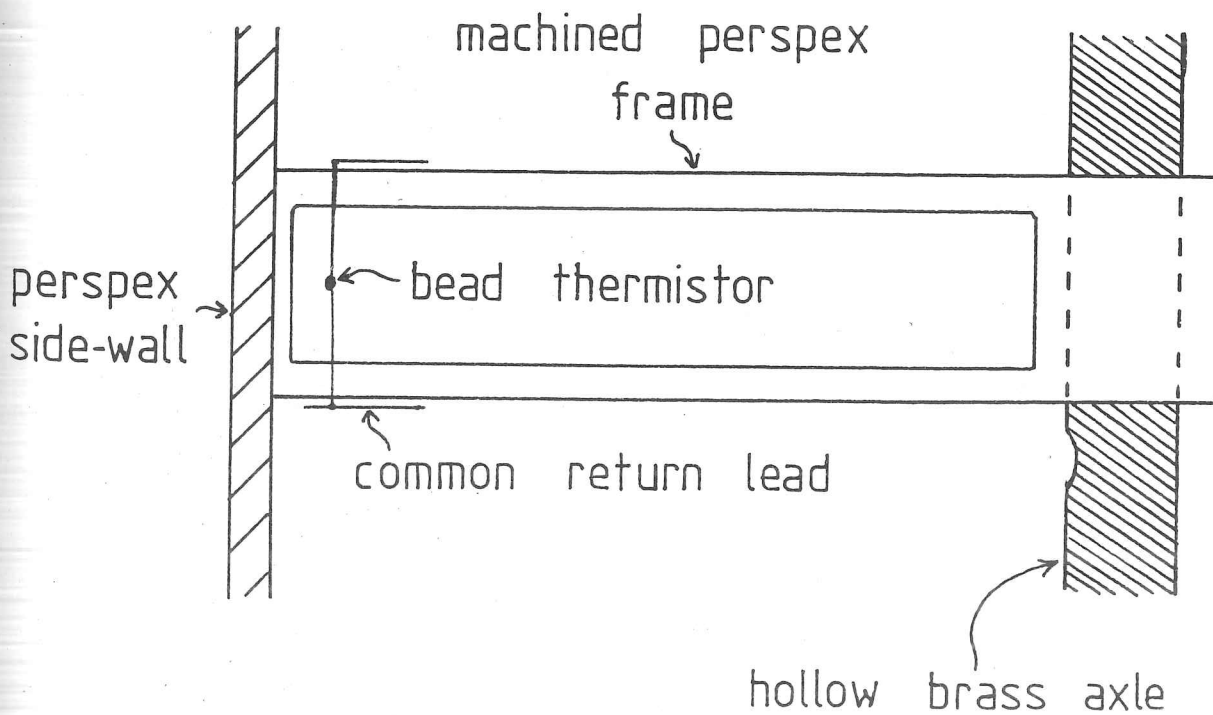


Fig. 6.3

Thermistor array . Only one thermistor shown .



Tank properties

Table 6.1

Axial length	L	=	0.2 m
Internal radius	R_o	=	$72 \times 10^{-3} \text{ m}$
Side-wall thickness		=	$3 \times 10^{-3} \text{ m}$
Construction material		=	perspex

Perspex properties (from ICI Ltd information sheets):

- i) density $\rho = 1.19 \times 10^3 \text{ kg.m}^{-3}$
- ii) thermal conductivity $k = 0.19 \text{ J m}^{-1} \text{ Ks}^{-1}$
- iii) specific heat $c_p = 0.35$
- iv) tensile strength $\approx 8 \times 10^6 \text{ Nm}^{-2}$

Distilled water at 30°C (from Batchelor (1967))

- i) thermal diffusivity $\kappa = 1.46 \times 10^{-7} \text{ m}^2 \text{ s}^{-1}$
- ii) kinematic viscosity $\nu = 8.02 \times 10^{-7} \text{ m}^2 \text{ s}^{-1}$

Thermistor beads: ITT U23UD miniature bead, nominally $2\text{K}\Omega$, diameter $\approx 0.3 \times 10^{-3} \text{ m}$, thermal reaction time $\approx 0.3 \text{ s}$.

air-space around the axis becomes a problem.

At the highest rotation rate in fact used, $80 \text{ radians s}^{-1}$, the Taylor number for the tank is approximately 10^{12} , based on an axial length $L = 0.2 \text{ m}$. This results in the tank being in the transition region between "Benard-type" and boundary-layer" convection for the expected unstable region depth d of approximately $d = 5 \text{ mm}$, for which we have an aspect ratio $\alpha = L/d = 40$. In practice, however, d did not greatly exceed 3 mm at the onset of convection, and so the boundary-layer contribution to the critical Rayleigh number is relatively small.

Measurement of the water jacket temperature is by a standard mercury thermometer (Gallenkamp THM-440-070M) immersed in the jacket, capable of being read to $\pm 0.01^\circ\text{C}$ by a Griffin & George thermometer reader. The two such thermometers in use were compared and found to agree to $\pm 0.02^\circ\text{C}$ in the range 7° to 37°C . Typical experimental temperatures are over the range $27\text{--}33^\circ\text{C}$ and, as only relative temperatures are of significant^{ce} for the thermal model, no further calibration of the thermometers (e.g. against a standard gas thermometer) has been thought necessary. Experimental temperatures are kept near 30°C both to allow the use of the 30°C values for properties of water tabulated in Batchelor (1967) in the thermal model and to avoid the need for refrigeration equipment in the temperature control bath.

Time lags in the measurement of water jacket temperatures are negligible: the thermometers were found to react to step changes in temperature with an exponential time constant of approximately 2.5 second, and the water jacket itself is very well stirred by the rotation of the experimental tank, so that the thermometer will experience the same temperature as the tank wall.

Observations of the convection in the tank are made visually under stroboscopic lighting from the side, using an inclined mirror above the water jacket to view along the axis of the experimental cylinder. Kalliroscope suspension AQ1000 is used in an approximately 1% solution in distilled water as a marker for the visual observations. It consists of a suspension of long thin quinine crystals which align themselves with the flow if there is a velocity shear, and as a result scatter light anisotropically. This method of observation is described by Chamberlain (1980) in more detail. However, unlike the case of the "Busse-rolls" observed in a sphere by Chamberlain (1980), no planform can be distinguished in the present study. The contrast between regions of shear and quiet regions is too slight to be recorded photographically when the convection is only slightly supercritical. As a result, the observations of the onset of convection and of its extent set out in § 6.4 are those recorded from direct observation by eye. In making these, it is found that a slight difference in frequency between the tank rotation and the stroboscope illumination greatly assists the observer in that the slow drift seen combines with the irregularities of the scattering to help in distinguishing the presence or absence of convection.

Tests of the numerical thermal model of the tank have been made with the use of bead thermistors mounted on a perspex frame extending from the central axis to the side-wall (fig. 6.3), with power leads to the thermistors fed through the hollow brass axis to a silver slip-ring assembly mounted above the water-jacket and thence to a Solartron 7045 digital resistance meter. Details of these tests are given in the next section. When using thermistors, no Kalliroscope suspension is added to the distilled water,

as the crystals are found to aggregate on the thermistor beads and their leads. Thus there are no combined observations of the convection by both visual means and temperature measurement. Whilst it would be desirable to use a thermistor array to examine the growth of the convecting region in strongly supercritical cases, this has not been done yet owing to frequent mechanical breakages in the thermistor system under rapid rotation.

6.3 Thermal conduction model

The thermal model for the experiments is a numerical integration of the thermal diffusion equation in a tank with cylindrical symmetry. Rather than use a Green's function method, a direct integration over time is performed based on a spatial array of 1 mm radial spacing, so that temperature profiles at successive time steps are available for analysis in terms of the Rayleigh number. If $T(r,t)$ denotes the temperature of the element centred on position r at time t , we have the equation:

$$cp \cdot \frac{\partial T}{\partial t}(r,t) = b_1 (T(r-1,t) - T(r,t)) + b_2 (T(r+1,t) - T(r,t))$$

where the constants b_1 and b_2 for each position r depend on the appropriate thermal conductivity k , position and on the appropriate surface area (cylindrical geometry):

$$b_1 = \frac{k_1}{\delta^2} \left(\frac{r - \frac{1}{2}}{r} \right)$$

$$b_2 = \frac{k_2}{\delta^2} \left(\frac{r + \frac{1}{2}}{r} \right)$$

where δ is the length scale of the grid spacing.

The temperature profile is then integrated by the first order method:

$$T(r, t + 1) = T(r, t) + \tau \frac{\partial}{\partial t} T(r, t)$$

where τ is the time step.

Boundary conditions on the temperature are described below, being

$$T(r, 0) \text{ for all } r_0 \leq r \leq r_i$$

$$T(r_0, t) \text{ for all } 0 \leq t \leq t_0$$

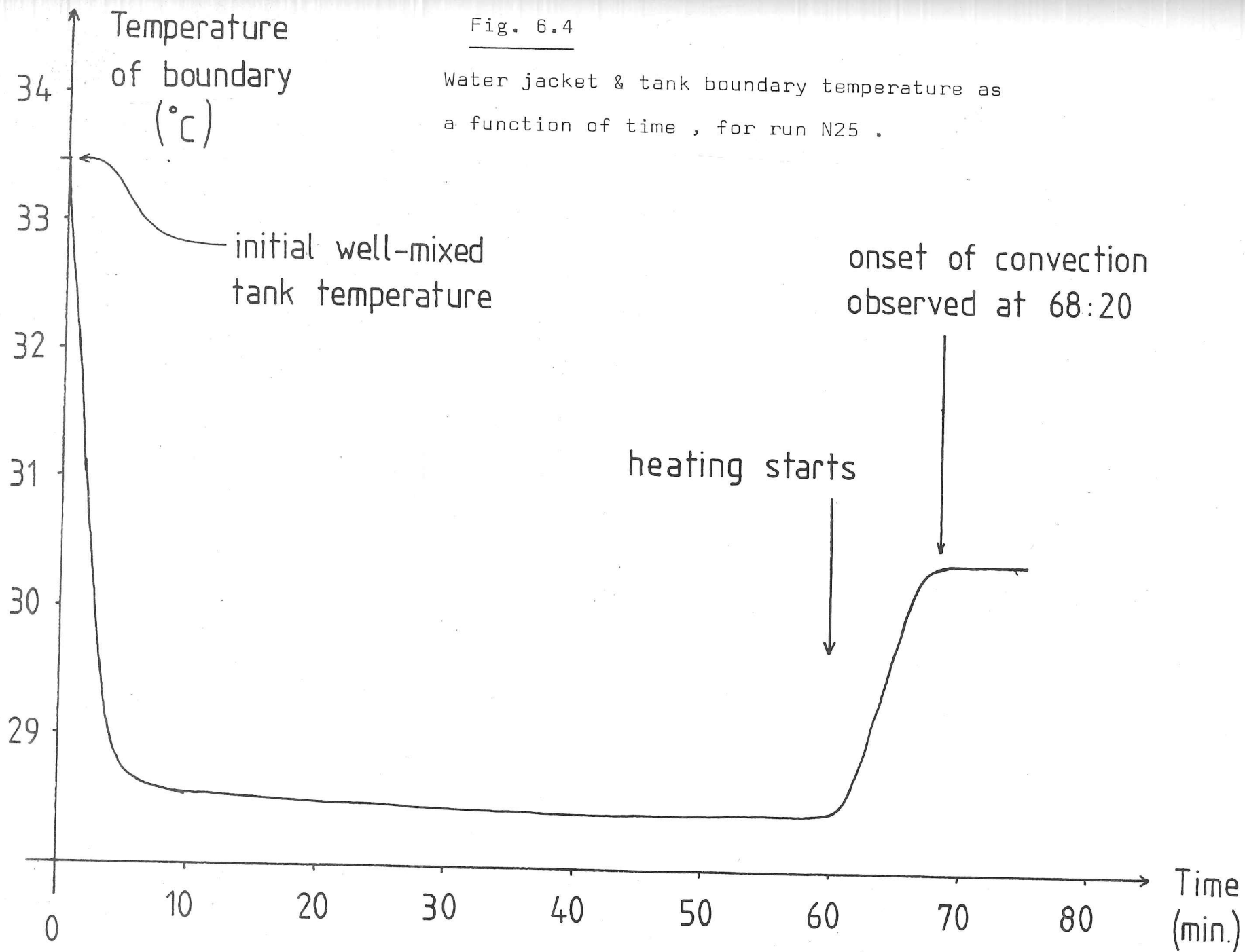
$$T(r_i, t) \text{ for all } 0 \leq t \leq t_0$$

where r_0 is the position of the outside of the tank wall, r_i is the axis of the tank (taken to be $r_i = 1$ mm to avoid the numerical problems of $r = 0$) and t_0 is a time limit, the duration of the experiment.

The temperature $T(r_0, t)$ of the water jacket in a typical experiment (N25) is shown in figure 6.4 as a function of time. At the start of the experiment, $t = 0$, the temperature throughout the tank is assumed constant. The inner boundary condition at $r = r_i$ (where $r_i = 1$ mm on a radial grid of 1 mm spacing) is that there is no heat flux through $r = 0$, by cylindrical symmetry. Alternatively, an inner boundary condition that $T(r_i) = T(r_0)$ can be applied to simulate thermal conduction through the metal shaft of the tank: no material effect on temperatures in the region of interest (near the outer wall) occurs. Figure 6.5 shows the resulting temperature profiles in the tank according to the thermal model at the end of cooling ($t = 60$ minutes) and at 5 minute intervals thereafter. Note the thin unstable region at t

Fig. 6.4

Water jacket & tank boundary temperature as a function of time, for run N25.



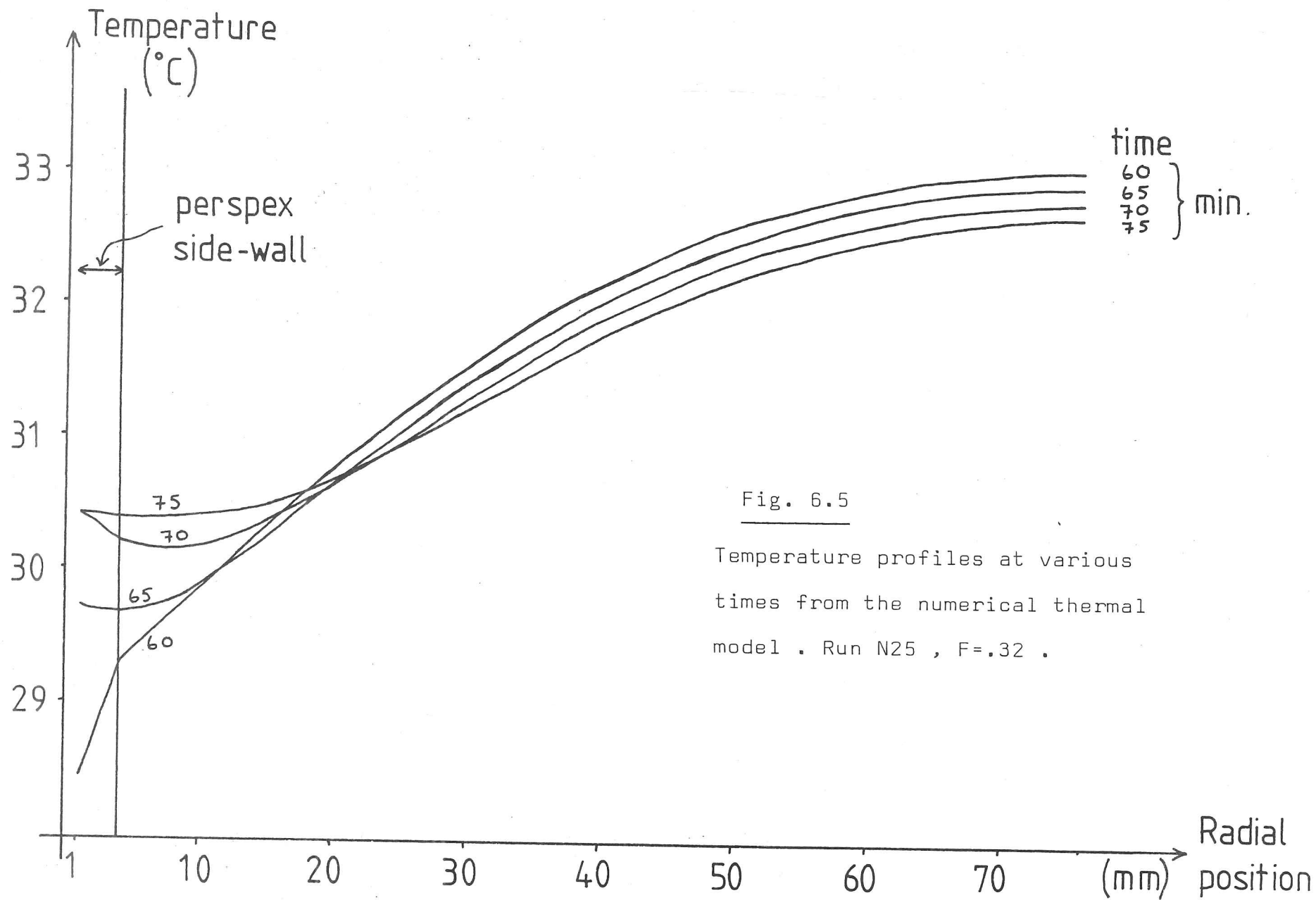


Fig. 6.5
 Temperature profiles at various times from the numerical thermal model . Run N25 , $F=0.32$.

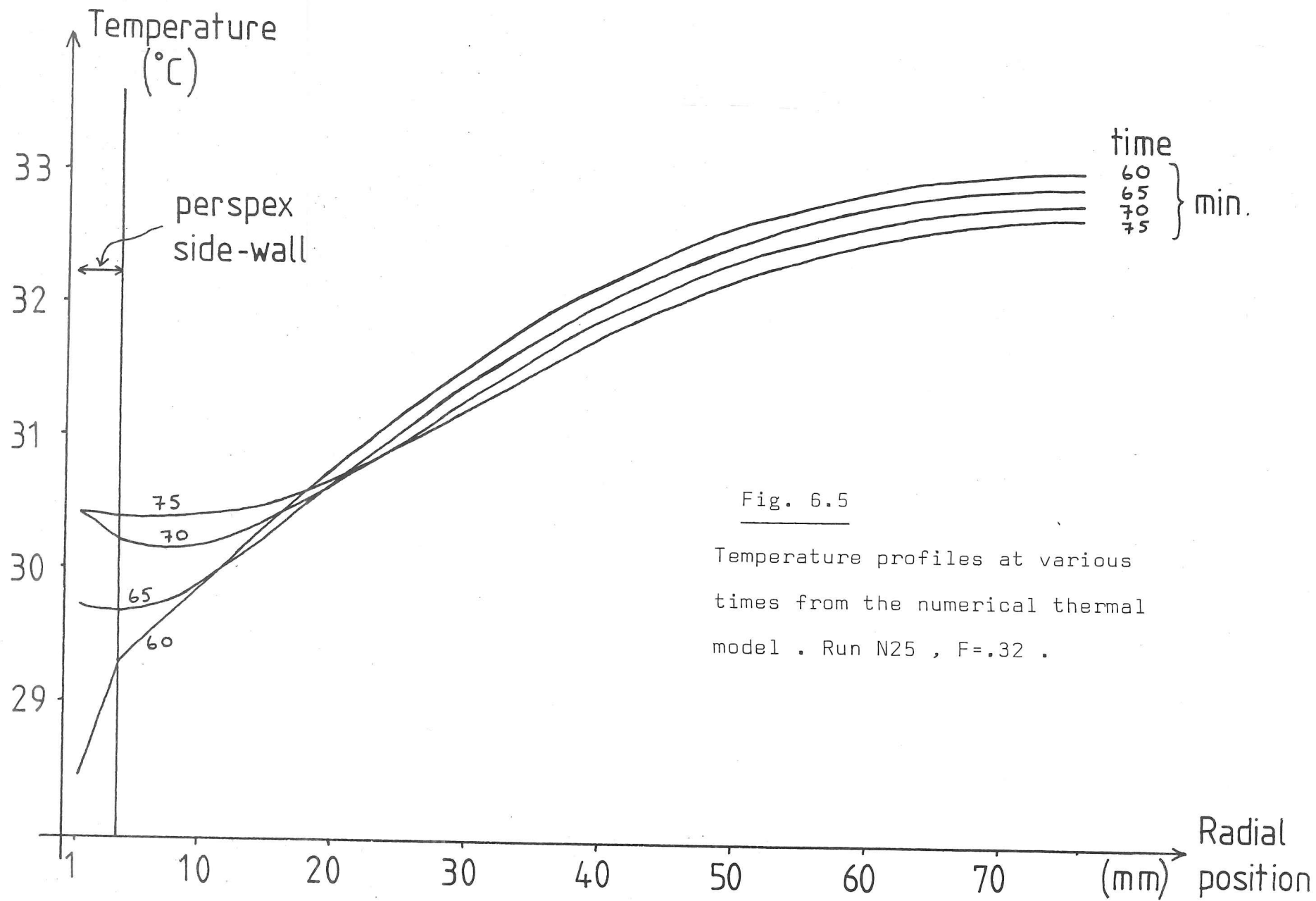


Fig. 6.5
 Temperature profiles at various times from the numerical thermal model . Run N25 , F=.32 .

= 70 minutes, which has almost disappeared by $t = 75$ minutes through diffusive decay.

Test of the model

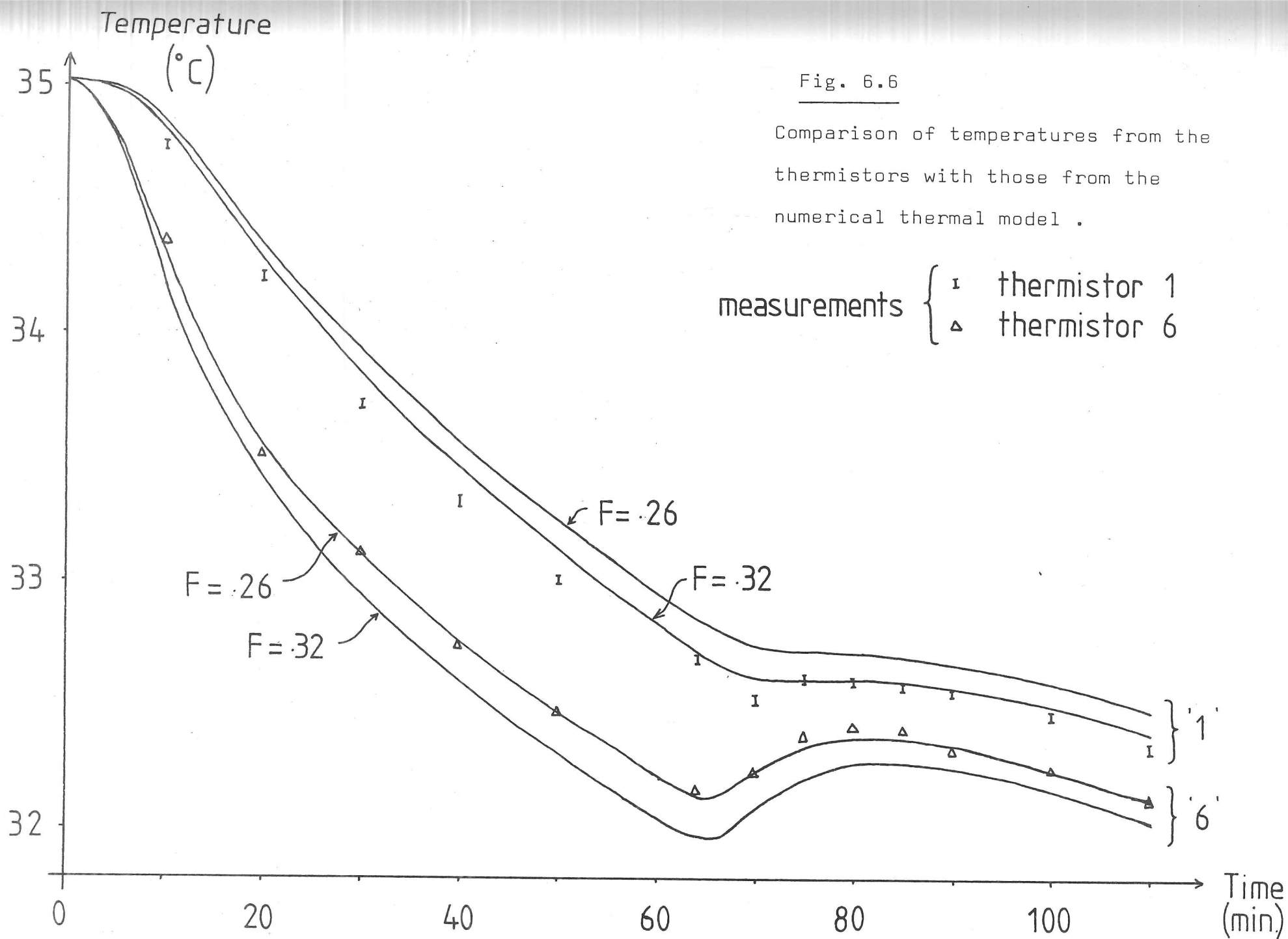
A comparison of the predictions of the model with measurements made using thermistors mounted inside the tank is shown in figs. 6.6 and 6.7. The first of these relates to run number N36 and to the thermistors mounted 16 mm ("1") and 6.5mm ("6") inside the tank wall (the other two thermistors then in use were giving very noisy signals and so have not been analysed). The second relates to run number N37, for which an extra thermistor had been attached to the wall of the tank (thermistor "3").

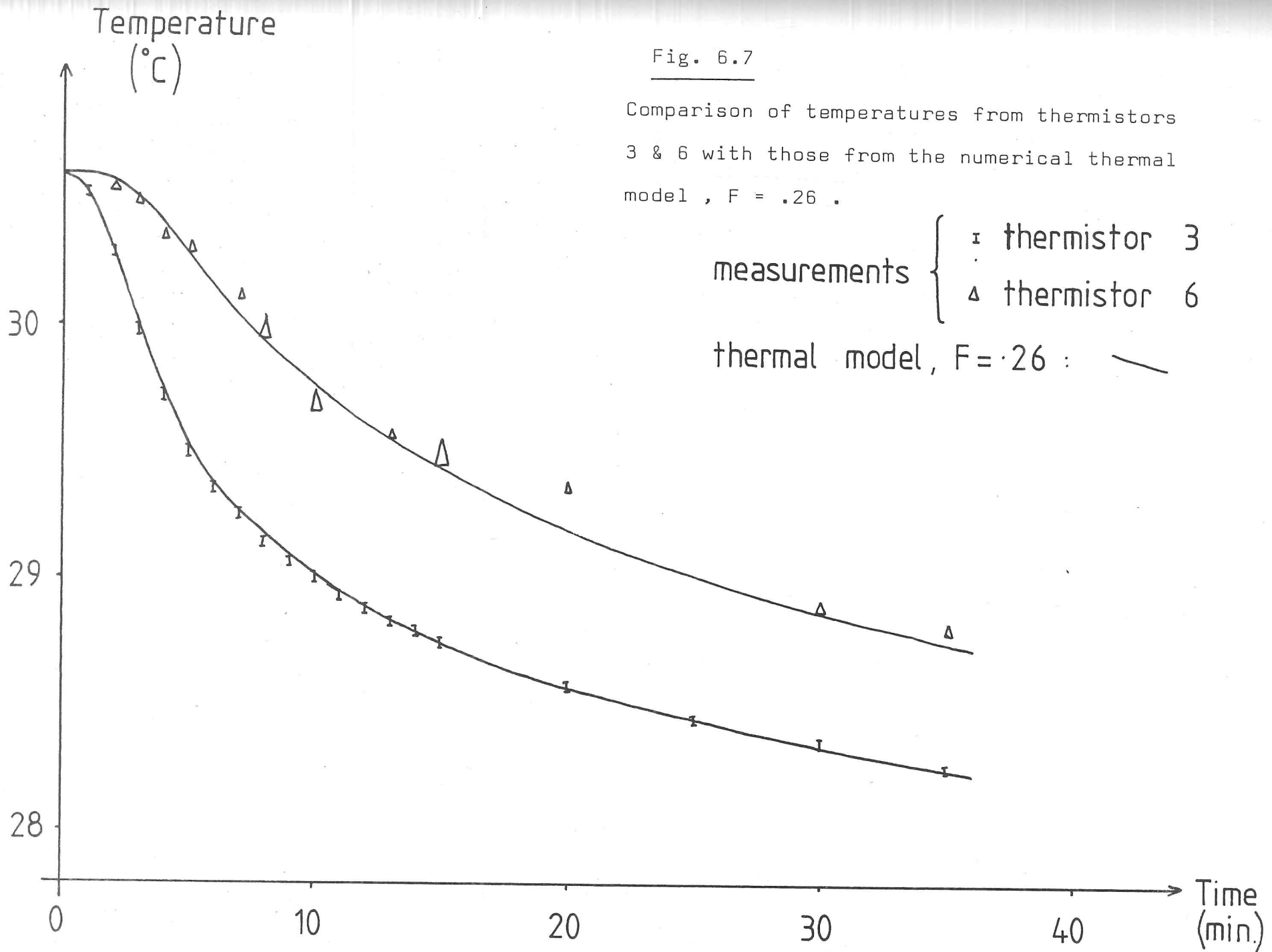
An uncertainty in the properties of the tank is the thermal conductivity of the perspex: in the numerical model this is represented as a fraction F of that of distilled water. The ICI literature value is $F = 0.32$, but variations of $\pm 10\%$ are possible. In addition, in designing the tank one worry was that there might be a boundary layer convection effect on the side-walls, where viscous drag would prevent a thermal wind from balancing the baroclinic pressure field that arises from the interaction of the radial temperature gradient and the axial laboratory gravity (§ 4.6). From the results shown in the figures, although $F = 0.32$ appears suitable with respect to the deeper part of the tank where thermistor '1' is located, it results in predicted temperatures noticeably too low for both thermistors '3' (0.2 mm from the wall) and '6' (6.5 mm from the wall). $F = 0.26$ results in a good fit to the measured temperatures in those latter positions, which span the region of the tank in which convective instabilities occur. Thus $F = 0.26$ is preferred, on the basis of the thermistors, in the analysis of

Fig. 6.6

Comparison of temperatures from the thermistors with those from the numerical thermal model.

measurements { I thermistor 1
 Δ thermistor 6





the experimental runs, but $F = 0.32$ has also been used in order to assess the sensitivity of the analysis to this factor, and will later be shown to be preferable.

One possible source of a systematic error between the thermistor measurements of temperature and the numerical model lies in the disturbance to the internal thermal wind (for which see § 4.6) caused by the presence of the thermistors mounting frame, a perspex "ladder" of side dimensions of order 3 mm. This constitutes a barrier to any azimuthal thermal wind flow by virtue of the change in the overall depth of the fluid. If this is the case, there will be a baroclinic flow in the tank resulting, as above, from the radial temperature gradient and the axial laboratory gravity. This flow will not be an azimuthal thermal wind, but instead will be a "meridional" convection cell leading to enhanced heat flow in the fluid away from the wall. Thus we must consider that the thermistor measurements of temperature, whilst being direct, may be misleading. This problem did not arise in the experiments in spherical tanks by Chamberlain (1980) because in a spherical tank there remains a path of constant depth along which geostrophic flow can occur even though there be a radial obstruction such as a thermistor array. The path merely has a radial kink, compensating for the obstruction (fig. 6.8).

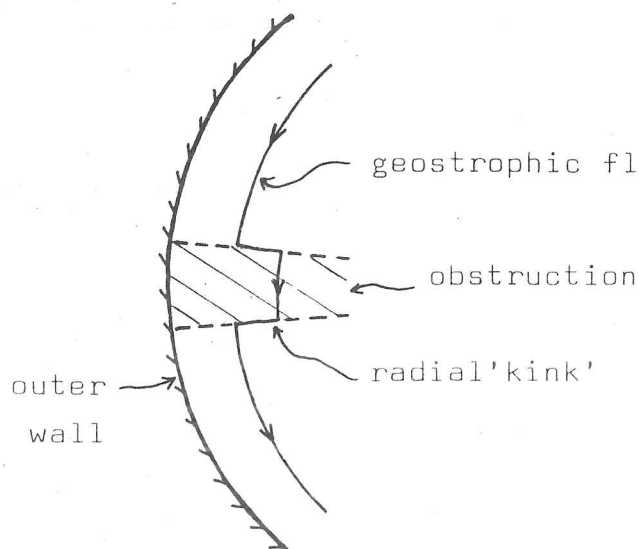


Fig.6.8

Effect of an obstruction on the flow path in a spherical tank geometry

Thermistors

As stated above, the resistances of the miniature bead thermistors and their leads are measured directly with a Solartron 7045 meter held on the 0-9 k Ω range, with sensitivity of $10^{-1} \Omega$. Changes of the meter range affect the reading (due to different internal impedance) but with the meter held on the one range it proves stable to $\pm 2 \times 10^{-1} \Omega$ between experiments. Calibration of the thermistors is based on measurements of their resistances while in place in the tank. In each case the tank is well-mixed (by spin-up then spin-down) and the water-jacket temperature adjusted until there is thermal equilibrium as shown by all the thermistors. The calibration measurements are made with the tank rotating, both to ensure that the water jacket is well mixed and to simulate the experimental conditions of the slip-rings incorporated in the thermistor lead circuits. Calibration tables are produced by an interpolation program that fits a cubic both to the two data points being interpolated and the next neighbouring data point on each side.

The sensitivity of the resistor meter, $\pm 0.1 \Omega$, corresponds approximately to a temperature sensitivity of $\pm 0.01^\circ\text{C}$ at the thermistors, i.e. in line with the accuracy to which the mercury thermometer in the water jacket can be read. As a combination of these two separate sources of measurement error, the measurements plotted in figs. 6.6 and 6.7 are given error estimates of $\pm 0.02^\circ\text{C}$, unless a noisy reading was noted at the time of the experiment (notably run N37 thermistor '6'). No sign of thermistor "warm-up" is ever observed with the thermistors immersed in water, but instead a slight cooling is observed over a period of about 3 seconds, typically involving an increase in resistance of .1 or .2 Ω over that period. In all

cases, measurements are taken after that change. This appears to be a result of the growth of local forced convection from the electrically heated thermistor bead, or perhaps due to the production of a thin gas layer on the bead surface by electrolysis, reducing the leakage current through the surrounding water. As the effect appears to be quite regular, no further investigation has been necessary.

6.4

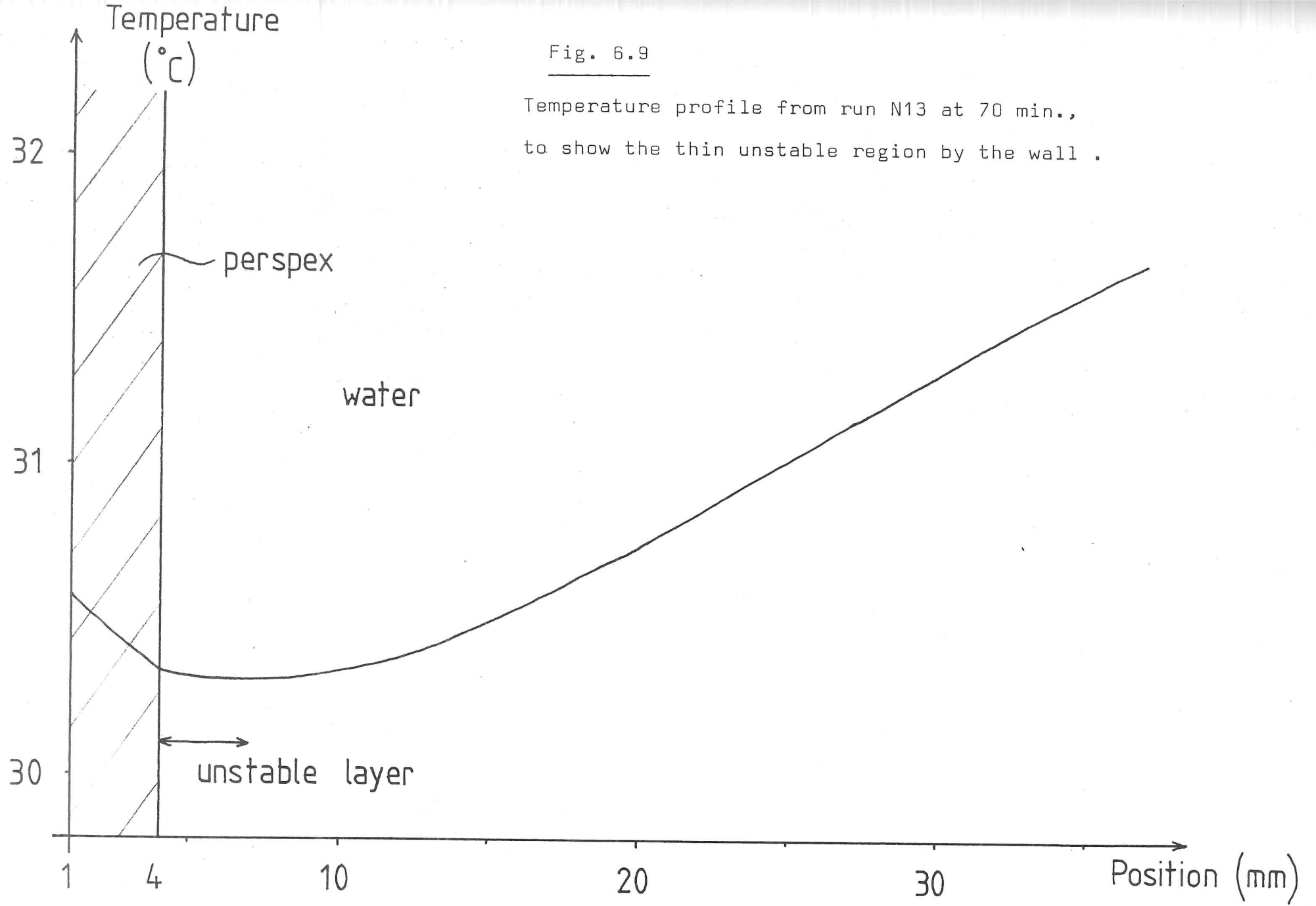
Observations

In general, observations have been made on experimental runs in which the tank is cooled for 60 minutes in order to set up a stable stratification and then heated over approximately 5 minutes in order to introduce an unstable region near the side-wall. Such a run is similar to that used in the thermistor temperature test run N36 shown in fig. 6.6. A typical temperature profile near the side-wall is shown in fig. 6.9, being at 70 minutes (i.e. after 10 minutes heating) in run N13, showing an unstably stratified region of depth 3 mm (positions 4 to 7 on the graph) and then stably stratified fluid further from the perspex sidewall. Runs were made at either 7.0 or 9.8 times the rotation unit of 2.5π radians s^{-1} : the accuracy of the speed controller was checked by observing the drive pulley under mains frequency stroboscopic lighting. The two speeds used give a variation of a factor of 2 in the centrifugal "gravity" in the tank.

The observations of the times of onset of convection are uncertain because convection only becomes visible at finite amplitudes: one needs both some degree of supercriticality and also a time interval for growth. As a result the Rayleigh number at the time observed for onset should be only an upper limit. In

Fig. 6.9

Temperature profile from run N13 at 70 min.,
to show the thin unstable region by the wall .



order to indicate how critical the timings are, the results are presented together with error estimates based on ± 10 seconds observation errors. The error due to the need for a growth period depends on the degree of supercriticality, but as an indication one can take the thermal diffusion time constant (d^2/κ) for the unstable layer depth, which is approximately 60 seconds, as an upper limit to this growth period.

Table 6.2 and fig. 6.10 give the results for the experimental runs, based on a thermal model with $F = 0.26$ (relative thermal conductivity of perspex) as indicated by the thermistor measurements. The Rayleigh numbers are calculated from temperatures interpolated to a 0.1 mm grid, and therefore do not always change smoothly with time. This result of grid "coarseness" leads to an uncertainty in the calculated value of R of approximately 10% at times of interest, which is not significant given the scatter in R_c shown in the table. The results are to be compared to the numerical results of the shooting program in § 5.5. For a rigid side-wall, parabolic temperature profile and a deep stable region, that model gives an approximate critical Rayleigh number of 730 for the appropriate Biot number, $\lambda \approx 0.15$. Clearly the scatter of the results is too great to be able to resolve the variations in R_c arising from different rotation rates.

The effect of using $F = 0.26$ in the thermal model rather than $F = 0.32$ can be seen by comparing Table 6.2 with Table 6.3, for which the latter value is used. The higher value of perspex conductivity results in markedly higher values for the Rayleigh number at the observed onset of convection. It also gives a greater length-scale d , which is of significance both to the effect of rotation (which enters as $\alpha^{-8} \times T$) and to the Biot

Table 6.2

Run Number N	Experimental Runs Observed time of onset of convection after start of heating (min : sec)	Rotation rate (2.5 rads ⁻¹)	Thermal model based on $F = 0.26$			Subse- quent peak R & time	d (mm) at onset	Notes
			10 sec. early	at onset	10 sec late			
13	7 : 30	9.8	620	754	751	1820 (10:35)	2.1	
14	-	9.8		-			-	
16	7 : 30	9.8	645	782	938	1497 (9:05)	2.1	
18 i) doubtful	9 : 30			0.06			-	
ii)	18 : 00	9.8	(after peak R = 3.5)					
			102	256	553	>18,000 (21:00)	1.8	
19	7 : 40	9.8	500	623	767	1386 (8:50)	2.0	
20	7 : 15	7.0	64	91	158	749 (8:55)	1.5	
21	4 : 10	7.0	875	1327	1888	12,590 (7:45)	2.4	
22	6 : 20	7.0	127	157	152	168 (7:05)	1.8	
23	5 : 50	7.0	277	274	333	473 (7:15)	1.9	
24	12 : 35	7.0	54	73	95	261 (13:50)	1.7	Previous peak R=64 at time 5:30 gave no observed convection

.../Cont'd

Table 6.2 (Cont'd)

<u>Run Number</u> N	Experimental Runs		Thermal model based on $F = 0.26$				<u>Subse- quent peak R & time</u>	<u>d (mm)</u> at onset	<u>Notes</u>
	<u>Observed time of onset of convection after start of heating</u> (min : sec)	<u>Rotation rate</u> (2.5π rads ⁻¹)	<u>R_c</u>						
			10 sec. early	at onset	10 sec. late				
25	8 : 20	7.0	509	489	471	509 (8:10)	2.3		
26	9 : 15	7.0	20	19	13	44 (7:30)	1.3	Peak R = 44 occurred at 7:30	
27	14 : 25 :	7.0	31	55	72	259 (16:10)	1.6		
28	-	9.8		-				Peak R = 0.3	
29	15 : 00	9.8	407	506	616	>17,000 (21:00)	2.2	Previous peak R = 3	
30	8 : 20	9.8	293	288	348	348 (8:30)	1.8		
31	7 : 25	9.8	318	412	519	1650 (9:10)	1.8		

Table 6.3

Run Number N	Experimental Runs Observed time of onset (min : sec)	Rotation Rate (2.5π rads ⁻¹)	Thermal model based on $F = 0.32$			Subse- quent peak R & time	d onset (mm)	Time delay since R = 730 (sec)	Notes
			10 sec. early	R _c at onset	10 sec. late				
13	7 : 30	9.8	4693	5307	5970	13,671 (10:20)	3.1	75	
14	-	9.8		-		0.12 (11:05)	-	-	No convection
16	7 : 30	9.8	5497	6185	6929	10,352 (8:55)	3.2	80	
18 i) doubt- ful	9 : 30	9.8	299	278	210	after 684 (7:55)	2.0	-	
ii)	18 : 00		1789	3082	4405	>67,000 (>21:00)	3.0	25	
19	7 : 40	9.8	4090	4695	5366	9215 (9:05)	3.0	70	
20	7 : 15	7.0	776	1129	1348	5157 (9:30)	2.5	10	
21	4 : 10	7.0	4075	5514	7131	40,374 (8:05)	3.2	50	
22	6 : 20	7.0	1525	1492	1672	1983 (7:05)	2.8	50	
23	5 : 50	7.0	1965	2225	2510	3710 (7:25)	2.9	50	
24	12 : 35	7.0	1214	1416	1641	3394 (14:10)	3.1	30	Previous peak R = 1158 at 6:25 gave no convection

.../Cont'd

Table 6.3 Cont'd

Run Number N	Experimental Runs		Thermal model based on $F = 0.32$					Time delay since $R = 730$ (sec)	Notes
	Observed time of onset (min : sec)	Rotation Rate (2.5π rads ⁻¹)	R_c		Subse- quent peak R & time	d onset (mm)			
			10 sec. early	at onset	10 sec. late				
25	8 : 20	7.0	3597	3481	3376	3841 (9:05)	3.4	95	
26	9 : 15	7.0	803	773	741	909 (8:30)	2.7	100	Earlier peak
27	14 : 25	7.0	792	1073	1237	3578 (16:45)	2.9	10	Previous peak $R = 413$ at 8:15 gave no convection
28	-	9.8	-	-	-	245 (7:55)	-	-	No convection
29	15 : 00	9.8	4507	5141	6466	>68,000 (>21:00)	3.5	80	Previous peak $R = 738$ at 8:50 gave no convection
30	8 : 20	9.8	3229	3625	3537	4196 (9:05)	3.0	95	
31	7 : 25	9.8	2691	3648	4207	11,197 (10:10)	2.8	50	
						average =		<u>58</u>	

number at onset (which rises in proportion to d). This sensitivity of the results to the value of the perspex conductivity leads to a large error-margin in the results, one that could be eliminated in future experiments most easily by using a material of higher and more uniform conductivity than perspex. The problem is one of finding a suitable material that is both strong in tension to withstand the centrifugal forces and is transparent to enable visual observations from side illumination.

Figures 6.10 and 6.11, plotting the results for $F = 0.26$ and $F = 0.32$ models respectively, show more clearly both the extent of the scatter of the results and also how compatible they are with the numerical prediction from the critical Rayleigh number. Clearly the $F = 0.32$ model is the more compatible; although the scatter of results is large, it is less than that for the $F = 0.26$ model. Further, if one concentrates attention on those runs for which onset was observed to occur at a model value for R_c within 30% of the peak R_c (i.e. runs in which conditions peaked near critical), runs 22, 25, 26 and 30, together with the "null" results, there is rather better agreement with the theory (figure 6.12). However, the results still cannot be said to verify the results from theory: the scatter involved is too great even after this selection of "best" runs.

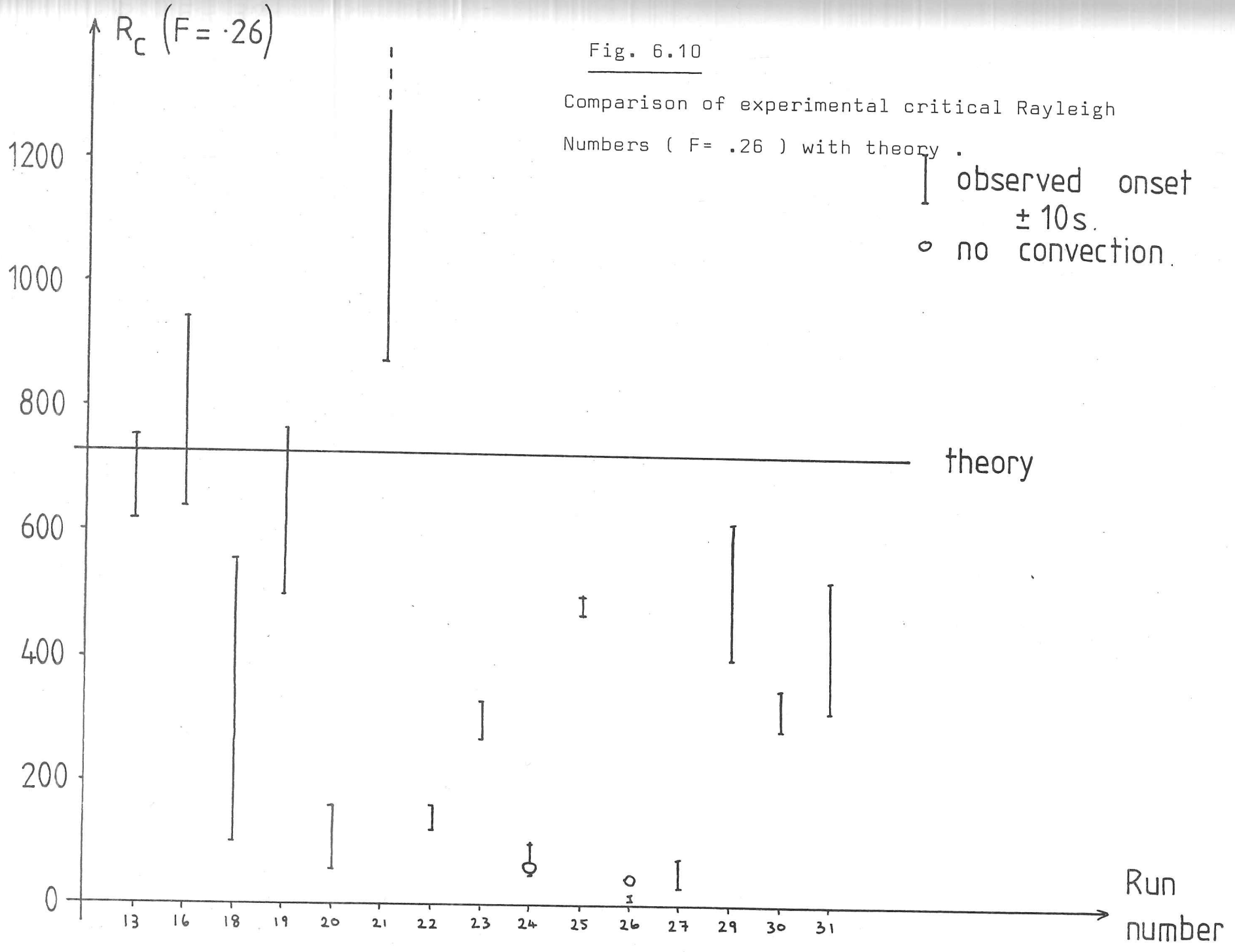
6.5 Growth of convecting region

After the onset of convection, observations were made when possible of the radial extent of the convection, as indicated by the region of scattering from the Kalliroscope. Immediately after onset, this was in general approximately 3 mm (all observations made to ± 1 mm), which is consistent with the thermal

Fig. 6.10

Comparison of experimental critical Rayleigh Numbers ($F = .26$) with theory .

| observed onset
± 10s.
○ no convection.



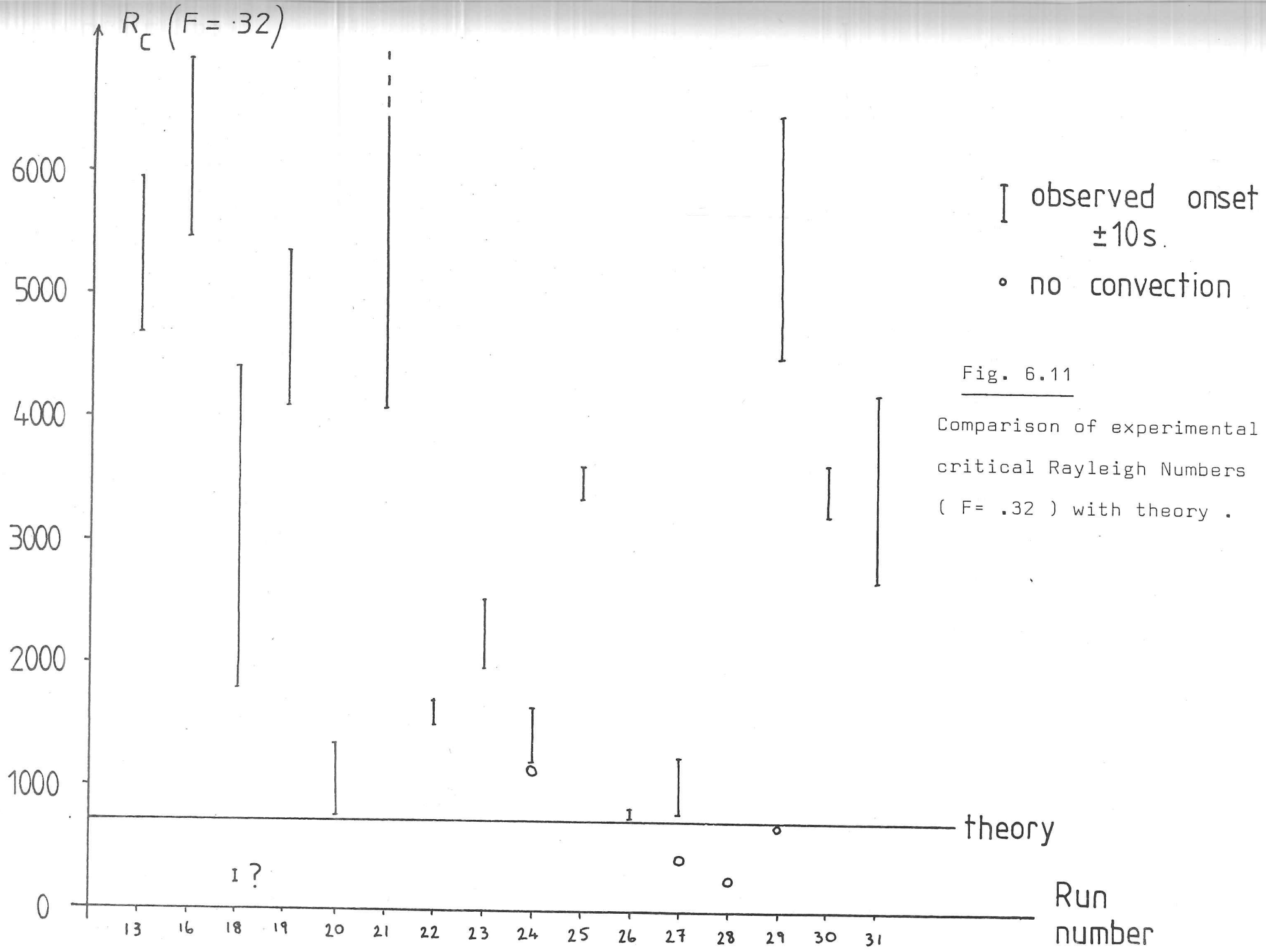


Fig. 6.11
 Comparison of experimental critical Rayleigh Numbers ($F = .32$) with theory .

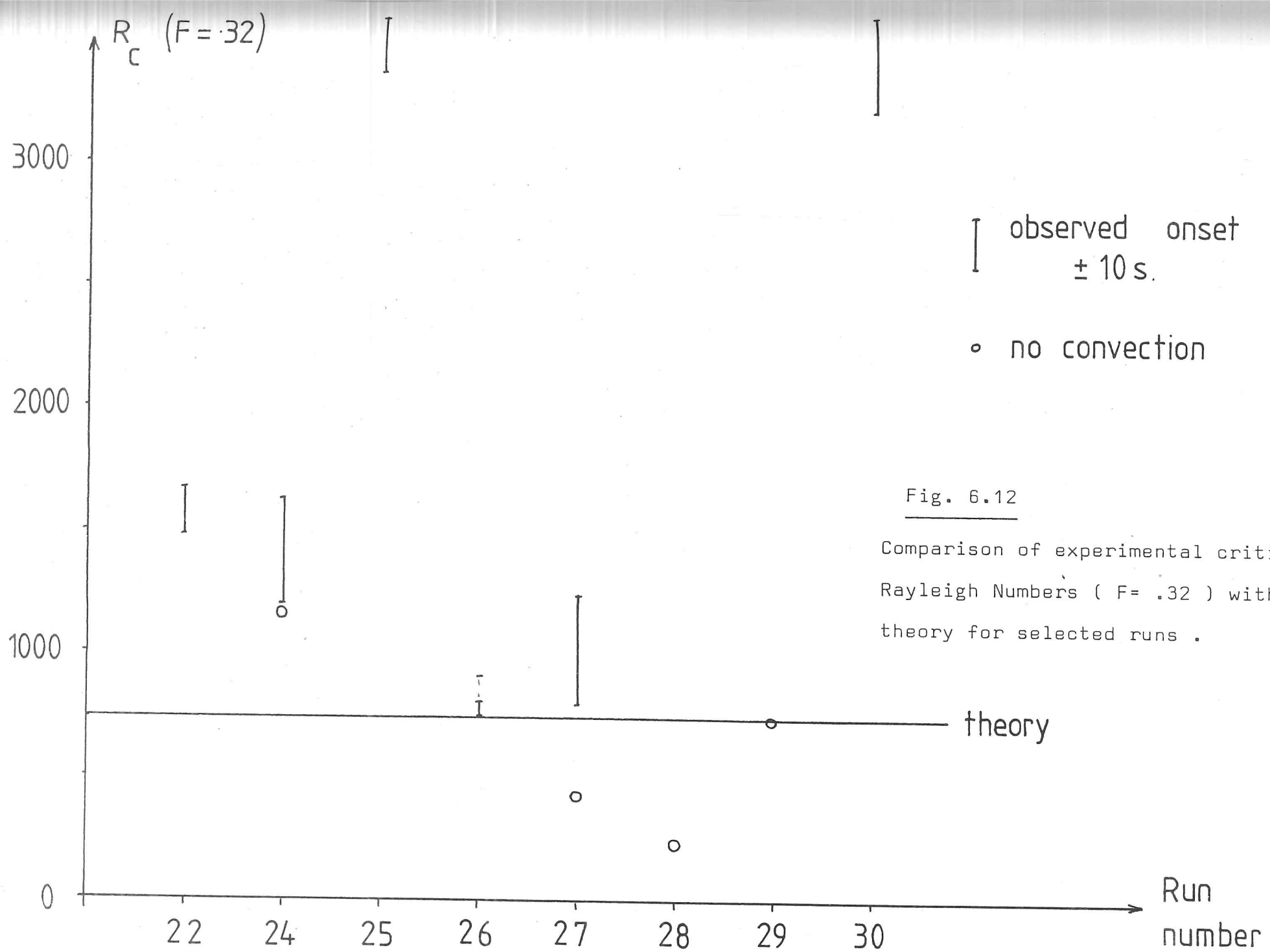


Fig. 6.12

Comparison of experimental critical Rayleigh Numbers ($F = .32$) with theory for selected runs .

models. Subsequent observations can only usefully be compared with the thermal model if the convection is only slightly supercritical, so that the Nusselt number (measuring heat transport relative to conduction) does not greatly exceed 1. Consideration of fig. 5.18 suggests that the Kalliroscope should reveal appreciable shear flows out to approximately $\alpha x = 2.0$, i.e. to about twice the depth of the unstable region. By the nature of the Kalliroscope suspension, it tends to remain aligned for some time after the shear flow it records may have decayed. Thus observations may continue to be made even though the underlying convection has ceased. A further point is that the greatest concentration of Kalliroscope, at the start of the heating that leads to instability, will be settled out on the side-wall owing to the centrifugal forces over the previous period (generally 1 hour) of cooling under rapid rotation. Thus little suspension will be available to show the existence of the countercell: $\alpha x = 2.0$ (where $U = 0$) is likely to act as a definite barrier to the Kalliroscope as a tracer.

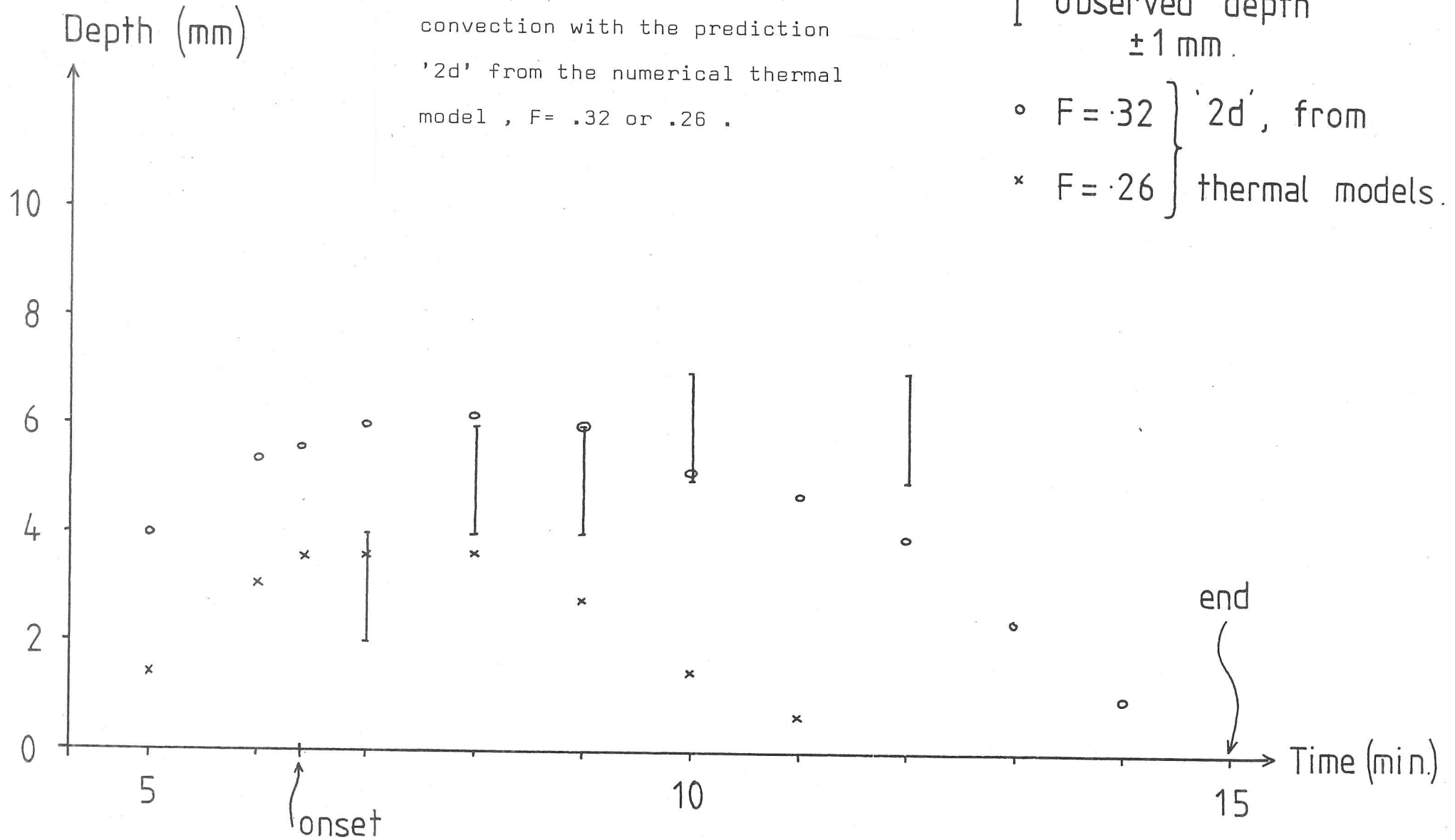
Figures 6.13, 6.14 and 6.15 compare the observations with the values for $2d$ given by the two thermal models for the experiments numbers 22, 25 and 30. Run number 26, which was observed to result in very faint convection which quickly faded, has no depth observational data. Instead figure 6.16 shows the variation of the Rayleigh number, as given by the two thermal models, over the time in which convection was observed. Taken together, these figures show better agreement with the model based on $F = 0.32$, but as expected the observed convection tends not to decrease in depth as it decays: the scattering merely becomes faint. Figure 6.16 clearly favours $F = 0.32$ as that model gives a peak Rayleigh number only some 40 seconds previous to the

Run N22

Fig. 6.13

Comparison of observed depth of convection with the prediction '2d' from the numerical thermal model, $F = .32$ or $.26$.

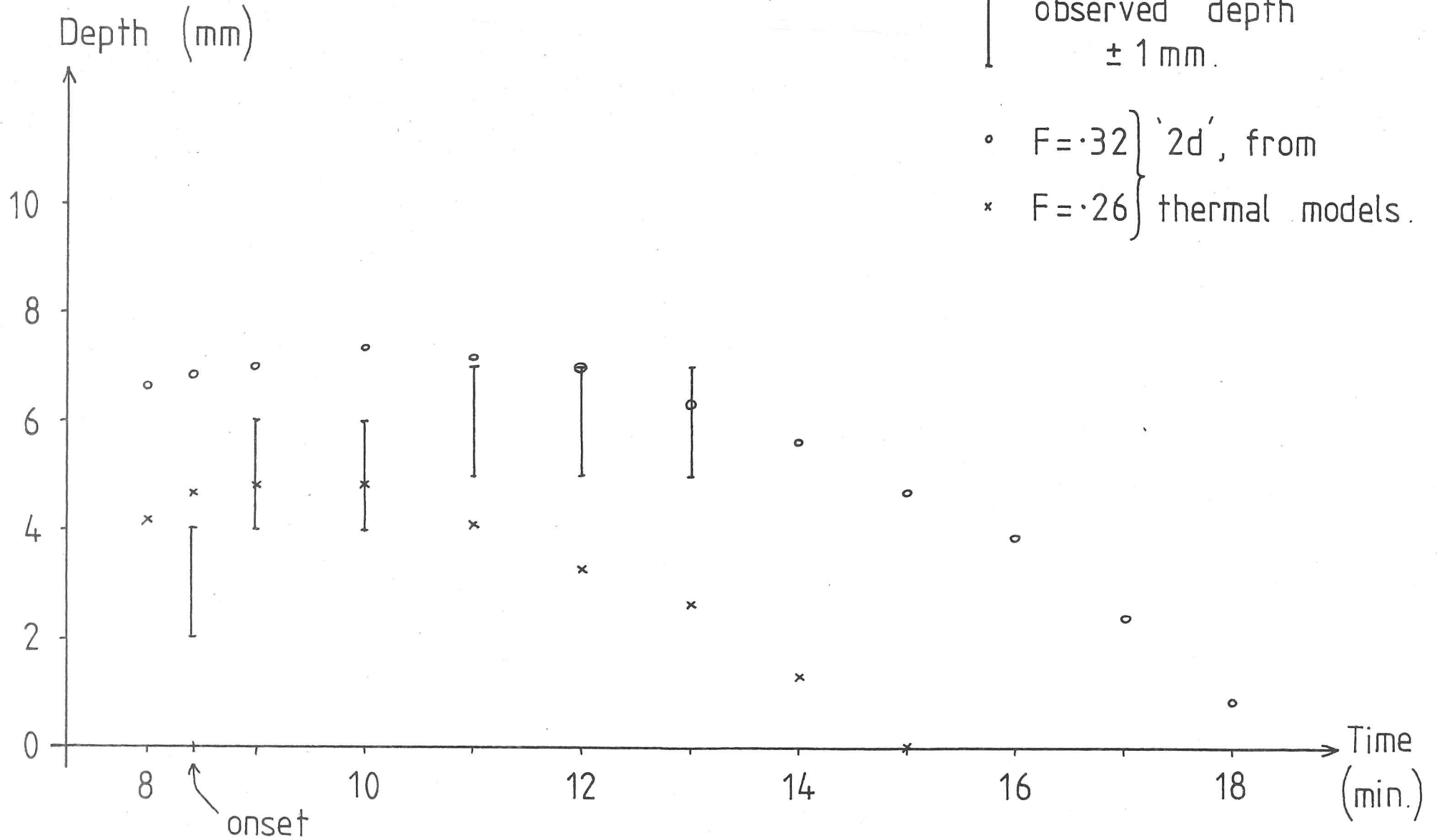
[observed depth ± 1 mm.
○ $F = .32$ } '2d', from
× $F = .26$ } thermal models.



Run N25

Fig. 6.14

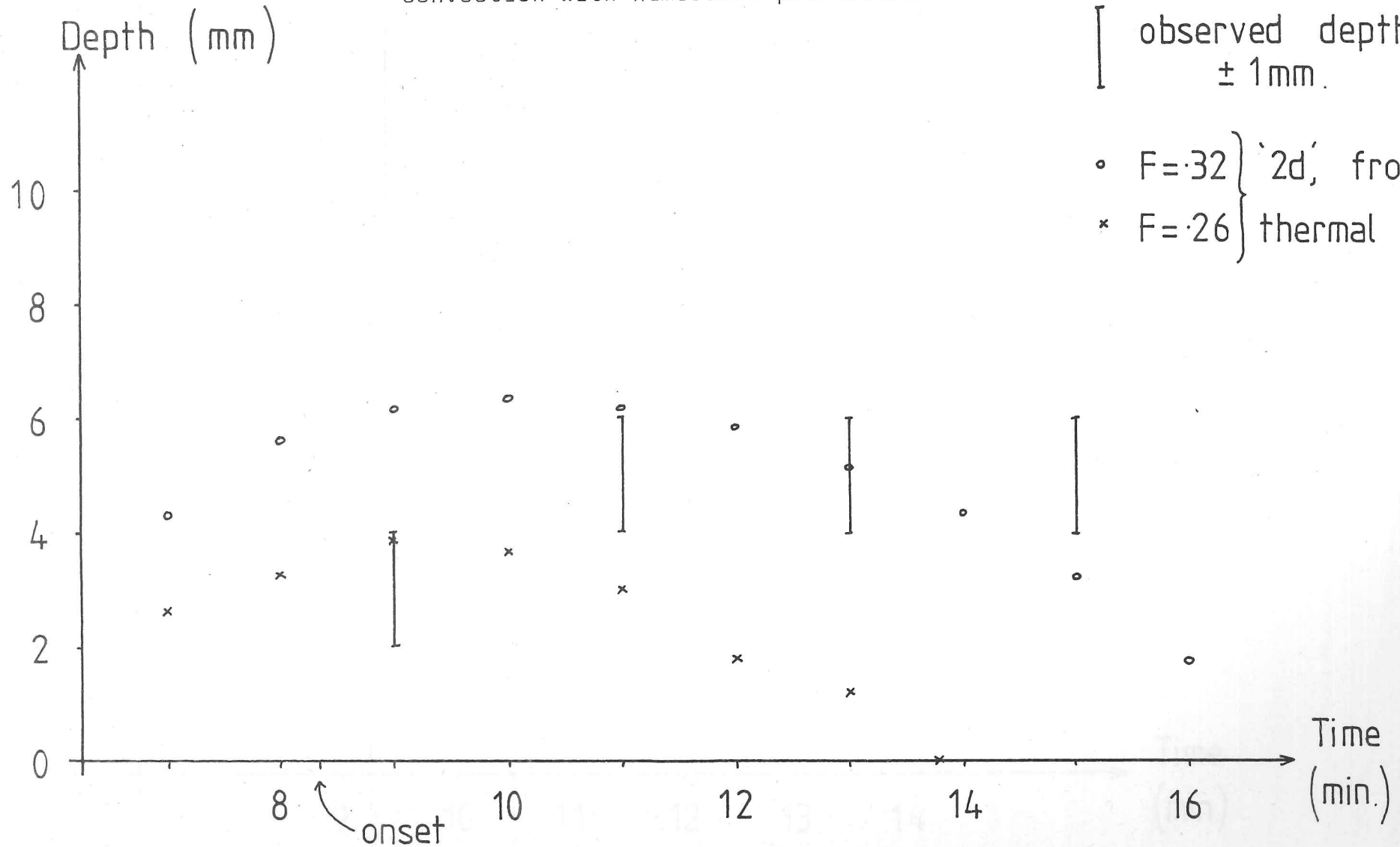
Comparison of observed depth of convection with numerical prediction.



Run N30

Fig. 6.15

Comparison of observed depth of convection with numerical prediction.



[observed depth ± 1 mm.

o $F=0.32$ } '2d', from
x $F=0.26$ } thermal models.

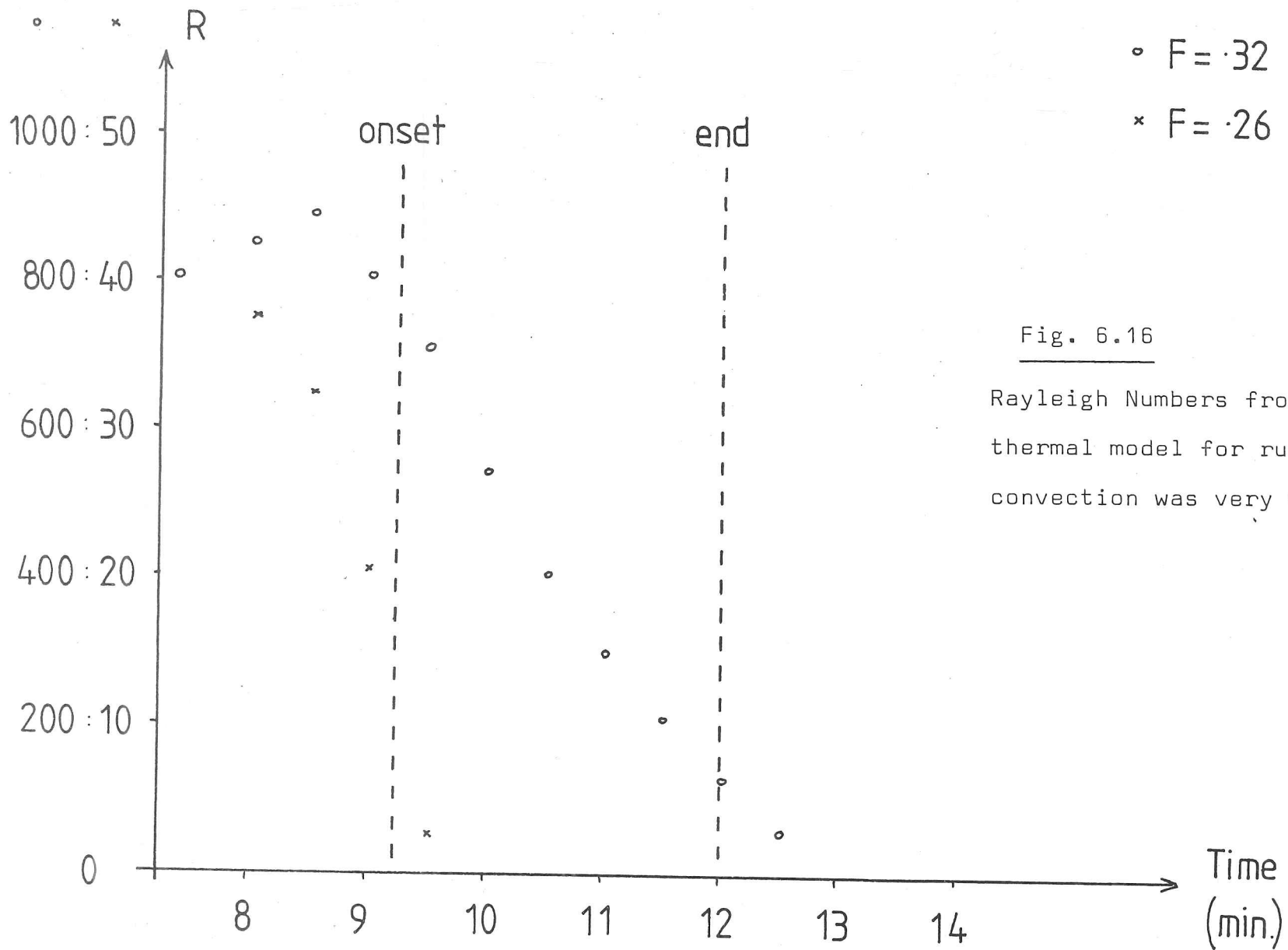


Fig. 6.16

Rayleigh Numbers from the numerical thermal model for run N26 in which convection was very weak .

observation of very weak convection (it is also heartening that that peak Rayleigh number of $R_c = 909$, is only about 25% above the prediction from the shooting program).

A greater time-span of depth observations is available for run N23, during which the Rayleigh number reached nearly twice its value at the time of onset, before convection died away and was then restarted, and then restarted again (fig. 6.17). The thermal model with $F = 0.32$ gives reasonable predictions of the observations: onset is observed later than the model prediction, but the fade-outs at 16 minutes and 25 minutes are in agreement. The later convection is observed to be deeper than is predicted by the thermal model, which presumably reflects the large degree of supercriticality (R peaks at $R = 32,500$ at 29:25).

6.6

Conclusions from the experiments

Thermal model based on $F = 0.32$

On the basis of the results for the onset of convection in §6.4 and those for the growth of the convecting region in § 6.5, the thermal model based on $F = 0.32$ (corresponding to the literature value for the thermal conductivity of perspex) is to be preferred. The use of $F = 0.26$ leads to critical Rayleigh numbers and predicted depths of convection markedly smaller than those predicted from the shooting program (§ 5). It therefore seems likely that the thermistor array used to make direct measurements of temperature does significantly alter the thermal regime in the tank by impeding the thermal wind and thereby making possible convective transport resulting from the axial laboratory gravity. In order to avoid this problem, a future rebuilt tank would need to allow the thermistor leads to be brought radially out from the axial shaft outside the tank,

Run N23

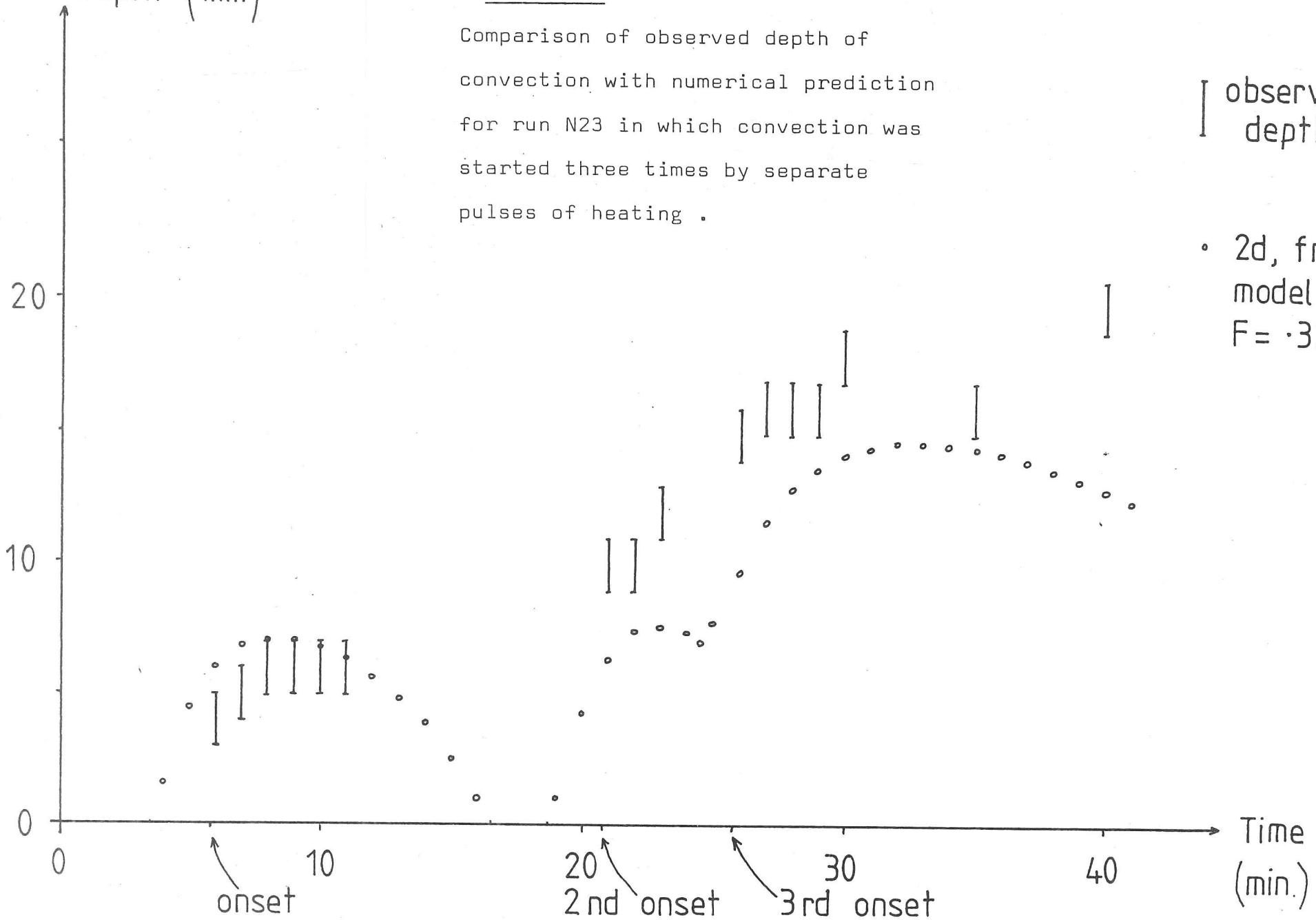
Depth (mm)

Fig. 6.17

Comparison of observed depth of convection with numerical prediction for run N23 in which convection was started three times by separate pulses of heating.

| observed depth

• 2d, from model, $F = .32$



perhaps within the end air-space. This will then create problems of sealing the entry ports for the leads, which would be under a substantial pressure difference.

Delay in observing onset of convection

Table 6.3, based on $F = 0.32$ models, gives the time delay between the prediction of the thermal model that the Rayleigh number R exceeds $R_c = 730$ and the time of onset observed in the experiment. These average 60 ± 30 seconds, and are not noticeably different between those runs at rotation rate 9.8 units and those at 7.0, whereas the crude data for the Rayleigh number at onset in general show distinctly higher values for the former set. The run N26, which has been noted as being close to marginal, is a notable example: although it yields a Rayleigh number at observed onset of $R = 773$ (approximately 6% above the theoretical value), that occurs only after a peak Rayleigh number of $R = 909$ and at a time 100 seconds after the time at which the Rayleigh number first exceeded the critical value. Thus the accuracy of this run stems not from being accurately observed in time, but from being a run in which the Rayleigh number went only marginally supercritical and remained so for a sufficiently long period.

As was noted before (§ 6.4), the diffusion time constant for the unstable layer is approximately 60 seconds: this is usually taken as an upper limit to the timescale for growth of the most quickly growing model of convection. Thus the observed delays are compatible with being primarily due to the time required for growth, except for those few runs where the delay was markedly short (e.g. N20, N27). No satisfactory reason for those very much shorter delays has been found.

Effect of rotation

This experiment has been unable to demonstrate the effect of rotation on the nature of the onset of convection, primarily because the aspect ratio a achieved is appreciably larger than expected (typically about 60-100, whereas $a \approx 40$ was expected). Since the effective Taylor number scales as a^{-8} , this leaves the rotation rate in a region in which R_c and b_c scarcely depend on T . Future rebuilding of the tank should therefore be based on a reduced vertical length L . A reduction to 3 cm, from 20 cm at present, should result in $a \approx 10$, and the currently obtainable rotation rate would give $T \equiv \frac{4\Omega^2 L}{\nu^2} \approx 10^{10}$. A combination of $a = 10$ and $T = 10^{10}$ would bring the results into the region in which boundary layer effects are appreciable, although not yet dominant. Whilst this proposed change of design will tend to give a stronger tank, supported by its end-plates, and therefore will ease the strength requirements, it will also tend to reduce the sensitivity of observation by the decrease in the depth of fluid illuminated by the stroboscope. This difficulty would probably prevent any further shortening of the tank.

Flows in stable region

In none of the experiments has any flow been observed in the stable region away from the convection zone. Thus, at the experimental levels of supercriticality, typically $R \lesssim 20 R_c$ (table 6.3), the convection does not cause strong shear flows in the adjoining stably stratified fluid. Penetrative convection is therefore only apparent to the extent of the immediate convecting region, corresponding to a depth of approximately $2d$ where d is the computed depth of unstable stratification (see figs. 6.13 to 6.17), which is in agreement with the linear theory (§ 5.5).

Summary

The experiment has demonstrated that a time-dependent temperature profile can be set up to investigate penetrative convections in terms of both the critical Rayleigh number for onset of convection and the resulting depth of convection. The accuracy is as yet poor. The present tank design is unable to investigate the "boundary-layer" dominated regime of rapid rotation, but this would be accessible to a redesigned tank, shorter along the axis. Observed times of onset of convection, using Kalliroscope suspension as a tracer for the presence of shear flows, are delayed by the period required for growth of the convection and so the critical Rayleigh number can only be measured by creating temperature profiles that are marginally supercritical at their peak, rather than by timing onset in runs that then go substantially supercritical.

7. Discussion

7.1 Discussion of results

The object of this work is to investigate two questions: firstly whether a stably stratified layer can occur in the core and secondly what effect rotation has on penetrative convection. The latter is a step towards understanding whether such a stably stratified layer might survive adjacent to a convecting region. The first of these questions must remain essentially speculative, as no direct observations are possible. However, the work presented in chapters 2 and 3 shows that no such stable layer is likely to arise from a subadiabatic temperature gradient. On the second question, the results of the analytical and numerical investigations of the linear equations, set out in chapters 4 and 5, indicate that the effect of rotation is to inhibit penetration into a stable region. The experimental observation described in chapter 6 are not sufficiently accurate to extend the investigation to the finite amplitude, non-linear problem. The lack of a treatment of either non-linear advection terms or Lorentz forces means that the results cannot yet be applied to the geophysical problem: much more work is required.

The model for the Earth's thermal history described in chapter 3 results in values for the present heat flux out of the core and for its dependence on the various parameter values adopted. The conclusion that a subadiabatic temperature gradient is unlikely to exist in the core depends on a consideration of the needs of a dynamo prior to the formation of the inner core. Thus the most critical aspect of the model is the assumption of a sufficiently hot start that the frozen inner core forms only relatively recently. If the inner core were an original feature,

then the core must have been at a remarkably constant temperature, one not consistent with the model used in that it requires a close equation of surface heat flux to radiogenic heating throughout the age of the Earth. Although the variation of mantle viscosity with temperature should favour this, it is unlikely to change the conclusions significantly, given the strength of the applied constraints.

Compositional gradients are discussed as an alternative cause of a stable stratification, in section 2.3: the problem for them is whether such gradients could form or survive in a vigorously convecting outer core, and this leads on to the fluid dynamics study in the later part of the thesis. A simple model following Fearn & Loper (1981) for such a compositional gradient is set out in section 2.3 in order to assess the possible degree of stability. This leads to a maximum Brunt-Vaisla frequency of approximately

$$N \approx 3 \times 10^{-3} \text{ s}^{-1}$$

Both analysis (chapter 4) and numerical solutions (chapter 5) of the linear Boussinesq equations at marginal stability lead to the conclusion that rotation inhibits penetration of a stable region in the plane-layer problem. Such a geometry would be appropriate to a "polar" region (fig. 2.4). Another effect of rotation is to inhibit the tendency of fixed flux boundary conditions to result in long horizontal wavelength flows. This reduces the geophysical applicability of the non-linear analysis of Chapman & Proctor (1980) and others, which depends on scale separation between the vertical and horizontal structure of the solutions.

The same problem is studied in the cylindrical geometry of Busse, both numerically (chapter 5) and experimentally (chapter 6), in the absence of any inclination of the end boundaries in order to avoid the Busse-roll type solution. Rotation has little effect on penetration in this geometry, owing to the secondary nature of the influence of rotation on the flows, through the end boundary layers. The experiments are of insufficient accuracy to confirm the results of the linear theory: the results reported are based on a numerical model of the temperature profile in the tank since direct temperature measurement leads to a disruption of the thermal wind balance in the cylindrical tank. Further, the effect of rotation has not been resolved as the effective aspect ratio of the convection (length of tank/depth of unstable layer) is found to be too large. This could be rectified in future work, by redesign of the experimental tank.

7.2 Suggestions for future work

No definitive answer can yet be given to the question of whether there is a region of stable stratification at the top of the outer core. However, the results of the thermal history model and the difficulty of a compositional layer surviving undisrupted raise sufficient doubts about the suggested stable layer that the next step should be a re-examination of the magnetic secular variation evidence for zero upwelling. Improvement of the thermal history model could come from a proper parameterisation of convective heat transport in a fluid of temperature dependent viscosity. However the constraints already placed on the model should ensure that any such improvement would have little effect on the results.

The fluid dynamics problem leads more directly to future

work. Apart from the redesign of the experimental tank suggested in chapter 6 to enable a verification of the linear theory, the next area of study should be on finite amplitude penetrative convection. The effect of rapid rotation on this is as yet quite unclear, and experimental observations on the growth of a convecting region, along the lines of those reported in section 6.5, are feasible with the techniques used already.

'Vous ne les lisez jamais, mon ami' (Stendhal, 'Le Rouge et le Noir').

- Acheson, D.J. (1980). Stable density stratification as a catalyst for instability. *J. Fluid Mech.*, 96, 723-733.
- Anderson, O.L., (1982). The Earth's core and the phase diagram of iron. *Phil. Trans R. Soc. Lond A.*, 306, 21-35.
- Backus, G.E., (1968). Kinematics of geomagnetic secular variation in a perfectly conducting core. *Phil. Trans. R. Soc. Lond. A.* 263, 239-266.
- Backus, G.E., (1975). Gross thermodynamics of heat engines in deep interior of Earth. *Proc. Nat. Acad. Sci. USA*, 72, 1555-1558.
- Batchelor, G.K., (1967). An introduction to fluid dynamics. Cambridge University Press.
- Benton, E.R. (1979). Magnetic probing of planetary interiors. *Phys. Earth Planet. Int.*, 20, 111-118.
- Benton, E.R. & Muth, L.A. (1979). On the strength of electric currents and zonal magnetic fields at the top of the Earth's core: methodology and preliminary estimates. *Phys. Earth Planet. Int.* 20, 127-133.
- Bolt, B.A., (1972). The density distribution near the base of the mantle and near the Earth's center. *Phys. Earth Planet. Int.*, 5, 301-311.
- Bolt, B.A., (1982). The constitution of the core: seismological evidence. *Phil. Trans. R. Soc. Lond. A*, 306, 11-20.
- Braginsky, S.I., (1963). Structure of the F layer and reasons for convection in the Earth's core. *Dokl. Akad. Nauk SSSR*, 149, 1311-1314.

- Braginsky, S.I., (1967). Magnetic waves in the Earth's core. *Geomagn. Aeron.*, 7, 851-859.
- Buell, J.C. & Catton, I. (1983). Effect of rotation on the stability of a bounded cylindrical layer of fluid heated from below. *Phys. Fluids* 26, 892-896.
- Bullard, E.C., Freedman, C., Gellman, H. & Nixon, J., (1950). The westward drift of the Earth's magnetic field. *Phil. Trans. R. Soc. Lond. A.* 243, 67-92.
- Busse, F.H., (1970). Thermal instabilities in rapidly rotating systems. *J. Fluid Mech.* 44, 441-460.
- Busse, F.H., (1975). Nonlinear interaction of magnetic field and convection. *J. Fluid Mech.*, 71, 193-206.
- Busse, F.H., (1981). Do Eddington-Sweet circulations exist? *Geophys. Astrophys. Fluid Dyn.*, 17, 215-235.
- Busse, F.H. & Carrigan, C.R., (1974). Convection induced by centrifugal buoyancy. *J. Fluid Mech.*, 62, 579-592.
- Chamberlain, J.A., (1980). Experiments on convection in rotating systems. Ph.D. thesis, Cambridge University.
- Chandrasekhar, S. (1954). The stability of viscous flow between rotating cylinders in the presence of a radial temperature gradient. *J. Rat. Mech. Anal.*, 3, 181-207.
- Chandrasekhar, S., (1961). Hydrodynamic and hydromagnetic stability. Oxford University Press, reprinted (1981) by Dover Publications, New York.
- Chapman, C.J. & Proctor, M.R.E., (1980). Non-linear Rayleigh-Benard convection between poorly conducting boundaries. *J. Fluid Mech.*, 101, 759-782.
- Davies, G.F., (1980). Thermal histories of convective Earth models and constraints on radiogenic heat production in the Earth, *J. geophys. Res.*, 85, 2517-2530.

- Deardorff, J.W., (1976). On the entrainment rate of a stratocumulus-topped mixed layer. *Quart. J. Roy. Met. Soc.*, 102, 563-582.
- Denton, R.A. & Wood, I.R., (1981). Penetrative convection at low Peclet number. *J. Fluid Mech.*, 113, 1-21.
- Dziewonski, A.M. & Anderson, D.L. (1981). Preliminary reference Earth model. *Phys. Earth Planet. Int.*, 25, 297-356.
- Eltayeb, I.A., (1972). Hydromagnetic convection in a rapidly rotating fluid layer. *Proc. R. Soc. Lond. A*, 326, 229-254.
- Eltayeb, I.A., (1975). Overstable hydromagnetic convection in a fluid layer. *J. Fluid Mech.*, 71, 161-179.
- Eltayeb, I.A., (1981a). Propagation and stability of wave motions in rotating magnetic systems. *Phys. Earth Planet. Int.*, 24, 259-271.
- Eltayeb, I.A., (1981b). Hydromagnetic stability of the Kennedy-Higgins model of the Earth's core. *Phys. Earth Planet. Int.*, 27, 1-5.
- Fearn, D.R., (1979) Thermal and magnetic instabilities in a rapidly rotating fluid sphere. *Geophys. Astrophys. Fluid Dyn.*, 14, 103-126.
- Fearn, D.R. & Loper, D.E., (1981). Compositional convection and stratification of Earth's core. *Nature*, 289, 393-394.
- Gans, R.F., (1972). Viscosity of the Earth's core. *J. geophys. Res.*, 77, 360-366.
- Green, D.H., (1972). Archaean greenstone belts may include terrestrial equivalents of Lunar Maria, *Earth Planet. Sci. Lett.*, 15, 263-270.
- Greenspan, H.P., (1968). The theory of rotating fluids. Cambridge University Press.

- Gubbins, D., (1977). Energetics of the Earth's core, *J. Geophys.* 43, 453-464.
- Gubbins, D., (1982). Finding core motions from magnetic observations. *Phil. Trans, R. Soc. Lond. A.*, 306, 247-254.
- Gubbins, D., Masters, T.G. & Jacobs, J.A., (1979). Thermal evolution of the Earth's core, *Geophys. J.R. astr. Soc.*, 59, 57-99.
- Gubbins, D., Thomson, C.J. & Whaler, K.A., (1982). Stable regions in the Earth's liquid core, *Geophys. J.R. astr. Soc.*, 68, 241-251.
- Haddon, R.A.W., (1982). Evidence for inhomogeneities near the core-mantle boundary. *Phil. Trans. R. Soc. Lond. A*, 306, 61-70.
- Hage, H. & Muller, G., (1979). Changes in dimensions, stresses and gravitational energy of the Earth due to crystallization at the inner core boundary under isochemical conditions, *Geophys. J.R. astr. Soc.*, 58, 495-508.
- Hewitt, J.M., McKenzie, D.P. & Weiss, N.O., (1975). Dissipative heating in convective flows. *J. Fluid Mech.* 68, 721-738.
- Hide, R., (1958). An experimental study of thermal convection in a rotating liquid. *Phil. Trans. R. Soc. Lond. A.*, 250, 441-478.
- Hide, R., (1966). Free hydromagnetic oscillations of the Earth's core and the theory of the geomagnetic secular variation. *Phil. Trans. R. Soc. Lond. A*, 259, 615-647.
- Hide, R., (1969). On hydromagnetic waves in a stratified rotating incompressible fluid. *J. Fluid Mech.*, 39, 283-287.
- Hide, R., (1978). How to locate the electrically conducting fluid core of a planet from external magnetic observations. *Nature*, 271, 640-641.

- Hide, R. & Roberts, P.H., (1979). How strong is the magnetic field in the Earth's liquid core? *Phys. Earth Planet. Int.* 20, 124-126.
- Higgins, G. & Kennedy, G.C., (1971). The adiabatic gradient and the melting point gradient in the core of the Earth. *J. geophys. Res.*, 76, 1870-1878.
- Hurle, D.T.J., Jakeman, E. & Pike, E.R., (1967). On the solution of the Benard problem with boundaries of finite conductivity. *Proc. Roy. Soc. A.*, 296, 469-475.
- Jacobs, J.A., (1975). *The Earth's Core*, Academic Press, London.
- Jeanloz, R. & Richter, F.M., (1979). Convection, composition and the thermal state of the lower mantle, *J. geophys. Res.*, 84, 5497-5504.
- Jensen, N.O. & Lenshow, D.H., (1978). An observational investigation of penetrative convection. *J. Atmos. Sci.*, 35, 1924-1933.
- Joseph, D.D. & Shir, C.C., (1966a). Subcritical convective instability. Part 1. Fluid Layers. *J. Fluid Mech.*, 26, 753-768.
- Joseph, D.D. & Shir, C.C., (1966b). Subcritical convective instability. Part 2. Spherical shells. *J. Fluid Mech.*, 26, 769-777.
- Kalinin, V.A., (1972). An equation which defines the variation of density with depth in a heterogeneous Earth. *Izv. Earth Phys. Engl. Transl.* 129-133.
- Kenyon, P.M. & Turcotte, D.L., (1983). Convection in a two layer mantle with a strongly temperature dependent viscosity. *J. geophys. Res.*, 88, 6403-6414.

- Kulacki, F.A. & Emara, A.A., (1977). Steady and transient thermal convection in a fluid layer with uniform volumetric energy sources, *J. Fluid Mech.*, 83, 375-395.
- Kumar, S. & Roberts, P.H., (1975). A three dimensional kinematic dynamo, *Proc. R. Soc. London A.*, 314, 235-258.
- Latour, J. & Zahn, J-P., (1978). On the boundary conditions imposed by a stratified fluid. *Geophys. Astrophys. Fluid Dyn.*, 10, 311-318.
- Loper, D.E., (1975). Torque balance and energy budget for precessionally driven dynamos. *Phys. Earth Planet. Int.*, 11, 43-60.
- Loper, D.E., (1978a). The gravitationally powered dynamo, *Geophys. J.R. astr. Soc.*, 54, 389-404.
- Loper, D.E., (1978b). Some thermal consequences of a gravitationally powered dynamo. *J. geophys. Res.*, 83, 5961-5970.
- Loves, F.J., (1974). Spatial power spectrum of the main geomagnetic field, and extrapolation to the core. *Geophys. J. R. astr. Soc.*, 36, 717-730.
- McElhinny, M.W. & Senanayake, W.E., (1980). Paleomagnetic evidence for the existence of the geomagnetic field 3.5 Ga ago. *J. geophys. Res.*, 85, 3523-3528.
- McKenzie, D.P. & Richter, F.M., (1981). Parameterized thermal convection in a layered region and the thermal history of the Earth. *J. geophys. Res.*, 86, 11,667-11,680.
- McKenzie, D.P. & Weiss, N.O. (1980). The thermal history of the Earth. *The Continental Crust and its Mineral Deposits*, ed. D.W. Strangway, Geological Association of Canada.

- McKenzie, D.P. & Weiss, N.O., (1975). Speculations on the thermal and tectonic history of the Earth, *Geophys. J.R. astr. Soc.*, 42, 131-174.
- Malkus, W.V.R., (1964). Boussinesq equations and convection energetics. Unpublished. Reproduced in Ref. 64-46 (1964). W.H.O.I. Geophysical Fluid Dynamics Notes.
- Malkus, W.V.R. & Veronis, G., (1958). Finite amplitude cellular convection. *J. Fluid Mech.*, 4, 225-260.
- Masters, T.G., (1979). Observational constraints on the chemical and thermal structure of the Earth's deep interior, *Geophys. J.R. astr. Soc.*, 57, 507-534.
- Mihaljan, J.M., (1962). A rigorous exposition of the Boussinesq approximations. *Astro. J.*, 136, 1126-1133.
- Moore, D.R. & Weiss, N.O., (1973). Nonlinear penetrative convection. *J. Fluid Mech.*, 61, 553-581.
- Nakagawa, Y. & Frenzen, P., (1955). A theoretical and experimental study of cellular convection in rotating fluids. *Tellus*, 7, 1-21.
- Olson, P., (1981). A simple physical model for the terrestrial dynamo. *J. geophys. Res.*, 86, 10875-10882.
- O'Nions, R.K., Evenson, N.M. & Hamilton, P.J., (1979). Geochemical modelling of mantle differentiation and crustal growth, *J. geophys. Res.*, 84, 6091-6101.
- Pedlosky, J., (1979). *Geophysical fluid dynamics*. Springer-Verlag, New York.
- Peltier, W.R., (1983). Constraint on deep mantle viscosity from Lageos acceleration data. *Nature*, 304, 434-436.
- Proctor, M.R.E., (1981a). Steady subcritical thermohaline convection. *J. Fluid Mech.*, 105, 507-521.

- Proctor, M.R.E., (1981b). Planform selection by finite-amplitude thermal convection between poorly conducting slabs. *J. Fluid. Mech.*, 113, 469-485.
- Richter, F.M., (1979). Focal mechanisms and seismic energy release of deep and intermediate earthquakes in the Tonga-Kermadec region and their bearing on the depth extent of mantle flow. *J. geophys. Res.*, 84, 6783-6795.
- Roberts, A.J., (1982). Nonlinear buoyancy effects in fluids. Ph.D. thesis, Cambridge University.
- Roberts, P.H., (1968). On the thermal instability of a rotating fluid sphere containing heat sources. *Phil. Trans. R. Soc. Lond. A*, 263, 93-117.
- Rossby, H.T., (1969). A study of Benard convection with and without rotation. *J. Fluid Mech.*, 36, 309-335.
- Schmitt, R.W. & Lambert, R.B., (1979). The effects of rotation on salt fingers. *J. Fluid Mech.*, 90, 449-463.
- Schubert, G., Stevenson, D. & Cassen, P., (1980). Whole planet cooling and the radiogenic heat source contents of the Earth and Moon. *J. geophys. Res.* 85, 2531-2538.
- Sclater, J.G., Jaupart, C. & Galson, D., (1980). The heat flow through oceans and continents, *Rev. geophys. Space Phys.*, 18, 269-311.
- Sharpe, H.N. & Peltier, W.R., (1979). A thermal history model for the Earth with parameterized convection, *Geophys. J.R. astr. Soc.*, 59, 171-203.
- Singer, H.A. & Olson, P.L., (1983). Dynamo action in a stably stratified core. *EOS*, 64, 18.
- Soward, A.M., (1979). Thermal and magnetically driven convection in a rapidly rotating fluid layer. *J. Fluid Mech.*, 90, 669-684.

- Soward, A.M., (1980). Finite-amplitude thermal convection and geostrophic flow in a rotating magnetic system. *J. Fluid Mech.*, 98, 449-471.
- Sparrow, E.M., Goldstein, R.J. & Jonsson, V.K., (1964). Thermal instability in a horizontal fluid layer: effect of boundary conditions and non-linear temperature profile. *J. Fluid Mech.*, 18, 513-528.
- Spiegel, E.A. & Veronis, G. (1960). On the Boussinesq approximation for a compressible fluid. *Astro. J.*, 131, 442-447.
- Spohn, T. & Schubert, G., (1982). Modes of mantle convection and the removal of heat from the Earth's interior. *J. geophys. Res.*, 87, 4682-4696.
- Stern, M.E., (1960). The salt fountain and thermohaline convection. *Tellus*, 12, 172-175.
- Stevenson, D.J., (1980). Applications of liquid state physics to the Earth's core. *Phys. Earth Planet. Int.*, 22, 42-52.
- Stevenson, D.J., Spohn, T. & Schubert, G., (1983). Magnetism and thermal evolution of the terrestrial planets. *Icarus*, 54, 466-489.
- Stix, M., (1970). Two examples of penetrative convection. *Tellus*, 22, 517-520.
- Stommel, H., Arons, A.B. & Blanchard, D., (1956). An oceanographical curiosity: the perpetual salt fountain. *Deep-Sea Res.*, 3, 152-153.
- Sun, W.Y., (1976). Linear stability of penetrative convection. *J. Atmos. Sci.*, 33, 1911-1920.
- Tough, J.G. & Roberts, P.H. (1968). Nearly symmetric hydromagnetic dynamos. *Phys. Earth Planet. Int.*, 1, 288-296.

- Townsend, A.A., (1966). Internal waves produced by a convective layer. *J. Fluid Mech.*, 24, 307-319.
- Tozer, D.C., (1972). The present thermal state of the terrestrial planets, *Phys. Earth Planet. Int.*, 6, 182-197.
- Turner, J.S., (1973). Buoyancy effects in fluids. Cambridge University Press.
- Verhoogen, J., (1961). Heat balance of the Earth's core. *Geophys. J.R. astr. Soc.*, 4, 276-281.
- Veronis, G., (1959). Cellular convection with finite amplitude in a rotating fluid. *J. Fluid Mech.*, 5, 401-435.
- Veronis, G., (1963). Penetrative convection. *Astrophys. J.*, 137, 641-663.
- Veronis, G., (1966). Motions at subcritical values of the Rayleigh number in a rotating fluid. *J. Fluid Mech.*, 24, 545-554.
- Veronis, G., (1968). Large amplitude Benard convection in a rotating fluid. *J. Fluid Mech.*, 31, 113-139.
- Whaler, K.A., (1980). Does the whole of the Earth's core convect? *Nature*, 287, 528-530.
- Whaler, K.A., (1981). Some applications of inverse theory to geomagnetic data. Ph.D. thesis, Cambridge University.
- Whitehead, J.A., (1971). Upon boundary conditions imposed by a stratified fluid. *Geophys. Fluid Dyn.*, 2, 289-298.
- Whitehead, J.A. & Chen, M.M., (1970). Thermal instability and convection of a thin fluid layer bounded by a stably stratified region. *J. Fluid Mech.*, 40, 549-576.
- Yukutake, T., (1981). A stratified core motion inferred from geomagnetic secular variations. *Phys. Earth Planet. Int.*, 24, 253-258.

Appendix 1 : algebra for section 4.4 .

Write c for $\cos \rho z$, s for $\sin \rho z$, e for $\exp(-\nu z)$ and Δ for $(\nu^2 - \rho^2)$.

$$u = A e^{-\mu z} + B e^{-\nu z} \cos \rho z + C e^{-\nu z} \sin \rho z$$

(in $z > 0$)

$$\equiv A e^{-\mu z} + B e c + C e s$$

$$\therefore u(0_+) = A + B$$

$$Du = -\mu A e^{-\mu z} + (\rho C - \nu B) e c + (-\rho B - \nu C) e s$$

$$\therefore Du(0_+) = -\mu A + (\rho C - \nu B)$$

$$D^2 u = \mu^2 A e^{-\mu z} + [(\Delta) B - 2\nu\rho C] e c + [2\nu\rho B + (\Delta) C] e s$$

$$\therefore D^2 u(0_+) = \mu^2 A + [\Delta B - 2\nu\rho C]$$

$$D^3 u = -\mu^3 A e^{-\mu z} + [\nu B(3\rho^2 - \nu^2) + \rho C(3\nu^2 - \rho^2)] e c$$

$$+ [-\rho B(3\nu^2 - \rho^2) + \nu C(3\rho^2 - \nu^2)] e s$$

$$\therefore D^3 u(0_+) = -\mu^3 A + [\nu B(3\rho^2 - \nu^2) + \rho C(3\nu^2 - \rho^2)]$$

$$D^4 u = \mu^4 A e^{-\mu z} + [B(\nu^4 - 6\nu^2\rho^2 + \rho^4) + C(4\nu\rho^3 - 4\nu^3\rho)] e c$$

$$+ [B(-4\nu\rho^3 + 4\nu^3\rho) + C(\nu^4 - 6\nu^2\rho^2 + \rho^4)] e s$$

$$\therefore D^4 u(0_+) = \mu^4 A + [B(\nu^4 - 6\nu^2\rho^2 + \rho^4) + C(4\nu\rho^3 - 4\nu^3\rho)]$$

$$D^5 u = -\mu^5 A e^{-\mu z} + [B\nu(-\nu^4 + 10\nu^2\rho^2 - 5\rho^4) + C\rho(5\nu^4 - 10\nu^2\rho^2 + \rho^4)] e c$$

$$+ [B\rho(-5\nu^4 + 10\nu^2\rho^2 - \rho^4) + C\nu(-\nu^4 + 10\nu^2\rho^2 - 5\rho^4)] e s$$

$$\therefore D^5 u(0_+) = -\mu^5 A + [B\nu(-\nu^4 + 10\nu^2\rho^2 - 5\rho^4) + C\rho(5\nu^4 - 10\nu^2\rho^2 + \rho^4)]$$

Now , in $z < 0$, we have the same solutions except for $-\nu \rightarrow +\nu$, and $-\mu \rightarrow +\mu$ throughout .

Hence, matching the two solutions through $z=0$, we get :-

$$\begin{aligned}
 A_1 + B_1 &= A_2 + B_2 \\
 -\mu A_1 + (\rho C_1 - \nu B_1) &= +\mu A_2 + (\rho C_2 + \nu B_2) = 0 \\
 \mu^2 A_1 + (\Delta B_1 - 2\nu\rho C_1) &= \mu^2 A_2 + (\Delta B_2 + 2\nu\rho C_2) \\
 -\mu^3 A_1 + [\nu B_1(3\rho^2 - \nu^2) + \rho C_1(3\nu^2 - \rho^2)] &= +\mu^3 A_2 + [-\nu B_2(3\rho^2 - \nu^2) + \rho C_2(3\nu^2 - \rho^2)] = 0 \\
 \mu^4 A_1 + B_1(\nu^4 - 6\nu^2\rho^2 + \rho^4) + 4C_1\nu\rho(-\Delta) &= \mu^4 A_2 + B_2(\nu^4 - 6\nu^2\rho^2 + \rho^4) + 4C_2\nu\rho\Delta
 \end{aligned}$$

and so,

$$\begin{aligned}
 A_1 &= A_2 = A \\
 B_1 &= B_2 = B \\
 C_1 &= -C_2 = C
 \end{aligned}$$

where, to 1st order accuracy in $|\mu|$,

$$\begin{aligned}
 B &= \mu A \left[\frac{\rho^2 - 3\nu^2}{2\nu(\nu^2 + \rho^2)} \right] \\
 C &= \mu A \left[\frac{3\rho^2 - \nu^2}{2\rho(\nu^2 + \rho^2)} \right]
 \end{aligned}$$

{ Note that $Du(0) = D^3u(0) = 0$ by symmetry }